Calcium regulation of spontaneous and evoked neurotransmitter release in small central synapses

Felicity Genevieve Alder

Declaration

I, Felicity Alder, confirm that the work presented in this thesis is my original research work. Where contributions of others are involved, this has been clearly indicated in the text.

Abstract

Synaptic neurotransmitter release is mediated by presynaptic voltage-gated calcium channels (VGCCs) via a tightly controlled mechanism. Naturally occurring mutations in the *CACNA1A* gene, which encodes the pore forming α_1-subunit of P/Q-type VGCCs, can disrupt synaptic neurotransmission and lead to neurological disorders such as migraine, ataxia and epilepsy.

Here, we aimed to understand how mutations linked to a severe form of migraine – familial hemiplegic migraine type 1 (FHM1) – affects neurotransmitter release in small central synapses. The effects of FHM1 mutations on both VGCC function and transmitter release are currently controversial. It is widely agreed that FHM1 mutations cause a shift to more negative potentials in the voltage activation threshold of P/Q-type channels. However, it is less understood whether this leads to a gain- or loss- of function of neurotransmitter release.

We studied the effects of two particular FHM1 mutations using a combination of genetic manipulations and fluorescent imaging methods. First, in order to overcome species-specific differences in subunit expression, we attempted to express human cDNA encoding mutant VGCCs in the human neuronal-like cell line, NT2. Second, we compared synaptic neurotransmission in neuronal hippocampal cultures prepared from mice harbouring FHM1 mutations, with wild-type controls. Our results revealed that synaptic transmission was highly heterogeneous among individual synapses. However, FHM1 mutations did not have a significant effect on synaptic vesicular release.

We also investigated the role of VGCCs in triggering spontaneous neurotransmission. We found that approximately 25 % of miniature excitatory post-synaptic currents were dependent on the stochastic opening of presynaptic VGCCs. Further analysis showed that the slow Ca^{2+} buffer EGTA blocks VGCC-dependent spontaneous and evoked release to a similar extent, suggesting that the two types of neurotransmission may share the same release machinery.

Taken together these data provide new insights into the regulation of evoked and spontaneous release by presynaptic VGCCs.

Acknowledgments

I would like to thank a number of people who have supported me during my PhD. Firstly to my primary supervisor Kirill Volynski, who has been very encouraging and patient throughout my time at the Institute and without whose help this project would never have got off the ground. Secondly to the Brain Research Trust who have generously sponsored me throughout my PhD (and who made me sell raffle tickets to earn my keep!) and the MRC.

I am very grateful to my secondary supervisor, Stephanie Schorge, for her excellent proof-reading skills, and help in making this thesis more legible. Also, thanks to Dimitri Kullmann for the opportunity to work in his lab.

To past and present members of the lab, who have generously given their time to assist me, especially my collaborators Yaroslav Ermolyuk, Ivan Pavlov and Rainer Surges. Also to the members of room 825 who continually make me laugh. Long may the insanity continue.

A substantial part of this project was based on work carried out in transgenic mice, which were a kind gift from Arn van den Maagdenberg and colleagues. Thanks also to Stuart Martin and Rahima Begum, who have assisted me with genotyping.

A big thanks to the Old Girl and Codger for their love and incessant questioning (no there will not be a parents evening!), and to the rest of my family and friends. And finally to David – thanks for all the fun (and for breaking up the sandwich diet with hot meals).

Table of contents

Table of figures

Table of tables

Abbreviations

ADP	Adenosine diphosphate
AMPA(R)	2-amino-3-(5-methyl-3-oxo-1,2- oxazol-4-yl)propanoic acid (receptor)
AP	Action potential
araC	Cytosine β-D-arabinofuranoside
ATP	Adenosine-5'-triphosphate
BPB	Bromophenol blue
BSA	Bovine serum albumin
CaM	Ca^{2+}/calmodulin
CCD	Charge-coupled device
cDNA	Complementary DNA
$\chi 2$	Chi^2
CMF-HBSS	Ca^{2+}, Mg^{2+}-free Hanks balanced salt solution
CNS	Central nervous system
CSD	Cortical spreading depression
CV	Coefficient of variation
DIC	Differential interference contrast microscopy
DIV	Days in vitro
DL-AP5	DL-2-Amino-5-phosphonopentanoic acid
DMEM/F12	Dulbecco's Modified Eagle Medium: Nutrient Mixture F-12
DMSO	Dimethyl sulfoxide
DNAse	Deoxyribonuclease
Doc2b	Double C2-like domain-containing protein beta
DPBS	Dulbecco's Phosphate Buffered Saline
EA2	Episodic ataxia type 2

EB	Extracellular buffer
EDTA	Ethylenediaminetetraacetic acid
EGTA	Ethylene glycol tetraacetic acid
EM	Electron microscopy
EPSC	Excitatory post synaptic current
FBS HI	Fetal bovine serum, heat inactivated
FDA	Fluorescein diacetate
FHM1	Familial hemiplegic migraine type 1
FHM2	Familial hemiplegic migraine type 2
FHM3	Familial hemiplegic migraine type 3
FM dye	Fei Mao dyes
FUdR	5-Fluoro-2'-deoxyuridine
$GABA_A$	γ-aminobutyric acid receptor type A
GABA	γ-aminobutyric acid
GM	Glial medium
GPCRs	G-protein coupled receptor
G-protein	Guanine nucleotide-binding proteins
GTP	Guanosine-5'-triphosphate
HBSS	Hanks balanced salt solution
HEK 293	Human embryonic kidney 293 cell line
HEPES	4-(2-hydroxyethyl)-1-piperazineethanesulfonic acid
HET	Heterozygous
hNT	Neuronal-like cells derived from NT2 cells
HOM	Homozygous
HVA	High-voltage activated

ITPR1	Inositol 1,4,5-trisphosphate receptor type 1
K&R	Kiss and run
K_{AP}	AP-evoked destaining rate
K_d	Dissociation constant
K_{ev}	Evoked destaining rate
KI	Knock-in
KO	Knock-out
K_{sp}	Spontaneous destaining rate
LEMS	Lambert–Eaton myasthenic syndrome
LSM	Laser scanning microscope
LVA	Low-voltage activated
MEM/N2	Minimal essential medium: nutrient mixture N2
mEPPs	Miniature end plate potential
mEPSC	Miniature excitatory post synaptic current
NAP	Average number of vesicles released during a single AP
NB	Neurobasal complete
NBQX	2,3-dihydroxy-6-nitro-7-sulfamoyl-benzo[f]quinoxaline-2,3-dione
NMDA(R)	N-methyl-D-aspartic acid (receptor)
NMJ	Neuromuscular junction
NSF	N-ethylmaleimide-sensitive factor
NT2	Neuronally committed human teratocarcinoma cell line
P0	Postnatal day zero
PCR	Polymerase chain reaction
EGFP	Enhanced green fluorescent protein
PI	Propidium iodide

PKC	Protein kinase C
PLL	Poly-L-Lysine
PMT	Photomultiplier tube
P_{rel}	Probability of neurotransmitter release in response to an AP
PTX	Picrotoxin
p_v	Average fusion probability of an individual vesicle
RP	Recycling pool
RPM	Revolutions per minute
R_{rel}	Release rate
RRP	Readily releasable pool
SCA6	Spinocerebellar ataxia type 6
SFCA	Surfactant-free cellulose acetate
SNAP-25	Synaptosomal-associated protein 25
SNARE	Soluble NSF attachment protein receptor
SPMs	Synaptic plasma membranes
SRC1	SynaptoRed C1
syt1	Synpatotagmin 1
Tris-HCl	Tris(hydroxymethyl)aminomethane-Hydrochloride
TTX	Tetrodotoxin
Urd	Uridine
VAMP-2	Vesicle-associated membrane protein 2
VGIC	Voltage gated ion channel
ω-aga	ω -agatoxin IVA
ω -ctx	ω –conotoxin GV1A
WT	Wild type

1. Introduction

In this report, we focus on the regulation of neurotransmitter release by voltage-gated Ca^{2+} channels (VGCCs) at small central synapses. VGCCs provide the major means of Ca^{2+} entry into excitable cells, and regulate a huge range of cellular responses, including the activation of Ca^{2+}-dependent enzymes, gene transcription, and of course neurotransmitter release (Reid et al. 2003). Neurotransmitter release links intrinsic changes in membrane potential to vesicular release of a wide range of transmitters into the extracellular space. The main goal of this thesis is to probe the tightness of the link that Ca^{2+} channels provide: in particular, how regulation of neurotransmitter release varies between presynaptic boutons, and how disease - linked mutations in VGCCs can alter synaptic properties. Here, we give an overview of the background and major unresolved questions that underlie this thesis.

1.1. Voltage gated ion channels

1.1.1. A brief history of the ionic theory of membrane excitability

The ionic theory of membrane excitability was first deduced by Alan Hodgkin, Andrew Huxley and Bernard Katz in Great Britain and by Kenneth Cole and Howard Curtis in the United States (Huxley 2002; Häusser 2000). After Cole and Curtis had shown that membrane resistance dramatically decreases during an action potential (AP) (Cole et al. 1939), Hodgkin and Huxley, by recording the potential across the membrane of the squid giant axon, showed the interior voltage became substantially positive during an AP, in contrast to Julius Bernstein's theory (Hodgkin et al. 1939; Bernstein 1902). After a false start at an explanation of the data (Hodgkin et al. 1945), and delayed by the war, Hodgkin and Huxley correctly described their observations as an increase in the permeability of the membrane for sodium ions, which flooded into the axon, carrying positive charge – a result which confirmed an overlooked publication by Overton in

1902 (Overton 1902). This explanation was experimentally substantiated by Hodgkin and Bernard Katz (Hodgkin et al. 1949).

In order to study the current-voltage characteristics of the membrane during an AP, both the UK and the US laboratories realised that a feedback circuit was needed to control the internal potential. Cole won this particular race, and published the observation that the current-voltage relation was continuous with a region of negative slope that makes it unstable, causing an all-or-none response (Cole 1949), although he did not analyse the results further. Hodgkin and Huxley expanded this work, varying the concentration of external sodium, and analysing the components of the membrane current. They fit the data exceedingly closely with equations to describe the dependence of the permeability of the membrane to sodium and potassium as a function of the membrane potential and time. Finally, after solving the non-linear differential equations for the time course of voltage change if there was no feedback, they showed their fit was remarkably close to the recorded AP (Hodgkin et al. 1952). The Hodgkin-Huxley model was so successful at quantitatively describing the AP that it is still the basis of biophysical and modelling work in neuroscience, and gained Hodgkin and Huxley the Nobel prize in Physiology or Medicine in 1963, alongside John Eccles (Häusser 2000).

1.1.2. *Introducing the main divisions of the voltage-gated ion channel super-family*

The original experimental work that Hodgkin and Huxley carried out identified several ion fluxes, which are now attributed to different types of voltage-gated ion channels (VGIC). It has since been recognised that these channels underlie, AP propagation along an axon, repolarisation and neurotransmitter release. At rest, neuronal membrane ion permeability is low and only K^+ ions can cross (Hodgkin et al. 1952), causing the neuron to sit at a negative potential with respect to the external solution. After an

external stimulus, the electromotive force of the membrane changes and generates an inward current, via opening of Na^+ channels, which increases permeability and depolarises the cell. Na^+ channels open extremely rapidly (Rosenberg et al. 1984), and remain open for ~ 1 ms, allowing roughly 5000 Na^+ ions to flow through the channel (Rosenberg et al. 1984). The inflow of sodium ions from a large number Na^+ channels produces the depolarising upstroke of the AP. The inward current is sufficient to depolarise neighbouring patches of membrane, opening more Na^+ channels, and propagating the electrical signal (Hille 2001). Na^+ permeability is arrested at the pinnacle of the spike when (i) the Na^+ driving force heads to zero as the membrane potential reaches the Na+ equilibrium potential, (ii) all the available Na^+ channels have opened and (iii) the open channels transition to the inactivated state, triggering the absolute refractory period (Hodgkin et al. 1952; Yu et al. 2003). Sodium is relatively biologically inactive, so once inside a neuron it plays little role in modifying enzyme activity, transcription or transmitter release. The primary consequence of sodium ion influx is a change in membrane voltage, which triggers the gating of other channels.

Not all potassium channels are voltage gated (Coetzee et al. 1999). However, the canonical delayed inward rectifier K^+ channels are sensitive to voltage, and these channels are crucial for the rapid membrane repolarisation after an AP (Isomoto et al. 1997; Doyle 1998; Neusch et al. 2003; Dodson et al. 2004). On opening, voltage-gated K^+ channels allow K^+ ions to flow down their concentration gradient and out of the cell, returning the membrane potential back to negative resting potentials. Most K^+ channels inactivate much more slowly than Na^+ channels, so continue to pass K^+ ions after Na^+ channels have inactivated, causing an after-hyperpolarisation as the temporary impermeablility to Na^+ and increased permeability to K^+ drives the membrane voltage

towards the potassium reversal potential, which is slightly more negative than the typical resting potential. This accounts for a relative refractory period, during which the cell is less likely to respond to another stimulus. Finally, as K^+ channels flip into their closed or inactive states, the membrane potential returns to rest (Hodgkin et al. 1952; Catterall 1995).

As the AP invades the synaptic terminal, the synaptic membrane is depolarised, allowing the third class of voltage gated channels, the Ca^{2+} channels, which are densely packed in pre-synaptic terminals, to open, causing a tightly-restricted jump in intra-terminal Ca^{2+}, which in turn triggers neurotransmitter release (Südhof 2004). Ca^{2+} channels open at an intermediate rate, more slowly than sodium channels but more rapidly than many potassium channels, and they also tend to de-activate slowly, meaning that these channels pass large tail currents upon re-polarisation of cells. The highly positive equilibrium potential for Ca^{2+} ions means that when these channels are open at negative potentials (for example after rapid hyperpolarisation after an AP) they have a larger driving force and although individual channel opening is likely to be temporally short, more ions will pass than would if the terminal was at the depolarised peak of the action potential.

1.1.3. *Ion channel structure is highly conserved among VGICs*
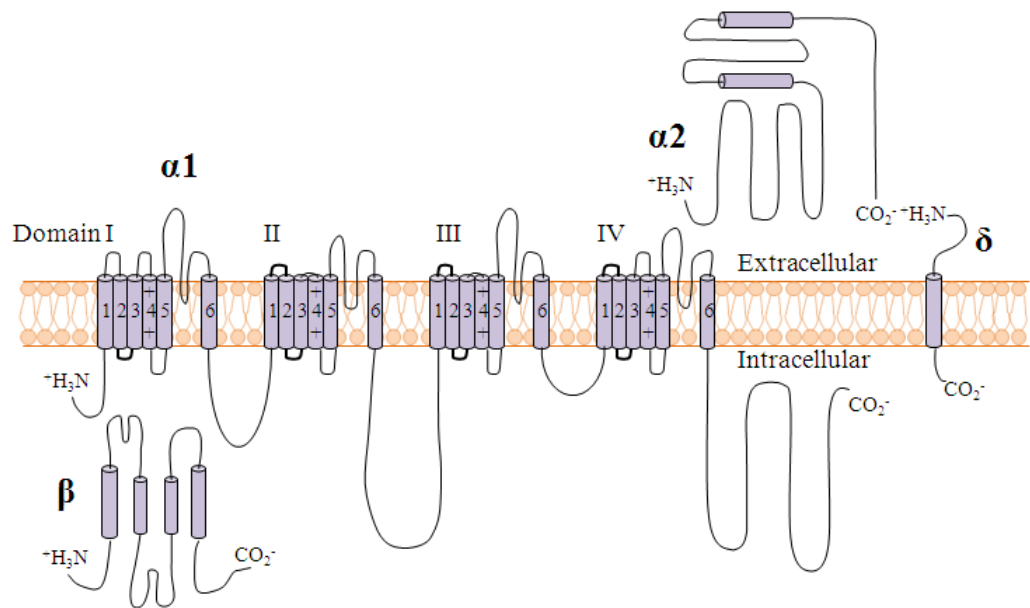
Figure 1.1: Structure of a voltage gated calcium channel. *VGCCs are comprised of several subunits. The α_1-subunit is the main pore-forming protein, consisting of four domains (I-IV), each divided into six transmembrane segments (S1-S6). The β- and $\alpha_2\delta$- subunits are auxiliary to the α_1-subunit.* ***Adapted from (Catterall 2011).***

Although voltage-gated ion channels were thought to be of importance only to animals with complex nervous systems, they are in fact relatively old proteins, and are present in a diverse range of prokaryotes, as well as plants (Anderson et al. 2001; Pohorille et al. 2005; Miller 2000). The finding that the pore-forming components of K^+, Na^+ and Ca^{2+} channels all consist of four highly homologous units comprised of six transmembrane segments (S1-S6) suggested that they all have a common ancestor (Strong et al. 1993) (see figure 1.1 for an illustration of a typical Ca^{2+} channel main pore-forming α_1-subunit, and associated auxiliary subunits). Indeed, several observations point towards a

6-TM K^+ domain being the common ancestor: (i) in K^+ channels, each homologous unit is a separate protein (Coetzee et al. 1999); (ii) of the four units, or domains, within each Na^+ and Ca^{2+} channel α-subunit, I and III are similar, and II and IV are similar, but the pairs are different from each other, suggesting two rounds of gene duplication of a K^+ channel (Kullmann 2002). Additionally, the distribution of Ca^{2+} and Na^+ channels in lower eukaryotes suggests that Na^+ channels evolved from low voltage-activated (LVA) Ca^{2+} channels (Hille 2001), as the dominant inward charge carrier.

1.1.4. *The ability to pass current in a voltage-dependent manner has evolved more than once*

While this thesis focuses on the voltage gated channel super family that descended from a primordial potassium channel, it is not intended to suggest these are the only channels. In fact the ability to gate in response to stimuli and selectively pass different ions has evolved at least three times. Chloride channels are structurally distinct from Na^+, K^+ and Ca^{2+} channels, as clearly indicated by the crystallised structure (Dutzler et al. 2003). A functional chloride channel is composed of two subunits, which can gate either together or independently (Duran et al. 2010). Ligand-gated channels mediate ion movement and generate electrical signals in response to specific chemical neurotransmitters, typically acetylcholine, glutamate, glycine or γ-aminobutyric acid (GABA) (Hille 2001). These ligand-gated channels mediate local membrane potential, depending on the channel ion selectivity, and it is this change in membrane potential that can be sensed and processed by the receiving cell (Madden 2002). Several of these ligand-gated channels have evolved the ability to link depolarisation to ion flow by developing voltage dependent pore block, with magnesium (NMDAR) or spermine (AMPARs). These channels therefore pass current in a voltage dependent manner.

1.1.5. Voltage-sensing and permeation modules are conserved in the voltage-gated ion channel super-family

While Hodgkin and Huxley were able to accurately describe the behaviour of voltage gated ion channels in their seminal studies, they had no information of what sort of molecules they were describing. It was not until the advent of molecular cloning and resolution of crystal structures that the distinct modules which allow them to detect voltage changes and pass ions became known. However, some features are still controversial.

In order to pass nerve impulses at velocities of up to 120 m/s, the cell membrane must have a method to quickly and accurately vary the permeability to various ions (Hodgkin 1964). Voltage-gated ion channels therefore have to respond rapidly to any changes in membrane potential, but how do they sense voltage? It is well known that the voltage sensor is located in the S4 transmembrane segment (figure 1.1), where several positive amino acids (mainly arginine or lysine) are located (Seoh et al. 1996; Aggarwal et al. 1996). Each model relies on the close interaction between S4 and the S5-S6 module which forms the selection pore, so when S4 moves, it opens or closes the pore.

Three models of voltage-gating have been suggested (figure 1.2): (i) the helical screw or sliding helix model (figure 1.2a) (Guy et al. 1986; Catterall 1986). Positive charges in S4 make contacts with negative charges elsewhere in the channel. When the membrane voltage changes, S4 moves 4.5 Å and rotates 60° around the length axis and makes new contacts. Several studies have used this model to explain functional data (Lecar et al. 2003; Silverman et al. 2003; Gandhi et al. 2000; Keynes et al. 1998; Tombola et al. 2007; Durell et al. 2004; Yarov-Yarovoy et al. 2006; Campos et al. 2007). (ii) Transporter model (figure 1.2b). This model suggests rather than a translational

movement of S4 across the membrane, a rotation is required to move the positive

charges across the membrane (Elinder et al. 2003; Blaustein et al. 2004; Cha et al. 1999;

Glauner et al. 1999; Chanda et al. 2005; Posson et al. 2005). (iii) The paddle model

(figure 1.2c). Based on X-ray crystallography data, the S4 and S3b (extracellular end of

S3) make up the paddle, and move freely in the lipid bilayer by 15-20 Å (Long et al.

2007; Y. Jiang et al. 2003; Ruta et al. 2005). However, it is possible that the crystal

structure produced are not accurate representations of the native conformation of the

voltage sensor (Ahern et al. 2004).

a. Model 1:
Helical screw

b. Model 2:
Transporter model

c. Model 3: Paddle
model
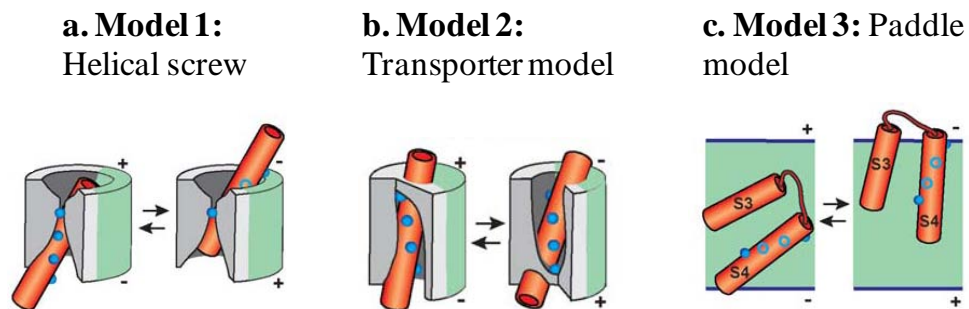
Figure 1.2: Models of voltage sensing. Three proposed models to describe the

*mechanism of voltage sensing (**a**) the helical screw (**b**) the transporter model and (**c**) the*

paddle model. Red cylinders represent the S4 segment unless otherwise indicated.

Protein surrounding S4 is gray. Lipid is green. The first four S4 arginines are

represented as blue spheres when they are in the foreground and empty blue circles

when they are behind the cylinder. In each model, the S4 resting position is shown on

*the left, and the activated position on the right. **Adapted from (Tombola et al. 2006).***

Each model has strong evidence in favour, although recently, the three models have

begun to converge towards each other (Börjesson et al. 2008; Long et al. 2007; Shafrir

et al. 2008; Campos et al. 2007; Pathak et al. 2007). A number of channelopathies (diseases caused by disturbed function of ion channel subunits) arise from mutations in the S4 voltage sensor, particularly familial hemiplegic migraine type 1 (FHM1), discussed below (Pietrobon 2010, 2007; Barrett et al. 2005).

Considerable work has also been done to elucidate the structural basis of ion permeation and selectivity, and the general conclusion that has emerged is that single amino acid mutations can be sufficient to radically alter the selectivity of each class of channel (Yang et al. 1993; Mikala et al. 1993). The S5 and S6 segments and the membrane-associated S5-S6 linker form the pore lining of the voltage-gated ion channel (Catterall 1995). A recent publication has elucidated the crystal structure of a VGSC from *Arcobacter butzleri* (Payandeh et al. 2011), which has furthered understanding in the structural basis of ion selectivity in a non-potassium selective VGIC. Although not identical, VGCCs share enough structural similarity with VGSCs that the results of this study can be extrapolated to VGCC ion selectivity. However, the full crystal structure of an α_1-subunit of a VGCC has not yet been reported.

1.2. Voltage-gated calcium channels

1.2.1. Discovery and classification of VGCCs

In 1953, Paul Fatt and Bernard Katz demonstrated that muscle cells submerged in a medium lacking sodium ions were still electrically excitable (Fatt et al. 1952), and correctly identified the excitable ion as Ca^{2+}. This was the first report of voltage-gated Ca^{2+} currents. Subsequently, in 1975, Susumu Hagiwara characterised Ca^{2+} conductances in invertebrate tissue (Hagiwara et al. 1975, 1981), followed later by work by Harald Reuter in mammalian tissue (Reuter 1967). Due to their prevalence in all excitable tissue, Ca^{2+} channels are said to define cell excitability (Hille 2001).

Since their original description in 1953, Ca^{2+} channels have emerged as a diverse family of transmembrane proteins, which pass multiple types of Ca^{2+} current – designated L-, N-, P-, Q-, R- and T-type – all of which have distinct physiological and pharmacological properties (Reuter 1967, 1979; Tsien et al. 1988; Bean 1989; Hess 1990; Llinas et al. 1992; Catterall 2000; Dolphin 2006). Originally different Ca^{2+} currents were dissected and described using pharmacological methods (Dolphin 2006). The first inkling that there was more than one type of Ca^{2+} channel came from the work by Hagiwara in starfish eggs (Hagiwara et al. 1975), and furthered by Carbone and Lux (Carbone et al. 1984) and Fedulova (Fedulova et al. 1985). This work distinguished two currents, flowing from a low- and a high- voltage activated channel (Carbone et al. 1984), which were separated using pharmacological methods. The L-type, denoted for "long-lasting" (Hess et al. 1984; Nowycky et al. 1985), was distinguished by blocking with 1, 4-dihydropyridine (DHPs). L-type currents were enriched in skeletal, cardiac

and smooth muscle (Peter Hess et al. 1984), as well as in endocrine cells (Milani et al. 1990) and neurons (Bean 1989). Work in invertebrate tissue (Hagiwara et al. 1975) and neurons (Llinas et al. 1981) demonstrated Ca^{2+} currents with different biophysical properties to L-type currents: activation at more negative potentials, faster inactivation, smaller channel conductance and insensitivity to DHPs. These currents were denoted T-type, for "transient" or "tiny".

Subsequently, the number of pharmacologically distinct HVA channels increased rapidly (Dolphin 2006). A component of the Ca^{2+} current in presynaptic terminals of hippocampal neurons was observed to be resistant to DHPs, but could be blocked by a peptide extracted from the cone shell mollusc *Conus geographus* ω-conotoxin GV1A (McCleskey et al. 1987; Nowycky et al. 1985). These channels were denoted N-type for "neuronal" or "non-L". Yet another subtype was discovered in cerebellar Purkinje cells, named P-type, which were blocked by the peptide ω-agatoxin IVA, a product of the venom of the American funnel web spider *Agelenopsis aperta* (Llinás et al. 1989; Mintz et al. 1992). P-type channels are extremely similar in physiology to Q-type channels, identified in cerebellar granule cells, which have a lower affinity for ω-agatoxin IVA (Randall et al. 1995). Generally, it is thought that P- and Q-type channels are either splice variants of the same gene (Bourinet et al. 1999) or different configurations of subunits (Richards et al. 2007), and these channels are usually denoted P/Q-type. Finally, an R-type current, for "residual" or "resistant", was isolated, and showed neither DHP nor peptide sensitivity (Randall et al. 1995). However, SNX-482 is now available to block this current (Newcomb et al. 1998; Giessel et al. 2011; Myoga et al. 2011) The variation in Ca^{2+} channel α_1-subunits, which is compounded by splice

variants and auxiliary subunit composition, reflects the diverse biological processes which Ca^{2+} channels underlie (Turner et al. 1995; Catterall 2011).

The main pharmacological features of Ca^{2+} channels are determined by the pore-forming α1 subunit of 190 kDa (Figure 1.1). To date, ten genes encoding distinct Ca^{2+} channel α1 subunits have been identified and almost all of these of these has been characterised by expression in mammalian cells or *Xenopus* oocytes. The pore subunit is associated with several auxiliary subunits, which have functions in trafficking, protein folding and promoting exit from the endoplasmic reticulum (ER), further discussed below in section 1.2.2 (Dolphin 2009). The nomenclature of Ca^{2+} channels has changed several times to reflect pharmacological, molecular, and genetic naming schemes, but was summarised in the compendium by Catterall *et al.*, in 2005, with the designation of the α1 subunit as Ca_vX.X becoming the accepted classification (Catterall et al. 2005). Table 1.1 outlines all known Ca^{2+} channel α1 subunits, their nomenclature (Ertel et al. 2000; Catterall et al. 2005), localisation and functions.

Table 1.1: Calcium channel α₁-subunit nomenclature

$α_1$ code	Ca^{2+} channel name	Current type	Gene	Specific blocker	Main localisation	Function
$α_{1S}$	Ca_v1.1	L	CACNA1S	DHPs	Skeletal muscle	Excitation-contraction, Ca^{2+} homeostasis, gene regulation
$α_{1C}$	Ca_v1.2	L	CACNA1C	DHPs	Cardiac muscle, endocrine cells,	Excitation-contraction, hormone secretion, gene

					neurons	regulation
α_{1D}	$Ca_v1.3$	L	CACNA1D	DHPs	Endocrine cells, neurons	Hormone secretion, gene regulation
α_{1F}	$Ca_v1.4$	L	CACNA1F	DHPs	Retina	Tonic neurotransmitter release
α_{1A}	$Ca_v2.1$	P/Q	CACNA1A	ω-aga	Nerve terminals, dendrites	Neurotransmitter release
α_{1B}	$Ca_v2.2$	N	CACNA1B	ω-ctx	Nerve terminals, dendrites	Neurotransmitter release
α_{1E}	$Ca_v2.3$	R	CACNA1E	SNX-482	Nerve terminals, dendrites, cell bodies	Neurotransmitter release
α_{1G}	$Ca_v3.1$	T	CACNA1G	None	Cardiac and skeletal muscle, neurons	Pace-making and repetitive firing
α_{1H}	$Ca_v3.2$	T	CACNA1H	None	Cardiac muscle, neurons	Pace-making and repetitive firing
α_{1I}	$Ca_v3.3$	T	CACNA1I	None	Neurons	Pace-making and repetitive firing

Ca^{2+} channels share little amino acid sequence between the different channel families. Typically, there is less than 40% amino acid sequence identity between channels in the Ca_v1 and Ca_v2 families, and less than 25% with Ca_v3 channels, suggesting that channels diverged early in evolutionary development (Stea et al. 1995). Within each family however, there is more than 70% amino acid sequence symmetry (Catterall 2000).

Like other voltage-gated ion channels, S5 and S6 and the membrane-associated S5-S6 linker form the channel pore (Catterall 2000). The narrow external pore is lined by the pore loop, which contains a pair of glutamate residues which are required for Ca^{2+} selectivity (Yang et al. 1993). Meanwhile, the inner pore is lined by the S6 segments, where the receptor sites for several Ca^{2+} channel antagonists are located (Catterall 2000). Other antagonists bind elsewhere, such as ω-agatoxin IVA (ω-aga) that binds to the S3-S4 linker (Adams 2004; Winterfield et al. 2000).

Ca^{2+} channels have been shown to inactivate after activation by depolarisation [apart from P-type channels which are non-inactivating (Llinás et al. 1989; Schorge et al. 2011)] by a little known mechanism which is voltage- and Ca^{2+}-dependent (Eckert et al. 1984; Dolphin 2006). The structural basis of this inactivation is poorly defined, but may be linked to the EF-hand in the intracellular c-terminus of the channels (Chang et al. 2007)

1.2.2. Ca^{2+} channel auxiliary subunits

The α_1 pore-forming subunits of VGCCs are associated with several auxiliary subunits, which recently have been shown to play diverse roles unrelated to voltage-gated Ca^{2+} entry (Figure 1.1, (Dolphin 2009). To date, four mammalian genes for β-subunits, and four for $\alpha_2\delta$-subunits have been identified, although due to alternative splicing, the potential complexity of complete Ca^{2+} channels is huge (Ellis et al. 1988; Castellano et al. 1993b, 1993a; B. Gao et al. 2000; Qin et al. 2002; Klugbauer et al. 2003).

The intracellular β-subunit of 55 kDa (Figure 1.1, (Takahashi et al. 1987)), contains four α-helices, but no transmembrane segment (Ruth et al. 1989), and interacts with the α_1-

subunit via high affinity binding to the alpha interaction domain (AID) located in the intracellular I-II linker of the α_1-subunit (Pragnell et al. 1994; Dolphin 2003; Richards et al. 2004; Buraei et al. 2010). Another interaction site has been located on the C-terminal region of the α_1-subunit (Walker et al. 1998). The β-subunit aids trafficking and anchoring and hence increases membrane expression of the α_1-subunit (Brice et al. 1997). Different variants can act to augment the physical properties of the α_1-subunit by shifting the activation to more hyperpolarised voltages, and increasing the channel opening probability which increases the current density (Dolphin 2003).

The α_2- and δ-subunits are encoded by the same genes, CACNA2D1-4, and the two subunits arise from post-translational cleavage (Figure 1.1, (De Jongh et al. 1990; Jay et al. 1991). The α_2-subunit is an extracellular membrane protein attached via disulphide links to the δ-subunit, which has a transmembrane segment and is consequently membrane bound (Gurnett et al. 1996). Of the four genes which code for $\alpha_2\delta$-subunits, $\alpha_2\delta$-2 and $\alpha_2\delta$-3 are highly expressed in neurons (Witcher et al. 1993; Liu et al. 1996; Barclay et al. 2001; Arikkath et al. 2003; Cantí et al. 2003; Klugbauer et al. 2003). Although the coexpression of $\alpha_2\delta$-subunits with α_1-subunits has much smaller functional effects than the β-subunits (Hofmann et al. 1994; Hosey et al. 1996), trafficking and the density of Ca^{2+} channels at the membrane is increased (Felix et al. 1997; Gao et al. 2000; Davies et al. 2006). It is thought that the $\alpha_2\delta$-subunit interacts with the pore-forming subunit at regions in the extracellular side of domain III (Cantí et al. 2005; Felix et al. 1997).

Eight genes have been found encoding γ-subunits, but thus far the γ-subunit has been found exclusively in skeletal muscle Ca^{2+} channel complexes, and its role in regulating

Ca^{2+} channels is poorly understood (Freise et al. 2000; Tomita et al. 2003). Early

experiments uncovered a novel γ-like subunit as the target of the *stargazer* mutation in

mice (Letts et al. 1998). This subunit was shown to be capable of modulating the

voltage dependence of heterologously expressed α$_1$A channels (Chu et al. 2001; Moss et

al. 2002). However, more recent work indicates that most γ-subunits may function as

trafficking regulators of AMPA receptors (Tomita et al. 2003; Jackson et al. 2011).

1.3. The P/Q-type Ca^{2+} channel

The family of Ca_v2 channels (P/Q-, N- and R-type) are often described as the neuronal channels for their predominantly neuronal expression and their key role in supporting Ca^{2+} dependent neurotransmission at synaptic terminals. In particular, P/Q-type channels are dominant in small central synapses like those of the hippocampus (Cao et al. 2004). The importance of P/Q channels for normal functioning of the nervous system is indicated by the large number of channelopathies (diseases related to ion channels) due to mutations located in the CACNA1A gene. The CACNA1A gene maps to chromosome 19p13.1 (Diriong et al. 1995; Jodice et al. 1997), and the mRNA is widely expressed in mammalian cortex, hippocampus and especially the cerebellum (Volsen et al. 1995). The channel itself (figure 1.1) was found to consist of α_1 -, β- and $\alpha_2\delta$- subunits via immunoprecipitation and purification studies (Liu et al. 1996).

P- and Q-type channels can be distinguished by their affinity for ω-aga [Q-type have a lower affinity for the toxin (Wheeler et al. 1996; Bucurenciu et al. 2010)], their distribution [P-type channels are by definition only located in Purkinje cells of the cerebellum (Hillman et al. 1991)], and by their inactivation properties [classic P-type channels do not inactivate (Hillman et al. 1991; Sather et al. 1993; Stea et al. 1994; Soong et al. 2002; Dolphin 2006)].

Like other Ca^{2+} channels, the voltage sensor of the P/Q-type Ca^{2+} channel is located in the S4 transmembrane segment of each domain, and contains a motif of the positively charged amino acids lysine and arginine. Two mutations used in this thesis are located

in the voltage sensor of domain I. Both of these mutations give rise to a severe form of migraine, familial hemiplegic migraine type 1 (FHM1) (Pietrobon 2007). The first mutation, S218L, is a substitution of a serine (S) for a leucine (L) at the 218th amino acid position (Ophoff et al. 1996; van den Maagdenberg et al. 2010)and the second mutation, R192Q, results in the exchange of an arginine (R) in the first S4 segment for a glutamine (Q) at position 192 (Ophoff et al. 1996; van den Maagdenberg et al. 2004). The clinical and electrophysiological data for these mutations are discussed in detail in section 1.6.9.

1.3.1. Alternative splicing of the P/Q-type Ca^{2+} channel

As with other genes encoding for Ca^{2+} channels, the CACNA1A gene is subject to alternative splicing, resulting in the expression of several structurally and functionally diverse α_1-subunit proteins (Tsunemi et al. 2002; Lipscombe 2005). Seven loci in the gene have been observed to undergo alternative splicing (Ophoff et al. 1996; Hans et al. 1999; Bourinet et al. 1999; Krovetz et al. 2000; Kanumilli et al. 2006) and the variants are differentially distributed throughout the brain (Soong et al. 2002). Alongside differences in auxiliary subunit composition, alternatively spliced protein subunits could contribute to variation in Ca^{2+} regulation of neurotransmitter release.

1.3.2. Distribution and regulation of the P/Q-type Ca^{2+} channel

P/Q-type channels are most highly expressed in Purkinje cells of the cerebellum, predominantly in their P-type form (Schorge et al. 2011). Elsewhere in the central nervous system, P/Q-type channels predominate in presynaptic boutons where they trigger neurotransmitter release (Dolphin 2009; Catterall 2011) most likely expressed in the dominant Q-type form (Wheeler et al. 1994; Bucurenciu et al. 2010). N-type

channels are also distributed throughout the central nervous system, although they are thought to predominate more in the periphery (Liu et al. 2003).
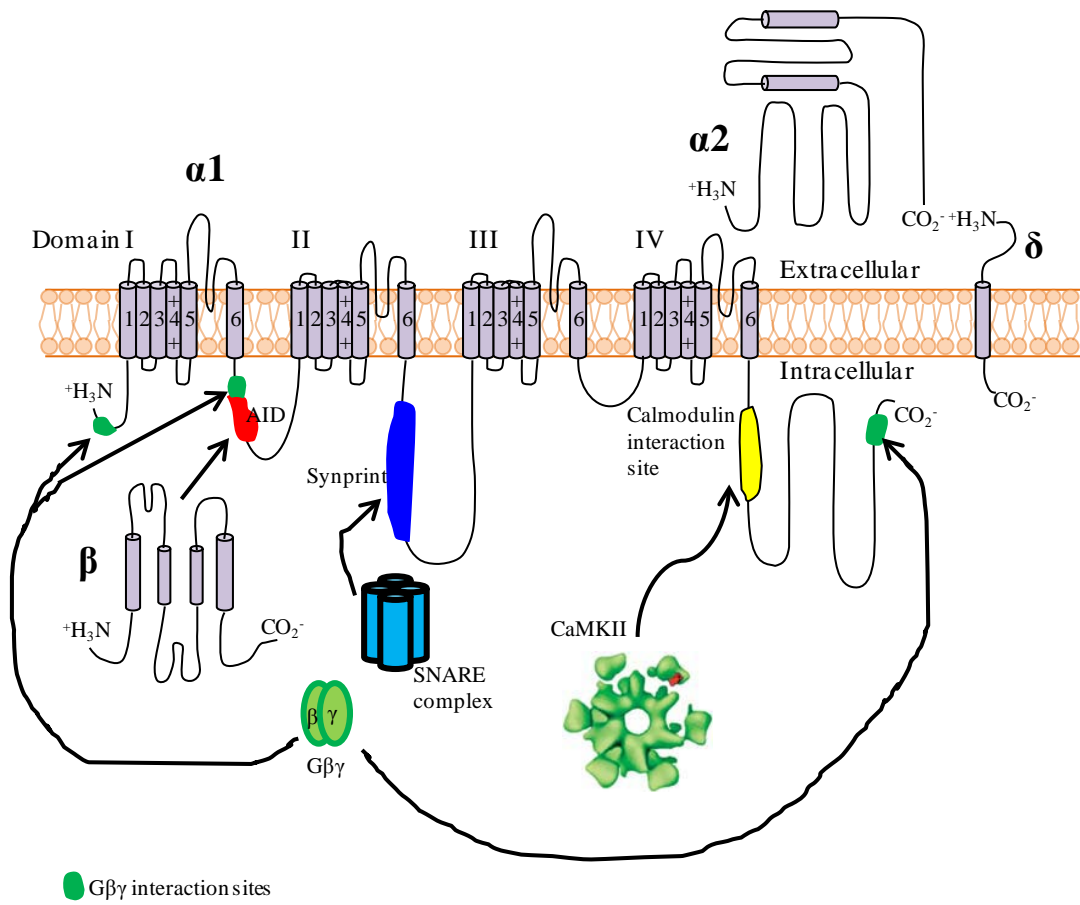
Figure 1.3: Binding sites of regulatory molecules on the P/Q-type VGCC. *A large number of molecules bind to and modify the properties of P/Q-type VGCCs. Binding sites tend to congregate on the intracellular domain linkers.* ***Adapted from (Catterall 2011).***

As the main Ca^{2+} channel subtype regulating neurotransmitter release in central synapses, P/Q- (and N-type) Ca^{2+} channels are the targets of extensive regulation by a large variety of mechanisms (figure 1.3) (Evans et al. 2006). Both types of channel undergo modulation by a number of molecular cascades, the main ones of which are summarised:

1. Synaptic protein interaction at the synaptic protein-interaction site ("synprint") (Catterall 1999). P/Q- and N-type Ca^{2+} channels contain a synprint region in the intracellular domain that links domains II and III, which binds synaptic proteins such as syntaxin 1, synaptosome-associated protein of 25 kDa (SNAP-25), cysteine string protein (CSP), Rim and synaptotagmin 1 (figure 1.3, blue) (Spafford et al. 2003; Zhong et al. 1999). In addition to linking Ca^{2+} channels to the vesicle release machinery in presynaptic terminals (discussed below), binding of syntaxin-1A and SNAP-25 to the synprint region regulates channel function by shifting potential at which channels inactivate, and therefore reducing channel activity (Bergsman et al. 2000; Stanley 2003; Verderio et al. 2004; Catterall et al. 2008).

2. G-protein coupled receptor activation (GPCRs, figure 1.3 green, (Zamponi 2001; Strock et al. 2004). G-protein coupled receptors (GPCRs) negatively regulate Ca^{2+} channels, but to different extents: N-type Ca^{2+} channel are much more susceptible to regulation than P/Q-type (Arnot et al. 2000; Zamponi 2001; Strock et al. 2004). Activation of a GPCR produces two molecules Gα-GTP and the Gβγ dimer, and it is Gβγ dimer that drives a signalling mechanism that terminates Ca^{2+} influx and hence inhibits neurotransmitter release (Ikeda 1996; De Waard et al. 2005), although the Gα-GTP does play a role in channel regulation (Kammermeier et al. 2000). There are a variety of binding sites for Gβγ on the intracellular side of Ca^{2+} channels (figure 1.3)

3. Ca^{2+}-binding proteins such as calmodulin (CaM) and protein kinase C (PKC) have the ability to regulate activity of Ca^{2+} channels (figure 1.3, yellow) (Halling et al. 2005; Evans et al. 2006; Catterall 2000). This modulation affects the ability of the

channel to open, close and inactive, and hence provides tight regulation of Ca^{2+} entry into the synapse (Catterall 2000; Evans et al. 2006; Catterall et al. 2008). It is well known that inactivation of L-type Ca^{2+} currents can occur by global Ca^{2+} influx promoting Ca^{2+} binding to calmodulin which is pre-associated with the channel (Soldatov 2003). P/Q- and N-type channels also contain calmodulin-interaction sites so it is possible that this method of interaction also occurs at these Ca^{2+} channel subtypes (Liang et al. 2003; Lee et al. 1999). Conversely, P/Q-type channels also exhibit a form of Ca^{2+}/calmodulin facilitation, a phenomenon which seems unique to P/Q-type channels (DeMaria et al. 2001). Ca^{2+} influx from an individual channel is enough to promote Ca^{2+}/calmodulin-dependent facilitation, and the splicing of the P/Q-type channel is important (Chaudhuri et al. 2004, 2005).

In addition, the modulation of Ca^{2+} channels can be regulated by the β-subunit, and there is evidence to suggest that the subtype of β-subunit drives the regulation of Ca^{2+} currents by second messengers (Viard et al. 2004; Finlin et al. 2000; Evans et al. 2006). Indeed, Ca^{2+} channel regulation by second messengers at central synapses is a hugely complex web of processes, which cannot be fully understood as a series of individual protein interactions. This is particularly true with Ca^{2+} dependent vesicular release, which although dependent on Ca^{2+} channels, by definition involves multiple proteins. Thus synaptic transmission can only be understood by looking at the interaction of multiple proteins.

1.4. Synaptic transmission

Synaptic transmission forms the basis of information transfer in the brain, and hence has been of interest since the time of the classical Greeks (López-Muñoz et al. 2009). The majority of the initial characterisation of neurotransmitter release was performed by Bernard Katz and colleagues, for which he won the Nobel prize in physiology or medicine in 1970 (Katz 1971). Katz built on work by Henry Dale (Dale et al. 1936) which showed that the motor nerve impulse was not simply passed on by continuous electrical excitation, but required a chemical mediator, in this case acetylcholine. It was further known that when acetylcholine was bath applied to muscle fibres, ionic channels opened allowing a current flow and a subsequent local depolarisation (Takeuchi et al. 1960). Katz and his colleague Paul Fatt observed the same local depolarisations on application of acetylcholine at the end-plate regions of motor nerves via intracellular recordings. In addition, they noticed in the absence of any stimulation, randomly occurring, discrete miniature end-plate potentials (Fatt et al. 1952). These miniature end-plate potentials were correlated with the fusion (and subsequent release of neurotransmitter) of synaptic vesicles with the synaptic membrane (De Robertis et al. 1954). Interestingly, miniature release has been shown at many, if not all synapses, posing the possibility that miniature release has a physiological function, rather than being just a phenomenon related to the probability of vesicular release at a synapse.

Further experiments performed by Katz and Ricardo Miledi determined that extracellular Ca^{2+} was necessary for effective neurotransmitter release (Katz and Miledi 1969b, 1969a; Katz et al. 1970). Synapses can be grouped into two types: electrical and chemical. Chemical synapses are much more diverse and widely studied, compared to electrical synapses.

1.4.1. Chemical synapses

Chemical synapses make up the majority of synapses in the adult brain, and play an intimate role in information processing. When an AP invades a synaptic bouton, VGCCs open, leading to a brief but relatively large rise in intra-terminal Ca^{2+} concentration. Ca^{2+} sensors located in the vicinity of the VGCCs respond to the increased Ca^{2+}, and trigger a cascade of fusion events which result in neurotransmitter-filled vesicles fusing with the synaptic membrane, and releasing their neurotransmitter via exocytosis (Katz 1971). Neurotransmitter diffuses across the synaptic cleft, where it is sensed by receptors, which open allowing ions to flow into the post-synaptic cell, producing a post-synaptic current. If this current is depolarizing and sufficiently large, it may trigger an AP in the post-synaptic neuron. After exocytosis, vesicles undergo endocytosis, recycle and refill with neurotransmitter for a new round of exocytosis (Südhof 2004). Synaptic transmission is "reliably unreliable" at central synapses, as only 10% - 20% of APs trigger release (Goda and Südhof 1997).

A number of vertebrate model synapses have been used to study synaptic function (figure 1.4) (Schneggenburger et al. 2006), including amongst others: the neuromuscular junction (Katz and Miledi 1969a); calyx of Held (Schneggenburger et al. 2006); chromaffin cells (Neher et al. 1982; O'Connor et al. 2007); hippocampal mossy fibre terminals (Geiger et al. 2000); chick ciliary ganglion (Stanley et al. 1991; Brain et al. 1995); retinal biopolar cells(Neves et al. 2001; Jockusch et al. 2005); synaptosomal preparations (Nicholls et al. 1986); and small central synapses such as those of the hippocampus (Branco et al. 2008).

Of these preparations, the hippocampal mossy fibre terminal (figure 1.4a), retinal bipolar cell (figure 1.4b), and calyx of Held (figure 1.4c), have all come to prominence as fast glutamateric synapses in the mammalian central nervous system which are large enough to allow direct presynaptic patch-clamp recordings (Geiger et al. 2000; Schneggenburger et al. 2006; Forsythe 1994; Palmer 2010). This method allows the voltage of the presynaptic membrane to be controlled and manipulated. Small central synapses although more prevalent in the brain, are less easily manipulated: being on average an order of magnitude smaller than the large synapses, it is practically impossible to patch-clamp small synapses such as those found in the hippocampus (figure 1.4d). Therefore studies of transmission at small CNS synapses have lagged behind those at other, larger synapses. However, as small CNS synapses predominate throughout the mammalian brain, it is important to determine the mechanisms underlying synaptic transmission at these synapses as well as at the larger, more accessible synapses. Because patch-clamp is not typically possible, small CNS synapses have been investigated by alternative methods, such as electron microscopy and fluorescence imaging, although there is a large difference in the type of information gained from these methods.
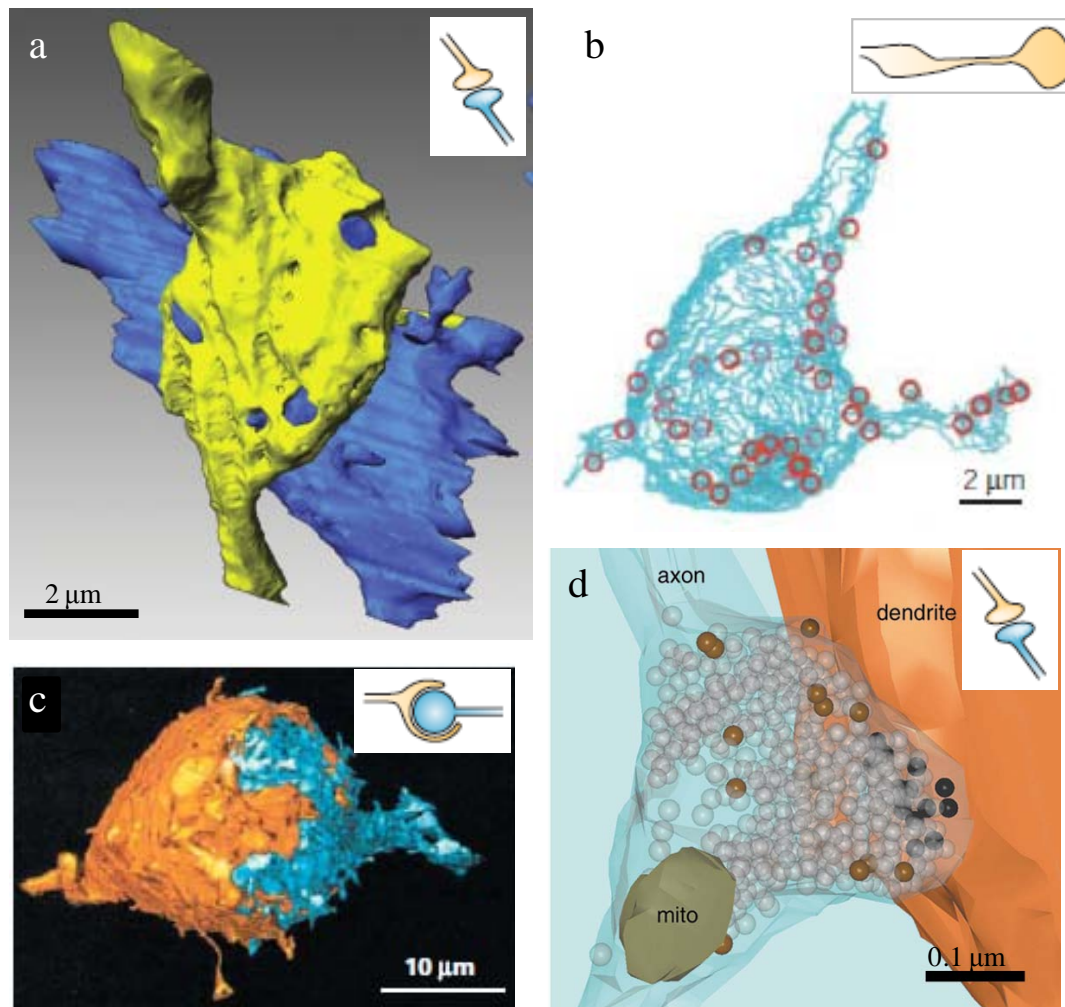
Figure 1.4: Typical vertebrate CNS synapses used to study synaptic transmission, (adapted from (Rizzoli and Betz 2005)). (a) Three-dimensional reconstruction of an adult mossy fibre bouton, depicting the presynaptic bouton (yellow), and the corresponding postsynaptic target dendrite (blue). Inset: schematic of the synapse, showing pre- (yellow) and postsynapse (blue). Adapted from (Rollenhagen et al. 2010). *(b) Dissociated goldfish retinal bipolar cell nerve terminal reconstruction indicating AZs (red circles). Inset: schematic of the presynapse. Adapted from* (von Gersdorff et al. 1996) *(c) Reconstruction of a rat calyx of Held, showing pre- (orange) and postsynapse (blue). Inset: schematic of the calyx of Held. Adapted from* (Sätzler et al. 2002). *(d) Rat hippocampal bouton reconstruction. Inset: schematic of the synapse, showing pre- (yellow) and postsynapse (blue). Adapted from* (Schikorski et al. 2001). *Note the*

*different scale bars used for the large (**a-c**) and small (**d**) synapses. For comparison, the tips of patch pipettes are typically 1-3 μm in diameter.*

1.4.2. The synaptic vesicle cycle
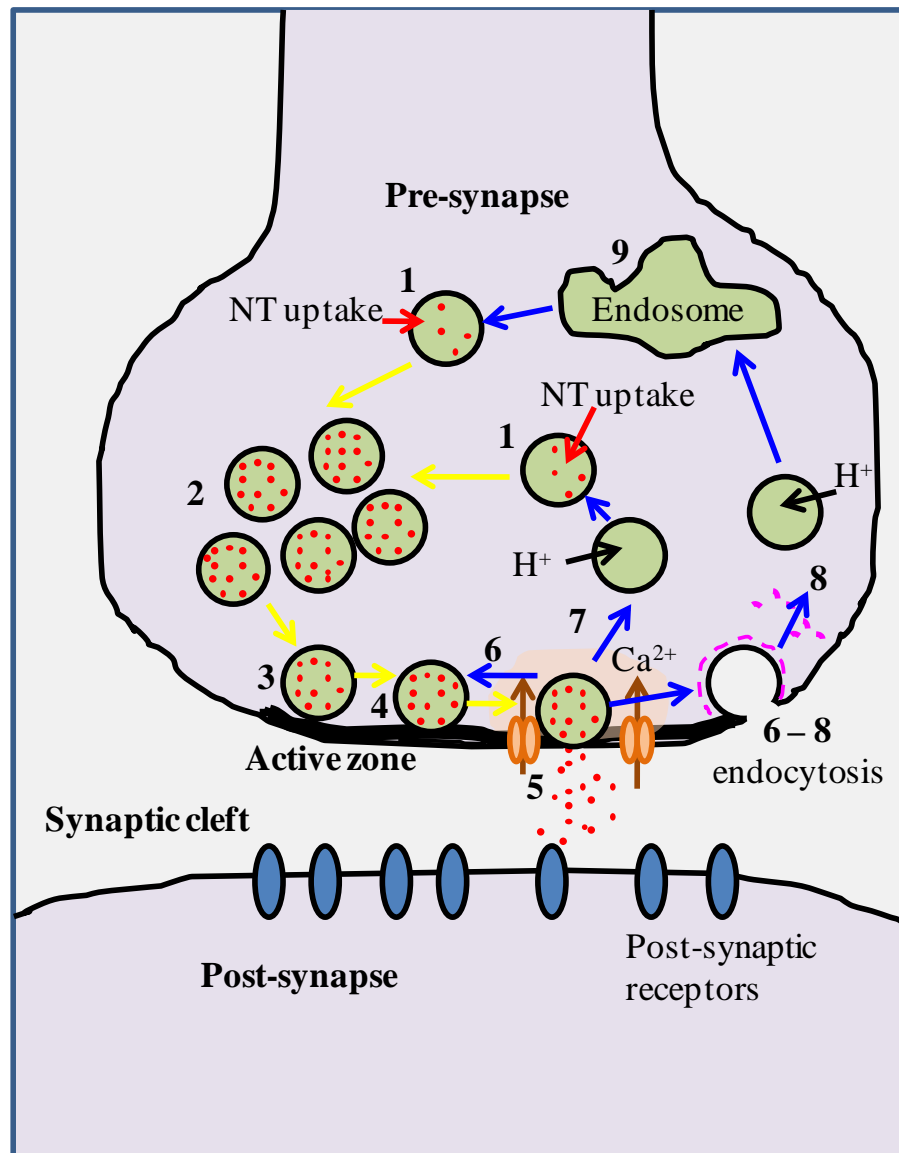
Figure 1.5: The synaptic vesicle cycle, (adapted from (Südhof 2004)) (1) *Synaptic vesicles (green circles) are filled with neurotransmitter (red particles) by active transport.* ***(2)*** *Vesicles cluster close to the active zone, ready for use.* ***(3)*** *Several vesicles dock at the active zone (possibly bringing them into the vicinity of* Ca^{2+}

*channels), where they undergo priming to make them fusion competent (**4**).*

Depolarisation of the synaptic plasma membrane activates voltage-gated Ca^{2+} channels

(orange), allowing influx of Ca^{2+} which triggers vesicle fusion and neurotransmitter

*release (**5**). The neurotransmitter diffuses across the synaptic cleft, and can activate*

post-synaptic receptors. After fusion pore opening, vesicles undergo endocytosis,

*although the method of retrieval is debated at small central synapses (**6 – 8**, see text for*

*more detail). The three debated cycles are shown as: (**6**) Local reuse, or kiss-and-stay,*

*(**7**) fast recycling with via kiss-and-run, and (**8**) classical full-fusion followed by*

*clathrin-mediated endocytosis (in pink), with recycling via endosomes (**9**). Yellow*

arrows: exocytosis processes, blue arrows: endocytosis processes.

A synapse has two components, the presynaptic terminal, or bouton, and the postsynaptic density, separated by a synaptic cleft, roughly 16 nm across [(Südhof 1995); Figure 1.5]. At the presynaptic bouton, functions are focussed on synaptic vesicles (Südhof 2004). In order to release neurotransmitter, synaptic vesicles undergo a cycling process, which can be broken down into several stages [figure 1.5, (Südhof 2004)].

Vesicles are loaded with neurotransmitter via active transport (stage 1, figure 1.5). Vacuolar-type proton pumps (ATPases) within the vesicle membrane transport H^+ to generate an electrochemical gradient, which forces neurotransmitter uptake via neurotransmitter transporters (Ahnert-Hilger et al. 2003), although the extracellular Cl^- concentration is also imperative for fast and full neurotransmitter uptake (Schenck et al. 2009; Xie et al. 1989)

Synaptic vesicles cluster at the active zone (stage 2, figure 1.5), an electron-dense region located directly opposite the postsynaptic density. Several vesicles dock at the active zone [stage 3, figure 1.5 (Rettig et al. 2002)]. This process involves syntaxin, and probably positions docked vesicles in the vicinity of presynaptic Ca^{2+} channels (Bennett et al. 1992). At hippocampal synapses, 8 – 10 vesicles are typically docked (Schikorski et al. 2001; Xu-Friedman et al. 2001). Once docked, vesicles are primed for release (stage 4, figure 1.5) to ensure they are in the correct state for Ca^{2+}-triggered fusion-pore opening [stage 5, figure 1.5 (Südhof 2004)].

After fusion-pore opening and release of neurotransmitter into the synaptic cleft, synaptic vesicles undergo endocytosis, a process which has been proposed to follow a number of mechanisms: (i) vesicles re-acidify and refill with neurotransmitter without undocking (stage 6, "kiss-and-stay" (van Kempen et al. 2011) (ii) a fast mode called 'kiss-and-run' (K&R) in which a transient pore forms between the vesicle and the synaptic membrane, releasing neurotransmitter, before the vesicle pinches off and recycles locally without losing its integrity [stage 7; (Ceccarelli et al. 1973; Klingauf et al., 1998b; Aravanis 2003; Richards et al., 2005a; Harata 2006)] or (iii) classical endocytosis where vesicles recycle via clathrin-coated pits (stage 8) and either refill immediately or pass via an endosomal intermediate (stage 9) (Heuser et al. 1973; Südhof 2004).

1.4.3. *Synaptic protein interactions underpin the synaptic vesicle cycle*

The synaptic vesicle cycle and subsequent neurotransmitter release is underpinned by a complex series of protein-protein interactions (Südhof 1995). Docking of vesicles at the active zone depends on the formation of SNARE (Soluble NSF Attachment Protein

REceptor) complexes. The formation of the SNARE complex brings the vesicle and synaptic plasma membrane into contact, and triggering via Ca^{2+} influx forces the two membranes to fuse (figure 1.6) (Südhof et al. 2009; Bajjalieh et al. 1995; Sollner et al. 1993; Südhof 1995, 2004).
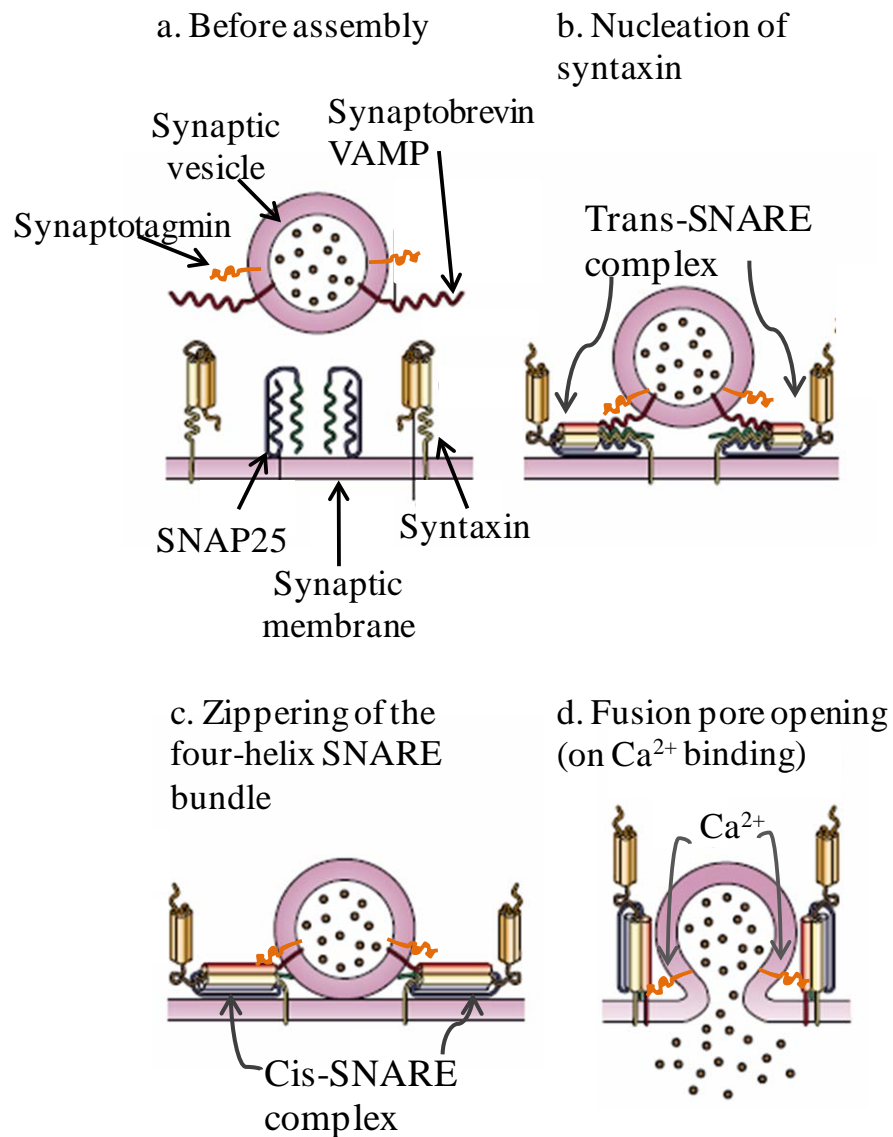
Figure 1.6: SNARE protein assembly. (a) Before assembly, syntaxin is in a closed conformational state and the proteins cannot bind. (b) Upon nucleation of syntaxin, zippering of the four-helix bundle occurs (c), bringing the vesicle and plasma

membranes together. (d) Membrane fusion may occur on binding of Ca^{2+} to synaptotagmin. **Adapted from (Rizo et al. 2002).**

The SNARE complex comprises of three membrane proteins (Sollner et al. 1993): syntaxin-1 and SNAP-25 extending from the presynaptic membrane (t-SNAREs), and VAMP (vesicle associated membrane protein or synaptobrevin) located on the vesicle membrane (v-SNAREs) (figure 1.6a) (Poirier et al. 1998; Bennett et al. 1992; Inoue et al. 1992; Oyler et al. 1989; Trimble et al. 1988; Südhof et al. 1989). These three proteins (and their homologs) are at the heart of membrane fusion, and are assumed, in the SNARE hypothesis, to be universal (Sollner et al. 1993; Südhof et al. 2009), although neurons do have other SNAREs.

Individually, SNARE proteins are unfolded and unstructured (Fasshauer et al. 1998; Dulubova et al. 1999), but spontaneously assemble via the formation of a stable, coiled coil four-helix bundle, comprised of two helices from SNAP-25 and one each from VAMP and syntaxin 1 (figure 1.6b, c)(Poirier et al. 1998; Hayashi et al. 1994; Sutton et al. 1998). Within this four-helix bundle, there are four classes of SNARE motif: the R- (corresponding to the v-SNARE) and Qa-, Qb- and Qc-SNARE motifs corresponding to the three types of t-SNAREs (Kloepper et al. 2007). The R/Q rule (Sutton et al. 1998; Kloepper et al. 2007) states that a SNARE complex has to contain one of each of the motifs. Syntaxin exists in a closed conformational state (figure 1.6a). Upon nucleation of syntaxin, the SNARE proteins are free to bind together (Rizo et al. 2002), and zipper up towards the carboxyl terminus (figure 1.6b, c).

When the SNARE complex forms between the synaptic and vesicle membrane, hemi-fusion may be catalysed by the trans-SNARE complex, which forces the membranes close together via a zipping up action (Hanson et al. 1997; Weber et al. 1998). The docked and primed stage of the vesicle cycle could be representative of a partial zippering up of the trans-SNARE complex (Reim et al. 2001; Maximov et al. 2009), which is held in an active but frozen state until release via Ca^{2+} triggering. The protein complexin (Rizo et al. 2008) acts as a grappling protein holding the SNARE complex in this state. When Ca^{2+} enters the terminal, it binds to the evoked-release Ca^{2+} sensor synaptotagmin, which releases complexin, allowing the trans-SNARE complex to fully zipper into the cis-SNARE configuration, forcing the adjacent membranes together to form a fusion pore, through which neurotransmitter escapes (figure 1.6d). (Geppert et al. 1994; Fernández-Chacón et al. 2001; Rizo et al. 2008; Südhof et al. 2009).

Synaptotagmin is a vesicle protein which can bind SNARE proteins (Bennett et al. 1992; Li et al. 1995; Chapman et al. 1995), and contains two protein kinase C-like C_2 domains, which can bind Ca^{2+} (Perin et al. 1990; Brose et al. 1992). It has been shown in mice that synaptotagmin is required for fast, synchronous release, but not for vesicle fusion *per se* (Geppert et al. 1994). When the Ca^{2+} binding affinity of synaptotagmin was lowered, a corresponding reduction in Ca^{2+} sensitivity of fusion was observed, supporting the hypothesis that synaptotagmin serves as the dominant Ca^{2+} sensor for membrane fusion and hence neurotransmission (Fernández-Chacón et al. 2001; Pang, Shin, et al. 2006).

A huge variety of other synaptic proteins play a role in synaptic neurotransmission. Over a thousand proteins populate the presynaptic terminal and hundreds are involved

in vesicular exocytosis (Südhof 2004), forming an exceptionally complex network of interactions.

1.4.4. Do vesicles kiss?

Although ample evidence shows K&R can occur at a number of different synapses (endocrine cells (Alés et al. 1999); calyx of Held (Wu et al. 2005); mast cells (Zimmerberg et al. 1987); bipolar cells (von Gersdorff et al. 1994), it is still controversial whether K&R takes place at small central synapses. Below is a summary of the history of the K&R hypothesis, and two sections highlighting experiments that support and refute the possibility of K&R.

1.4.4.1.   History of vesicle fusion studies and the Kiss and Run hypothesis

Full collapse fusion was first described by Heuser and Reese in 1973 in the frog neuromuscular junction (NMJ) using electron microscopy techniques (Heuser et al. 1973). To study the effects of prolonged stimulation on the nerve terminals, preparations were stimulated in the presence of extracellular markers (horseradish peroxidise), fixed and examined with electron microscopy. Using this method synaptic vesicles were observed to fuse completely with the synaptic membrane and to flatten, releasing their neurotransmitter, followed by slow retrieval of the membrane by clathrin-coated pits (Heuser et al. 1973; Keen et al. 1979), uncoating and recycling via endosomal compartments (Pfeffer et al. 1985; Takei et al. 1996). Since then, full-fusion has been demonstrated at various central nervous system synapses (Sankaranarayanan et al. 2000; Z. Li et al. 2005; Sankaranarayanan et al. 2001; Klyachko et al. 2002; Zenisek et al. 2002; Aravanis 2003; Gandhi et al. 2003; Richards et al., 2005a; Harata 2006).

The idea behind K&R was first proposed from the work of Bruno Ceccarelli also using the NMJ preparation by a combination of EM and end-plate potential measurements (Ceccarelli et al. 1973). However, it was not until 1994 that the term K&R was coined by his colleagues (Fesce et al. 1994). The experiments carried out were similar to those of Heuser and Reese, but Ceccarelli and colleagues came to different conclusions. As they did not observe any stimulation-induced change in the number of vesicles after prolonged stimulation (which would be expected from full fusion collapse), Ceccarelli and colleagues suggested vesicles fuse with the plasma membrane and reform directly from it without a loss of structure (Ceccarelli et al. 1973).

The concept of K&R at small central synapses is appealing because of the potential for fast turnover, less energy consumption and modulated transmitter release amounts, however, evidence is currently conflicting, and so a summary of the current state of the field is included here.

1.4.4.2. Evidence for K&R at small central synapses

Several lines of evidence derived via different techniques have been presented, suggesting the presence of K&R at hippocampal synapses (Gandhi et al. 2003; Aravanis 2003; Richards et al., 2005a; Harata 2006).

Gandhi and Stevens used a pH-sensitive fluorescent tag linked to the synaptic vesicle protein VAMP-2 (synaptopHluorin, (Miesenbock et al. 1998)), (Gandhi et al. 2003). During rest, the fluorescent tag is located on the synaptic vesicle, facing the lumen, which is acidic. Therefore the tag is protonated and the fluorescence is quenched. Upon exocytosis, vesicles lose their protons, which removes the fluorescence quenching, and

the fluorescence increases. Using this tag, Gandhi and Stevens showed that hippocampal vesicles which fused after a single AP could endocytose by one of three methods: a fast K&R mode (< 900 ms); a slower mode possibly representing full fusion (8-21s); and a stranded mode which did not recover over long periods of time.

A second method used FM dyes (a technique which we have used extensively in this thesis, and which is described later, in chapter 6) to minimally load only one vesicle per synapse. In response to APs, some labelled vesicles lost their total quanta of FM dye, suggesting full collapse of the vesicle into the synaptic membrane. However, other labelled vesicles only lost a proportion of their dye, suggesting dye escaping through a fusion pore, followed by rapid endocytosis, trapping the remaining dye (Aravanis 2003). Importantly, the proportion of vesicles undergoing this incomplete dye loss was similar to the proportion of K&R observed by Gandhi and Stevens.

A third method, using bromophenol blue (BPB) to quench fluorescence of FM dye also suggested that kiss-and-run was present at hippocampal synapses (Harata 2006). The motivation behind the use of BPB was as follows: if FM dye loaded vesicles recycled by full fusion collapse, all FM dye would be lost, and the addition of the quencher BPB would have no further effect on fluorescence. If however, vesicles recycled by kiss-and-run, and retained some dye, the addition of BPB would provoke a further decrease in fluorescence. By measuring the time course of FM dye fluorescence decrease in the presence and absence of BPB, Harata and colleagues noted a difference in the fluorescence decay, suggesting that K&R was present (Harata 2006).

1.4.4.3. Evidence against K&R at small central synapses

There is also strong evidence against the idea of K&R occurring at hippocampal synapses. Granseth and colleagues used the same genetic tag as Gandhi and Stevens (synaptopHluorin), but only observed one mode of endocytosis, which could be blocked by clathrin-mediated endocytosis inhibition (Granseth et al. 2006). They found no evidence of a fast mode of retrieval, and could not repeat the observations of Gandhi and Stevens (Gandhi et al. 2003). A compounding factor of synaptopHluorin is that it is also expressed in the plasma membrane, which leads to considerable background fluorescence. There is also evidence to suggest that synaptopHluorin molecules in the plasma membrane are mobile (Sankaranarayanan and Ryan 2000). Granseth and colleagues concluded that the fast component observed by Gandhi and Stevens (Gandhi et al. 2003), was most likely an artefact produced by lateral diffusion in the plasma membrane (Granseth et al. 2006). They repeated their observations with an alternative genetic tag, sypHy (linked to the synaptic vesicle protein synaptophysin). This appeared to be more specific to synaptic vesicles and they observed a slow endocytosis component with a time constant of ~ 15 s.

A second line of study (Balaji et al. 2007) suggested that positive evidence for kiss-and-run can be explained by the stochastic nature of a slower endocytic process. Here another genetic fluorescent tag, targeted to the vesicular glutamate transporter vGlut1, was used, which had a much lower surface expression, improving the signal-to-noise ratio. They observed that endocytosis was well described by a single Poisson process, with a time constant of ~14 s, in close agreement with (Granseth et al. 2006).

A third study carried out early on by Sankaranarayanan and Ryan (Sankaranarayanan and Ryan 2000), showed similar results using pH-sensitive fluorescent tags combined with alkaline trapping, a method which separates exo- and endocytosis. By applying bafilomycin A1 - a V-type ATPase inhibitor – they blocked acidification of recently endocytosed vesicles, trapping them in an alkaline state, and hence blocking the fluorescence from being quenched. By comparing the rate of fluorescence increase with and without bafilomycin, they could determine the rate of endocytosis, and found no evidence for K&R.

1.4.5. *Synaptic vesicle pool configurations*

One aspect which might contribute to the conflicting findings about the occurrence of K&R, is that not all synaptic vesicles, even within an individual pre-synaptic terminal are necessarily equivalent. In hippocampal boutons, synaptic vesicles are thought to be arranged in different pools, and although there is controversy surrounding the nature of these, the widespread view is that there are three distinct pools (figure 1.7): the readily releasable pool (*RRP*), the releasable or recycling pool (RP) and the reserve pool (Rizzoli and Betz 2005).

1.4.5.1.   *RRP*

The RRP contains vesicles which are immediately available for release on Ca^{2+} stimulation, and are assumed to be the docked and primed vesicles (figure 1.7, red vesicles) (Schikorski et al. 2001; Rettig et al. 2002). They lie docked in the active zone, close to voltage-gated Ca^{2+} channels (Heuser et al. 1973; Ceccarelli et al. 1980; Neher et al. 2008). In hippocampal boutons, the RRP comprises of ~ 5 – 20 vesicles, as shown by electron microscopy studies where these vesicles are identified by their position near the

membrane (Schikorski et al. 1997, 2001). The vesicles in the RRP can be released by a brief pulse of high frequency stimulation (Rosenmund et al. 1996; Murthy et al. 1999).
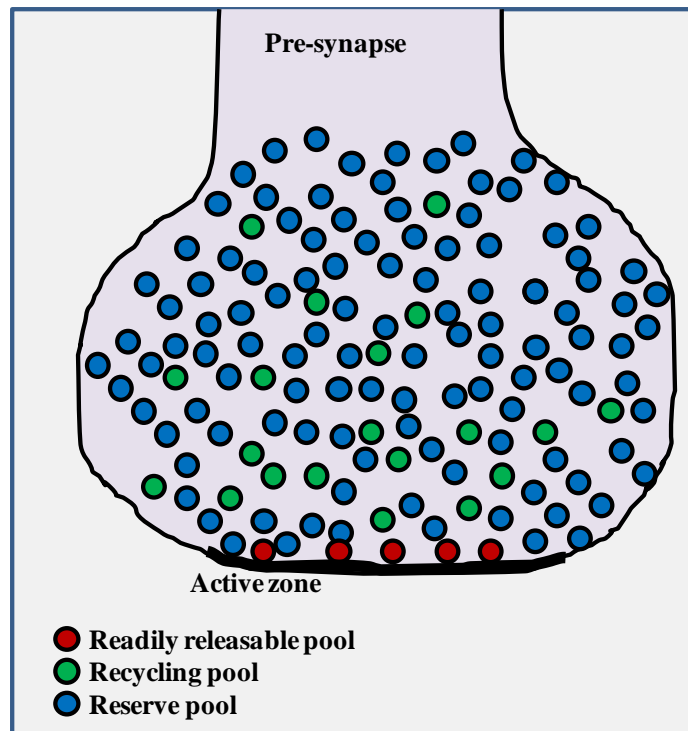
Figure 1.7: Distribution and proportion of vesicle pools in a hippocampal presynaptic terminal. Vesicles are distributed amongst three pools, of which ~ 5% are part of the RRP (in red) which are located close to the active zone, ~20% are in the RP (in green) and the rest in the reserve pool (in blue)

1.4.5.2. RP

RP vesicles maintain continuous synaptic release under moderate physiological stimulation, and this pool is refilled by newly recycled vesicles (figure 1.7, green vesicles) (Richards et al. 2003; Kuromi et al. 2004; Harata et al. 2001; de Lange et al. 2003). In hippocampal synapses, the RP has been visualised using two methods: (i) imaging photoconverted FM 1-43 labelled vesicles with electron microscopy (EM), and

(ii) minimal FM dye labelling to measure the fluorescence of a single vesicle (Harata et al. 2001). It comprises roughly 10-20% of the total number of vesicles, although this value is highly variable between boutons (Harata et al. 2001; Aravanis 2003). A recent study has shown preferential recycling in the RP. By sequentially labelling synaptic vesicles with the spectrally distinct dyes FM 1-43 and FM 5-95 using high- and low-frequency stimulation, the authors showed that vesicles from the RP recycled by low frequency stimulation are preferentially reused ahead of those released at high-frequency stimulation (Vanden Berghe et al. 2006).

1.4.5.3.   *Reserve pool*

Finally, the reserve pool provides vesicles only under intense stimulation, possibly after depletion of the RP (figure 1.7, blue vesicles) (Kuromi et al. 1998; Richards et al. 2000; Richards et al. 2003). Although vesicles are seldom recruited from the reserve pool under physiological conditions, it constitutes 80% - 90% of the total number of vesicles (Schikorski et al. 2001). Although mixed with the recycling pool, vesicles in the reserve pool tend to be located further from the active zone.

Mixing of vesicles between the various pools occurs at a fast rate between the RP and RRP and at a slower rate with the reserve pool. However, it has been shown that vesicles are preferentially recycled to their own pools (Pyle et al., 2000b). The absolute size of the synapse is not static, but has the ability to change under certain conditions, which are linked to activity. For example when synapses were pharmacologically silenced for several days using the AMPA receptor antagonist NBQX or the sodium channel blocker TTX, synaptic strength was increased, and this correlated with an increase in the size of synapse (Murthy et al. 2001). The active zone, post-synaptic

density, bouton and total number of vesicles all increased (Murthy et al. 2001). This sort of change has been designated homeostatic plasticity, and may be a theme in studies of cultured neurons where activity levels can be maintained (Pozo et al. 2010). It is possible that by disrupting Ca^{2+} influx, mutations in P/Q channels could drive homeostatic plasticity, but this has only been studied at the fly NMJ (Frank et al. 2006). This observation prompted our investigation of whether mutations in P/Q-type Ca^{2+} channels - which could detrimentally affect neurotransmitter release - would have an effect on the size of the synaptic vesicle pools. This idea is elaborated in chapter 7.

1.5. Calcium triggering of neurotransmitter release

During this project, we were particularly interested in Ca^{2+} regulation of neurotransmitter release at individual synapses, both using normal and mutant Ca^{2+} channels. The classical view is that when an AP invades a pre-synaptic terminal, the depolarising pulse forces a conformational change in the Ca^{2+} channel voltage sensor (Südhof 2004), which opens the channel, allowing an influx of Ca^{2+} ions into the terminal. In hippocampal synapses, the majority of the current is carried by P/Q- and N-type Ca^{2+} channels, although R-type channels are thought to make a small contribution (Dietrich et al. 2003). The Ca^{2+} influx is rapid and large, but local: concentrations of 5 – 20 µM are obtained (Bollmann et al. 2000; Schneggenburger et al. 2000), at submicromolar distances from the channel (Neher 1998) but only last 400 – 500 µs, due to effective buffering by endogenous buffers (Meinrenken et al. 2002).

This brief Ca^{2+} pulse can effectively trigger neurotransmission, suggesting vesicles are located in the close proximity of the Ca^{2+} channels (Jarvis et al. 2005). Indeed, both P/Q- and N-type cannels are thought to interact physically with the key proteins of the

vesicular release machinery (Stanley 1993; Sabatini et al. 1996; Stanley 1997; Koh et al. 2003; Kaeser et al. 2011; Y. Han et al. 2011). The three proteins of the SNARE complex, Syntaxin 1, SNAP-25, VAMP/synaptobrevin, and synaptotagmin can all bind to the synprint motif on the II-III linker (Figure 1.3). (Bennett et al. 1992; Yoshida et al. 1992; Sheng et al. 1996; Mochida et al. 1996; Sheng 1997; Catterall 1999; Atlas 2001; Jarvis et al. 2001; Jarvis et al. 2002; Spafford et al. 2003). However, immunohistochemical studies from several laboratories have indicated that there is tight association of syntaxin and synaptotagmin with P/Q-type channels (Bennett et al. 1992; Far et al. 1993; Lévêque et al. 1994; O'Connor et al. 1993).

Ca^{2+} influx through voltage-gated channels triggers at least two modes of neurotransmitter release. Fast, synchronous release initiated at about 50 µs after Ca^{2+} influx (Sabatini et al. 1996) and slower, asynchronous release, which extends for about one second after Ca^{2+} influx (Barrett et al. 1972; Geppert et al. 1994; Goda et al. 1994; Atluri et al. 1998). Both are Ca^{2+} dependent but change differently upon repetitive stimulation (Hagler et al. 2001). A third mode of release – spontaneous neurotransmission – also has a large Ca^{2+} dependent component (Xu et al. 2009; Groffen et al. 2010), although a proportion of this sort of release can continue in the absence of extracellular Ca^{2+}.

AP-independent, spontaneous neurotransmitter release may be a ubiquitous feature of synapses. It was first observed by Paul Fatt and Bernard Katz as miniature end-plate potentials (mEPPs) in muscle fibres (Fatt et al. 1952). In neuronal synapses, spontaneous neurotransmission can be observed as miniature post synaptic currents (either excitatory mEPSCs or inhibitory mIPSCs or 'minis') by patch-clamp recordings

from the post-synaptic cell (Simkus and Stricker 2002b, 2002a; González et al. 2011). Once thought to be a phenomenon of the stochastic nature of neurotransmitter release (Katz and Miledi 1969a), recent evidence (summarised below) has shown that minis play an important role in a number of physiological functions, including (1) maintenance of spines (McKinney et al. 1999), (2) dendritic protein synthesis (Sutton et al. 2004), and (3) firing rate in small interneurons (Carter et al. 2002).

1. Miniature release has been implicated in the maintenance of dendritic spines (McKinney et al. 1999). Blocking all vesicular release (with botulinum toxin) to cultures for seven days depleted the density of dendritic spines by 4-fold, whereas inhibition of evoked release alone (by TTX application) had no effect. This suggests that dendritic spine maintenance requires miniature synaptic events, by preventing spine retraction at inactive spine connections (McKinney et al. 1999).

2. A second study suggested that miniature release acutely inhibits dendritic protein synthesis (Sutton et al. 2004) contributing to the rapid changes in synaptic strength that may underlie long-term memory storage (Casadio et al. 1999; Kang et al. 1996; Sherff et al. 1999; Huber et al. 2000; Zhang et al. 2002; Ostroff et al. 2002). Furthermore, the same group showed that spontaneous neurotransmitter release is a specific regulator of postsynaptic sensitivity to neurotransmitters, by suppressing the dendritic protein translation machinery locally and therefore maintaining receptor composition at synapses (Chung et al. 2006; Sutton et al. 2006).

3. Individual quantal release has been shown to be sufficient to shape neuronal firing in small interneurons which have high input resistances and long membrane time

constants (Carter et al. 2002). In particular, the study showed that in small stellate cells, small numbers of coincident excitatory minis were sufficient to reliably evoke firing, making stellate cells well suited to perform rapid synaptic computations. This mini-dependent firing may be important elsewhere in the brain at other small interneurons.

As miniature release has been implicated in a range of physiological functions, it is important to understand the underlying mechanisms behind the origin and regulation of minis. Since the implication of synaptotagmin-1 (Syt1) as the major Ca^{2+} sensor for spontaneous release at murine cortical neurons (Xu et al. 2009), there has been an increased interest in the molecular mechanisms behind miniature release (Groffen et al. 2010; Pang et al. 2011). Although there are a proportion of minis which appear to be truly Ca^{2+}-independent (Erulkar et al. 1978; Malgaroli et al. 1992; Maximov et al. 2007), the majority (~75 %) of miniature release relies on Ca^{2+} influx (Xu et al. 2009; Groffen et al. 2010).

Two Ca^{2+} sensors of spontaneous release have been suggested. Firstly, Syt1 plays a dual role of Ca^{2+} sensor for spontaneous release and acts as a clamp on another alternative Ca^{2+} sensor (Xu et al. 2009). By recording miniature release in WT and syt1 KO synapses, the study revealed that both evoked and spontaneous release were both triggered by Ca^{2+} binding to syt1. However, a large (~ eight times) increase in the mini frequency in both cultures and slices was observed when recording from syt1 KO synapses (Xu et al. 2009). This increase in mini frequency was explained by a second Ca^{2+} sensor which became unclamped and functional in the absence of syt1. This second Ca^{2+} sensor was shown to have a higher apparent Ca^{2+} affinity and a lower Ca^{2+}

cooperatively than syt1, and was suggested to be the sensor which also drives slow, asynchronous release (Sun et al. 2007). A recent study has suggested the synaptotagmin analogue Doc2b as a possibility for the second sensor (Groffen et al. 2010). Doc2b is a soluble protein containing C2 domains similar to syt1, which binds Ca^{2+} with high affinity (Orita et al. 1995; Verhage et al. 1997; Groffen et al. 2006). However, the role of Doc2b as a Ca^{2+} sensor for spontaneous release has been bought into dispute (Pang et al. 2011). By introducing mutant Doc2b proteins lacking Ca^{2+} binding sites into Doc2b knock-out (KO) mice, the group showed that spontaneous release could be fully rescued, suggesting that Ca^{2+} binding to Doc2b was not necessary for spontaneous neurotransmission. These conflicting data on the identity Ca^{2+} sensor for minis suggests that further research is still needed to elucidate the mechanism behind spontaneous neurotransmission.

The implication of synaptotagmin-1 as the Ca^{2+} sensor for spontaneous release as well as evoked release was a surprising result, as it was thought that the Ca^{2+} affinity of synaptotagmin was too low to be activated by resting Ca^{2+} concentrations (Xu et al. 2009; Fernández-Chacón et al. 2001). Indeed, it has been suggested that spontaneous release is not triggered by resting Ca^{2+} in the presynaptic terminal, but by Ca^{2+} sparks from internal stores (Llano et al. 2000; Emptage et al. 2001). In particular, half of spontaneous transmitter release in hippocampal slice cultures is due to spontaneous release of Ca^{2+} from internal stores via ryanodine receptors (Emptage et al. 2001). By blocking Ca^{2+} induced Ca^{2+} release from internal stores with ryanodine, Emptage and colleagues showed that the frequency of spontaneous miniature synaptic events were reduced by around half (Emptage et al. 2001). Local Ca^{2+} transients ("Ca^{2+} sparks") from internal stores have been also observed in hippocampal cultures using the Ca^{2+}

indicator Fluo-3 (Koizumi et al. 1999), providing an origin of Ca^{2+} which could trigger spontaneous release. However, this only accounts for half of all minis, and as the majority ($< 90\%$) (Xu et al. 2009) of spontaneous release is Ca^{2+} dependent, there is possibly another origin of Ca^{2+} triggering minis. This alternate source of Ca^{2+} is currently unknown.

In light of these questions, we have asked: *Could a proportion of miniature release be triggered by Ca^{2+} entry through voltage-gated Ca^{2+} channels, using the same presynaptic release machinery as evoked release?* There is evidence that spontaneous and evoked transmitter release are regulated by shared mechanisms (Malgaroli et al. 1995), and in chapter 8 we aim to elucidate whether miniature release can be regulated via Ca^{2+} entry through voltage-gated Ca^{2+} channels.

1.6. Physiological consequences of mutations in P/Q channels: calcium channelopathies

One challenge of probing how altered voltage-gated Ca^{2+} channels are linked to vesicular release is that these channels are variable *in vivo*, in poorly defined ways. Heterologous expression provides a single channel splice variant, which may or may not co-assemble in the correct stoichiometry with accessory subunits, SNARE protein complexes, Ca^{2+} binding proteins, and G-protein regulatory subunits. Thus manipulating channel activity with heterologously expressed proteins may not provide an accurate measure of what endogenous channels are doing, as the endogenous channels may exist in different variants, at tightly localised anchored 'slots' (Cao et al. 2010), or in specific combinations with SNARES. A promising recent approach to surmounting this problem is to use mice with mutations known to disrupt channel function expressed in the endogenous genes. Because the genes are intact, splicing and expression is expected to be preserved, and because the mutations are associated with clinical dysfunction in humans, they are essentially 'experiments of nature' indicating the amino acid substitutions disrupt channel function in critical ways.

During this project, we were interested in the Ca^{2+} regulation of synaptic neurotransmission at small central synapses, particularly the well-characterised synapses of the hippocampus. We were predominantly interested in the role that P/Q-type Ca^{2+} channels play, as these channels are thought to be major supporters of central neurotransmission, and mutations arising in the α1-subunit coding gene have been implicated in a wide range of neurological channelopathies. It is thought that these mutations de-stabilise synaptic transmission, disrupt Ca^{2+} signalling and lead to neurological disorders such as ataxia and migraine. We studied synaptic

neurotransmission in neurons isolated from mice carrying two mutations in P/Q-type channels (S218L and R192Q) both of which lead to a severe form of migraine called familial hemiplegic migraine type 1 (FHM1) (Ophoff et al. 1996; Pietrobon 2007). We also investigated the effect of P/Q-type channel KO (CACNA1A KO) which is genetically similar to human episodic ataxia type 2 (Kaja et al. 2007). Below is a brief description of the different channelopathies resulting from mutations in P/Q-type Ca^{2+} channels.

1.6.1. Episodic Ataxia type 2

Mutations in P/Q-type Ca^{2+} channels are the origin of episodic ataxia type 2 (EA2) (Ophoff et al. 1996). EA2 presents in the second decade (Kullmann 2002), and manifests as attacks of midline cerebellar disturbance, vertigo, diplopia and nystagmus (Gancher et al. 1986), with asymptomatic periods in between. Although EA2 is most commonly due to nonsense, frame-shift or splice-site mutations (Denier et al. 1999), it can also be caused by missense mutations (Denier et al. 2001), which lead to a loss-of-function associated with the channel. (Guida et al. 2001; Kullmann 2010). In particular, it is thought that EA2 arises from a failure to adequately modify inositol 1,4,5-triphosphate receptor type 1 (ITPR1)-dependent plasticity in Purkinje cells in the cerebellum (Schorge et al. 2010). Mutations leading to EA2 are likely to allow no channel function at all, as truncations almost always encroach on one of the α_1-subunit domains (Kullmann 2002), suggesting that the origin of the EA2 phenotype may be haploinsufficiency (Guida et al. 2001).

If haploinsufficiency leads to EA2 in humans, heterozygous (HET) CACNA1A KO mice provide a model of EA2, although there are differences in phenotype between the

mouse model and the human disease (Fletcher et al. 2001; Jun et al. 1999). CACNA1A+/- mice are not generally overtly ataxic (possible due to being quadrupedal), but do exhibit motor learning deficits (Katoh et al. 2007). We have a colony of CACNA1A KO mice, a kind donation from tha laboratory of Arn van den Maagdenberg (Fletcher et al. 2001; Kaja et al. 2007), and in chapter 7 we examine the effects of the loss of functional P/Q-type Ca^{2+} channels on synaptic transmission.

1.6.2. Spinocerebellar ataxia type 6

Spinocerebellar ataxia type 6 (SCA6) is a relatively pure, slowly progressive cerebellar degeneration, caused by an expansion of a polyglutamine repeat in the intracellular C-terminus of the channel (Zhuchenko et al. 1997). The disease is thought to be due to disregulation of ITPR1 signalling caused by the polyglutamine repeat (Durr 2010), although alterations in the voltage sensitivity of activation or inactivation (Matsuyama et al. 1999; Restituito et al. 2000; Kullmann 2010) as well as differences in surface expression of the channel (Piedras-Renteria et al. 2001) have also been suggested as mechanisms. SCA6 leads to a severe loss of Purkinje cells (Pietrobon 2010).

1.6.3. Epilepsy

A higher (7%) proportion of patients with EA2 have epilepsy than the general public (Rajakulendran et al. 2010; Sander 2003), suggesting that P/Q-type Ca^{2+} disorders may also be linked to human epilepsy (Jouvenceau et al. 2001; Imbrici et al. 2004; Jen et al. 2004; Jen et al. 2007; Haan et al. 2008). However, the underlying mechanisms between mutations in CACNA1A and human epilepsy remain unclear (Chioza et al. 2001; Khosravani et al. 2006).

1.6.4. Lambert Eaton myasthenic syndrome

Although not a disease arising from mutations in P/Q-type channels, Lambert Eaton myasthenic syndrome (LEMS) is an autoimmune disease associated with antibodies that are thought to bind to pre-synaptic P/Q channels at the neuromuscular junction, interfering with neurotransmission and causing muscle weakness (Spillane et al. 2010; Vincent 2010). Although the specific antibody targets are unknown, LEMS may confirm the importance of P/Q-type Ca^{2+} channels in regulating neurotransmission in peripheral as well as central neurons. LEMS is also associated with cerebellar ataxia, underlying the importance of P/Q-type channels in the regulation of cerebellar control of movement (Pinto et al. 1998; Graus et al. 2002).

1.6.5. Migraine

Migraine is a complex, episodic headache disorder affecting around 10% of the general population (Pietrobon 2005; Goadsby et al. 2009), with a strong hereditary component. Migraine can be broadly divided into two subtypes, with aura (MA) and without (MO). Attacks are characterised by unilateral, pulsating headaches lasting 4 to 72 hours, often accompanied by nausea, photo- and phono- phobia, and in the case of MA, visual auras (although other sensory auras can occur) (Pietrobon et al. 2003; Kullmann 2010).

The mechanisms behind the primary cause of migraine remain poorly understood despite substantial research. Within the skull, pain sensitivity is restricted to the meningeal blood vessels, which are densely innervated by sensory afferent fibres of the trigeminal nerve, and it is activation of these afferents which is generally understood to underlie the pain of migraine (Pietrobon et al. 2003). Migraine aura is thought to be caused by cortical spreading depression (CSD), a slow propagating wave (2-6 mm^{-1}) of

strong neuronal depolarisation that generates a transient (seconds), intense spike activity, followed by neural suppression (Leao 1944; Lauritzen 1994). A recent study has shown that in the rat cortex, CSD activates trigeminovascular afferents, evoking a series of alterations in the meninges consistent with migraine pain development (Bolay et al. 2002). However, more work is needed to elucidate the mechanism behind migraine pain and aura.

Migraine has a strong genetic component (up to 50%), although causative genes have not yet been identified, except in the case for familial hemiplegic migraine (FHM), a rare autosomal dominant subtype of MA (Pietrobon 2007; Kullmann 2010). FHM is characterised by aura (typically occurring in the order visual, sensory, motor, aphasic), motor weakness or unilateral paralysis (Thomsen et al. 2002). Other than the paralysis and length of an attack, FHM symptoms are similar to those of MA, and indeed FHM episodes may alternate with MA in patients and occur simultaneously within FHM families. This has led to the idea that FHM and MA lie on the same spectrum, and may share some mechanistic similarities (Pietrobon et al. 2003). Therefore it may be possible to generalise the study of mechanisms behind FHM mutations to migraine.

Although the majority of cases of FHM (FHM1) are caused by mutations in the gene encoding the P/Q-type α_1-subunit, there are three known subtypes of FHM (FHM1, FHM2 and FHM3), all caused by mutations in genes encoding proteins important in neuronal excitability. However, as not all patients with FHM symptoms have mutations in these three genes, there may be further subtypes of FHM found in the future (Pietrobon 2007).

1.6.6. FMH1

The FHM1 locus was identified in 1996 (Ophoff et al. 1996) and is the CACNA1A gene, which encodes the pore-forming α_1 subunit of the P/Q-type voltage-gated Ca^{2+} channel ($Ca_v2.1$). To date, eighteen different missense mutations have been described, the majority of which substitute conserved amino acids in either the voltage sensor or pore lining regions of the channels (See figure 1.8 and table 1.2). FHM1 mutations make up roughly 50% of all FHM cases, and will be looked at in more detail later.
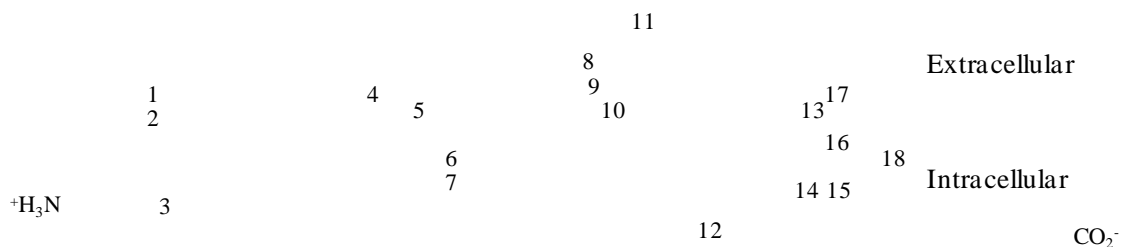
Figure 1.8: Location of FHM1 mutations. There are currently 18 missense mutations of the P/Q-type VGCC which lead to familial hemiplegic migraine, the majority of which are located either on the voltage sensor or on the pore-forming S5-S6 transmembrane segments. See table 1.2 for a description of the individual mutations. Adapted from (Pietrobon 2007).

Table 1.2: FHM1 mutations

Mutation (figure 1.8)	Mutation name*	Model systems
1	R192Q	*Xenopus laevis* oocytes (Kraus et al. 1998) HEK 293, cerebellar granule cells (Tottene et al. 2002) HEK 293 (Hans et al. 1999) Hippocampal neurons (Cao et al. 2005) KI mouse (van den Maagdenberg et al. 2004)
2	R195K	
3	S218L	HEK 293, cerebellar granule cells (Tottene et al. 2005) KI mouse (van den Maagdenberg et al. 2010)
4	R583Q	*Xenopus laevis* oocytes (Kraus et al. 2000)
5	T666M	*Xenopus laevis* oocytes (Kraus et al. 1998) HEK 293 (Hans et al. 1999) HEK 293, cerebellar granule cells (Tottene et al. 2002) Hippocampal neurons (Barrett et al. 2005) Hippocampal neurons (Cao et al. 2005)
6	V714A	*Xenopus laevis* oocytes (Kraus et al. 1998) HEK 293, (Hans et al. 1999) HEK 293, cerebellar granule cells (Tottene et al. 2002) Hippocampal neurons (Cao et al. 2005)
7	D715E	*Xenopus laevis* oocytes (Kraus et al. 2000)
8	K1336E	*Xenopus* oocytes (Müllner et al. 2004)
9	R1347Q	
10	Y1385C	
11	V1457L	*Xenopus laevis* oocytes (Kraus et al. 2000) HEK 293, cerebellar granule cells (Tottene et al. 2002)

12	C1534S	
13	R1667W	
14	L1682P	
15	W1684R	*Xenopus* oocytes (Müllner et al. 2004)
16	V1696I	*Xenopus* oocytes (Müllner et al. 2004)
17	I1710T	
18	I1811L/I1815L/I1819L	*Xenopus laevis* oocytes (I1819L) (Kraus et al. 1998) HEK 293 (I1815L) (Hans et al. 1999) HEK 293, cerebellar granule cells (I1815L) (Tottene et al. 2002) Hippocampal neurons (I1811L) (Cao et al. 2005)

*where A is the correct amino acid, B is the substituted amino acid and # is the substitution position

1.6.7. FHM2

In 2003, the gene for FHM2 was discovered (De Fusco et al. 2003) in two Italian families. This gene, ATP1A2 encodes the α_2 subunit of the Na+, K+-ATPase, an active transport pump which transports three Na^+ out and two K^+ into the cell, using energy from the hydrolysis of ATP to ADP. This transmembrane pump, localised in both neuronal and glial cells, has two major functions: maintaining the resting membrane potential and providing the driving force for neurotransmitter uptake. To this end, the pump plays a vital role in controlling neuronal excitability (Benarroch 2011).

The twenty-three missense mutations in the ATP1A2 gene found to date all lead to either severe or in some cases complete loss-of-function of pump activity (Vanmolkot et

al. 2003; Vanmolkot et al. 2003; Jurkat-Rott et al. 2004; Spadaro et al. 2004; Dreier et al. 2005; Riant et al. 2005). In patients with FHM2, this loss-of-function leads to impaired clearance of K^+ from the extracellular space, and a decrease of glutamate scavenging efficiency in the synaptic cleft, which in turn increases neuronal excitability (Pietrobon 2007). It has been suggested that this leads to enhanced susceptibility to CSD in migraineurs with FHM2.

1.6.8. FHM3

Mutations in the SCN1A gene encoding the α1 subunit of the $Na_v1.1$ voltage-gated Na^+ channel leads to FHM3 (Dichgans et al. 2005). The mutation, Q1489K, is located on the cytoplasmic segment that links domains III and IV, and has been shown to accelerate recovery from fast inactivation (in recombinant human $Na_v1.5$ channels), which is thought to increase neuronal firing. This suggests a likely mechanism for increased susceptibility to CSD.

1.6.9. Controversy surrounds FHM1 mutation functions

The effects of FHM1 mutations on the biophysical properties of P/Q-type Ca^{2+} channels have been widely studied, but remain controversial. To date, eighteen different missense mutations are associated with FHM1 (Figure 1.8; and table 1.2), all of which produce substitutions in conserved amino acids, particularly in the voltage sensor region (S4) and the pore lining (S5 and S6 and the S5-S6 linker) (Pietrobon 2007; Ducros et al. 2001), with T666M (figure 1.8, number 5) being the most prevalent (Barrett et al. 2005), and S218L (figure 1.8, number 3) the most severe (van den Maagdenberg et al. 2010).

Three models have been used to study FHM1 mutations. Twelve of the mutations have been studied in heterologous expression systems, characterising recombinant P/Q-type Ca^{2+} channels in either *Xenopus* oocytes or HEK 293 cells (see table 1.2 for references). As P/Q-type Ca^{2+} channels are most prevalent in neurons, five mutants have been studied in neurons from $Ca_v2.1^{-/-}$ mice expressing human $Ca_v2.1\alpha_1$ subunits (see table 1.2 for references). Finally, mice carrying two of the mutations (S218L and R192Q) have been generated, allowing the analysis of mutant channels expressed at endogenous levels in neurons (see table 1.2 for references) (Pietrobon 2007).

Attempts to connect channel dysfunction with biophysical properties in these different FHM1 models have resulted in conflicting results, as opinion is divided as to whether the mutations cause gain- or loss-of-function (Hans et al. 1999). It is generally accepted that mutations result in a shift in activation voltage to more negative potentials (Hans et al. 1999). The greatest shift is seen with the S218L mutation, which correspondingly has the most severe phenotype (Tottene et al. 2005). However translating a change in activation potential to altered influx of Ca^{2+} and release of neurotransmitter in a pre-synaptic terminal is not straightforward.

Here, an overview of the evidence for gain- and loss- of function is outlined, along with possible explanations for the controversy.

1.6.9.1.   Evidence for gain-of-function for FHM1 mutations in VGCCs

A gain-of-function was seen by Tottene and colleagues (Tottene et al. 2002) in five mutations studied in transfected HEK 293 cells and cerebellar granule cells from $Ca_v2.1^{-/-}$ mice. They observed an increase in the Ca^{2+} influx mediated by individual channels over a range of depolarisations, arguing for a gain-of-function at the level of

individual synapses (Tottene et al. 2002). Combined with the shift of activation voltage increasing the open probability, they suggested that this could lead to Ca^{2+} influx through mutant channels in response to small depolarisations insufficient to open wild type (WT) channels. They also observed a decrease in maximal current density in cerebellar granule cells transfected with mutant channels, consistent with another study by Cao and colleagues (Cao et al. 2005). However, in the study by Tottene and colleagues, this decrease in maximal current density was presumed due to a decrease in functional Ca^{2+} channels at the membrane surface, suggesting that the mutation interferes with protein expression or transportation.

A further study by the same group confirmed their findings by studying the S218L mutation in both neurons and HEK 293 cells. S218L produced a shift to lower voltages of the single channel activation curve and consequently an increase in both the single channel and whole cell Ba^{2+} influx (Tottene et al. 2005). Moreover, the group showed the S218L mutation had a unique effect on the kinetics of inactivation. Whilst the fast component of inactivation was accelerated, a large component of current inactivated very slowly, resulting in a residual current twice as large as in WT after a 1 s depolarisation. They suggested that this current could account for the increased cortical spreading depression seen later in FHM1 mice (van den Maagdenberg et al. 2010).

1.6.9.2.   Evidence for loss-of-function in FHM1 mutated VGCCs

In contrast to the studies by Tottene and colleagues, when expressed in HEK 293 cells, a reduction in Ca^{2+} current was seen for the most prevalent FHM1 mutation T666M, without a corresponding reduction of functional channels at the surface membrane,

discounting the idea that the mutation interferes with protein expression or transportation (Barrett et al. 2005; Cao et al. 2005). They proposed the model that while a subset (~30%) of mutant channels were able to undergo gating with normal WT properties, the majority were unavailable for gating (Barrett et al. 2005). This work was extended by analysing synaptic transmission at both excitatory and inhibitory synapses in hippocampal cultures prepared from CACNA1A$^{-/-}$ KO mice transfected with human α_{1A} subunits (Cao et al. 2004, 2005). Although overall synaptic strength was maintained and synaptic transmission was not affected, the amplitude of the EPSCs and IPSCs dependent on P/Q-channels was reduced, and shifted in favour of N-type channels (Cao et al. 2004, 2005).

1.6.9.3. Loss-of-function in FHM1 mutations could be due to a shift in dependency towards N-type VGCCs

This shift towards N-type Ca^{2+} channels being the dominant carrier of Ca^{2+} current, whilst maybe not having an effect on overall synaptic strength, would affect the synapse susceptibility to neuromodulation by GPCRs, as N-type channels are more vulnerable to GPCRs (Currie et al. 1997; Zamponi et al. 1998). Cao and Tsien proposed that this shift in Ca^{2+} channel subtype dominance could underlie migraine onset. As migraine is an episodic disease, commonly triggered by emotional or physical stress, they suggested that a heightened level of neuromodulation could occur before a migraine attack, leading to a state of weakened neurotransmission (Cao et al. 2005).

Although shifting transmission to be more reliant on N-type channels, and hence more susceptible to neuromodulation by GPCRs, a number of studies have suggested that the mutated channels themselves may be less prone to GPCR inhibition (Melliti et al.

2002). This could explain the perceived gain-of-function seen by Tottene and colleagues (Tottene et al. 2002; Tottene et al. 2005). In the study by Melliti et al. carried out in transfected HEK tsA-201 cells, the R192Q mutation reduced the G-protein inhibition of P/Q-type Ca^{2+} channels, by possibly altering mechanisms by which Gβγ-subunit binding induces a change in channel gating (Melliti et al. 2002). They argued that altered G-protein modulation and the consequent reduction in presynaptic inhibition may contribute to migraine attacks. A second study by Weiss et al., came to a similar conclusion, in HEK 293 cells transfected with S218L (Weiss et al. 2008). They suggested that the S218L mutation did not affect G-protein association onto the channel in the closed state but promoted dissociation from the activated channel, decreasing the inhibitory pathway. A similar result was seen in R192Q, but to a lesser extent. Finally, a third study confirmed acceleration of Gβγ dissociation from the P/Q-type channel in the Y1245C mutation (Serra et al. 2009). The group suggested that the effect could account for the reduced P/Q channel voltage-dependent inhibition by Gβγ subunits at voltages that may be attained during CSD (Serra et al. 2009).

1.6.9.4. Evidence is variable even in FHM1 KI mice

Two transgenic knock-in (KI) mice have been produced harbouring the R192Q and S218L mutations (van den Maagdenberg et al. 2004; van den Maagdenberg et al. 2010). The effects of the mutations on synaptic transmission have been studied at various synapses, but give differing results possibly due to differences in splice variants or auxiliary subunit composition at the different synapses (Tottene et al. 2009). Increased spontaneous neurotransmission was observed at the neuromuscular junction (miniature end plate potentials, mEPPs) in both R192Q and S218L (van den Maagdenberg et al. 2004; van den Maagdenberg et al. 2010), but not at cultured cortical pyramidal cells

harbouring the R192Q mutation (Tottene et al. 2009). The same study saw an increase in evoked excitatory neurotransmitter release, but no corresponding increase in inhibitory synapses of fast spiking interneurons (Tottene et al. 2009). This increased excitation susceptibility could underlie the lowered threshold for cortical spreading depression and the increased velocity of wave (van den Maagdenberg et al. 2004).

Studies of evoked neurotransmission at the NMJ in both R192Q and S218L showed no increase in the probability of release at physiological Ca^{2+} levels (2 mM). However, lowering the Ca^{2+} level to 0.2 mM unmasked a gain-of-function effect of neurotransmission (van den Maagdenberg et al. 2004; van den Maagdenberg et al. 2010). Interestingly, at the calyx of Held, Ca^{2+} current amplitude and kinetics were similar in WT and R192Q synapses, and evoked neurotransmission was unaffected. However, when a longer-duration, small-amplitude AP waveform was used to trigger synaptic release, presynaptic Ca^{2+} influx was significantly increased compared to WT, enhancing transmission (Inchauspe et al. 2010).

1.6.9.5.   What possible reasons could explain the conflicting views of how FHM1 mutations affect P/Q-type VGCCs?

There are several explanations for the conflicting results from studies of FHM mutations. Firstly, overexpression of mutations in recombinant expression systems such as HEK 293 cells and *Xenopus* oocytes can lead to different results (Südhof 2004). While often giving the most dramatic, but variable results, overexpression can lead to difficulty in interpretation due to inconsistency in the amount of functional channels in the membrane (Tottene et al. 2002). Consequently, although overexpression may be suitable for single channel studies, it is not appropriate for studying properties at the

whole-cell level. The combination of human cDNA expressed in cells from other species can also cloud effects, potentially by altering binding to endogenous proteins (Kraus et al. 1998; Hans et al. 1999).

Studies of the effect of FHM1 mutations in neurons derived from $Ca_v2.1^{-/-}$ mice are more physiological, but run into difficulty when controlling for auxiliary subunit expression and discerning the interaction between the mutant channels and other Ca^{2+} channel subtypes. Whole-cell studies are more successful when the protein is expressed in an endogenous system (van den Maagdenberg et al. 2004; van den Maagdenberg et al. 2010). However, there is still huge variability in results from different synapses taken from transgenic animals (van den Maagdenberg et al. 2004; Tottene et al. 2009; van den Maagdenberg et al. 2010; Inchauspe et al. 2010), underlying the strong dependence of Ca^{2+} channel properties on external factors such as splice variants, auxiliary subunit composition and modulation by various up-stream molecules.

In all previous work, neurotransmitter release from synapses expressing FHM1 mutations was simultaneously recorded from large populations of heterogeneous synapses (i.e. summating all the synapses onto an individual neuron). This could lead to masking of a loss- or gain-of-function effect seen at individual synapses. We are in the unique position where we can monitor synaptic neurotransmission in individual synapses harbouring FHM1 mutations, using a fluorescence imaging technique (see chapter 6) (Betz et al. 1996). In chapter 7 we apply our approach to ask what the effects of two migraine mutations (S218L and R192Q) are on synaptic transmission in individual synapses. In particular, we will measure the spontaneous (K_{sp}) and evoked destaining rates (K_{AP}) (which give an indication of the release rate), the size of the RRP

and RP of vesicles and the probability of release of a vesicle (p_v) at individual synapses with mutated and WT Ca^{2+} channels.

1.7. Questions to answer in this thesis

In summary, in this thesis, we will aim to answer the following questions:

1. **Are differentiated human-derived neurons suitable for characterising the functional consequences of FHM1 mutations in Ca^{2+} channels?**

We asked whether expression of FHM1 mutant cDNA into a human-derived cell-line, which can be differentiated into neuronal-like cells (Andrews 1984; Hartley et al. 1999), was likely to produce robust data on vesicular release. The differentiation and transfection of the human-derived cell-line NT2 are discussed in chapter 3.

2. **What conditions are optimal for producing stable dissociated hippocampal cultures for characterisation of Ca^{2+} dependent vesicle release?**

Much of this thesis used cultured hippocampal neurons, as synaptic transmission is well characterised at these synapses (Kaech et al. 2006) and the heterogeneity of cell types is low (Benson et al. 1994). The optimisation of a culturing procedure from WT and mutant animals to produce neurons suitable for imaging and electrophysiological experiments is described in chapter 4.

3. **What is the dissociation constant of the most common FM dyes on membranes derived from dissociated hippocampal cultures?**

In this study, the main method used to characterise synaptic transmission at individual synapses is loading vesicles with FM dyes, and imaging synaptic recycling (Gaffield et

al. 2006). In order to analyse our data accurately, it is necessary to measure the binding properties of FM dyes with the membrane of our cultures. The measurement of K_d on our cultured neurons, and a comparison to another membrane model is presented in chapter 5.

4. **How heterogeneous are synaptic neurotransmitter characteristics at individual synapses in WT cultures?**

The FM dye destaining experiment protocol and analysis is described in detail in chapter six. In particular, we asked *how heterogeneous are the synaptic neurotransmitter release parameters (K_{sp}, K_{AP}, RRP, RP and p_v) at individual synapses*? In chapter 6, we focus on data from WT cultures.

5. **How do the specific FHM1 mutations R192Q and S218L modulate synaptic transmission? Do the mutations lead to a loss- or gain-of-function in neurotransmitter release properties at the level of individual synapses? How does knock-out of the P/Q-type Ca^{2+} channel affect synaptic transmission?**

In chapter 7 we build on data from WT neurons in chapter 6 to ascertain whether *spontaneous release is increase at hippocampal synapses with R192Q and S218L mutations* in accordance with previous studies at the NMJ (van den Maagdenberg et al. 2004; van den Maagdenberg et al. 2010). With our method, we can also compare the size of the *RP* or *RRP* pools. In particular, we will investigate *whether FHM1 mutations lead to homeostatic changes in the size of either vesicle pool.*

6. Does spontaneous synaptic transmission depend on the opening of voltage-gated Ca^{2+} channels? If spontaneous neurotransmitter release is enhanced in FHM1 mutations at hippocampal synapses, what is the mechanism behind this enhancement?

In chapter 8 we study spontaneous synaptic transmission in cultured neurons by combining FM dye destaining experiments with electrophysiological methods. We will look at Ca^{2+} regulation of spontaneous neurotransmission at WT and mutated cultures, and address the extent to which it is dependent on opening of voltage-gated Ca^{2+} channels.

2. Materials and Methods

This chapter describes the general methods that were used to produce data for this thesis. It is subdivided into the following sections:

1. Preparation and maintenance of neuronal cultures.

2. Maintenance, transfection and differentiation of the NT2 cell culture line.

3. Preparation and quantification of synaptic plasma membranes (SPMs).

4. Imaging of vesicular recycling with FM dyes.

5. Electrophysiological methods.

2.1. Preparation and maintenance of neuronal cultures

The comparison of different protocols for preparation of primary hippocampal cultures is discussed in chapter 4. Here we describe in detail the final optimised protocol for preparation and maintenance of hippocampal neuronal cultures from rats and mice. This protocol is used in all functional imaging and electrophysiological experiments.

The protocol is divided into three major stages:

1. Preparation and expansion of cortical glial cells.

2. Preparation of coverslips and plating the glial cell feeding layer.

3. Isolation of hippocampal neurons.

2.1.1. *Materials, media and timeline for hippocampal cell culture*

The following tables list all the reagents and equipment needed for producing a dissociated hippocampal culture. Table 2.1 describes all the cell culture media and reagents, table 2.2 catalogues all consumables used and table 2.3 logs all apparatus

needed. Finally, a timetable for production of the culture is listed in table 2.4, which is divided into three columns detailing the three major stages of the protocol.

Table 2.1 – Cell culture media and other reagents for dissociated hippocampal cell cultures

Media and other cell culture reagents	Component	Source	Amount
2.5 % trypsin		Invitrogen	
Trypsin/EDTA		Invitrogen	
Trypan Blue		Sigma	
CMF-HBSS Store at 4°C	Tissue culture grade H$_2$0	Sigma	1000 ml
	10x HBSS	Invitrogen	100 ml
	10 m M HEPES	Invitrogen	10 ml
Glial Medium, (GM) Store at 4°C	MEM	Sigma	500 ml
	D-glucose	Sigma	6.7 ml
	1% Penicillin-streptomycin	Invitrogen	5 ml
	10% Horse serum	Invitrogen	50 ml
	1% L-Glutamine	Sigma	5 ml
2x cell freezing medium Make fresh	FBS	Invitrogen	40 ml
	20% DMSO	Sigma	10 ml
Wash solution Store at 4°C	HBSS	Sigma	500 ml
	10 mM HEPES	Invitrogen	5 ml
Dissection solution Make fresh	Wash solution	From stock	40 ml
	20% FBS	Invitrogen	10 ml
Neurobasal complete, (NB) Store at 4°C	Neurobasal A medium	Invitrogen	500 ml
	2% B27 supplement	Invitrogen	10 ml
	25 µM Glutamax	Invitrogen	1.25 ml

araC stock Filter (0.2 µm) and store at -20 °C	Cytosine β-D-arabinofuranoside (araC)	Sigma	4.20 mg
	Tissue culture grade H_2O	Sigma	5 ml
DNAse stock Freeze at -20 °C	DNAse, 75 u/µl	Sigma	150 KU
	H_2O	Sigma	2 ml
Digestion solution Adjust pH to 7.2 with 10 M NaOH, filter (0.2 µm, SFCA membrane). Freeze at -20 °C	Tissue culture grade H_2O	Sigma	
	137 mM NaCl,	Sigma	
	5 mM KCl,	Sigma	
	7 mM Na_2HPO_4	Sigma	
	25 mM HEPES	Sigma	
Digestion mix Make on the day of neuronal preparation. Filter (0.2 µm)	Trypsin XI	Sigma	25-30 mg
	Digestion solution	Stock	2.5 ml
	DNAse	Stock	10 µl
Dissociation solution Filter (0.2 µm). Freeze at -20 °C	Wash solution	Stock	
	12 mM $MgSO_4$	Sigma	
Dissociation mix Make on the day of neuronal preparation.	Dissociation solution	Stock	2.5 ml
	DNAse	Stock	12.5 µl
Borate buffer titrate to pH 8.5 with sodium tetraborate, store at room temperature	100 mM Boric acid	Sigma	
	100 mM Sodium tetraborate	Sigma	
Poly-L-lysine	Poly-L-Lysine	Sigma	1 mg

Make fresh, Filter (0.2 μm)	Borate buffer	Stock	1 ml
Fluorescein diacetate (FDA) Freeze at -20°C	Fluorescein diacetate	Sigma	50 mg
	Acetone	Sigma	10 ml
Working FDA Make fresh	FDA	Stock	0.04 ml
	Neurobasal complete, (NB)	Stock	10 ml
Propidium iodide (PI) Store at 4°C	Propidium iodide	Sigma	1 mg
	CMF-HBSS	Stock	50 ml
Incubation solution Make fresh	Neurobasal complete, (NB)	Stock	5 ml
	Working FDA	Stock	0.5 ml
	PI	Stock	0.15 ml
Nitric Acid	65 % Nitric acid	Sigma	
Ethanol	70 % ethanol	UCL Chemistry	

Table 2.2: Cell culture consumables

Cell culture materials	Type	Source
Plasticware	Centrifuge tubes (15 ml, 50 ml)	Sigma
	Culture dishes (30, 60, 90 mm)	Sigma
	Pasteur pipettes	Sigma
	Serological pipettes (5, 10, 20 ml)	Sigma
	Freezing vials	Sigma
	T25, T75, T225 flasks	Sigma

	12-well culture plates	Sigma
	Sterile eppindorff tubes	Sigma
Pasteur pipettes	Plugged and unplugged	Sigma
Filters	70 μm, 0.2 μm	VWR
Coverslips	18 mm diameter	Fisher Scientific

Table 2.3: Cell culture equipment

Cell culture equipment	Type	Source
Laminar flow hood	Gelaire BSB4	Labcaire
Tissue culture incubator, 37 °C, 5% CO_2 atmosphere	Galaxy S, Galaxy S+	Wolf laboratories
Water bath	JB series	Grant
Dissection Microscope	-	Zeiss
Dissection tools	2 x Dumont #5 2 x Dumont #55 Scissors	WPI 500233 WPI500235 WPI 500228
Centrifuge	Universal 32 R	Hettich
Hemacytometer	Bright-line	Sigma
Liquid nitrogen storage facility	-	-
Ceramic coverslip staining racks	-	Thomas Scientific, 8542E40
Pipetters	Powerpette	Jencons Scientific
	Labmate pipettors (2 μl, 20 μl, 200 μl, 1000 μl)	Jencons Scientific
Oven	Autoclave oven	Binder

Table 2.4: Timetable for dissocitated hippocampal culture preparation

Day	Glial cells	Coverslips	Neurons
Prior	Prepare and freeze glial cells		
-14	Defrost and plate glial cells into T75 flasks		
-13	Feed with GM		
-10	Feed with GM	Soak coverslips in 70% nitric acid	
-7	Feed with GM	Rinse and bake coverslips	
-6		Coat with PLL	
-5	Dislodge cells and re-plate on coverslips	Rinse and seed glial cells	
-4	Feed with GM		
0	Feed with NB		Prepare and plate neurons onto glial cells
1			Add araC
7			Feed with NB
14 - 24			Use neurons for experiments

2.1.2. Animal husbandry

All animal procedures were carried out in accordance with Home Office regulations, under the UK Animal (Scientific Procedures) Act 1986. Animals were housed under controlled environmental conditions (24-25°C; 50-60% humidity; 12h light/dark cycles) and had free access to food and water. To produce primary rat hippocampal neuronal and cortical glial cultures, newborn (P0) Sprague Dawley rats were obtained from UCL Central Biological Unit.

Three transgenic mice strains - S218L KI (van den Maagdenberg et al. 2010), R192Q KI (van den Maagdenberg et al. 2004) and CACNA1A KO (Kaja et al. 2007) - were a kind gift from the lab of Arn van den Maagdenberg. Transgenic mice were bred on a C57BL/6J background for at least 8 generations before being used for experiments. The individual strains were propagated by breeding HET KI or CACNA1A$^{+/-}$ mice with C57BL/6J animals (Charles River, UK) with one pair per cage (Gerlai 1996). Breeding pairs were replaced if they did not produce a litter for three months or if litters did not survive. Litters were weaned at three weeks and ear-tagged in order to ascertain genotype (PCR based genotyping was kindly carried out by Stuart Martin of the Biosciences Huxley Building Molecular Biology Facilities).

For experiments where homozygous (HOM), HET and WT littermates were required, pairs of HET KI or CACNA1A$^{+/-}$ mice were set up. Newborn pups were used for preparation of cultures at P0-P1 or culled before weaning to ensure that HOM mice did not reach maturity (in accordance with the project licence.)

2.1.3. Dissection
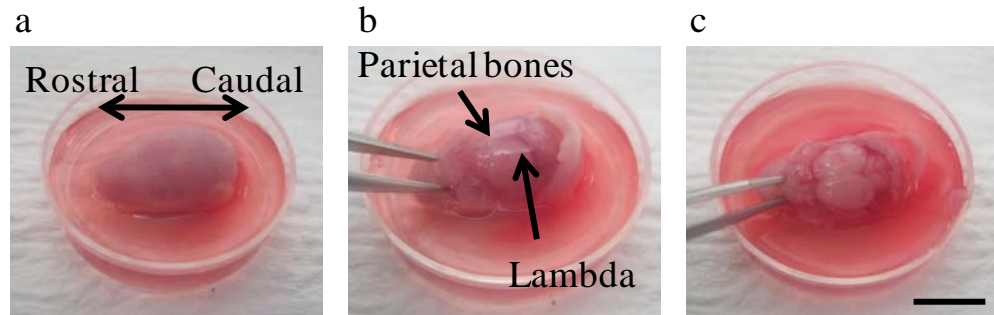
Figure 2.1: Dissction of a P0 rat. (a) The rat was decapitated and the head submerged in ice cold wash solution. (b) The head was clamped between the eyes to stabilise it during dissection. The skin covering the top of the head was peeled back to expose the skull. The parietal bones were pierced at the lambda and pulled apart. (c) The skull was gently but completely removed to expose the brain. Scale bar (a) - (c) ~1 cm.

All media for the preparation of neuronal cultures was ice cold before trypsin application, and at 37°C after. P0 rat pups were culled by an appropriate method and decapitated. The heads were rinsed with 70% ethanol, washed four times in ~ 30 ml of wash solution, and placed into a 10 cm dissection plate with wash solution (figure 2.1a). The skin was removed (figure 2.1b), using Dupont 5 forceps, the skull pierced at the lambda and the parietal bones peeled back and removed, exposing the brain (figure 2.1c).

The brain was scooped out and placed into a 3.5 cm dissection plate, fully submerged with dissection solution (figure 2.2a). Under the dissection microscope the cortices were separated from the brain stem using Dupont 55 forceps (figure 2.2b), and meninges fully removed, exposing the hippocampus. Finally, the hippocampii were separated

from the cortices by snipping along the outside edge and teasing them apart (figure 2.2c). The cortices and hippocampii were transferred to separate plates filled with dissection solution and cut into several pieces with the forceps. The dissection process was repeated for all pups being used.

2.1.4. Preparation, amplification and freezing/defrosting of cortical astroglial cells

The pieces of cortices were transferred to a 50 ml tube containing 9.5 ml CMF-HBSS, 1.5 ml 2.5% tryspin and 1.5 ml DNAse stock. The tissue was incubated for 5 minutes at 37°C in a water bath and swirled occasionally. The tissue was triturated through a 10 ml pipette ten times in order to break up large clumps of cells, then returned to the water bath for a further 10 minutes. Any remaining clumps were triturated again, with a 5 ml pipette until the suspension was mostly homogenous.
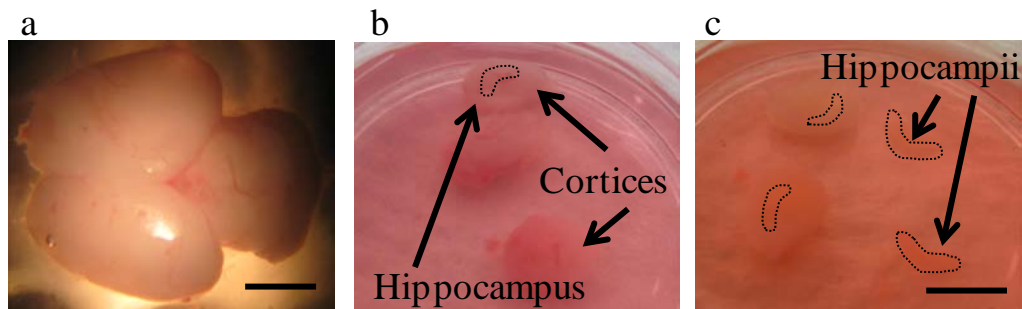
Figure 2.2: Dissection of the cortex and hippocampus of a P0 rat. (a) The brain was removed from the skull and head and submerged in ice cold dissection solution. Both cortices and cerebellum can clearly be seen, covered in the meningeal membranes. (b) The cortices were separated from the cerebellum and brain stem, and the hippocampus located. The meninges were peeled away from the brain tissue. (c) The hippocampii were removed from the cortices, leaving a gap. The cortices were used to produce

*astroglia, and the hippocampii to make neuronal cultures. Scale bars (**a**) 2.5 mm, (**b**) and (**c**) 6.5 mm.*

The cell suspension was passed through a 70 μm filter, and collected in a 50 ml tube containing 15 ml of glial medium (GM). The cells were centrifuged for 10 minutes at 2000 RPM to remove the enzymes. The supernatant was discarded and the pellet resuspended in 20 ml of GM. The cells were counted using the 0.4% trypan blue exclusion method to ascertain viability. Cells were seeded at a density of 7-10 x 10^6 cells per T75 flask (roughly one pup per flask), and topped up to a final volume of 12-13 ml with GM. Cells were grown in an incubator at 37 ^{o}C, 5% CO_2. The day after plating, the media was exchanged to remove dead cells, and thereafter media was changed every two to three days, until cells reached 90-100% confluence.

The glial cells were split when confluent and each T75 flask divided into 8 in order to amplify the colony. The cells were rinsed with 10 ml of warmed CMF-HBSS, and treated with 2 ml of trypsin/EDTA until cells had dislodged. The trypsin/EDTA was inactivated by 8 ml GM, and the cells pelletted (10 minutes at 2000 RPM). The pellet was resuspended in GM and divided between 8 flasks. This process was repeated in order to obtain a large batch of cells (roughly 150 flasks).

The cells were frozen in liquid nitrogen, in order to create a stock of glia which could be defrosted for weekly neuronal cell preparations. The cells were dislodged with trypsin/EDTA as described above, but resuspended in 0.5 ml GM and 0.5 ml ice-cold 2x cell freezing medium, and transferred to individual 1.8 ml cryotubes (2 T75 flasks per

tube). Tubes were frozen for 2 hours at -20°C then overnight at -80°C, before being placed in liquid nitrogen for long term storage.

Glial cells were defrosted two weeks before neuronal preparation to form a feeding layer on glass coverslips. One tube was defrosted and resuspended in ice cold GM, before pelletting (10 minutes at 2000 RPM) to remove DMSO. The pellet was resuspended in warmed GM and plated in 9 T75 flasks. Media was changed the following day, and cells grown to reach 95-100% confluence over several days (feeding every two to three days with fresh GM).

2.1.5. Preparation of coverslips

19 mm glass coverslips were placed into ceramic racks and submerged in 70% nitric acid for several days. They were rinsed four times for two hours in ddH$_2$O and baked overnight at 225°C. The coverslips were placed in 12-well plates (6 coverslips per plate) and coated with 150 μl PLL solution. They were incubated overnight, then rinsed twice for two hours with ddH$_2$0.

Glial cells were dislodged with trypsin/EDTA, resuspended in GM and plated onto the coated coverslips at a density of 60K per cm^2. Media was changed the following day, and cells left to grow to form a continuous monolayer before the neuronal preparation was added.

2.1.6. Preparation of rat neuronal cultures

Dissected hippocampi were transferred to a new dish with dissection buffer and then transferred to a 15 ml centrifuge tube where they were washed 5 times in 5 ml wash buffer. The hippocampal tissue was transferred to a tube containing digestion mix and

incubated for 10 minutes at 37°C. The enzyme was inhibited by 5 ml of dissection

buffer, before being rinsed a further 4 times, twice with dissection buffer and twice with

wash buffer.

The digested tissue was triturated in 2 ml dissociation mix, for roughly 5 stokes with a

half-diameter fire-polished, cotton-plugged Pasteur pipette. Roughly 1 ml of cell

solution was removed to a new 15 ml tube (in order to minimise cell death by

mechanical trituration), then the remainder triturated with a third-diameter, fire-polished

Pasteur pipette. Large clumps of tissue were allowed to settle before the cell solution

was removed and added to the 15 ml tube. 10 ml dissection solution was added and cells

centrifuged for 5 minutes at 2000 RPM.

The supernatant was discarded and the cell pellet broken. Cells were resuspended in

Neurobasal complete (NB) and counted. GM was removed from the glial cell coated

coverslips and 1 ml NB added to each well. The cell solution was diluted to a

concentration of 30K cells per ml with NB and 1 ml added to each well (giving a

density of ~10 K cells/cm^2). Cells were returned to the incubator and stored at 37°C and

5% CO_2. The following day, cells were fed with 1 ml per well of warmed NB

containing 3 μM araC (This gave a final concentration of 1 μM). On day 7 after plating,

cells were fed with NB. 1 ml of medium was removed from each well, and replaced

with fresh medium. Cells were used for experiments 14 to 21 days after plating.

2.1.7. Modifications for transgenic mouse cultures

A number of modifications were made when culturing mouse hippocampii, due to their

relative size, and the number of pups in a litter (typically 6-12 pups). As the genotype of

each pup was determined after the culture preparation littermates had to be cultured

separately (PCR based genotyping by Stuart Martin was carried out on tail clippings after culturing). Typically 3-4 pups would be dissected at a time, with the surgical instruments cleaned with 70% ethanol between each to avoid cross contamination of genotypes. Less media was required during the washing processes, trypsin application and trituration, due to the physical size of the tissue samples. The cells were not counted; instead 4 coverslips per pup were plated. This gave a roughly consistent density, without delaying plating during counting. After genotyping, experiments were ideally carried out on all three genotypes on the same day to control for differences in development.

2.1.8. Cell viability method

The method for assessing cell viability used in chapter 4 was adapted from the paper by Jones et al. (Jones et al. 1985). This technique was based on using two dyes in contrast to the typical Trypan Blue exclusion method. These were: fluorescein diacetate (FDA), a non-polar ester which exclusively stains viable cells; and propidium iodide (PI), an analogue of ethidium bromide, which intercalates with DNA and RNA of damaged and dead cells forming a bright red fluorescence complex in the nuclei of dead cells. PI is excluded by intact cell membranes so is an effective stain to identify non-viable cells. FDA passes through cell membranes and is hydrolysed by intracellular esterases, forming fluorescein. Fluorescein is a polar compound that accumulates in the cell, emitting green fluorescence when excited by a blue light (450-490 nm). This is a slow process and the fluorescence emission develops over time.

FDA, PI, working FDA and incubation solution stocks were made according to table 2.1. Incubation solution was added to a 35 mm plate containing a coverslip of interest, and incubated at room temperature for 5 minutes. The cells were observed under a

fluorescent microscope with a 20x objective, illuminated by an epi-illumination 100 W halogen bulb. A band pass excitation filter (450-490 nm) and long pass 520 nm emission filter were used (this filter combination permitted both green and red fluorescing cells to be seen consecutively, viable cells in green, nonviable cell nuclei in red). Typically images were taken of 10 regions per coverslip, using three coverslips for each condition. All cells in each region were counted, and the ratio of red to green cells was calculated.

2.2. Maintenance, transfection and differentiation of the NT2 cell culture line

The NT2 precursor cell line was a kind gift from Prof. Ushkaryov, Imperial College London

2.2.1. Materials, media and timeline for NT2 cell culture

Table 2.5 lists all the reagents and equipment needed for culturing and transfecting of NT2 cells. All consumables and apparatus are as detailed in tables 2.2 and 2.3.

Table 2.5: All cell culture media and supplements

Culture media and reagents	Component	Source	Amount
Complete DMEM/F12	DMEM/F12	Invitrogen	500 ml
	FBS HI	Invitrogen	50 ml
	Penicillin-streptomycin	Invitrogen	5 ml
Retinoic Acid,100 mM	Retinoic Acid	Sigma	30.04 mg
	DMSO	Sigma	1 ml
Differentiation medium	DMEM/F12	Invitrogen	500 ml
	FBS HI	Invitrogen	50 ml
	Penicillin-	Invitrogen	5 ml

	streptomycin		
	Retinoic Acid, 10 µM	Stock	50 µl
Versene	Ca^{2+}, Mg^{2+} chelator	Sigma	
D-PBS	With Ca^{2+}, Mg^{2+}	Sigma	
	Without Ca^{2+}, Mg^{2+}	Sigma	
Mitotic Inhibitors Filter with 0.2 µm syringe filter	5-Fluoro-2'-deoxyuridine (FUdR), 1 mM	Sigma	10 mg
	Water, cell culture grade	Sigma	40.6 ml
	Uridine (Urd), 1mM	Sigma	10 mg
	Water, cell culture grade	Sigma	41 ml
	araC, 1 mM	Sigma	2.4 mg
	Water, cell culture grade	Sigma	10 ml
Conditioned medium	Condition medium from cells	From cells	50 ml
	Complete DMEM/F12	From stock	50 ml
	FUdR, 10 µM	From 1 mM stock	1ml
	Urd, 10 µM	From 1 mM stock	1 ml
	araC, 1 µM	From 1 mM stock	0.1 ml
Trypsin/EDTA		Invitrogen	
CMF-HBSS Store at 4°C	Tissue culture grade H_20	Sigma	1000 ml
	10x HBSS	Invitrogen	100 ml
	10 m M HEPES	Invitrogen	10 ml
Lipofectamine 2000 reagent	Transfection reagent	Invitrogen	
pEGFP-N2 construct	DNA construct	Stock	1 µg/µl stock

2.2.2. Culturing of NT2 cells

NT2 cells were maintained and propagated in an undifferentiated state prior to transfection or differentiation. Sufficient cells were defrosted and resuspended in ice cold DMEM/F12 complete, before pelletting (10 minutes at 2000 RPM) to remove DMSO. The pellet was resuspended in warmed DMEM/F12 complete and plated in a T75 flask. Media was changed the following day with DMEM/F12 complete, and cells grown to reach 95-100% confluence over several days (feeding every two to three days).

Once confluent, cells were split every two to three days. Cells were rinsed with DPBS, loosened with 4 % trypsin/EGTA application, and divided one to ten. Media was changed the following day, and cells grown to reach 95-100% confluence.

2.2.3. Transfection of NT2 cells

NT2 cells were plated directly onto 12-well plates and grown to be 90-95% confluent on the day of transfection (~80K cells per well). DNA (pEGFP-N2, concentration 1 µg/µl) was diluted to a concentration of 4 µg per 250 µl in DMEM/F12 (without additives). The transfection reagent Lipofectamine was diluted 4 µl into 250 µl of DMEM/F12. The DNA and Lipofectamine solutions were combined, mixed gently by finger tapping and incubated for 20 minutes at room temperature to allow DNA/liposome complexes to form. During incubation of the DNA/liposome, cells were washed twice with DMEM/F12 (without additives) to remove FBS and penicillin-streptomycin. 0.5 ml of DMEM was added to each well followed by 0.5 ml of the DNA/liposome complex. The solution was mixed by gently swirling the plates.

After 6 hours, the cells were removed by trypsin application. Cells were plated 1:2 into new 12-well plates, containing DMEM/F12 complete, and incubated for 24 hours (giving ~80 – 100 transfected cells per well).

To produce stable clones, transfected cells were plated at low density (10 K cells per well, 12-well plate) and incubated for 24 hours. 0.5 mg/ml geneticin (diluted in DMEM/F12) was applied (to kill un-transfected cells) and cells incubated for a further 24 hours. The media was changed after 24 hours to remove dead cells, and clones allowed to grow for a further 48 hours before analysis.

2.2.4. Differentiation into hNT neuron and purification

Table 2.6: Timetable of differentiation of NT2 cells into hNT neurons

Process	Timing
Differentiating NT2 cells	6-7 weeks
Replate 1 – separation of differentiated cells	48 hours
Replate 2 – addition of mitotic inhibitors	1 week
Replate 3 – harvesting of neuronal-like cells	3 weeks +

NT2 cells were split one to two into a T75 flask, to reach ~ 50 % confluence at the start of differentiation. The following day, media was exchanged for warmed DMEM/F12 complete, supplemented with 10 μM retinoic acid. This process was repeated three times a week for six to seven weeks.

After 6-7 weeks of retinoic acid treatment differentiated hNT neurons were purified

over three replating processes, to separate them from undifferentiated NT2 cells

(roughly 10% of the original NT2 cells develop into hNT neurons (Stratagene Cloning

Systems 1998). During the first replating all cells were removed from the T75 flask and

replated into a T225 flask. The cell layer was thick as it had been dividing for several

weeks, so in order to aid the trypsin process, cells were washed with DPBS without

Ca^{2+} and magnesium, then with versene and finally with 4% trypsin/EDTA to free all

the cells. Cells were incubated for 48 hours in DMEM/F12 complete after this replate.

The second replate was designed to remove only differentiated hNT neurons, which had

formed a layer over the NT2 cells after the first replate. Cells were washed with DPBS

containing Ca^{2+} and Mg^{2+} prior to adding 4% trypsin/EDTA and incubated until the

hNT neurons were just lifting off. These cells were transferred to a T25 flask and fed

three times per week with filtered conditioned medium (made from media incubated for

several days with NT2 cells) containing the mitotic inhibitors 20 µM 5-Fluoro-2'-

deoxyuridine (FUdR),20 µM Uridine (Urd) and 2 µM Cytosine (araC) in order to assist

the purification process. The third replate was intended to plate cells onto a 100%

confluent glial culture, as well as to purify the hNT neurons further. Cells were

dislodged as for replate 2, and plated at a density of ~10 K cells/cm^2 onto pre-plated rat

glial cells (see section 2.1.4 for preparation of glial cells). After this final replate, cells

were matured for an additional two weeks before experiments commenced, feeding

weekly with conditioned media.

2.3. Preparation and quantification of synaptic plasma membranes (SPMs)

Synaptic plasma membranes were used in chapter 5 to quantify the biophysical properties of FM dyes.

Table 2.7: Reagents for the preparation of SPMs

Buffer	Component	Source	Amount
Buffer A	Tissue culture grade water	Sigma	500 ml
	0.32 M Sucrose	Sigma	54.76 g
	10 mM HEPES	Sigma (1 M solution)	5 ml
12 % Ficoll	Ficoll	Sigma	24 g
	0.32 M Sucrose	Sigma	21.9 g
	10 mM Hepes	Simga (1 M solution)	2 ml
	Tissue culture grade water	Sigma	Up to 200 ml
7.5 % Ficoll	12 % Ficoll	Stock	62.5 ml
	Buffer A	Stock	37.5 ml
Extracellular buffer	See table 2.8		
Lysis buffer Balance to pH 7.6 with HCl	5 mM Tris-HCl	Sigma (1 M stock)	5 ml
	50 μM CaCl$_2$	Stock (100 mM)	500 μl
	Tissue culture grade water	Sigma	1 L
Bradford assay	Bradford reagent	Sigma	
BSA	BSA	Sigma	
NaOH	1 M NaOH	Sigma	

2.3.1. Purification of synaptic plasma membranes

All solutions and centrifugations were at 0 - 4 °C. The cerebral cortices from 4 adult rats were dissected and placed in 40 ml of ice-cold buffer A. The brains were rinsed several times to remove blood. Cortices were homogenised in 40 ml of buffer A using a Potter-Elvehjem homogenizer (clearance 0.2 mm, 800 rpm, 8 strokes). The homogenate was transferred into two 50 ml centrifuge tubes and spun for 10 minutes at 1,000 revolutions per minute (RPM). The supernatant was collected and centrifuged for 30 minutes at 6,000 RPM. The resulting pellet was resuspended in 4 ml of buffer A, and loaded on pre-prepared Ficoll gradients. The gradients were centrifuged for 1 hour at 30,000 RPM. The 7.5 %/12 % (w/v) interphase Ficoll were separated into Eppindorf tubes. The Ficoll was washed three times using extracellular buffer (1.5 ml buffer per tube, centrifuge 2,000 RPM, 15 minutes, pellet resuspended between washes). The washed synaptosomes were resuspended in 0.5 ml/tube extracellular buffer. The synaptosomes were osmotically lysed in 200 ml of lysis buffer, and incubated for one hour, constantly stirring. The lysis solution was centrifuged for 30 minutes at 24,000 RPM. The pellets were resuspended in 4 ml of extracellular buffer and frozen with ethanol and dry ice. The synaptsomes were thawed and re-frozen two times. Finally, synaptic membranes were harvested by centrifugation at 18,000 RPM for 30 minutes. Synaptic membranes were resuspended in 2 ml extracellular buffer and aliquots made for use.

2.3.2. Bradford assay

To measure the protein content of the synaptic plasma membranes (SPMs), a calibration scale of BSA was prepared (BSA 0 – 100 μg/ml) in water. SPMs were diluted 1:10 with 1 M NaOH, then samples were prepared in water (0 – 100 μl/ml). Samples were vortexed, diluted 1:1 with Bradford reagent and incubated at room temperature for 10

minutes. Samples were loaded onto a plate reader and absorbance was measured at 595 nm. Three samples were taken for each concentration, and compared to the BSA calibration to calculate the total protein content.

2.4. Apparatus and recording buffers for imaging and electrophysiological experiments
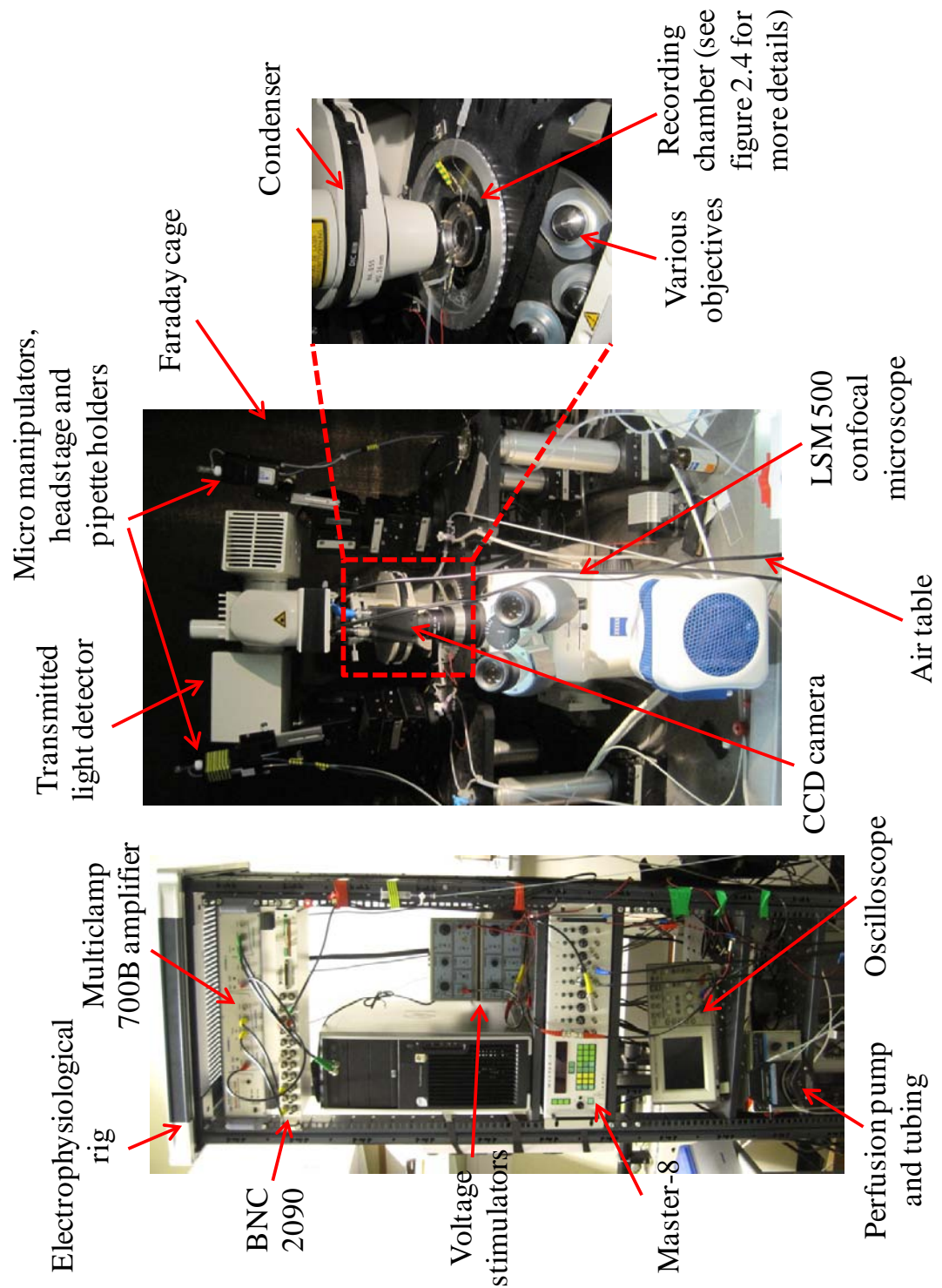
Figure 2.3: The experimental rig. *The electrophysiological and imaging setup. Left: the electrophysiological rig contained the amplifier, stimulators, Master8 programmer,*

oscilloscope and perfusion pump. Middle: the Zeiss LSM 510 confocal microscope was placed on an air table to minimise vibrations, and surrounded by a Faraday cage to eliminate electrical interference during electrophysiological recordings. The perfusion system was attached to the outside of the Faraday cage. Micromanipulators were used to perform electrophysiological experiments. Right: the recording chamber (see figure 2.4 for more detail) was placed in the light path of the microscope. The condenser was used to focus the DIC image into various objectives.

As there was a large overlap in apparatus and buffers used for confocal imaging and electrophysiological experiments, the entire experimental set-up is illustrated (figure 2.3), and is described in table 2.8. The custom-made recording chamber is depicted in figure 2.4. The recipe for the extracellular buffer (EB) used in all experiments (unless otherwise stated in the results) is listed in table 2.9.
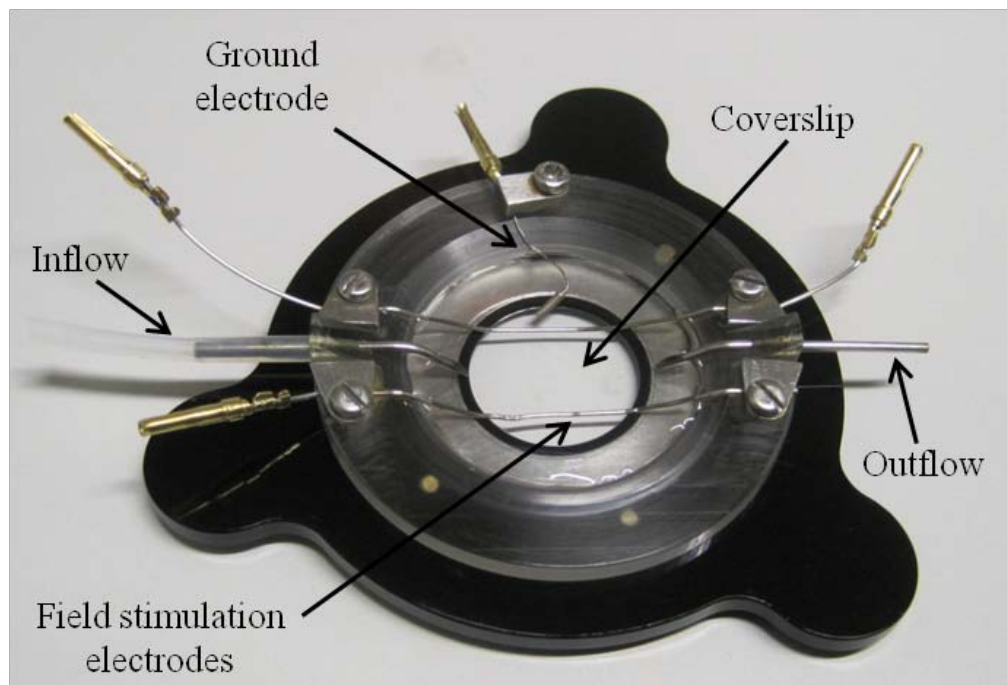
Figure 2.4: The recording chamber. *The cells were plated onto glass coverslips and secured in a custom-made recording chamber for the duration of the experiment. A*

rubber O-ring was used to prevent leakage of the extracellular buffer. Two parallel

platinum electrodes were used to evoke field stimulation across the coverslip. A

silver/silver chloride ground pellet was used during electrophysiological experiments to

reduce electrical noise. The coverslip was perfused with fresh EB during experiments

via the in- and outflow.

Table 2.8: Confocal microscope and periphery apparatus

Equipment	Source	Usage
LSM 500 confocal microscope	Zeiss	Used for confocal microscopy imaging experiments, including various objectives, condenser and photomultiplier tube (see text). Run from computer 1
Air table	TMC	Isolates vibrations for steady imaging. The microscope, recording stage and chamber, and micromanipulators for electrophysical recordings are placed on the air table.
Faraday cage	Custom made	Reduced electrical noise. The Faraday cage confines the microscope and electrophysiological recording apparatus. Everything in the faraday cage is electrically grounded.
CCD Camera	Sony: XC–ST 30CE	Used to visualise cells in transmitted light settings. The image acquired is observed using PatchVision software, run on computer 2.
Perfusion system	Custom made	Gravity perfusion system used to continually perfuse cells in the chamber with fresh extracellular buffer. The perfusion was rinsed with ddH$_2$O between experiments and with 20% ethanol daily.

Perfusion pump	Masterflex: Easyload II	Pump used to drive perfusion.
Master-8	A.M.P.I	Programmed to apply different electrical stimulation paradigms to the recording chamber. The Master-8 is programmed via a software interface, run on computer 3. It is connected to the chamber via two constant voltage isolated stimulators.
Constant voltage isolated stimulators	Digitimer: DS2A – Mk II	2 connected in series to apply voltage across the stimulation chamber. These are used in conjunction with the Master-8 to apply a voltage of 15 V across the chamber.
Oscilloscope	Tektromix: TDS 1002	The oscilloscope monitors voltage stimulation applied to the chamber.
Micro manipulators	Scientifica	Micro manipulators used to direct recording pipettes during electrophysiological recordings.
Headstage	Axon Instruments	Contains voltage clamp and voltage follower circuits for voltage and current clamp recording (see text). Connected to the micromanipulators.
Pipette holder	Custom made	Used to securely hold pipettes. Connected to the headstage.
Multiclamp 700B amplifier	Axon instruments	Amplifier used for electrophysiological recordings (see text). Run on computer 3
BNC 2090	National instruments	Analogue-to-digital signal converter. Used to communicate the output of the amplifier with the data acquisition (DAQ) board.
Recording chamber (figure 2.4)	Custom made	Holds coverslip during experiment. The chamber includes an inflow and outflow for the perfusion, parallel platinum field

		stimulation wires (attached to the voltage stimulators) and a ground pellet.
P97, Flaming/brown micropipette puller	Sutter Instruments Company	Used to pull recording pipettes
Filamented borosilicate glass pipettes	Warner Intruments	Pipettes pulled to a resistance of 3.5-6 MΩ

The EB (table 2.9) was used in all experiments, unless otherwise indicated in the results.

Table 2.9: Composition of experimental extracellular buffer (EB)

Buffer	Composition (mM)	Provider
Extracellular pH 7.4 with 10 M NaOH, Osm 310 mmol/Kg Made daily	125 NaCl	Sigma
	2.5 KCl	Sigma
	2 $CaCl_2$	Sigma
	2 $MgCl_2$	Sigma
	30 Glucose	Sigma
	25 HEPES	Sigma

Several software programs were used throughout the project to acquire and analyse data (table 2.10).

Table 2.10: Acquisition and analysis software table

Software	Source	Usage
LabView software	National Instruments and custom written	Acquisition software for electrophysiological experiments, used to record output from the

		amplifier. Software run on computer 3.
Windows Electrophysiology Disk Recorder (WinEDR v 3.0.1) software	Dr. John Dempster, University of Strathclyde, Glasgow	Software for mEPSC acquisition, run on computer 3.
LSM Viewer	Zeiss	Viewing confocal images offline.
PatchVision CCD camera software	Scientifica Ltd.	Viewing coverslip in transmitted light mode. Software run on computer 2.
ImageJ	Wayne Rasband, National Institutes of Health, USA	Viewing and analysing confocal images offline.
SigmaPlot	Systat Software Inc.	Data analysis and manipulation
Mathcad	PTC	Data fitting and modelling

2.5. Imaging of vesicular recycling with FM dyes

All experiments were performed at room temperature (20 - 22°C).

2.5.1. Reagent and buffers

The extracellular buffer was supplemented with neurotransmitter receptor antagonists (table 2.11) to inhibit recurrent activity.

Table 2.11: Extracellular ion channel blockers used to minimise recurrent activity

Drug	Target	Stock conc.	Final conc.	Storage	Provider
NBQX (2,3-dihydroxy-6-nitro-7-sulfamoyl-benzo[f]quinoxaline-2,3-dione)	AMPA receptor antagonist	25 mM	10 μM	-20°C	Ascent Scientific
DL-AP5 (DL-2-Amino-5-phosphonopentanoic acid)	NMDA receptor antagonist	100 mM	50 μM	-20°C	Ascent Scientific
Picrotoxin (PTX)	$GABA_A$ receptor antagonist	50 mM (in DMSO)	50 μM	-20°C	Sigma

The following styryl FM dyes were used in different experiments to label recycling vesicles and study synaptic recycling dynamics (and see chapter 5, figure 5.1 for dye molecular structures).

Table 2.12: FM dyes and analogues for labelling recycling vesicles

Fluorescence dye	Ex/Em wavelength (nm)	Stock conc.	Final conc.	Storage	Provider
SynaptoRed C1 (SRC1)	558/734	20 mM	200 μM	-20°C	Biotium, USA
FM 1-43	510/626	1 mM	12.5 μM	-20°C	Invitrogen
FM 2-10	506/620	20 mM	200 μM	-20°C	Invitrogen
FM 4-64	558/734	1 mM	10 μM	-20°C	Invitrogen

2.5.2. Confocal microscope settings

All imaging experiments were carried out using a 63x/1.4 NA oil immersion objective. Cultures were imaged at a resolution of 1024x1024 pixels, with the pixel size set to 0.14 μm and a pixel dwell time of 1.60 μs. This gave a total area of ~ 143 μm^2, which typically contained several hundred boutons.
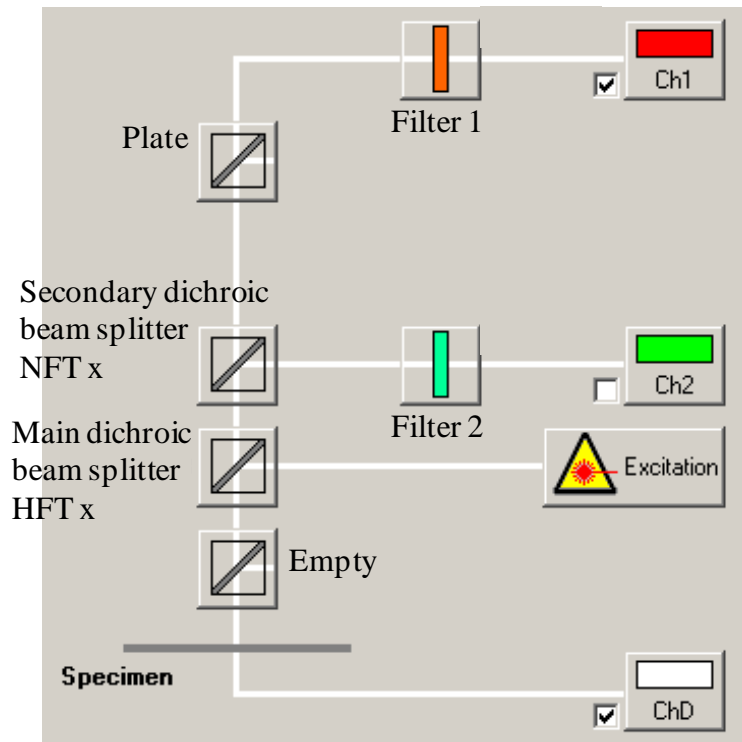
Figure 2.5: Light path of the confocal laser setup. *The laser beam (labelled excitation) passed through the main dichroic beam splitter, which diverted the beam towards the specimen. The fluorescence signal from the SRC1 passed back through the main dichroic beam splitter, and through the secondary dichroic beam splitter, which directed the beam to one of two recording channels (Ch1 or Ch2). The light passed through a filter and was collected by the channel PMT. See text for filter combinations. Image modified from Zeiss LSM software*

The pinhole was opened fully (1000 μm) to maximise photon collection, as high spatial resolution in the z-direction was not required. Three z-stacks were imaged, 0.75 μm apart, to incorporate boutons which may be in different focal planes. The laser light (figure 2.5) passed through the main dichroic beam splitter (HFT x, where x is the threshold wavelength), which reflected light of a lower wavelength than x and passed higher wavelengths. Laser light illuminated the specimen, and the subsequent emitted fluorescent light passed back through the main beam splitter and either passed through or was reflected by the secondary beam splitter (NFT x) into channel 2. Emitted light was collected in either channel 1 (Ch1) or channel 2 (Ch2), after being filtered by filter 1 or 2.

Different filter and beam splitters were used to measure the emission from the different dyes. SRC1 and FM 4-64 were excited with the 488 nm line of an argon laser and emission fluorescence collected via a long pass (LP) 585 nm filter by Ch1. The light passed through a HFT 488 and a NFT 543 beam splitter. FM 1-43 and FM 2-10 were excited with the 488 nm line laser and emission fluorescence collected via a long pass (LP) 505 nm filter by Ch2. The light passed through an HFT 488/543 (which is optimised to reflect light of wavelength 488nm and 543 nm, and transmits all other wavelenghts) and a NFT 543 beam splitter.

Gains on the photomultiplier tubes (PMT) were determined for individual experiments using the range indicator pallet to eliminate saturation of the fluorescent signal. The amplifier offset was set to 0 and the amplifier gain to 1 throughout experiments. The laser was allowed to warm up and stabilise for two hours before imaging. It was set to

50% of the maximal power and 1% output, to provide sufficient illumination whilst reducing the risk of photodamage to the culture.

2.5.3. Calibration of the optical efficiency of the microscope

Experiments were carried out over several months, during which time there were changes in the efficiency of the confocal microscope in converting photons into the fluorescence signal. These changes were due to a number of factors: fluctuations in the laser power, shifts in the optical path alignment, the effectiveness of the PMT in amplifying the signal, and the cleanliness of the optics. These changes were monitored using a fluorescent standard – an Alexa 555 calibration slide – that allowed individual experiments to be compared accurately, by adjusting the fluorescence signal against a constant standard. The calibration was based on the following theoretical idea:

Considering a typical experiment, the fluorescence signal collected could be described as:

$$F = y_0 + \alpha S \qquad\qquad \textbf{Equation 1.1}$$

where,

F = Measured fluorescence signal of the experiment

y_0 = Dark current offset. The PMT response when there was no illumination.

α = Scaling factor determined by laser intensity, PMT gain and variations in the optical path of the microscope

S = Number of fluorescent molecules in the confocal volume

The dark current offset, y_0 was measured daily with the Alexa 555 calibration slide after switching off the laser. This value could be subtracted from F, to give the adjusted fluorescence signal, f.

$$f = F - y_0 = \alpha S \hspace{4cm} \textbf{Equation 1.2}$$

Similarly, the Alexa 555 calibration slide fluorescence could be denoted as:

$$F_C = y_0 + \alpha S_C$$

where,

F_C = Measured fluorescence signal of the calibration slide

y_0 = Dark current offset. The PMT response when there was no illumination

α = Scaling factor arising from fluctuations in the optical efficiency of the microscope (as above)

S_C = Number of fluorescent molecules in the confocal volume of the calibration slide

Again, the signal can be adjusted for the dark current:

$$f_C = F_C - y_0 = \alpha S_C$$

To normalise the experimental fluorescence to the calibration fluorescence,

$$f_{normalised} = \frac{f}{f_c} = \frac{\alpha S}{\alpha S_c}$$

$$f_{normalised} = \frac{S}{S_c} \hspace{4cm} \textbf{Equation 1.3}$$

By dividing by the maximal signal from the Alexa 555 calibration slide, the normalised fluorescence no longer depended on α and experiments carried out over several months could be accurately compared with each other.

The calibration slide itself was made from a large stock of 20 μM Alexa 555 in 50% glycerol. Alexa 555 was of particular use as the fluorescence spectrum overlapped with the FM dyes and Fluo-4. Each day, a slide was prepared with a 10 μl drop of 20 μM Alexa 555, and a z-stack through the dye was imaged (21 slices, 3.5 μm apart) using the same optical settings as the experiment (figure 2.6a, upper panel). The fluorescence signal for 5 areas (mean ± s.e.m) was imaged (figure 2.6a, lower panel). After measuring the z-stack, the laser was switched off in order to get a value of the dark current offset (Y_0, figure 2.6b). To estimate F_c, we took the mean of maximal values measured in five different areas. To ensure that this gives an unbiased estimate of F_c, we also checked the linearity of the fluorescence signal with concentration. Serial dilution slides of Alexa 555 were made from the stock, and a z-stack measured as before (figure 2.7). Once F_c and y_0 had been established for each experiment, the measured fluorescence signal could be adjusted in order to compare individual experiments.
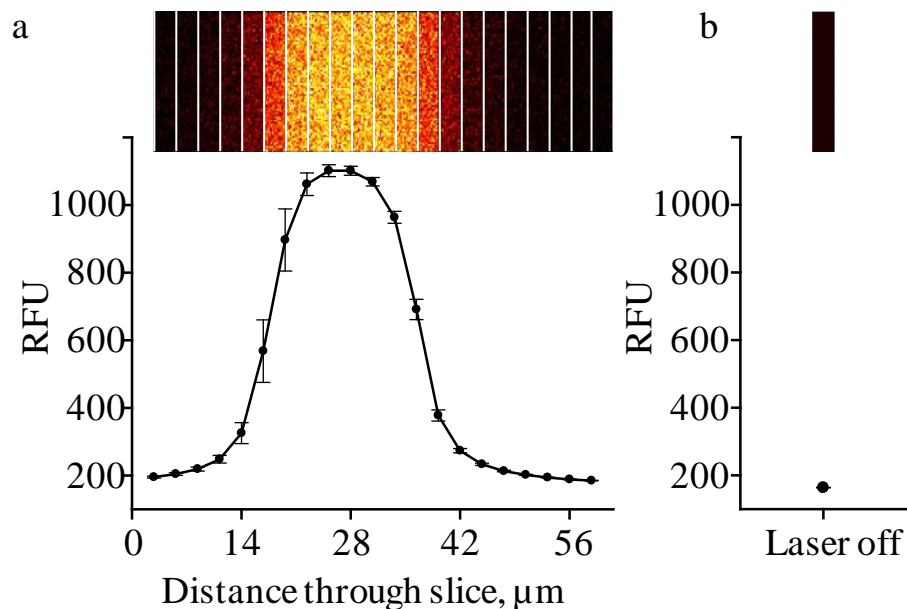
Figure 2.6: Calibration of the confocal setup with Alexa 555. (a) *Top panel, z-stack images of Alexa 555 fluorescence in a slide containing a drop of 20 μM Alexa 555.*

*Each slice was 3.5 μm apart. Bottom panel, dependence of Alexa 555 fluroescence signal on z coordinate. (n=5 regions from one slide, mean ± s.e.m) (**b**)Top panel, dark image of the same sample when the laser was switched off. Bottom panel, fluorescence signal when the laser was switched off, giving a measure of the dark current (n=5 regions from one slide, mean ± s.e.m)*
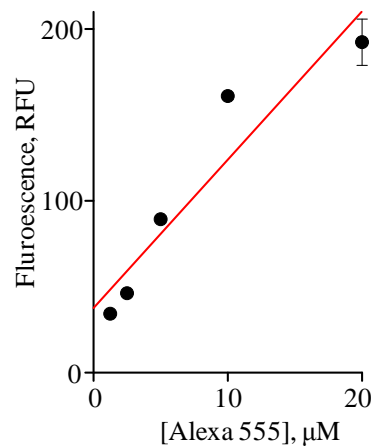
***Figure 2.7: Linearity of fluorescence signal with increasing concentrations of Alexa 555.** Increasing concentrations of Alexa 555 were measured using the same type of slide as in figure 2.6, to confim the linearity of Alexa 555 with concentration.*

2.5.4. Experimental procedure – destaining experiments

Exact protocols for individual experiments are described in the results chapters, although the loading process was identical in all experiments. Here, the main experimental method is described. The electrical stimulation paradigms used during the experiment are listed in table 2.13.

Table 2.13: Master8 stimulation protocols

Paradigm	Frequency, Hz	Number of pulses	Number of rounds	Delay between rounds, sec
Loading	30	120	4	20
RRP drop	30	60	1	-
Low frequency stimulation	0.5	300	1	-
Complete destaining to determine background fluorescence	10	300	3	120

A coverslip was placed in the chamber, and connected to the gravity perfusion system, at a flow rate of ~1 ml per minute. The perfusion was stopped and buffer allowed to drain, leaving ~400 μl remaining in the chamber. The stimulation intensity was adjusted to 12.5 V, and the selected dye was added and mixed. The loading paradigm was applied. 40 seconds after the last pulse the dye was removed with fresh extracellular buffer (5 x 1 ml washes), then the perfusion restarted for 15 minutes. During washing, an area with sufficient individual puncta was located and the optimal focus found. A focus template was created, using the laser reflection from the coverslip, so there would be a fixed distance between the surface of the coverslip and the region of interest. The gain of the PMT was adjusted to avoid signal saturation.

After 15 minutes of washing, imaging was started. The total recycling pool, RP was estimated as the total fluorescence at either the start of washing or at the start of imaging. The region was imaged every minute (refocusing between each image) in the absence of stimulation to obtain measurements for the spontaneous destaining rate, K_{sp}.

The *RRP* drop paradigm was applied to measure the relative size of the *RRP* in comparison to the *RP* (*RRP/RP*), followed by further imaging with no stimulation. The low frequency stimulation was applied for 10 minutes to measure the AP-evoked destaining rate K_{ev}. At the end of experiments, cells were subjected to the complete destaining paradigm. The region was imaged 5 times to determine the background fluorescence.

2.5.5. Analysis

Images were analysed in two steps: first, boutons were selected, and then the fluorescence trace from each boutons fitted. Boutons were selected using a custom written ImageJ macros. This incorporated the following pre-written plugins: LSM Toolbox ver 4.0d (2008, Patrick Pirrotte), Image 5D (Joachim Walter), MultiStackReg (Brad Busse) Substack Maker (Anthony Padua, Daniel Barboriak, MD). Time stacks of Ch1 (fluorescence channel) images were run through the macros to time-sort, z-project and x-y align the images. Active boutons were identified – a mask was created by subtracting an average of the background images (last 5 images) from the average of the initial 5 images. Boutons were selected using the LUT green fire blue for easy visualisation. Any boutons with overlapping signals were discarded, as were any in regions of high background fluorescence. Once all potential boutons were identified, the selected regions of interest were applied to the time stack images, and the area and mean grey value at each time point for each individual bouton was extracted to a SigmaPlot file. At this point, data was adjusted to take into account the Alexa 555 calibration (see figure 2.6 and section 2.5.3)

The data from the selected boutons were run through a specially written MathCad program in order to fit the destaining curves to obtain values for K_{AP}, K_{sp}, *RP*, *RRP*,

RRP/RP and the average fusion probability of individual vesicles, p_v. This program split the data into several stages, depending on the experimental protocol used. For typical experiments, these were: before the *RRP* drop, after the *RRP* drop, during low frequency destaining, and after background destaining. For each stage, the start and end times and corresponding frame numbers were specified. The MathCad program fitted data in each stage with an exponential fit, $F = ae^{-bt}$. For each bouton, the parameters a, b and the goodness of the fit χ^2 were calculated, using both absolute and normalised values. These values were placed in separate columns of a table and could be further sorted to remove outliers.

For the two spontaneous stages (before and after the *RRP* drop), the values K_{sp1} and K_{sp2} were fitted with the same exponential fit $F = ae^{-bt}$, to give a single value for K_{sp}. This also removed boutons where K_{sp1} and K_{sp2} were substantially different. Boutons with χ^2 for any stage larger than 2.5×10^{-3} were removed. For the third stage (during 0.5 Hz stimulation) the exponential fit, $F = ae^{-bt}$ was implemented to estimate K_{ev}. As for the spontaneous fitting, any boutons with χ^2 larger than 2.5×10^{-3} were removed. The MathCad program allowed the plotting of both the average trace of all boutons in the experiment, and individual boutons, giving a visual confirmation that the experiment was successful.

Once all unselected boutons were removed by the MathCad program, the parameters for the remaining boutons were transferred back into SigmaPlot. In SigmaPlot, a specially designed transform was applied to the data to extract several parameters. For each bouton, the absolute size of the *RP* was calculated by approximating $F = ae^{-bt}$ for K_{sp} to the beginning of imaging (i.e. at t=0), and to the beginning of the wash (i.e. at t = -

900s). The ratio *RRP/RP* was estimated by calculating the difference between $F = ae^{-bt}$ at end of stage one and the beginning of stage two. An estimate of the size of the *RRP* was then determined.

The measured evoked destaining rate, K_{ev} was calculated by estimating the parameter b for stage 3. As K_{ev} and K_{sp} were in units of rate (s^{-1}), each was multiplied by destaining frequency (0.5) to get a rate per AP (AP^{-1}). The evoked destaining rate corrected for spontaneous release, K_{AP} ($K_{AP} = K_{ev} - K_{sp}$) could be deduced. Finally, all selected boutons from a particular set of experiments were combined, and parameters plotted in SigmaPlot.

2.6. Electrophysiological methods

2.6.1. Reagents and Buffers

The recipe for the intracellular buffer used in all electrophysiological experiments is listed in table 2.14. As only excitatory synaptic transmission was to be observed, the extracellular buffer (table 2.9) was supplemented with GABAa and GABAb receptor antagonists (table 2.15) to block inhibitory synaptic transmission. mEPSCs were recorded in the presence of tetrodotoxin (TTX) to inhibit AP. The contribution of P/Q- and N-type VGCCs to spontaneous and evoked neurotransmitter release was determined using the specifc VGCC blockers ω-conotoxin GVIA (ω-ctx) and ω-aga Iva (ω-aga).

Table 2.14: Intracellular solution recipe

Buffer	Composition (mM)	Provider
Intracellular pH 7.2 with 10 M KOH, Osm 290 mmol/Kg. Stored at -20°C Filtered with 0.2 µm filter	130 Potassium gluconate	Sigma
	10 KCl	Sigma
	1 EGTA	Sigma
	4 Mg-ATP	Sigma
	0.5 Na_2GTP	Sigma
	10 HEPES	Sigma
	10 phosphocreatine	Sigma

Table 2.15: Ion channel and post-synaptic receptor antagonists and Ca^{2+} chelators

Drug	Target	Stock conc.	Final conc.	Storage	Provider
Picrotoxin (PTX)	$GABA_A$ receptor antagonist	50 mM (in DMSO)	50 µM	-20°C	Sigma
CGP 55845	$GABA_B$ receptor antagonist	1 mM (in DMSO)	1 µM	-20°C	Tocris Bioscience
Tetrodotoxin (TTX)	Na^+ channel antagonist	1 mM	1 µM	-20°C	Ascent Scientific
ω-conotoxin GVIA (ω-ctx)	N-type Ca^{2+} channel antagonist	500 µM	5 µM	-20°C	Ascent Scientific
ω-agatoxin IVA (ω-aga)	P/Q-type Ca^{2+} channel antagonist	25 µM	250 nM	-20°C	Ascent Scientific
EGTA-AM	Slow Ca^{2+} chelator	20 mM	20 µM	-20°C	Sigma

2.6.2. Experimental procedure – recording miniature synaptic currents

Cells were patched in the somatic whole-cell voltage-clamp configuration and both miniature excitatory post-synaptic currents (mEPSCs, or 'minis') and evoked excitatory post-synaptic currents (EPSCs) were recorded, via a MultiClamp 700B operational amplifier, filtered at 4 kHz and digitized at 10 kHz. Filamented borosilicate glass pipettes were pulled to a resistance of 3.5-6 MΩ. These were filled with intracellular buffer and placed in a pipette holder over an Ag/AgCl$_2$ electrode (The chloride coating was regularly replaced by electroplating to avoid tip potential drift.) attached to the headstage.

A coverslip was placed in the microscope-mounted recording chamber and was continually perfused throughout the experiment (~1 ml per minute flow rate) at room temperature. The perfusion was allowed to stabilise before commencing, to reduce noise. A suitable cell was located before a pipette was filled and placed into the headstage. Positive pressure was applied to the pipette (to reduce blocking) before it was lowered into the bath using the coarse manipulators. The pipette resistance was calculated using a 5 mV seal test, and the pipette offset zeroed (to ensure the membrane voltage and command voltages were equal). The pipette was located over the cell, and then lowered. The objective was changed from 10x to 63x, and the pipette brought into the vicinity of the cell. Just before patching, the pipette offset was zeroed again, and the cell gently touched by the tip of the pipette (in a diagonally-moving approach mode), observed as a dimple forming on the cell surface. The pressure was released and a gentle suction applied to achieve a gigaseal between the membrane and pipette. Cells were discarded at this point if a gigaseal was not obtained. The cell was clamped to a

holding potential of -70mV, and fast and slow capacitance transients cancelled by the multiclamp software.

Once a gigaseal was deemed stable, a short sharp suction was applied to rupture the membrane and enter whole cell configuration, and a timer started to reliably record drug application times. The access resistance was monitored and more suction applied in order to stabilise it to below 25 MΩ if necessary (cells were discarded if the access resistance drifted by more than 25% over the course of the experiment). The patch was held for 7 minutes before recording to allow for equilibrium between the cell and the pipette. Meanwhile, the software was toggled between WinEDR v3.0.1 and LabView 8.0 to ascertain whether there were any mEPSCs (roughly 1 in 4 cells had no apparent mini activity) whilst monitoring the stability of the patch.

If mEPSCs were present, the baseline was recorded in WinERD for 10 minutes. A test pulse (5 mV, 200 ms in duration) was applied every two minutes to monitor access resistance, and gentle suction applied to the pipette if it was drifting. VGCC blockers were added to the perfusion at 10 minutes (either ω-aga alone or with ω-ctx), and the cell continuously recorded for a further 25 minutes (The drugs typically took 10 minutes to equilibrate and take effect). The perfusion was rinsed with ddH$_2$O and ethanol between experiments to remove any trace of previous toxins.

For experiments with the Ca^{2+} buffer EGTA-AM, EGTA-AM was added to the buffer after 5 minutes of recordings to measure the time-course of application and effect. For pre-incubated experiments, either EGTA-AM or the vehicle (DMSO) was added to the perfusion at the start of experiments, and cells incubated for 25 minutes before patching.

2.6.3. Analysis – mEPSC recordings

16 pA

100 ms
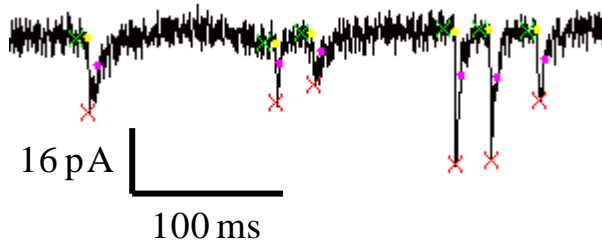
Figure 2.8: Analysis of mEPSCs. *A small section of a typical mEPSC trace, analysed using Mini Analysis Program 6.0.3. The program automatically detected miniature events and fitted them with four points: Baseline between the green cross and yellow dot; maximum amplitude with the red cross and the decay time with the pink dot.*

Raw traces were exported from WinEDR to Mini Analysis Program 6.0.3 and converted to .ABF files, using ABF Utility Program. The mEPSCs were initially detected using a peak detection algorithm (figure 2.8), which measured baseline (green cross to yellow dot), peak amplitude (red cross), and decay time (pink dot). Traces were checked manually for false positives and undetected events. The threshold was set to three times the root mean square of the baseline noise amplitude. Cumulative mini frequency directly before and 10 minutes after drug application was calculated and the acute effect of toxins quantified. Cells were discarded if there was a drift in the holding current (>100 pA) or access resistance (>25%), or if the frequency did not stabilize before drug applicaion.

2.6.4. Experimental procedure – recording evoked synaptic currents

Cells were patched in the same way as for mEPSC recordings, with one modification. Two cells, separated by no more than 100 μm were patched (figure 2.9) and were

checked for synaptic connections. Two typical examples (figure 2.9a and b) of paired

cells, at 10x (figure 2.9ai, bi) and 63x (figure 2.9aii, bii) magnification are illustrated.

The distance between the cells was ~30 μm (figure 2.9a), and ~24 μm (figure 2.9b), and

in these cases, the cells were synaptically connected in both directions (i.e. both cells

could be used as either pre- or post-synaptic).
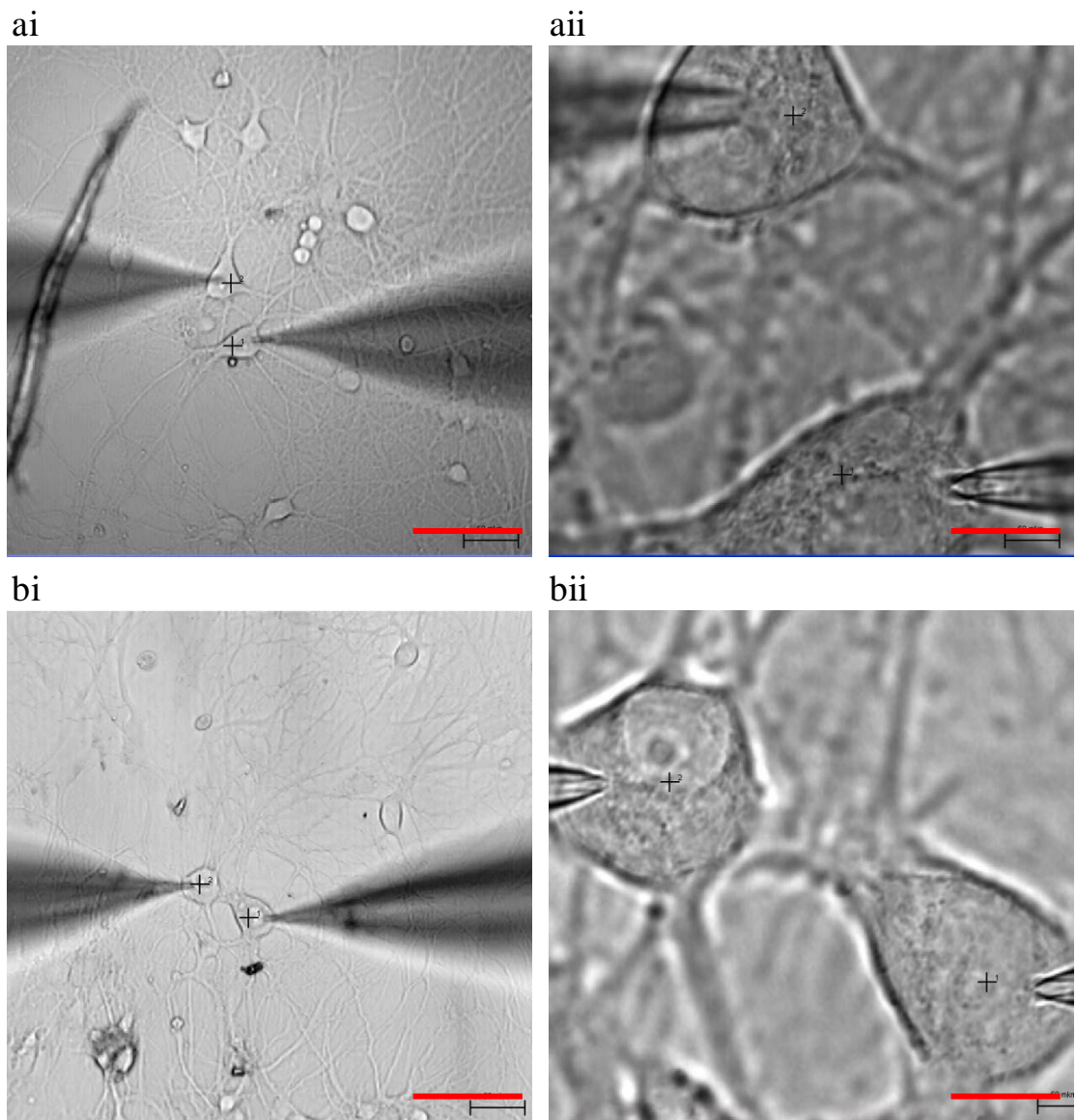
Figure 2.9: Two examples of pairs of cells patched for evoked EPSC recordings. (ai)

Two patched cells (under the 10x objective) were tested to see whether they were

*synaptically connected. (**aii**) The same cells in (**ai**) under 63x magnification. (**bi**) As in (**ai**). (**bii**) As in (**aii**). Scale bars: (**ai**), (**bi**) 50 μm.(**aii**), (**bii**) 8 μm.*

Both cells were held in voltage clamp at -70 mV using LabView 8.0, and a brief 3 ms voltage step of 80 mV (to +10 mV) was applied to one of the cells to produce an unclamped 'escape' current and pre-synaptic AP. The cells were toggled between pre- and post-synaptic to identify whether they were connected in either direction. Once a strong response (an EPSC of >50pA, with minimal failures) was established, the baseline was recorded for 15-20 minutes.

Toxins (ω-aga alone or with ω-ctx) were applied at 15 minutes to the perfusion system, and the effect on EPSC amplitude recorded. Drug application was alternated between experiments, and chamber and perfusion cleaned with ethanol and water in between applicaitons.

2.6.5. Analysis – eEPSC recordings
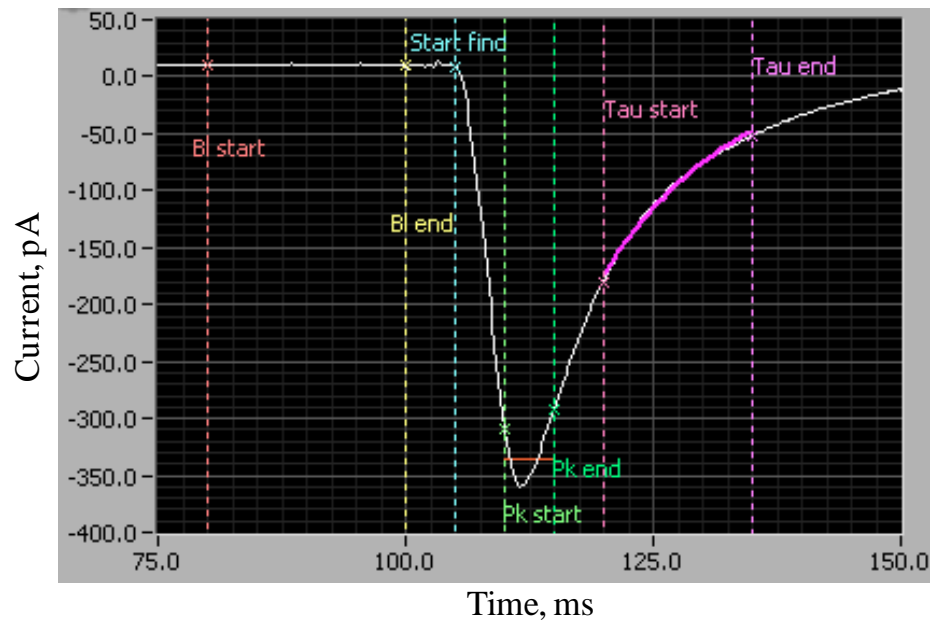
Figure 2.10: Analysis of EPSCs. The average EPSC peak for each experiment was calculated in LabView in order to calculate where to place the baseline and peak constraints. The baseline start (red cursor) and end (yellow cursor) were placed roughly 20 ms apart, 10 ms before the start of the peak. The start-find (blue cursor) was placed at the start of the EPSC to initiate the search for the EPSC. The maximum of the peak was calculated to be the maximal point between the peak start and end (green cursors). Typically the start-find, peak start and peak end were placed at 5 ms intervals, although this was adjusted for individual experiments. The time course of the EPSC decay could also be calculated (between tau start and end, purple cursors) although we did not use this in our measurements. The positions of the cursors were then applied to individual EPSC traces and the maximal amplitude of each EPSC calculated.

Data was analysed in LabView 8.0. The EPSC traces were averaged to find the position of the first peak, then start and end constrains were applied (Figure 2.10). These

constraints were: start and end of baseline; start-find; peak start and end; and tau start

and end. The experiment was then processed and the peak of each EPSC trace found.

The data was extracted and exported to SigmaPlot.

2.6.6. Statistical methods

All data (unless otherwise stated) was described by the mean and standard error of the

mean (mean ± s.e.m). Several different statistical tests were used throughout this thesis,

and are stated where used. The tests are listed in table 2.16.

Table 2.16: Statistical tests

Test	Use	Assumptions
One sample t-test	Tests whether the mean of a population has a value specified in the null hypothesis (e.g. chapter 6, figure 6.8b)	1. Population is normally distributed 2. Populations have similar variance
t-test	Tests whether the difference between two unrelated samples can be accounted for by sample error alone (e.g. chapter 4, figure 4.3)	1. Population is normally distributed 2. Populations have similar variance
Mann-Whitney	Tests whether the difference between two unrelated samples can be accounted for by sample error alone (e.g. chapter 4, figure 4.3)	Population is not normally distributed
Paired t-test	Tests whether the difference between two related samples can be accounted for by sample error alone (e.g. chapter 6, figure 6.11a-c)	Population is normally distributed
Kolmogorov-Smirnov test	Tests whether two sample cumulative distributions are drawn from the same distribution (e.g.	Population is not normally distributed

	chapter 8, figure 8.12b)	
One way ANOVA	To test whether several unrelated samples originate from the same distribution (e.g. chapter 7, figure 7.1a)	Population is normally distributed
Kruskal-Wallis ANOVA	Tests whether populations from which several unrelated samples originate have the same median (e.g. chapter 7, figure 7.1e)	Population is not normally distributed
Spearman-rank correlation	Tests the null hypothesis that the correlation between two variables is zero (e.g. chapter 6, figure 6.8a and b)	Population is not normally distributed

3. Development of an in vitro model to study disease-linked ion channel mutations in human neuronal-like cells

3.1. Introduction

Traditionally the functional effects of disease-linked human ion channel mutations (channelopathies) are studied using mouse neuronal models. There are two common strategies to do this: over-expression of WT and mutated human cDNAs encoding the ion channels of interest in primary cultures of hippocampal or cortical neurons from WT or KO mice; and generating KI mice that carry human disease linked mutations. Both approaches however can give controversial results due to: over-expression artefacts (van den Maagdenberg et al. 2004); differential effects of the same mutation in different species (Toru et al. 2000); differences in species auxiliary subunits and artefacts due to different splicing patterns (Kraus et al. 1998; Hans et al. 1999). To study human ion channel mutations with optical techniques, we wanted to develop a human neuronal-like cell culture model to compliment our experiments in mouse hippocampal cultures. To this end, we carried out preliminary experiments in the Ntera2 clone D2 (NT2) cell line which has been shown to differentiate into neuronal-like hNT post-mitotic cells (Andrews 1984; Pleasure et al. 1992, 1993; Görtz et al. 2004; Misiuta et al. 2006; Hartley et al. 1999).

NT2 is a human embryonal teratocarcinoma cell line, which was originally derived from a lung metastasis associated with a testicular germ cell tumour. Upon application of retinoic acid, approximately 5 % of NT2 cells differentiate into neuronal-like hNT cells (Andrews 1984), (Pleasure et al. 1993), and have been reported to exhibit characteristics similar to cultured neurons.

In hNT cells under phase-contrast microscopy, extensive neurite networks were observed, and identified to contain the same molecular markers as axons and dendrites

(Pleasure et al. 1992). Electron microscopy (EM) experiments carried out on hNT cells grown on an astrocytic feeding layer illustrated that synapse morphology was remarkably similar to previous reports at small central synapses from murine cultures (Pleasure et al. 1992; Hartley et al. 1999). In particular, the abundant synaptic profiles clearly showed copious small clear vesicles, located close to membrane specialisations, and several large dense-core vesicles, suggesting the formation of functional synapses. However, other studies suggested that neurite arborisations in hNT cells were shorter and thicker than in primary cultured neurons (Görtz et al. 2004), which led to a difference in network activity observed by microelectrode array experiments.

Extensive immunohistochemical studies have shown that during differentiation, NT2 cells loose neuroepithelial markers and gain markers specific for mature neurons (Munir et al. 1995; Mantione et al. 1995). The presence of synapsin I (Hartley et al. 1999), synaptophysin (Görtz et al. 2004), cytoskeletal polypeptides and cell surface antigens typical to CNS neurons (Pleasure et al. 1992) on differentiated hNT neruons have all been confirmed. The presence of these neuron-specific markers suggests that retinoic acid treatment does indeed differentiate NT2 cells into functional neurons. Furthermore, hNT cells can be electrically excitable. Spontaneous miniature excitatory and inhibitory post-synaptic currents were recorded at 5-week old hNT cells (Hartley et al. 1999) as were evoked post-synaptic currents (PSCs) in paired whole-cell recordings.

hNT cells have been shown to use several different neurotransmitters for signalling, including dompamine, GABA, acetylcholine and glutamate (Zeller et al. 1995; Saporta et al. 2000; Hartley et al. 1999; Misiuta et al. 2006). Indeed, when grown on a glial cell feeding layer, synapses from hNT cells were 71 % glutamatergic and 29 % GABAergic,

a very similar ratio to cultured hippocampal neurons (Vicario-Abejón et al. 1998, 2000; Christie et al. 2003; Varley et al. 2011). Furthermore, hNT cells contain TTX-sensitive Na^+ channels (Rendt et al. 1989), K^+ channels (Hartley et al. 1999) and L-, N-, P/Q- and R-type Ca^{2+} channels (Neelands et al. 2011).

For these reasons, we investigated whether this cell line was suitable as a human neuronal-like cell model for our optical and electrophysiological experiments.

3.2. Specific aims

- Create a stably transfected clonal NT2 cell line using a GFP marker construct, with the long term goal of transfecting cells with different WT and mutated voltage-gated Ca^{2+} channel subunits.
- Differentiate NT2 cells into hNT cells.
- Assess whether differentiated hNT cells are functionally comparable to dissociated cultured murine neurons.

3.3. Results

3.3.1. Major findings

- NT2 cells can be transfected and the production of stable clones is possible.
- Retinoic acid treatment over several weeks differentiates NT2 cells into hNT neuronal-like cells.
- Although hNT cells are morphologically similar to cultured hippocampal neurons, and produce spontaneous Ca^{2+} sparks, their firing properties differ significantly from cultured hippocampal neurons.

3.3.2. Transient transfection efficiency of NT2 cells is roughly 0.2 %
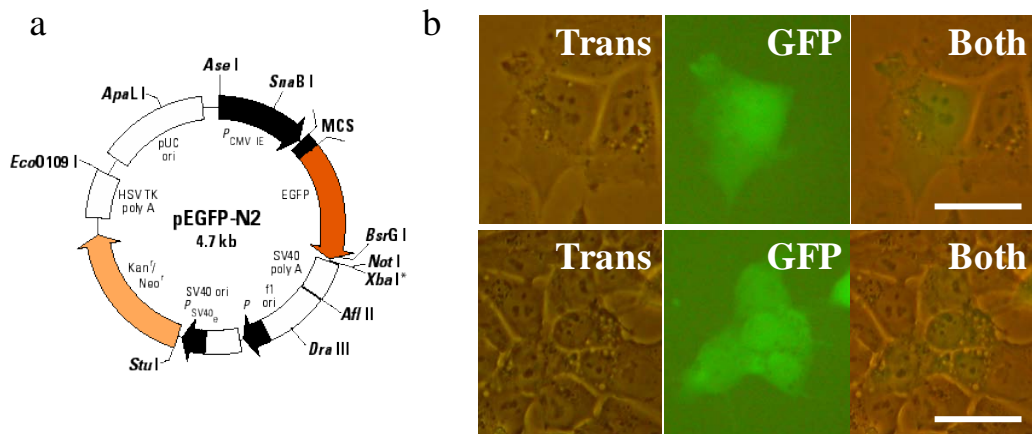
Figure 3.1: Optimisation of transient transfection using an enhanced green fluorescent protein (EGFP) marker. (a) pEGFP-N2 plasmid used to optimise transfection protocol. (b) Undifferentiated NT2 cells were transfected with the pEGFP-N2 construct using the transfection reagent Lipofectamine 2000. Two example regions with EGFP-positive cells are shown (top and bottom panels) in transmitted, GFP fluorescent and combined channels (left, middle and right respectively). Scale bar: (b) 50 μm

To study genetic mutations in VGCCs in hNT cells, we developed a transfection protocol which would allow us to stably transfect a gene of interest into the NT2 precursor cells before differentiation (Pleasure et al. 1992). To optimise the transient transfection protocol (see chapter 2, section 2.2.3), we used a marker plasmid (pEGFP-N2, figure 3.1a) which has resistance to the antibiotic geneticin and allows identification of transfected cells by GFP fluorescence

During optimisation, we attempted to use two transfection reagents - Escort III and Lipofectamine 2000 - to assess which produced the highest transfection efficiency. By

varying the amount of transfection reagent (0 – 10 µl per ml), we found that

Lipofectamine 2000 gave increasing efficiency up to 4 µl/ml, but was toxic to cells

above this amount. In contrast, Escort III was lethal to NT2 cells at all concentrations.

Next we varied the concentration of DNA (0 – 20 µg/ml), whilst keeping the amount of

Lipofectamine 2000 constant. 4 µg/ml of DNA gave an optimised efficiency of ~ 0.2 %

(Average number of green fluorescent cells counted over N =10 regions from n = 4

coverslips). Example NT2 cells transfected with pEGFP-N2 construct are illustrated

(figure 3.1b).

3.3.3. NT2 cells can be stably transfected
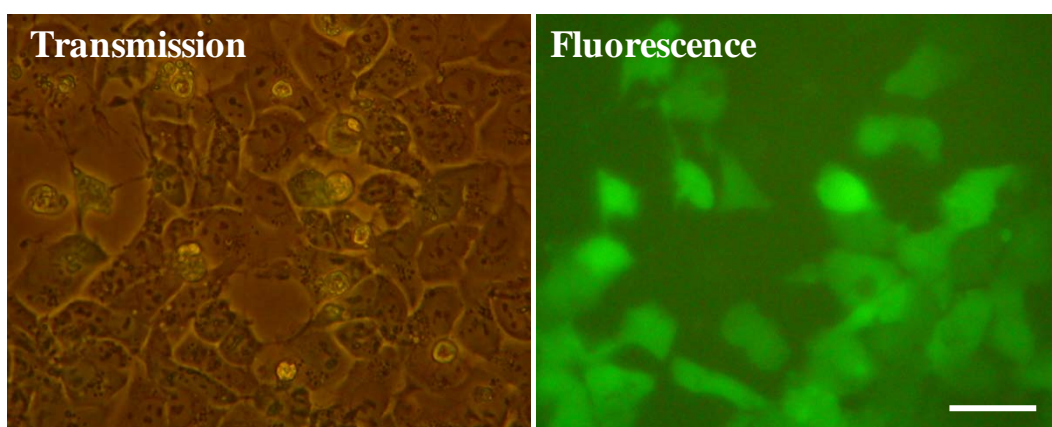
Figure 3.2: Stable transfection of NT2 cells with pEGFP-N2. Transfected cells were selected with the antibiotic geneticin. A region of a clonal cell group is illustrated in transmitted and fluorescent channels. Scale bar: 50 µm

To achieve stable transfections, 24 hours after transfection we removed cells by trypsin

application and seeded into 12-well plates at a density of ~10K cells per well (~20 – 50

transfected cells per well). To separate transfected from non-transfected cells, we

applied the antibiotic geneticin. 0.5 mg/ml geneticin per well was found to be optimal

for killing un-transfected cells, whilst not affecting cells expressing GFP. After several days' growth, clumps of green fluorescent cells could be seen (figure 3.2, note that the fluorescence optics on the tissue culture microscope were not optimised, hence cells with low expression were not seen as green)

3.3.4. NT2 cells are differentiated into neuronal-like hNT cells after retinoic acid application

To differentiate cloned NT2 cells into postmitotic hNT cells, we followed the guidelines in the Stratagene Cloning Systems guide (Stratagene Cloning Systems 1998). The differentiation process followed very closely previously published observations (figure 3.3, (Pleasure et al. 1993; Stratagene Cloning Systems 1998; Misiuta et al. 2006; Mantione et al. 1995; Kleppner et al. 1995; Pleasure et al. 1992). After two weeks in culture, cells became super-confluent, and by around 4 weeks, we clearly observed cluster of cells lying on top of a lower layer of cells, which can be seen in the image taken at 42 DIV. These clumps have been reported previously (Andrews 1984; Pleasure et al. 1993), and were found to be islands of hNT cells overlying progenitor cells.

After 6-7 weeks of differentiation, we began to purify the differentiated cells (figure 3.4). We performed three replating procedures, each of which aimed to separate hNT cells from the NT2 progenitor cells which had not differentiated. After the first replate the NT2 cells attached to the flask first and the phase-bright hNT cells could clearly be seen lying on top (figure 3.4, left hand panel). After the second replate, differentiated cells could clearly be seen and looked remarkably like cultured rat neurons, with rounded bodies and processes (figure 3.4, middle panel).
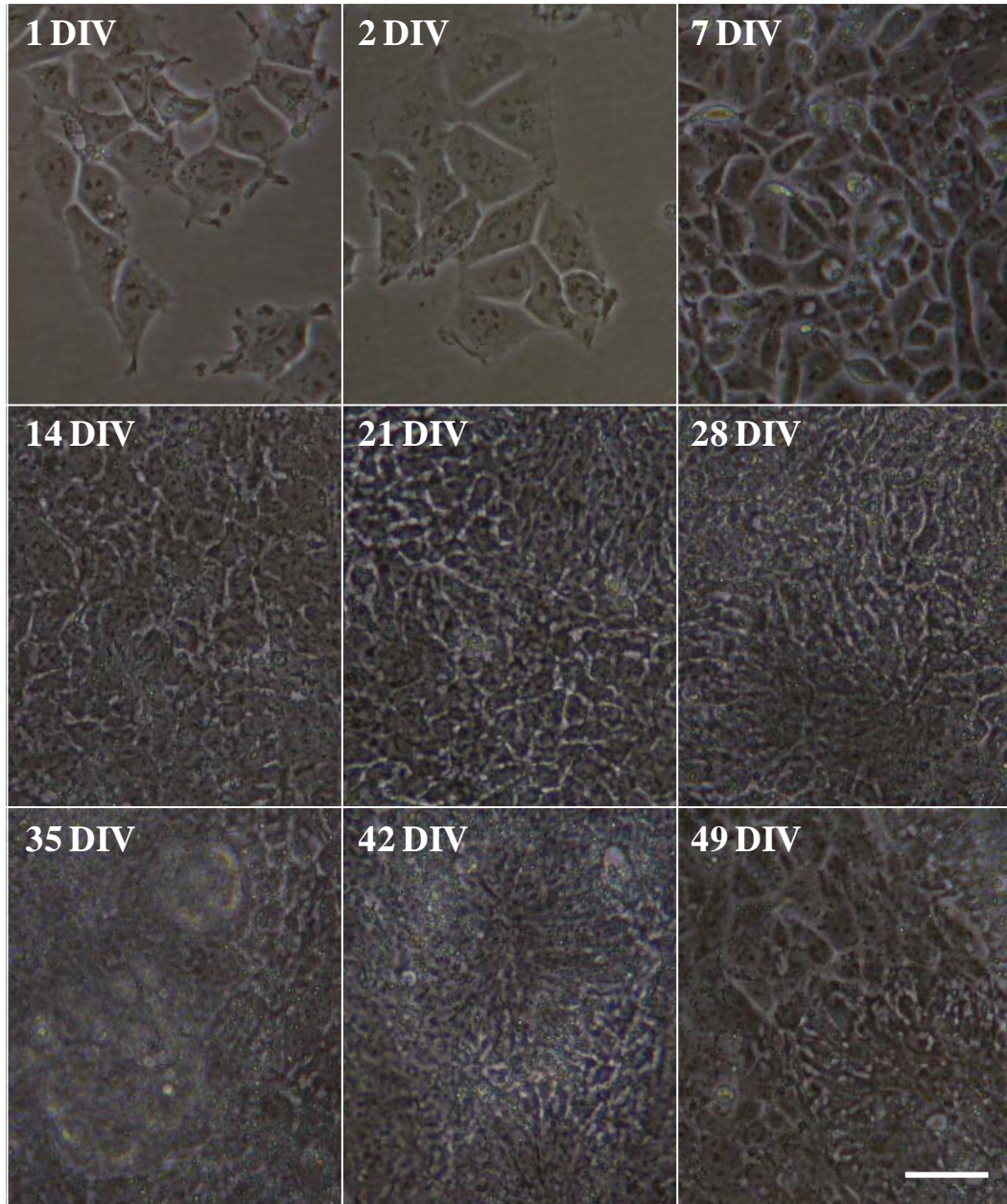
Figure 3.3: Differentiation of the NT2 cell line into hNT cells. *Images illustrating the*

development into hNT cells over time due to differentiation by retinoic acid treatment.

Cells are shown at 1 DIV, 2 DIV then at weekly intervals until 7 weeks. Cells became

super-confluent by 14 DIV, and formed islands (containing hNT cells) by 28 DIV, which

can clearly be seen here at 35 and 42 DIV. Scale bar: 50 μm
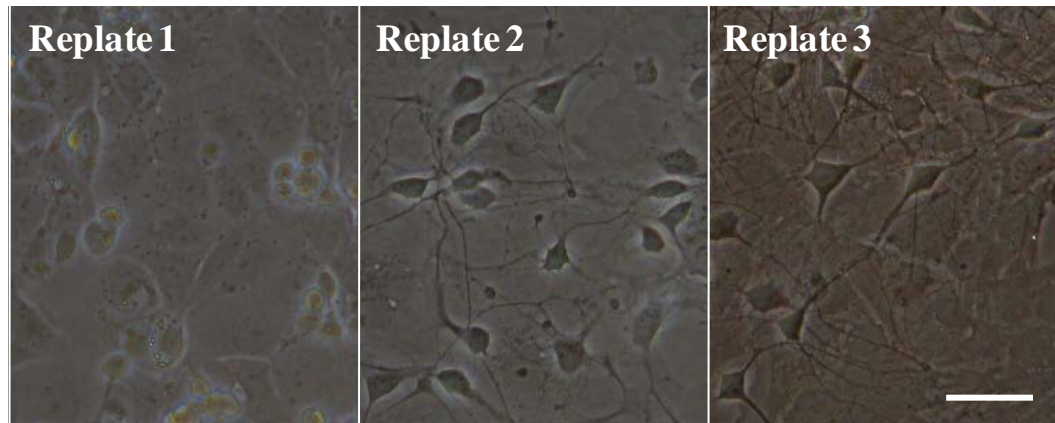
Figure 3.4: Replating differentiated hNT cells. There were three steps in the replating process to purify hNT cells. During replate 1, all cells were removed from flasks by trypsin application, and replated into large T225 flasks. Undifferentiated cells had a higher affinity for the plastic, so attached first, with the differentiated cells forming clusters on top of them. Replate 2 used gentle trypsin application (in Mg^{2+} and Ca^{2+}) to only remove this top layer of cells in order to purify the hNT cells. Mitotic inhibitors were included in the medium to inhibit cellular division. Finally, replate 3 was a further purification process and allowed the hNT cells to be plated onto rat glial cells. Scale bar: 50 μm

The intention of replate 3 was to plate cells onto a 100% confluent glial culture. In the study by Hartley and colleagues, they showed that hNT cells plated on rat glial cells underwent physiological, morphological and biochemical changes which resembled maturing rat neuronal cultures. This was in contrast to hNT cells plated on poly-D-lysine/Matrigel coated coverslips, which did not show such changes and had a lower survival rate. NT2 cells plated on glial cells had a similar morphological form to dissociated murine hippocampal neurons (figure 3.4, right hand panel). While the morphology was consistent with neuronal differentiation, our wider investigation of Ca^{2+} channel function also required neuronal physiological function, and the next set of

experiments were designed to characterise the biophysical properties of these differentiated neuron-like cells.

3.3.5. hNT neuronal-like cells do not have similar physiological properties to neurons

We performed several functional property tests on hNT cells after two weeks growth on glial cells (figures 3.5, 3.6 and 3.7), in the absence of NBQX, DL-AP5, and PTX. First, we patched cells in the whole-cell configuration and loaded with 200 μM of the morphological tracer Alexa 568 (figure 3.5, experiment performed by I. Pavlov). We observed developed neurites similar to those in cultured rat hippocamal neurons, including filopodia-like processes. However, the dendritic tree was not as extensive as we would expect from cultured neurons, as was also noted in the study by Görtz and colleagues (Görtz et al. 2004).
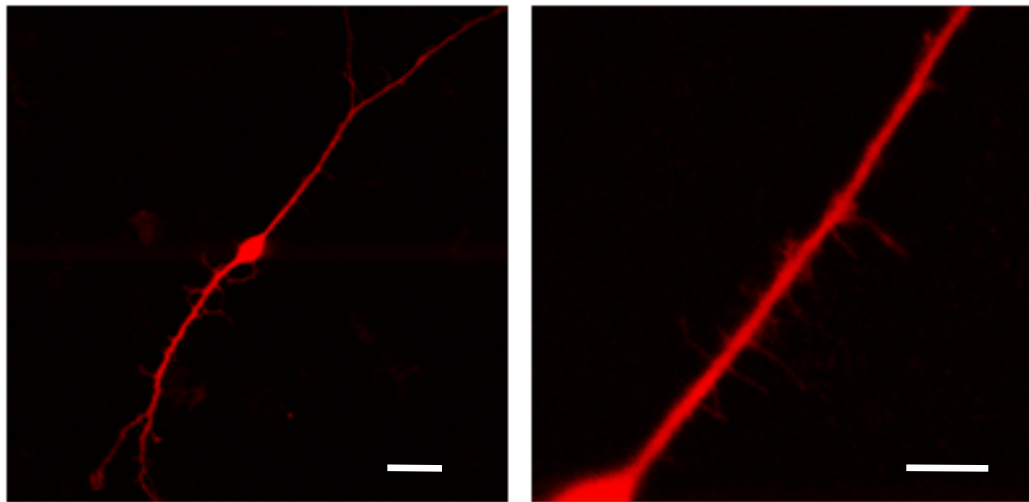
Figure 3.5: Morphology of a typical hNT cell, filled with the fluorescent tracer 200 μM Alexa 568. The differentiated hNT cells (after two weeks growing on a glial cell feeding layer) shared some similar morphological properties with other cultured hippocampal neurons of the same age. From the cell soma, there were projections (left

hand image) which contained filopodia-like structures (right hand image). Scale bar:

40 μm (left), 20 μm (right). **Experiments performed by K. Volynski**
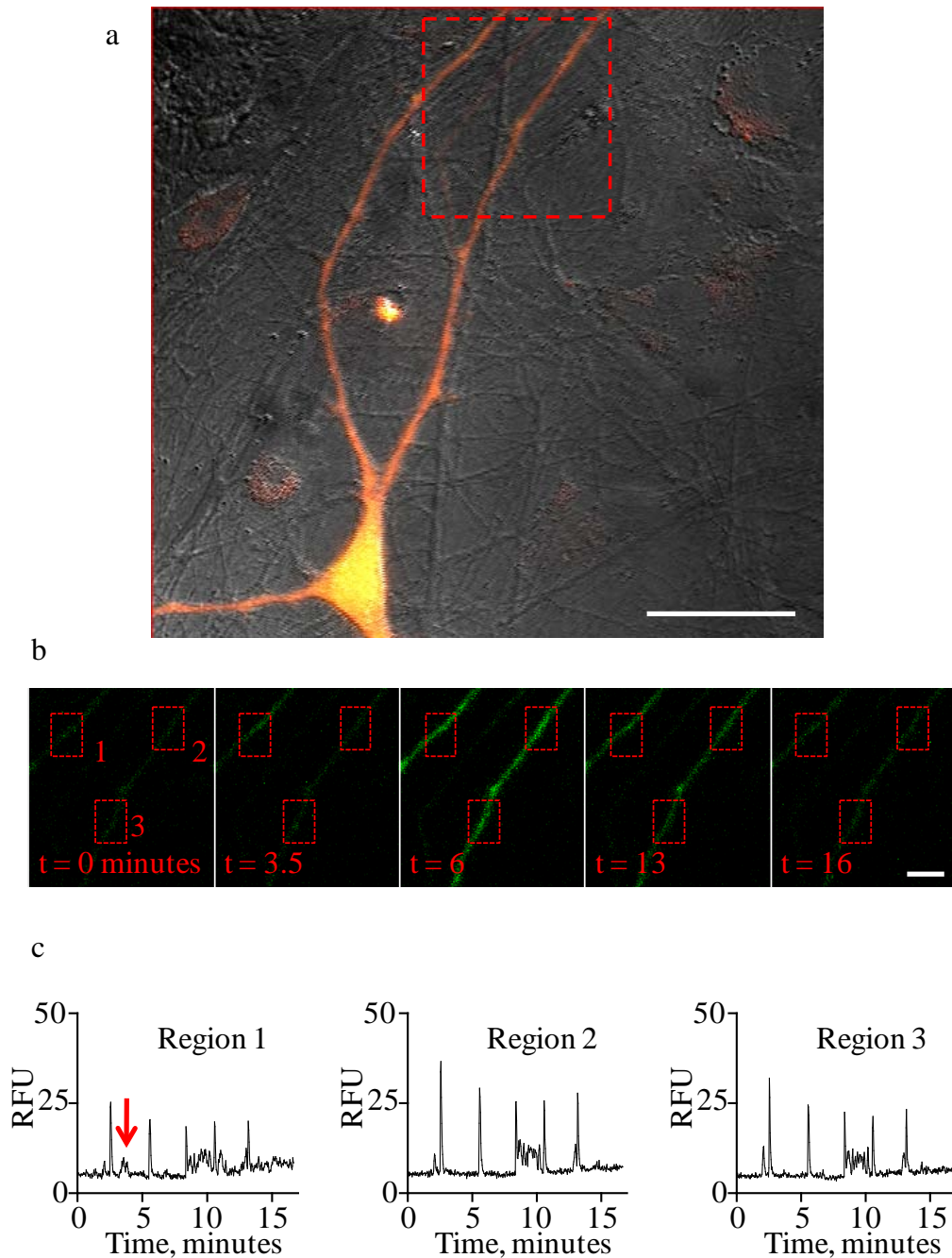
Figure 3.6: Ca²⁺ dynamics in hNT cells. *(a) Cells were loaded with 200 μM Alexa 568*

and 200 μM Fluo-4. (b) Boxed region from (a), showing time-delayed images of two

individual dendrite-like branches (c) Ca²⁺ traces for the three boxed regions in (b),

Secondly, we performed Ca^{2+} imaging experiments on hNT cells to ascertain whether there was any spontaneous Ca^{2+} signalling in these cells. Cells were whole-cell patch loaded with 200 μM Fluo-4 and 200 μM of the morphological tracer Alexa 568 (figure 3.6, experiment performed by I. Pavlov). After allowing for equilibration, cells were imaged for ~ 15 minutes and Ca^{2+} fluctuations recorded via Fluo-4 fluorescence changes (figure 3.6b). Interestingly, not only did we observe spontaneous global Ca^{2+} sparks (figure 3.6c), we also noticed local Ca^{2+} increases (region 1, red arrow), which were highly localised (~ 10 μM) within a branch.

Next, we carried out whole-cell current injection experiments in hNT cells that have been grown on a glial cell layer for two weeks (figure 3.7a), and compared the voltage traces to cultured hippocampal rat neurons of the same age (figure 3.7b, experiments carried out by K. Volynski). In these recordings the hNT cells failed to reproduce behaviour of primary neurons. The example hNT cell patched (figure 3.7a) showed amplitudes of APs comparable to that in rat neurons, and each was followed by a hyperpolarising component, suggesting that the hNT cells had functional sodium and potassium channels. However the APs produced by the hNT cells were significantly longer in duration (figure 3.7c, full width at half maximum, FWHM = 5.5 ± 0.13 ms) compared to those from rat neurons (FWHM = 2.44 ± 0.11 ms)

We also found that the apparent resting membrane potential for hNT cells to be around -30 mV in normal KMS intracellular solution in comparison to -58 mV for rat cells.

Therefore during our experiments -15 pA of current was injected to hold the cells at -60 mV. This suggested that the hNT cells did not possess the full complement of potassium channels that are present in primary neuronal cultures, leading to depolarised resting membrane potentials.
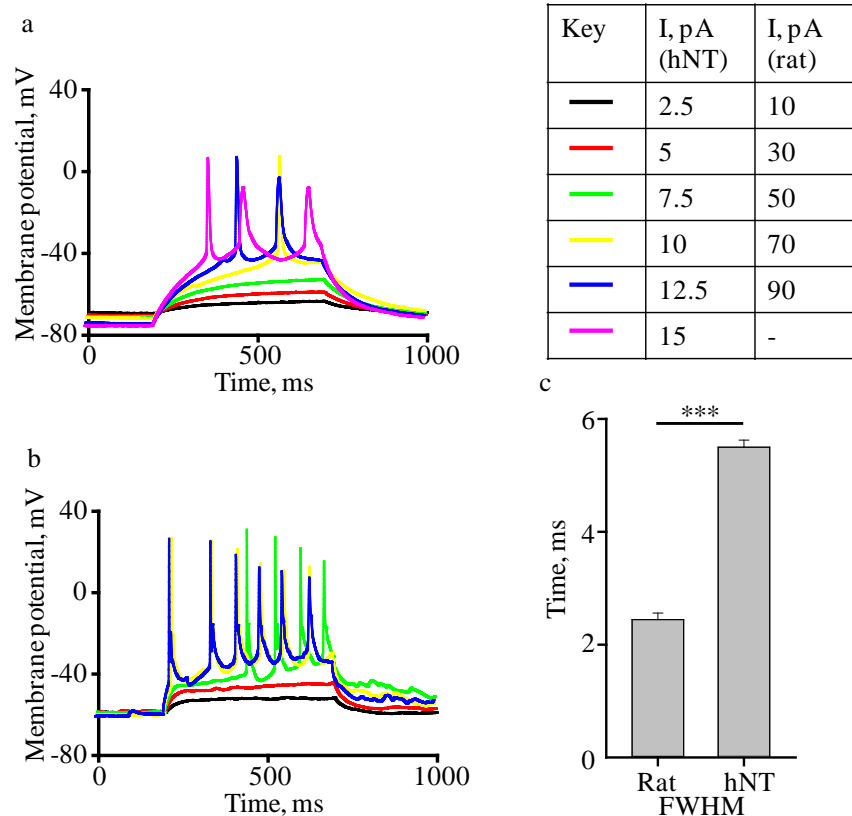
Figure 3.7: Firing patterns of a typical hNT cell and a rat hippocampal neuron for comparison. (a) During voltage-clamp experiments, when subjected to depolarising current steps, the hNT cell fired a train of action potentials. However, when compared to rat hippocampal cultured neurons (b) the elicited action potentials were much wider in hNT recording. (c)FWHM analysis on the evoked APs. n=7 APs for each condition.
*** P < 0.001, T-test. **Experiments performed by I. Pavlov, analysis by F. Alder**

3.4. Discussion

Although we were able to stably transfect and differentiate hNT cells, our functional data revealed several limitations which could severely limit their use as model neurons for probing functional consequences of ion channel mutations. Stable transfection of NT2 cells has been shown previously, using the β-gal expression plasmid SPUD1 (Pleasure et al. 1992), confirming our finding that NT2 cells could easily be transfected with common protocols. Furthermore, when treated with retinoic acid, pure cultures of β-gal positive hNT cells were harvested, suggesting that hNT cells continue to express exogenous gene products introduced into NT2 cells. This would have been the next logical step for us to take if the functional experiments had provided more positive results.

Our differentiation protocol produced hNT neuronal-like cells that were equivalent to previously published data (Andrews 1984; Pleasure et al. 1992; Kleppner et al. 1995). Interestingly, our hNT cultures exhibited spontaneous Ca^{2+} sparks, an observation which has previously not been recorded in the literature. The source of this Ca^{2+} increase is unknown, but could indicate the presence of functional VGCCs (Neelands et al. 2011) or internal Ca^{2+} stores (Alford et al. 1993; Emptage 1999; Ross et al. 2005). We observed global increases in Ca^{2+} levels, possibly indicating Ca^{2+} influx through VGCCs due to recurrent AP-evoked activity. In addition, we noted brief, local Ca^{2+} increases in several small dendritic compartments. Further functional experiments could be performed using specific Ca^{2+} channel blockers and variable external Ca^{2+} concentrations to dissect the source of the Ca^{2+} sparks.

However, there is a large discrepancy in the time-frame of maturation of hNT cells after differentiation, with experiments performed across a long time scale (21 days (Görtz et al. 2004); 1 month (Saporta et al. 2000; Misiuta et al. 2006); 5 months (Pleasure et al. 1992); 1 - 12 months (Hartley et al. 1999)). The discrepancies between hNT and rat hippocampal neurons in our electrophysiological data could be explained by lack of maturation of the hNT cells at the time of experiment, as several studies have observed slow maturation times of neurons from human origin compared to other species (Gossler et al. 1989; Pleasure et al. 1992, 1993; Bain et al. 1995).

3.5. Conclusions

Although hNT cells have been described as neuronal cells in previously published studies, in our hands, the electrical properties of the hNT cells exclude them as a model for studying functional consequences of human ion channel mutations on synaptic transmission. Secondly, the long length of differentiation and maturation time (~ 9 weeks, plus maturation time on astrocytes) made experiments impractical. Therefore we abandoned this cell model and focused on rodent primary cultures.

4. Optimising the preparation of dissociated primary hippocampal cultures from ante- and post-natal rodents

4.1. Introduction

In 1910, Ross Harrison established the method of neuronal tissue culture and used it to validate the neuron doctrine (Harrison 1910). He described in detail how axons grew out from neurons after isolation from tissue, and paved the way for modern tissue culture standards. Over the last hundred years, culturing methods have been developed greatly, and dissociated neuronal cultures are now an extensively used tool (Banker et al. 1988; Kaech et al. 2006; Vicario-Abejón 2004; Viesselmann et al. 2011; Chen et al. 2011; Fath et al. 2009; Yang et al. 2010).

Dissociated neuronal cultures were of particular interest to us for a number of reasons. Dissociated cell cultures are much less complex than intact neural tissue (such as that found in brain slices or *in vivo*) and provide a means to delicately control the surrounding experimental environment, whilst being easy to observe using standard microscopy techniques (Segal et al. 1992; Regehr et al. 2001). In addition, advances in fluorescence imaging over the last thirty years have allowed fluorescently labelled molecules to be observed at the low intensity light levels needed to avoid cell photo-damage (White et al. 1987; Amos 2003). In particular, confocal microscopy techniques can be effectively used in conjunction with isolated cultures, as the neurons are confined to a semi two-dimensional substrate. Although this two-dimensional architecture is unphysiological, dendrites and axons of dissociated cultured neurons are functionally comparable to those in slices (Higgins et al. 1988; Boyer et al. 1998).

Normal neuronal inputs and outputs are lost during cell dissociation (as many of them are during brain slice preparation), which may change neuronal phenotype. However, as juvenile animals are used (typically E18 to P1 pups), dendritic arborisation is not

complete at the time of preparation, and after dissociation developing processes demonstrate a large propensity for plasticity (Banker et al. 1988). Furthermore, dissociated neuronal cultures form extensive synaptically-connected networks connections after several days (Friedman et al. 2000). The synapses themselves were comparable with those in more intact preparations (McBain et al. 1994; Jones et al. 1995; Boyer et al. 1998; Regehr et al. 2001), (but see (Bekkers et al. 1996, 1991) for differences in translation and trafficking of NMDA receptors between cultures and slices).

Finally, dissociated cultures are the optimal neuronal model for our electrophysiological patch-clamp experiments as the cell surface is easily accessible, and post-synaptic currents can be readily observed. In addition, due to their exposed nature, cultured neurons can be easily perfused with drugs, which will be useful for the experiments we have planned, especially with specific VGCC blockers.

The hippocampus is one of the most widely studied formations in the brain. Dissociated hippocampal cultures have been studied for over twenty-five years and an extensive database of all aspects of their development and functional properties has been built, especially in the field of vesicle recycling (Kaech et al. 2006; Miyawaki et al. 2011; Branco et al. 2008; Bouron 2001) etc). In comparison to other cortical areas, the hippocampus contains relatively few cell types, and pyramidal neurons (the most widespread excitatory neurons in the hippocampus) are morphologically distinct from other cell types, particularly interneurons (Benson et al. 1994; Buchhalter et al. 1991; Grosse et al. 1998; Miyawaki et al. 2011). Furthermore, the hippocampus is relevant to

disease, because it is often the focal point of temporal lobe epilepsy, and is highly susceptible to seizures (de Lanerolle et al. 2005; Chang et al. 2003).

When compared to pure primary neuronal cultures, co-cultures with glial cells enhance synapse density, the amplitude of spontaneous postsynaptic currents, and the frequency of AP-independent quantal release (Pfrieger et al. 1997). It appears that glial paracrine trophic support of neuronal survival is species independent. Human hNT cells and mouse hippocampal neurons have both been shown to survive when co-cultured with rat glial cells (Schmalenbach et al. 1993; Matthiessen et al. 1988).

In this chapter we describe and compare two conceptually different protocols that use glial cell layer in order to support neuronal development and survival: the Banker's "sandwich" method (Brewer et al. 1989; Kaech et al. 2006) and direct plating of neurons onto a glial cell feeding layer (Bekkers et al. 1991; Morales et al. 2000). The "sandwich" technique was of particular interest to us because the glial cells and neurons were physically separate. This would be a benefit during imaging experiments, as glial cells can raise the background fluorescence and expand or contract during experiments, adding noise to the signal.

4.2. Specific aims

- Optimise a protocol for dissociated rat and mouse hippocampal cultures which can be implemented to produce long-lasting (up to 25 DIV), viable cells.
- Ensure that differences between individual cultures are minimal.

4.3. Results

4.3.1. Major findings

- Using a Banker's "sandwich" approach did not result in stable cultures.

- HEPES is necessary in the growth medium to increase cell viability

- Plating directly onto a glial cell feeding layer produced excellent cultures, suggesting that neurons need to be in physical contact with glial cells to reap the benefit of trophic support.

4.3.2. Optimising the Banker's "sandwich" method

We adapted a protocol by Kaech and Banker (Kaech et al. 2006). The method is outlined in figure 4.1. Briefly, the protocol followed that which was described in the methods (section 2.1) with several differences. Glial cells were produced and amplified as described, but plated on the plastic base of 6-well plates and left to reach confluence. Coverslips were acid-treated as described in the methods section, but wax dots applied to act as feet. Finally, neurons were harvested from embryonic E18 pups, and plated onto coverslips, before being flipped upside down on top of the glial cells. We systematically tested several conditions to optimise our cultures. To compare between different conditions, we used the cell viability method described in the methods section (Jones et al. 1985). Fluorescein diacetate (green cells) stained living cell membranes, whereas propidium iodide (red) labelled the nucleus of dead cells (figure 4.2).

a   Glial cells

Dissect cortex of P0 pups, prepare cells and freeze → Defrost and plate. Grow until confluent → Plate into culture dishes and grow until confluent → Day before culture, change medium

b   Coverslips

Acid wash coverslips, bake at 225 C and place in dishes → Add wax dots and treat with poly-l-lysine → Rinse and add plating medium

c   Neurons

Dissect E18 hippocampi → Trypsin application and trituration to single cell suspension → Plate onto coverslips → Flip coverslips and add to glial cells

Figure 4.1: Schematic of culturing process, adapted from Kaech and Banker (Kaech et al. 2006). The protocol was split into three stages. (a) Glial cells were prepared from rat cortex, amplified and frozen to make a large stock. They were defrosted when needed and plated into culture dishes and allowed to grow until confluent. (b) Meanwhile, coverslips were sterilised by acid-wash and baking. Wax dots were applied to the coverslips to act as feet, and they were treated with poly-L-lysine. (c) Neurons were harvested from embryonic rat hippocampi, dissociated with trypsin application and trituration and plated onto the prepared coverslips. After allowing several hours for attachment, coverslips were flipped over onto the glial cell feeding layer.
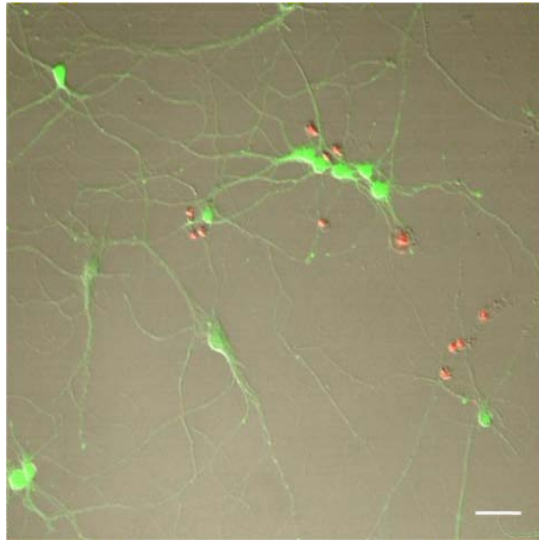
Figure 4.2: Double fluorescent dye viability test. Combined fluorescence and transmitted light image of cultured neurons. Live cells were stained with green fluorscein diacetate, whilst the nuclei of dead cells were labelled with red propidium iodide. Scale bar: 50 μm.

Two types of culturing media were described in the original protocol: Neurobasal/B27 (Brewer et al. 1993); and MEM/N2 (Bottenstein 1979). According to the original protocol, neurons grown on Neurobasal/B27 survived better in the long-term, but the probability of a high-quality culture was lower. Grown in MEM/N2, early neuronal development occurred more rapidly but long-term survival was problematic. There were several differences between the two media (table 4.1). The biggest difference was the sodium concentration: 3 g/L (51 mM) in Neurobasal/B27; 6.8 g/L in MEM/N2 (116 mM). The sodium concentration in MEM/N2 was much closer to that of our physiological buffer, which would reduce environmental changes to our cells when transferring to our experimental buffer. However, the sodium concentration in Neurobasal/B27 was lower, which would decrease spontaneous electrical activity in

cultures and may explain why cells survived longer in this medium. We decided to test neuronal survival in both media.

Table 4.1: Compositional differences in MEM and Neurobasal growth media

Component	MEM (mM)	Neurobasal (mM)
NaCl	116	51
HEPES	0	11
Glucose	6	25

When we grew cultures in Neurobasal/B27 medium, they did indeed show superior survival, in particular more than twice as many cells were still alive after 16 DIV than on MEM/N2 (figure 4.3). However, as we wished to carry out experiments at 14-21 DIV, and in both media the survival rate was not acceptable during this time frame, we further tried to optimise our cultures.

In general the glial cell feeding layer appeared healthy up until 8–9 DIV at which point the glial cells started to demise. We attempted to rectify this by transferring the neurons after 7 DIV to new plates containing fresh glial cells but this had no effect on cell survival, possibly due to the neurons being accustomed to the composition of conditioned media. We minimised disruption of the glial cell layer by reducing mechanical movements of the overlying coverslips, but this also had no difference on survival rates.
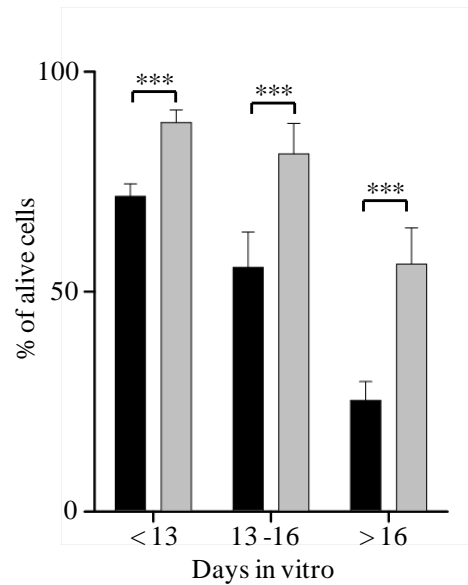
Figure 4.3: Comparison of MEM/N2 and Neurobasal/B27 neuronal growing mediums shows that cells survive better in Neurobasal/B27. Neurons were grown in both medias and viability assessed at different time points (< 13, 13-16, and >16 DIV). Cells grown in Neurobasal/B27 had a better survival rate. n=30 regions from N=3 coverslips for each condition. Black bars: MEM/N2, grey bars: Neurobasal/B27. ***P < 0.001.

As these simple measures did not improve the quality of the glial layer, we optimised the concentration of cytosine arabinoside (araC) - an antimetabolic agent which damages DNA when the cell cycle holds in the S phase, which is commonly used to curb glial proliferation in culture (Kaech et al. 2006). At high concentrations, araC is also toxic to non-dividing cells. In the original protocol media was supplemented with 5 μM araC, but any concentration down to 1 μM can be used effectively (Yataganas et al. 1974). Neuronal cultures grown in the absence of araC were overgrown with glial cells after 2 weeks. We found that 1 μM araC effectively curbed growth of glial cells on the

coverslips without destroying the glial feeding layer. At this concentration, the feeding layer was healthy for the length of the culturing period (>3 weeks).
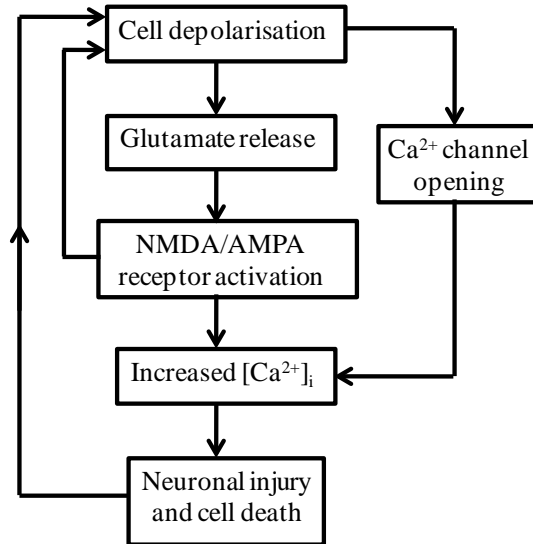
Figure 4.4: Glutamate excitotoxicity idea, adapted from (Mark et al. 2001). Cell depolarisation leads to activation of voltage gated Ca^{2+} channels and glutamate release, which in turn activates NMDA and AMPA receptors. This increases intracellular Ca^{2+} levels which can lead to cell injury. There is a feedback loop which exacerbates the situation.

Unfortunately, the improved viability of the glial cell layer did not increase neuronal survival. One possible explanation for the cell death was excitotoxicity caused by excessive glutamate in the extracellular solution. If the concentration of glutamate is raised to 100 μM or more, it becomes excitotoxic (figure 4.4, adapted from (Mark et al. 2001)). Cell depolarisation leads to Ca^{2+} channels opening and glutamate release, which activates NMDA and AMPA receptors. This increases cell depolarisation and intracellular Ca^{2+} concentrations, which can lead to cell injury and death. Cell death leads to the breakdown of the lipid bilayers and release of vesicular and cytosolic

glutamate into the extracellular space. This begins the cycle again. At 7 DIV, cultured neurons undergo a period of extensive neurite elongation and branch formation and are not vulnerable to excitotoxicity. By 14 DIV this vulnerability has increased, coinciding temporally with a period of synapse formation and changes in NMDA receptor subunit expression (King et al. 2006). This could explain why our cultures did not survive well after two weeks in culture.

To test this idea, we buffered glutamate in our cultures using the scavenger enzyme glutamic-pyruvic transaminase (GPT) in conjunction with the equilibrium reaction driver pyruvate. The enzyme catalysed the equilibrium reaction:

$$Glutamate + Pyruvate \overset{GPT}{\rightleftharpoons} \alpha - ketoglutorate + alanine$$
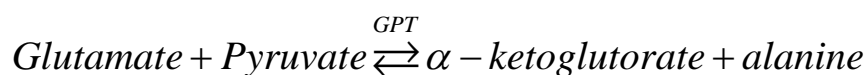
GPT has been shown to be the most effective enzyme catalyst for this reaction (Matthews et al. 2000). MEM/N2 media contained no alanine or pyruvate, so we added pyruvate in order to drive the forward reaction. It was shown that concentrations of 5 U/ml of GPT and 2 mM pyruvate were sufficient to rapidly convert glutamate to α-ketoglutarate, leading to a decrease of glutamate levels in the extra-synaptic environment (Min et al. 1998; Tsvetkov et al. 2004).

We performed experiments with GPT in MEM/N2 medium only. We found that a concentration of pyruvate between 2-4 mM was optimal, as concentrations about 6 mM were toxic. Adding pyruvate alone did not aid cell survival (figure 4.5). With 5 U/ml of GPT and 4 mM pyruvate, we also found no significant difference in cell viability (figure 4.6).
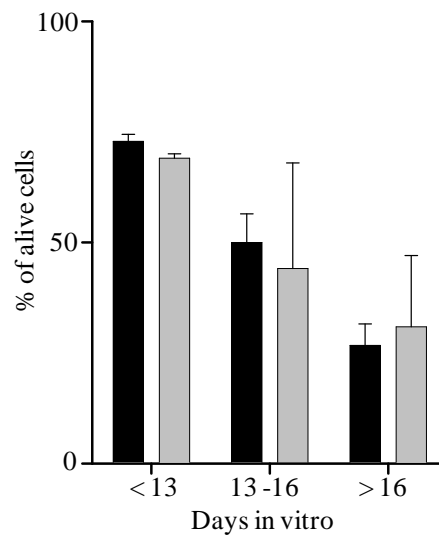
Figure 4.5: Application of pyruvate has no effect of cell survival. Cells were grown in MEM/N2 supplemented with 4 mM pyruvate, which had no effect on cell survival rates at any time point. Black bars: 4mM pyruvate, grey bars: control. n=30 regions from N=3 coverslips for each condition. All time points were not significant (T-test).
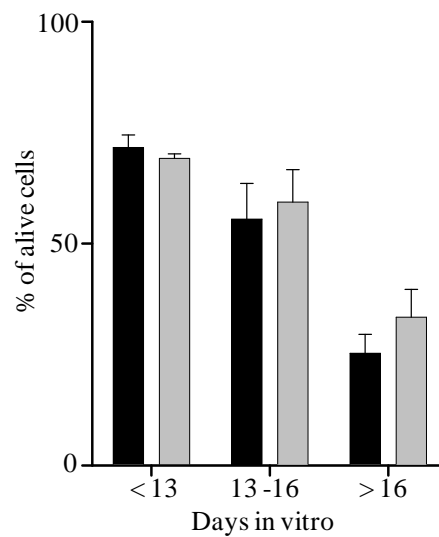
Figure 4.6: Application of the enzyme glutamic-pyruvic transaminase (GPT) had no effect on cell survival. Cells were grown in MEM/N2 supplemented with 5 U/ml GPT and 4 mM pyruvate. This had no beneficial effect on cell survival rates at any time

point. Black bars: 4mM pyruvate+5 U/ml of GPT, grey bars: control. n=30 regions

from N=3 coverslips for each condition. All time points were not significant (T-test).

As we did not find any improvement using the enzyme GPT, we returned to the differences between the two media, to see if we could optimise other parameters. We noticed that neurons growing in the middle of the coverslip died sooner in comparison to the neurons growing towards the coverslip edge when grown in MEM/N2. Unlike Neurobasal/B27, which contained 11 mM of the pH buffer HEPES, MEM/N2 had no pH buffers. We hypothesised that due to the absence of HEPES in MEM/N2, the pH of the media was not sufficiently buffered under the glass coverslip. The volume under the coverslip was very limited (assuming that diffusion between the media under the coverslip and the rest in the well was restricted), so it was feasible to suggest that if there was a small pH change (due for example to excretion from the cells), this would make a large difference to the microenvironment under the coverslip.

We added 10 mM HEPES to MEM/N2 culture medium on the day of culturing. This significantly increased cell viability for the entire culturing duration (figure 4.7), and reduced the difference between the two media in terms of survival rates.
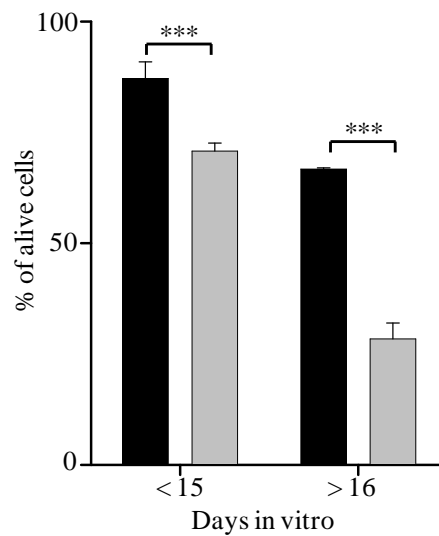
Figure 4.7: Application of HEPES to MEM+N2 had a significant positive effect of survival rates. MEM+N2 growing medium was supplemented with 10 mM HEPES, which increased the cell viability, especially in cells over 16 DIV. Black bars: MEM+N2 supplemented with HEPES, grey bars: control. n=30 regions from N=3 coverslips for each condition. ***P<0.001, T-test

4.3.3. Plating neurons directly onto a glial cell feeding layer

Although we had increased the cell viability, there was still a large proportion of cells (~30 %) which died before reaching three weeks in culture. Therefore, in parallel with optimising the Banker's "sandwich" protocol, we also tried to plate hippocampal cells directly onto glial cells (Tokuoka et al. 2006; Morales et al. 2000), see the materials and methods chapter, section 2.1). The method was similar to the Banker's "sandwich" protocol, although the glial cells were plated directly onto poly-l-lysine coated coverslips and the neurons layered on top. This immediately improved the viability of cultures and we found cells to be healthy up until ~25 DIV.

We tested these cultures in typical FM dye imaging experiments to see whether there would be a high background or significant movement due to the glial cells (the protocol and results are discussed in chapter 6). We found minimal movement during experiments, presumably because the glial cells formed a complete sheet underneath the neurons, and therefore were less likely to expand or contract. We therefore decided to abandon the Banker's "sandwich" protocol and concentrate on neurons plated directly onto glial cells. Using this protocol, we plated cells derived from both pre- and postnatal rats, and found no difference in culture viability, and proceeded with postnatal pups, as this reduces the number of animals sacrificed. We grew cultures on both Neurobasal/B27 and MEM/N2 medium supplemented with 10 mM HEPES and found no difference between the two in cell survival rates. We therefore decided to grow cultures in Neurobasal/B27 as it is more commonly used, and would allow our data to be comparable with a larger number of other laboratories.

Once we had optimised the hippocampal protocol for rats, we adapted the protocol to cultures from transgenic mice. Each mouse had to be cultured separately as they were different genotypes (it was not possible for us to genotype the mice before culturing). Therefore, we cultured mice in batches of three or four pups, keeping the tissue from each individual separate. As the hippocampus was much smaller, we used smaller volumes of culturing solutions. In order to reduce culturing time, we did not count cells prior to plating. Instead we plated neurons from each pup onto 4 coverslips, which produced cultures with consistent density.

4.4. Discussion

Our experiments have shown that in order to thrive for longer than 16 days in vitro, hippocampal neurons grown in culture need to be in physical contact with glial cells. It is commonly known that astroglia are necessary for the development and longevity of neuronal cultures (Banker 1980), but whether the responsible factors for optimised survival are membrane bound or diffusive or both is unknown.

The importance of physical contact has long been noted to contribute to optimal survival (Lasek et al. 1977). Physical contact was also necessary for substantial axonal and dendritic growth (Gasser et al. 1990; Piontek et al. 2002), regulation of voltage-gated Ca^{2+} channels (Mazzanti et al. 2003), synaptogenesis (Hama et al. 2004) (although here the authors could not distinguish between physical contact and short-range diffusible factors), and synaptic efficacy (Pfrieger et al. 1997).

However, other published data has suggested that neurons are able to survive in conditioned medium (Pyka et al. 2011). A soluble form of cholesterol is a likely diffusible candidate (Mauch et al. 2001), and has been shown to be crucial in synaptogenesis. However, the origin of the cultured neurons creates differences in the neuronal responses to soluble glial factors (Schmalenbach et al. 1993). This origin-dependence of response could partly explain the differing opinions on whether soluble or membrane-bound factors are necessary for cell survival.

Cell plating density also plays a major role in cell survival (Adler et al. 1986; Schmalenbach et al. 1993). It is commonly understood that the denser the culture, the higher the survival rate. However, in order to have cultures optimised for imaging

experiments, it is important to not have extremely dense neurons as at high densities individual synaptic boutons can be difficult to image. Plating directly onto a glial cell feeding layer allowed us to plate neurons at a reasonable density (~10 x 10^3 cells/cm^2, compared to a typical high density of ~30 x 10^3 cells/cm^2).

It has been suggested that the Banker's "sandwich" technique creates a microenvironment between the glass coverslip and plastic well which can reduce the oxygen level in the culture, increasing neuronal survival (Brewer et al. 1989). However, we found that cells in the middle of the coverslip were not viable, most likely due to poor pH buffering. The addition of HEPES reduced this problem (Chesler 1990; Tombaugh 1998) which was not surprising given that pH must be tightly regulated for efficient functioning of most enzymes, ion channels and other macromolecules (Tombaugh et al. 1996).

4.5. Conclusions

In conclusion we found that co-culturing neurons at low density in direct contact with glia gave optimal conditions for imaging experiments. Moreover was important to regulate the pH of the growing medium with a buffer, in our case 10 mM HEPES, particularly in "sandwich" cultures where media movement was restricted.

5. Biochemical characterisation of FM dyes

5.1. Introduction

Fluorescent styryl FM dyes have been used extensively to investigate synaptic vesicle recycling since their introduction in 1992 (Betz et al. 1992; Cochilla et al. 1999). The FM dye family all have a similar molecular structure (figure 5.1): a lipophilic tail region, which can partition into membranes; a pair of aromatic rings making up the fluorophore, bridged by double bonds (the number of which determine the fluorescence spectrum); and a positively charged head which stops the molecule from flipping across the membrane (Gaffield et al. 2006; Wu et al. 2009). On contact with non-polar solvents (i.e. membranes), the fluorescence increases by more than two orders of magnitude, hence almost the entire signal is from dye molecules buried within the membrane (Gaffield et al. 2006).

FM dyes have been used in numerous studies on a large variety of preparations (Gaffield et al. 2006) including: goldfish bipolar cells (Rouze et al. 1998; Neves et al. 1999; Joselevitch et al. 2009); frog (Betz et al. 1992; Richards et al. 2003; Groemer and Rizzoli 2010a), drosophila larval (Ramaswami et al. 1994), crayfish (Wang et al. 1998), and snake (Teng et al. 1999) neuromuscular junction; rat cerebellar granule cells (Pocock et al. 1995; León et al. 2008); slices (Kay et al. 1999; Pyle et al. 1999; Winterer et al. 2006); and most relevant to our current project in hippocampal cultures (including (Ryan et al. 1993; Klingauf et al., 1998a; Harata et al. 2001; Hopf et al. 2002; Darcy et al. 2006; Staras et al. 2010; Laviv et al. 2010) amongst others)

a. FM 1-43

b. FM 2-10
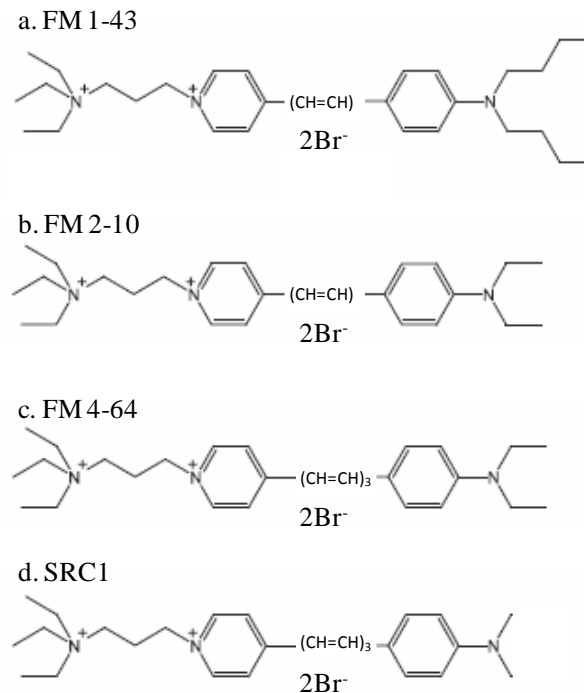
c. FM 4-64

d. SRC1

Figure 5.1: Molecular structures of styryl FM dyes. (a) FM 1-43, (b) FM 2-10, (c) FM 4-64 and (d) SRC1. Adapted from (Wu et al. 2009).

There are a number of FM dyes and their analogues which are used to monitor recycling synaptic vesicles (Wu et al. 2009). The most common dye used is FM 1-43 (Fig 5.1a), which has been well characterised in many different synapses (Harata et al. 2001; Schikorski et al. 2001). FM 2-10, (Sara et al. 2002; Baldwin et al. 2006; Clayton et al. 2008) has a shorter tail group than FM 1-43 (Fig 5.1b), and hence can departition faster from biological membranes. This could potentially be a useful property when measuring fast vesicle recycling events. There is another set of dyes with red-shifted emission spectra (due to more double bonds in the bridge region of the molecule), which can be used in conjunction with green emission dyes, such as the Ca^{2+} indicator Fluo-4 (figure 5.1c, d). This was an important consideration for this project as we wanted to combine FM dye destaining experiments with calcium imaging. In particular, FM 4-64 (figure 5.1c) (Tsai et al. 2009; Sankaranarayanan et al. 2001; Laviv et al. 2010) is a red shifted

form of FM 1-43. There is also a FM 4-64 analogue - SynaptoRed C1 (SRC1, figure 5.1d) - available, with one carbon less on the lipophilic tail, which (like FM 2-10) is expected to have a faster departitioning rate from biological membranes. To our knowledge, SRC1 has not been used in any previously published work, although it has a similar quantum yield to FM 1-43.

Due to the red shift in emission spectrum and the faster departitioning rate, SRC1 was very promising for our proposed work. We carried out some preliminary destaining experiments with FM 4-64 and SRC1 and found that SRC1 was more specific than FM 4-64, and therefore gave a better signal-to-noise ratio. This was most likely due to the shorter tail group making SRC1 less sticky and easier to wash out of the surrounding cellular membrane (Gaffield et al. 2006; Wu et al. 2009).

To obtain consistent results in imaging experiments, it is crucial to use an appropriate amount of the FM dye during vesicle loading. This is notably important as styryl dyes can act as surfactants to modify fusion pore open probability at high concentrations (Zhu and Stevens 2008). Indeed using FM dye at concentrations much lower than its membrane dissociation constant (K_d) would lead to incomplete labelling of vesicular membranes, lower fluorescence signal, and poor signal-to-noise ratio. If however, too much FM dye is applied, loading will be unspecific and bulk loading may occur (Clayton et al. 2008), and again the signal-to-noise ratio would be poor. Typically roughly two times the dissociation constant of the dye is used. The values of K_d for FM 1-43, FM 2-10 and FM 4-64 have been previously published (Smith et al. 1996; Neves et al. 1999; Richards et al., 2005b; Wu et al. 2009), but the methods and hence results vary. As K_d can vary with membrane composition (Wu et al. 2009), it was important for

us to measure the dissociation constant of each dye with hippocampal neuronal membranes. Here, we discuss two complementing methods for measuring binding of FM dyes to fixed hippocampal neurons and to synaptic plasma membranes (SPMs).

5.2. Specific aim

- Measure membrane dissociation constants and determine optimal working concentrations for several commonly used FM dyes in our experimental conditions.

5.3. Experimental design/theoretical considerations

In order to estimate the K_d of FM dyes on our biological membrane, we used standard first-order ligand-receptor equations. By assuming that the dye is in excess during an experiment, staining of membranes can be approximated by a pseudo-first order reaction:

$$Ligand\ (L) + Receptor\ (R) \underset{K_{-1}}{\overset{K_1}{\rightleftarrows}} Ligand.Receptor$$
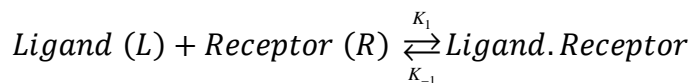
where in this case, the *Ligand* is the FM dye, the *Receptor* is the membrane and K_1 and K_{-1} are the dissociation rated for the forward and reverse process.

K_d for the FM dye can be estimated as:

$$K_d = \frac{L_f.R_f}{L_B} = \frac{L_f.(B_m - L_B)}{L_B}$$

where:

L_f = the concentration of free ligand

R_f = the concentration of free receptor

L_B = the concentration of bound ligand

B_m = the total number of binding sites on the receptor

$$K_d.L_B = L_f.B_m - L_f.L_B$$

$$L_B = \frac{L_f.B_m}{K_d + L_f}$$

Equation 5.1

By measuring the fluorescence signal from increasing concentrations of FM dyes applied to membranes, we can fit the dose-response curve with a hyperbola regression, of the form:

$$y = \frac{a.x}{b + x}$$

and hence estimate K_d for each FM dye.

Values of K_d for FM 1-43, FM 2-10, FM 6-64 and SRC1 were estimated using two complementary techniques. In the first method, we measured the change in fluorescence signal to increasing concentrations of the dyes, when applied to fixed dissociated hippocampal cultures, using the confocal set-up. Increasing concentrations of dye was added to the recording chamber, and the fluorescence signal recorded. Three independent experiments were performed.

In the second method we used synaptic plasma membranes (SPMs). The aim was to compare our results with previously published data (Richards et al. 2005b), and to verify our results from neuronal membranes. Using this SPMS method, we only tested

FM 1-43 and FM 2-10 as sadly fluorescence filter sets suitable for FM 4-64 and SRC1 were not available for the fluorescence plate reader used. After SPMs (Gordon-Weeks 1987; Berninghausen et al. 2007) were purified and the total protein content measured (using Bradford's assay, see methods, section 2.3.3), they were diluted (to 50 μg/ml total protein content) with increasing concentrations of FM dyes (The dye concentration range was 0-50 μM for FM 1-43 and 0-150 μM for FM 2-10). Aliquots were loaded into a 96-well plate and fluorescence at each well measured using a fluorescence plate reader (Fluoroscan Ascent). We used the 485 ± 10 nM excitation and 555 ± 25 nm emission filter sets throughout. For control experiments, increasing concentrations of SPMs (0-100 μg/ml) or FM dyes were mixed with 20 μM Alexa 488, and loaded into the plate reader.

5.4. Results

5.4.1. Major findings

- K_d was measured successfully using two methods: on fixed hippocampal cultured neurons and using synaptic plasma membranes (SPMs)
- The results from the two techniques were comparable, and were similar to previously published data.

5.4.2. K_d measured on fixed cultured neuronal membranes

We first measured the value of K_d of the four dyes (FM 1-43, FM 2-10, FM 4-64 and SRC1) binding to fixed hippocampal cultured neurons. The emitted fluorescence increased as expected for increasing concentrations of each dye (figure 5.2). In a typical experiment, the fluorescence signal for each dye tended towards a maximal, after which

further increases of dye could no raise the fluorescence further (figure 5.3), suggesting that the membrane was saturated at this point.

Dose response curves for each coverslip was fitted with a hyperbola regression, and a value of K_d calculated. The values of K_d calculated using this method are summarised in table 5.1.

Table 5.1: K_d for four FM dyes, measured on fixed neuronal membranes.

Dye	K_d (neuronal membranes, mean ± s.e.m for n = 3 independent experiments)
FM 1-43	5.24 ± 0.16 μM
FM 2-10	73.2 ± 1.4 μM
FM 4-64	9.58 ± 0.52 μM
SRC1	142.9 ± 8.1 μM
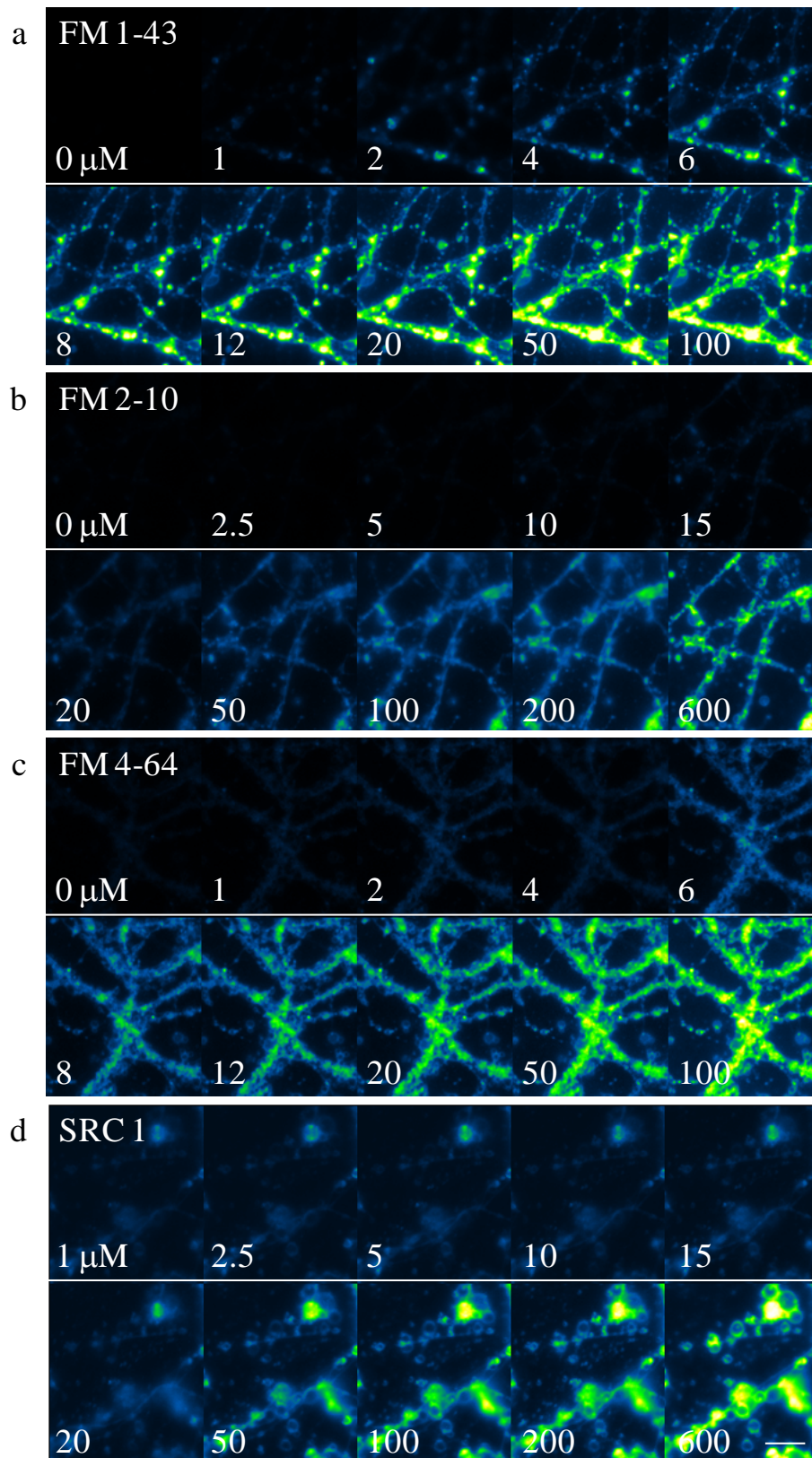
Figure 5.2: Typical regions showing binding of FM dyes to fixed neuronal cultures.

*Example increase of fluorescence with rising concentrations of (**a**)FM 1-43, (**b**) FM 2-*

10, (c) FM 4-64, and (d) SRC1, on fixed cultured hippocampal neurons. The

concentration of dyes is as shown (in µM). Scale bar: 5 µm.
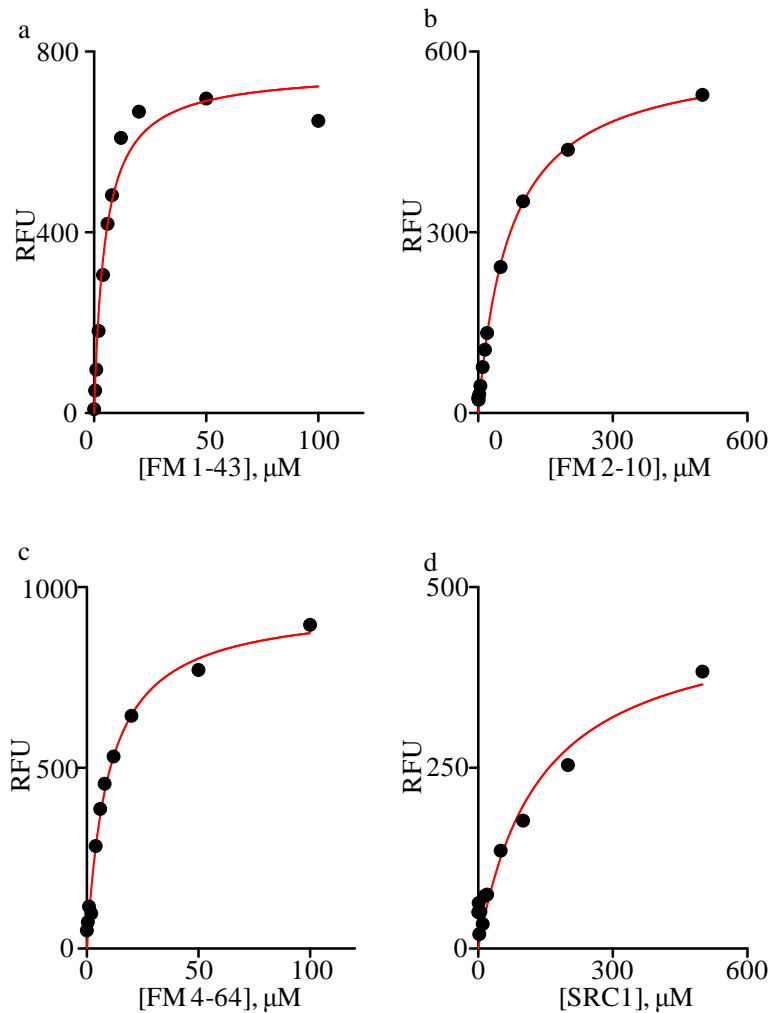
Figure 5.3: Dose response curves of four FM dyes to fixed cultured hippocampal

neurons. *Binding of FM dye to neuronal membrane resulted in a dose response curve,*

*each for an example experiment using (**a**)FM 1-43, (**b**) FM 2-10, (**c**) FM 4-64, and (**d**)*

SRC1. Curves fitted with a non-linear hyperbola regression (in red), to calculate K_d

according to equation 5.1.

5.4.3. K_d measured on synaptic plasma membranes (SPMs)

Next, we measured K_d using a second method. We produced purified SPMs, and measured the protein content using Bradford's assay method (see section 2.3.3). In total, we had 3.7 mg/ml of protein in our SPM sample. In figures 5.4 – 5.6 a typical experiment is illustrated, although three independent experiments were performed to calculate the mean $\pm$ s.e.m of K_d for both dyes.
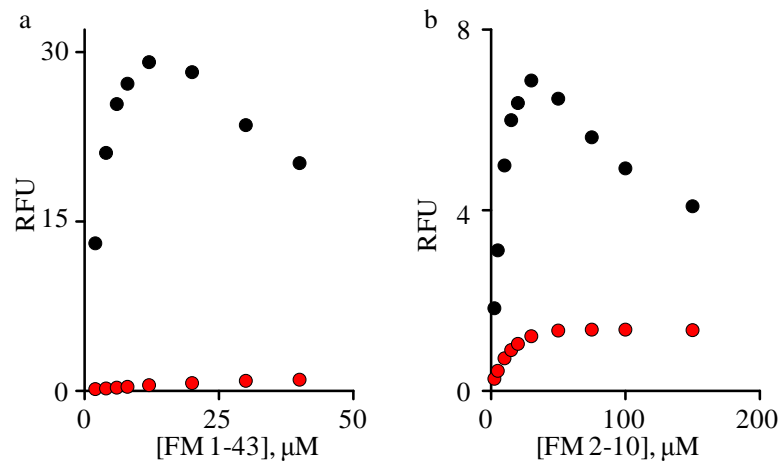
Figure 5.4: Binding of FM dyes to purified SPMs. Dependencies of FM dye fluorescence on dye concentrations for two typical experiments. (a) Red circles FM 1-43 alone, black circles FM 1-43 mixed with 50 µg/µl of SPMs. (b) Red circles FM 2-10 alone, black circles FM 2-10 mixed with 50 µg/µl of SPMs.

We first measured the dose dependency of both FM 1-43 and FM 2-10 fluorescence in the presence and absence of 50 µg/ml SPMs, using a fluorescence plate reader (figure 5.4). The data did not follow a typical dose-response curve for two reasons (figure 5.5a). Firstly, a proportion of the emission signal was lost via scattering from the membranes. We overcame this by measuring the dependence of Alexa 488 fluorescence on increasing concentrations of SPMs (figure 5.5b). Secondly, the raw trace had a bell

shape due to an increasing inner-filter effect of the FM dye. To correct for this, we measured the fluorescence of Alexa 488 in the presence of increasing concentrations of the FM dye, using the same filter sets as in the original experiment (figure 5.5c and d).

To correct our data for the inner filter effect, for each experiment, we divided the dose-response trace (figure 5.4) by the normalised Alexa 488 fluorescence traces in figures 5.5c and d. To account for the effect of light scattering from the membranes, we multiplied the membrane-free FM traces (figure 5.4, red circles) by 0.68 (figure 5.5b), the reduction of fluorescence due to light scattering at 50 μg/ml SPM concentration). By correcting for these effects, we obtained typical dose-dependency curves for both FM 1-43 and FM 2-10 (figure 5.6). By again fitting with a hyperbolar regression, we calculated values of K_d for both dyes (table 5.2)

Table 5.2: K_d for two FM dyes, measured on synaptic plasma membranes.

Dye	K_d (SPMs, mean ± s.e.m for n = 3 independent experiments)
FM 1-43	7.56 ± 0.24 μM
FM 2-10	105.3 ± 4.3 μM

Although the measured value of K_d for FM 1-43 and FM 2-10 was significantly different using the two methods (P < 0.001, t-test for both FM 1-43 and FM 2-10),

importantly, the values of K_d using these two independent methods were of the same order of magnitude.
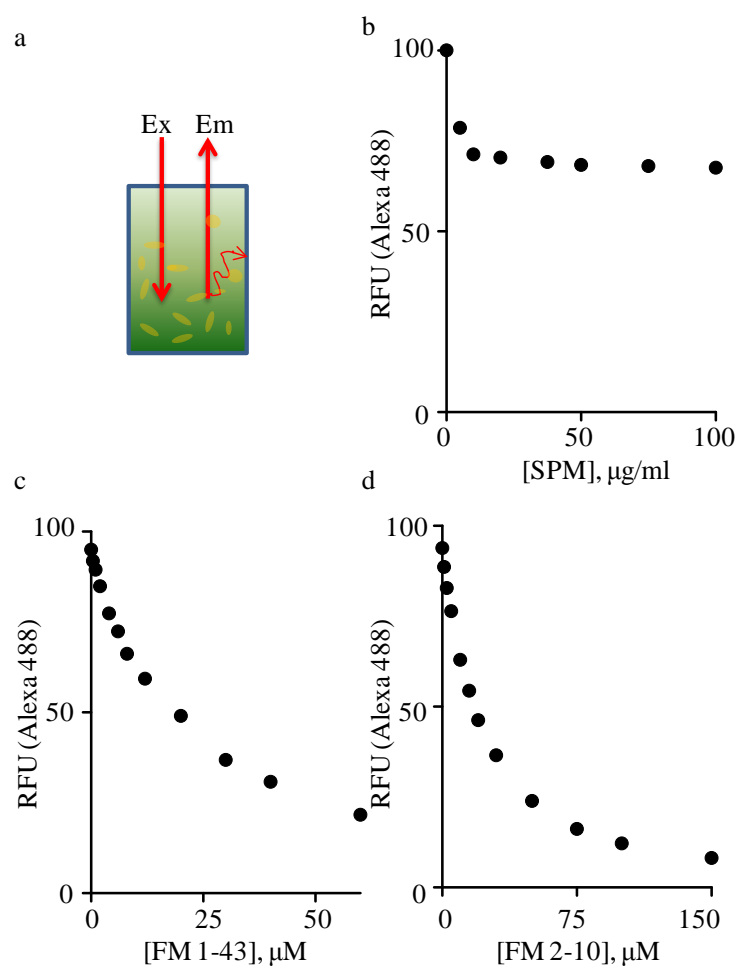
***Figure 5.5: Control for FM dye/SPM binding experiments.** **(a)** Schematic showing scattering of emission (Em) and excitation (Ex) fluorescence by SPMs and the inner filtering effect of the FM dyes. **(b)** Measurement of light scattering at different concentrations of SPMs **(c, d)** Measurements of the inner filter effect of **(c)** FM 1-43 and **(d)** FM 2-10 using Alexa 488 fluorescent dye.*
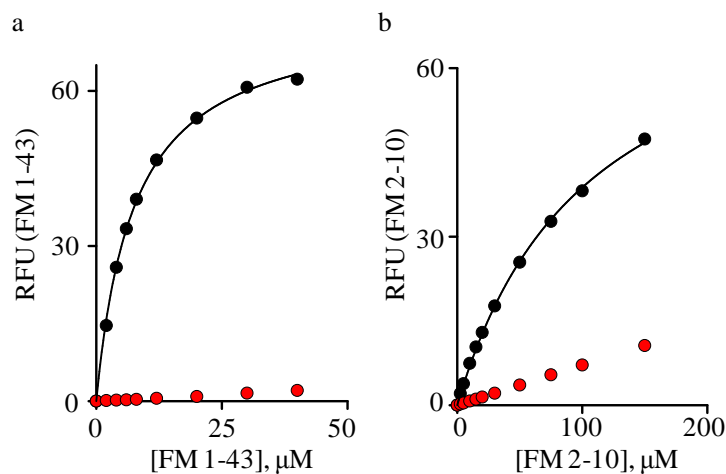
Figure 5.6: Dependency of fluorescence on dye concentration after correction for the inner filter effect and membrane scattering. (a) Black circles FM 1-43 alone, red circles FM 1-43 mixed with 50 µg/µl of SPMs. (b) Black circles FM 2-10 alone, red circles FM 2-10 mixed with 50 µg/µl of SPMs.

5.5. Discussion

We measured the dissociation constant, K_d, of three commonly used FM dyes and an analogue (SRC1), on fixed neuronal membrane and K_d for FM 1-43 and FM 2-10 on SPMs . Although the results for FM 1-43 and FM 2-10 from each method were significantly different (tables 5.1 and 5.2, P < 0.001, t-test for both FM 1-43 and FM 2-10), they were comparable, indicating that although the methods used different approaches, each produced a reliable estimate of K_d. For the first time, we have determined the K_d of SRC1. Although SRC1 has a short lipophilic tail (giving it a faster departitioning rate than FM 1-43), and a red-shifted emission spectrum (making it idea to use in conjunction with green-shifted dyes such as the Ca^{2+} indicator Fluo-4), it is not yet commonly used.

Our results are comparable with previously published data. The dissociation constant has been reported for FM 1-43 in several publications. In the study on goldfish retinal bipolar cell membranes by Neves and Lagnado (Neves et al. 1999), the K_d of FM 1-43 was measured to be 3.5 μM using a stopped-flow design, and 3.8 μM using a steady-state protocol similar to ours. In comparison, Smith and Betz (Smith et al. 1996) measured K_d to be 1.33 μM on chromaffin cells. All these values are within the same order of magnitude, but differences most likely arise due to variability in membrane composition, temperature or pH (Richards et al., 2005b).

Interestingly, in the studies using liposomes by Richards (Richards et al., 2005b) and Wu (Y. Wu et al. 2009), the dose dependencies of FM 1-43 (figure 5b, (Richards et al., 2005b); figure 2c (Wu et al. 2009)), FM 2-10 (figure 2E, (Wu et al. 2009)) and FM 4-64 (Figure 2F, (Wu et al. 2009)) were measured, but values for K_d were not calculated. By crudely fitting this set of data, we could derive approximate values of K_d (although this data was not corrected for the inner filter effect of the dye of membrane scattering). K_d = 5.1 μM (FM 1-43, Richards), K_d = 2.9 μM (FM 1-43, Wu), K_d = 27.4 μM (FM 2-10), K_d = 25.1 μM (FM 4-64). These values are within the same order of magnitude as our results, although they are very rough estimates, and are derived using a completely different model system to ours, further suggesting that the K_d values for these dyes are consistent in a wide range of systems, membranes and applications.

5.6. Conclusions

These experiments enable us to determine the optimal range of concentrations of FM dyes to use during our destaining experiments (see chapter 6). In particular, in order to optimally load synaptic vesicles (65% - 75% of maximal fluorescence) whilst minimising non-specific staining we used FM dyes at a concentrations ~ 2 times higher than their determined dissociation constants.

6. Simultaneous measurements of functional vesicular pool sizes and release probability in individual synaptic boutons

6.1. Introduction

The efficiency of information transfer at a given synapse is regulated by the probability of neurotransmitter release in response to an AP, which is denoted P_{rel}. P_{rel} varies widely, even amongst neighbouring synapses along the same axon, and is thought to be due to local adjustment in synaptic strength (Koester et al. 2005; Branco et al. 2008). However, the molecular mechanisms that determine variability of P_{rel} at small central synapses are not completely understood.

The probability of neurotransmitter release P_{rel} at a synapse can be related to the average fusion probability of an individual vesicle, p_v, and the size of the RRP, docked at the active zone (AZ) (Murthy et al. 1997, 2001; Schikorski et al. 2001; Rizzoli and Betz 2005), by the classical binomial equality:

$$P_{rel} = 1 - (1 - p_v)^{RRP}$$
Equation 6.1

RRP, RP and AZ sizes have all been shown to scale with the size of the synapse in both neuronal cultures and *in situ* (Murthy et al. 2001; Schikorski et al. 1997), and hence P_{rel} is typically higher at synapses with larger presynaptic compartments.

However, P_{rel} has been shown to vary extensively in imaging experiments, even in boutons of similar sizes (Waters et al. 2002). There are two reasons why this variability may occur. Either the relative size of the RRP varies between boutons [i.e. the ratio RRP/RP varies, (Waters et al. 2002)] or the average fusion probability of an individual vesicle, p_v is heterogeneous among presynaptic boutons. Since p_v has not been directly

compared among individual boutons it remains unknown whether heterogeneity in p_v significantly contributes to variability of P_{rel}.

Here, we devised a protocol based on loading and destaining of recycling vesicles with fluorescent FM dye SRC1, which allowed us to simultaneously estimate P_{rel} and the vesicular pool sizes (*RP* and *RRP)* in individual synaptic boutons. From these measurements, we could estimate p_v, and hence determine to what extent heterogeneity of p_v contributes to variability of P_{rel}.

6.2. Specific aims

- Simultaneously measure the size of the *RRP* and *RP,* and AP-evoked (K_{AP}) and spontaneous (K_{sp}) SRC1 destaining rates at individual synapses in cultured hippocampal neurons.
- Compare the above vesicular recycling parameters among synapses.
- Test whether heterogeneity of P_{rel} is mainly determined by the variability of *RRP* size or whether the variation of p_v between synapses also plays a role.

6.3. Experimental design/theoretical considerations
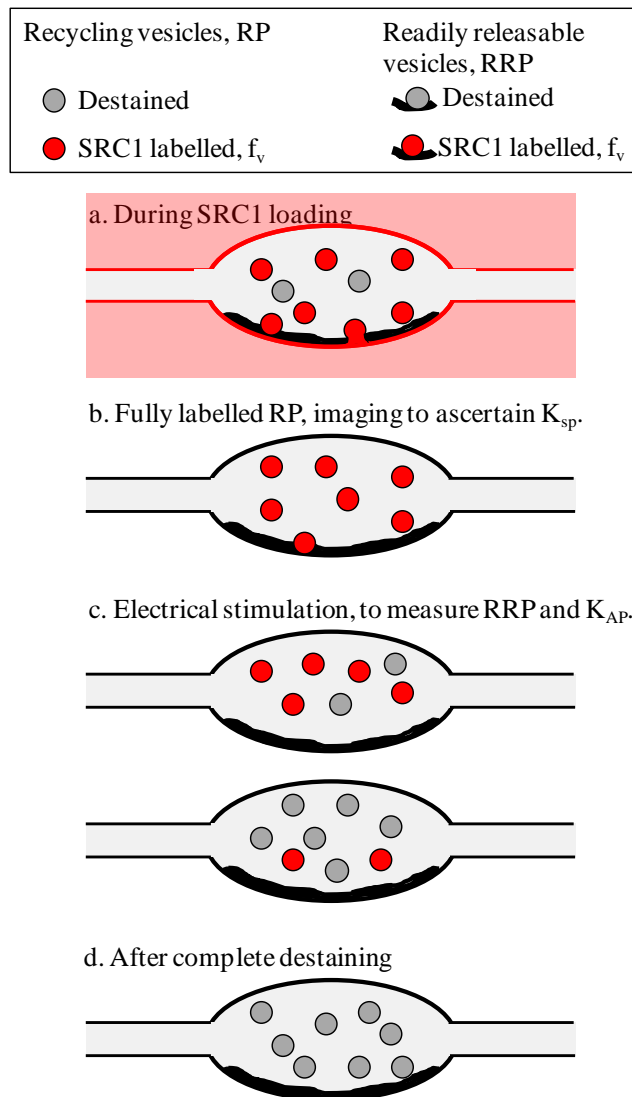
*Figure 6.1: Model synapse outlining the SRC1 protocol. (**a**) During loading of vesicles with SRC1, all exposed synaptic membrane is loaded with SRC1. Vesicles recycle on application of high frequency electrical stimulation, and internalise SRC1. (**b**) After complete loading of the RP, excess dye is washed from synaptic membranes. The spontaneous destaining rate (K_{sp}) is estimated in the absence of stimulation. (**c**) Electrical stimulation is applied to synapses to estimate both the size of the RRP and the evoked destaining rate K_{AP}. (**d**) High frequency stimulation is applied to completely destain vesicles of SRC1, to estimate the background fluorescence.*

We used the styryl dye SRC1 to label synaptic vesicles and monitor vesicular recycling to collect data for this chapter. The experimental protocol was designed to simultaneously estimate several aspects of vesicle recycling at individual boutons. We could directly measure: RP, RRP/RP, K_{sp} and K_{AP}. From these, we were able to calculate RRP, p_v, P_{rel} and the vesicular release rate R_{rel}. A simplified synapse undergoing SRC1 labelling and destaining is illustrated in figure 6.1. During loading (figure 6.1a) SRC1 was bound to all plasma membranes. As vesicles underwent exo- and endocytosis, their membranes became labelled with SRC1. After several rounds of stimulation to mobilise the entire RP, the SRC1 was washed out of the bath, and hence from the cell membrane. The fluorescence signal at this point (figure 6.1b) gave a measure of the number of synaptic vesicles in the total recycling pool, RP (after the background fluorescence was taken into account). Boutons were imaged for several minutes in the absence of stimulation to garner an estimate of the spontaneous destaining rate, K_{sp}. This destaining rate gave only an estimate of the true spontaneous destaining rate, as it was also affected by non-specific loss of fluorescence.

A brief, high-frequency burst of stimulation was applied to measure the size of the RRP (figure 6.1c) (Pyle et al., 2000a; Murthy et al. 2001; Stevens et al. 2007). Several minutes later (to allow time for labelled and unlabelled vesicles to mix between pools), low frequency stimulation (0.5 Hz) was applied (figure 6.1c), to estimate the rate of AP-evoked vesicular exocytosis (K_{AP}). During 0.5 Hz stimulation recycling vesicles could be assumed to be in equilibrium between the RRP and the RP; in other words, SRC1-labelled vesicles were equally distributed throughout the RP (Murthy et al. 1999). Consistent with this assumption, the fluorescence decay during 0.5 Hz stimulation, K_{ev} could be fitted with a mono-exponential function. The fluorescence decrease measured

during this period gave a measure of the specific AP-evoked destaining rate, $K_{AP} = K_{ev} - K_{sp.}$ Finally, boutons were subjected to strong stimulation, to recycle any vesicles which still contained SRC1, and to measure the background fluorescence (figure 6.1d).

By simultaneously measuring the values of *RRP/RP*, *RP*, K_{sp} and K_{AP} for each bouton, we were able to theoretically calculate several other parameters. By assuming that vesicles in the *RRP* fused independently from each other and hence follow a binomial distribution (Schneggenburger et al. 2002), we could relate the average number of vesicles released during a single AP, N_{AP}, to the size of the *RRP* and to the average release probably as:

$$N_{AP} = RRP \cdot p_v \qquad\qquad \textbf{Equation 6.2}$$

The SRC1 fluorescence (F_{SRC1}) decay during low frequency stimulation could be described by the differential equation:

$$\frac{d\ _{SRC1}F(t)}{dt} = -N_{AP}.f_v.\frac{F_{SRC1}(t)}{F_{SRC1total}}$$

Where f_v is the specific fluorescence of individual SRC1 labelled vesicles and $F_{SRC1total}$ is the total fluorescence of completely loaded *RP*. By taking into account that:

$$F_{SRC1total} = RP \cdot f_v \qquad\qquad \textbf{Equation 6.3}$$

And by substituting for N_{AP} and $F_{SRC1total}$, we obtained:

$$\frac{dF_{SRC1}(t)}{dt} = -\frac{RRP}{RP}.p_v.F_{SRC1}(t)$$

and

$$F_{SRC1}(t) = F_{SRC1total}.e^{-\left(\frac{RRP}{RP}.p_v.t\right)}$$

Here, the coefficient of the exponential decay is equal to the observed specific AP-evoked SRC1 destaining rate:

$$K_{AP} = \left[\frac{RRP}{RP}\right].p_v \qquad\qquad \textbf{Equation 6.4}$$

Therefore from our experimental protocol, where we measured K_{AP}, RRP/RP and RP we could indirectly calculate the average release probability, p_v, of vesicles within the RRP as:

$$p_v = \frac{K_{AP}}{\left[\dfrac{RRP}{RP}\right]}$$

Also, another experimentally determined parameter of interest is the vesicular release rate:

$$R_{rel} = F_{SRC1total}.K_{AP}$$

Equation 6.5

Since $F_{SRC1total}$ is proportional to the size of the RP (Equation 6.3), the observed R_{rel} is proportional to the average number of vesicles released during a single AP. Indeed, by combining 6.3, 6.4 and 6.5:

$$R_{rel} = F_{SRC1total} \cdot K_{AP} = RP \cdot f_v \cdot \frac{RRP}{RP} \cdot p_v = f_v \cdot RRP \cdot p_v$$

And hence:

$$R_{rel} = f_v.N_{AP}$$

Equation 6.6

Finally, the variation of parameters was determined by the coefficient of variation, CV, where

$$CV = \frac{Std.dev}{mean} = \frac{\sigma}{\mu}$$

Equation 6.7

6.4. Results

6.4.1. Major findings.

- The sizes of the *RP* and *RRP* vary widely across boutons.

- *RRP* does not correlate with K_{AP}, arguing that release ready vesicles fuse independently from one another, and hence a binomial model is valid.

- The variation in *RRP/RP* cannot fully explain the variation in K_{AP}, indicating a substantial heterogeneity of p_v among individual synaptic boutons.

6.4.2. Labelling recycling synaptic vesicles with SRC1
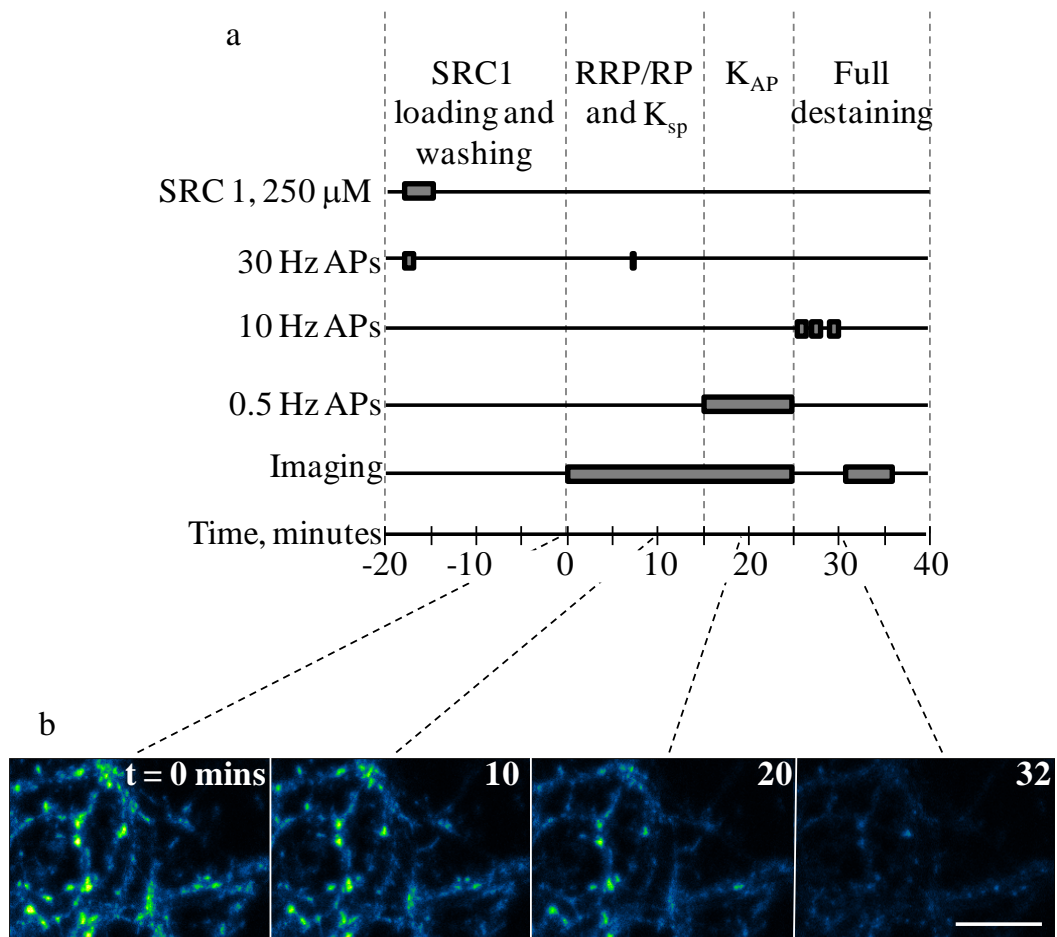
Figure 6.2: Experimental paradigm and example region containing several putative boutons. (a) Experimental paradigm for SRC1 labelling and destaining experiments. (b)

Example region from one experiment, showing several putative boutons during the course of the experiment. Scale bar: 10 μm.

We performed experiments on cultured hippocampal neurons extracted from post-natal WT mice, using our established protocol (figure 6.2a and see section 2.5 for more details). After complete labelling of recycling vesicles with 250 μM SRC1 using four trains of 120 APs at 30 Hz (20 s delay between trains), the chamber was washed of the dye for 15 minutes before imaging commenced. The spontaneous destaining rate K_{sp} was estimated first, before the *RRP* was depleted by 60 APs at 30 Hz. The evoked destaining rate K_{ev} (and hence $K_{AP} = K_{ev} - K_{sp}$) was estimated by applying 0.5 Hz stimulation. Finally a measure of the background fluorescence was taken by releasing all the vesicles in the recycling pool with three rounds of 300 APs at 10 Hz.

A typical region with several putative boutons at 10 minute intervals during the SRC1 destaining experiment is shown in figure 6.2b. We selected potentially active boutons by circling regions of interest (ROIs) on a mask image (see section 2.5.5 in Chapter 2 for detailed method), and then analysed fluorescence traces from each bouton using specially written MathCad program as detailed below.

6.4.3. Average synaptic vesicle recycling parameters in a typical SRC1 destaining experiment
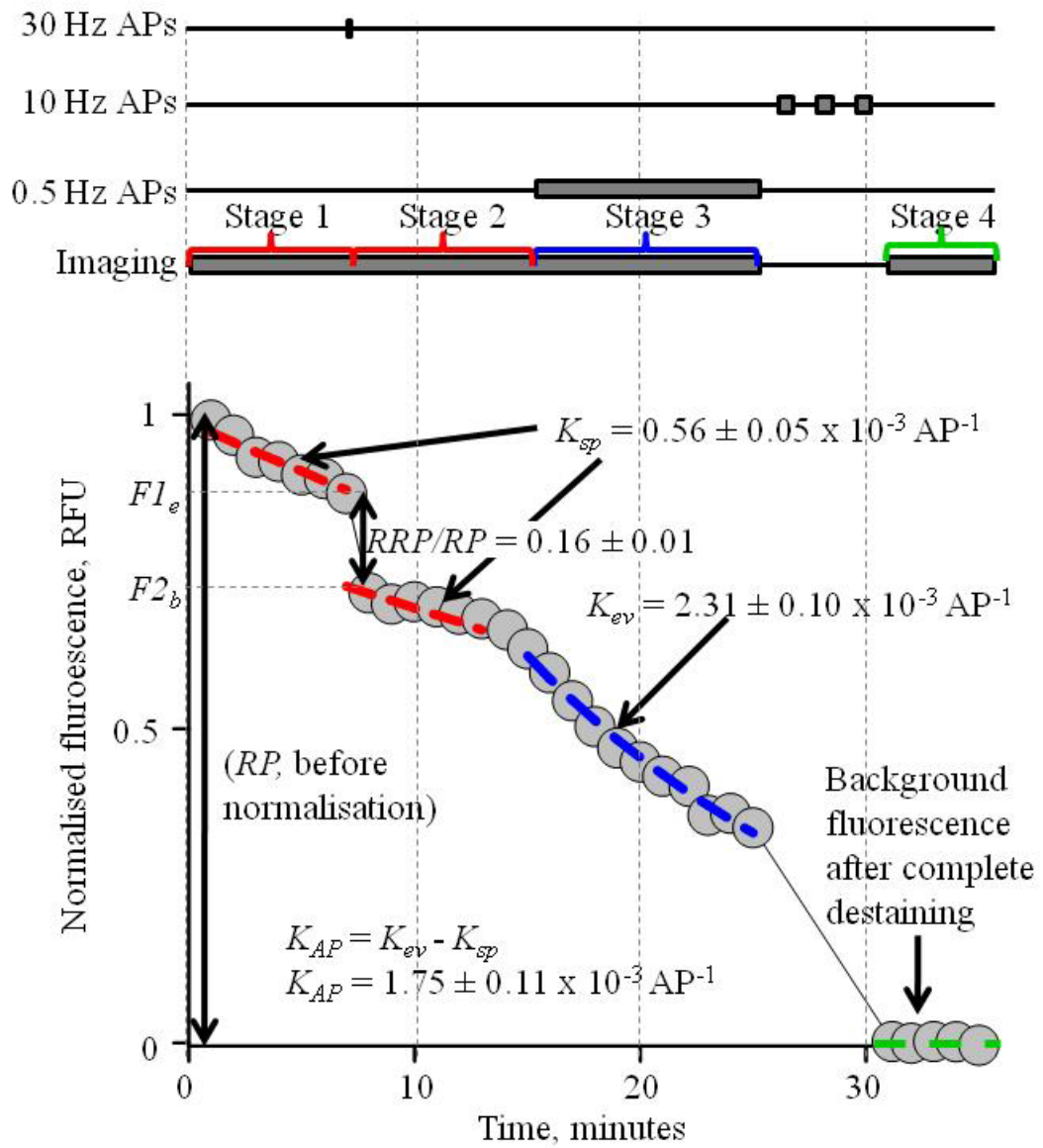
Figure 6.3: Example average trace from a typical experiment. *The fluorescence trace was fitted with mono-exponential functions to determine K_{sp} (red traces) and K_{ev} (blue trace). The RRP / RP ratio was estimated as $(F1_e - F2_b)/F1_e$, where $F1_e$ is the specific SRC1 fluorescence immediately before RRP deletion (last frame of stage 1) and $F2_b$ is the specific SRC1 fluorescence immediately after RRP depletion (first frame of stage 2).*

The size of RP was estimated as the total fluorescence at t = 0, after taking background fluorescence into consideration (and before normalisation)

The average destaining trace for selected boutons normalised to the initial fluorescence at t = 0 minutes from a typical WT mouse experiment showed a slow fluorescence decrease in the absence of stimulation, pertaining to the spontaneous destaining rate K_{sp} (red trace, figure 6.3). A distinct drop in fluorescence during high frequency (30 Hz) stimulation gave an estimate of the average size of the *RRP*. Applying low frequency (0.5 Hz) stimulation to the culture led to a faster decrease in fluorescence, which gave an approximation of the average evoked destaining rate K_{ev} and hence K_{AP} (blue trace, figure 6.3). Finally, the background fluorescence could be estimated after complete destaining (three rounds 300 APs at 10 Hz). This gave us an estimate for *RP* in each bouton (before normalisation). The average values from this typical experiment were interesting to study the overall neurotransmission profile in our cultures, but more interesting for us was the distribution of synaptic parameters at the level of individual boutons.

6.4.4. *Estimating synaptic vesicle recycling parameters in individual synapses*

The typical region from figure 6.2b contained several putative synaptic boutons (figure 6.4a). Even in this small region, we observed a large heterogeneity in *RRP/RP* ratios and K_{AP} values among different boutons (figure 6.4b and table 6.1 for values). In particular, we obtained similar estimates of *RRP/RP* for boutons 2 and 3, but K_{AP} was 2.4 times larger in bouton 2. Also, the size of the *RRP/RP* in bouton 1 was smaller than all other example boutons, but the destaining rate K_{AP} was relatively fast.
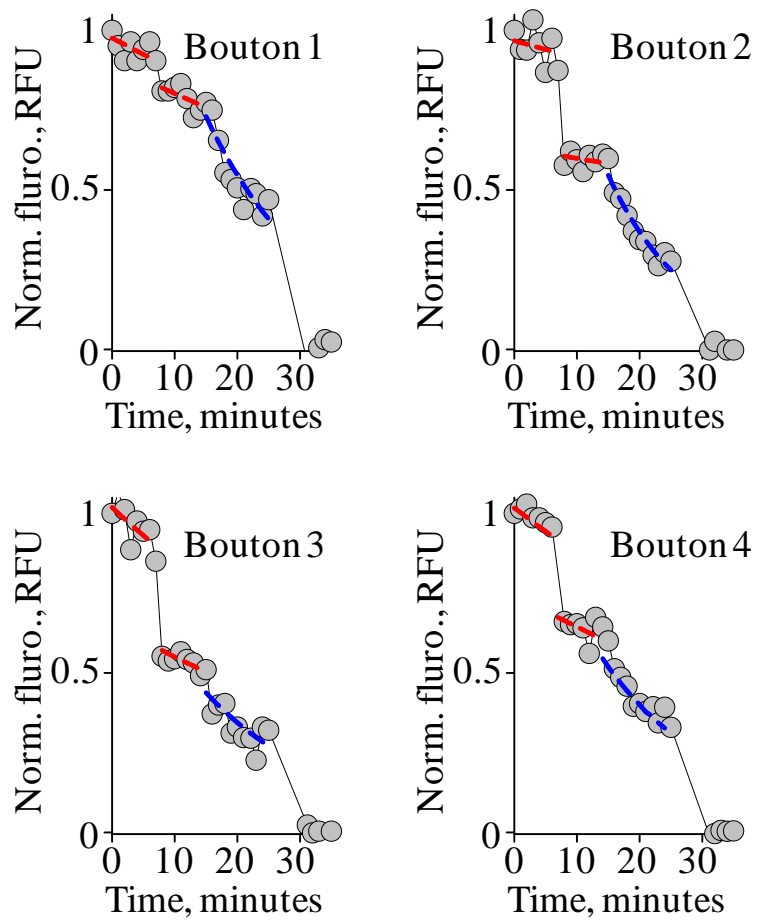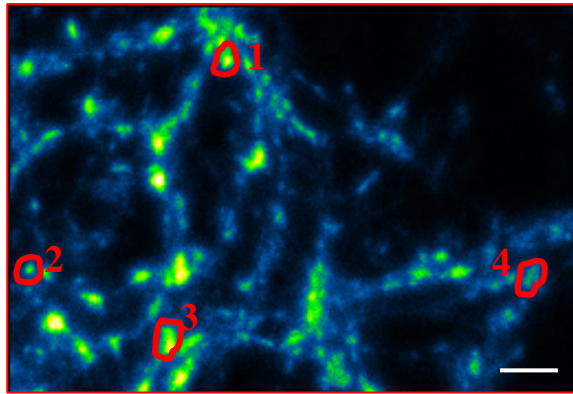
Figure 6.4: Example traces for four selected boutons from a typical experiment. (a)
*Typical region from the example experiment in figure 6.2b and 6.3. (**b**) Traces for four*
boutons which passed the selection criteria. Values of parameters for these boutons are
*listed in table 6.1. Scale bar: (**a**) 10 μm*

Table 6.1: Recycling parameters of 4 example boutons shown in figure

Bouton	K_{sp}, x 10^{-3}, AP^{-1}	K_{AP}, x 10^{-3}, AP^{-1}	*RRP/RP*	Stage 1, χ^2 x 10^{-3}	Stage 2, χ^2 x 10^{-3}	Stage 3, χ^2 x 10^{-3}
1	0.36	1.57	0.08	0.92	0.70	2.20
2	0.19	2.43	0.34	2.33	0.53	0.68
3	0.60	1.01	0.35	2.04	0.32	1.98
4	0.50	1.21	0.25	2.30	1.30	0.85

For each bouton, the χ^2 of the fit of K_{sp} and K_{ev} was calculated as outlined in Chapter 2, section 2.5.5. By varying the cut-out of χ^2 for each stage of the experiment, we determined that $\chi^2 = 2.5$ x 10^{-3} was sufficient to remove boutons where movement artefacts were present (e.g. figure 6.5). In order not to bias our analysis, the cut-out of χ^2 was the only parameter we initially used to select boutons. However, it was a powerful method, as a large number of destaining profiles which did not correspond to synaptic boutons were removed (~ 90% removed, figure 6.5 and table 6.2). These boutons all had signals which were either too noisy to fit accurately (figure 6.5b, regions 1 and 2) or where obvious movement of the fluorescence signal occurred (figure 6.5b, regions 3 and 4, red arrows). Movement of fluorescence during an experiment could be due to mobile vesicles leaving or entering a synapse (Staras et al. 2010), movement of the synapse itself, or a particles of dirt in the perfusion.
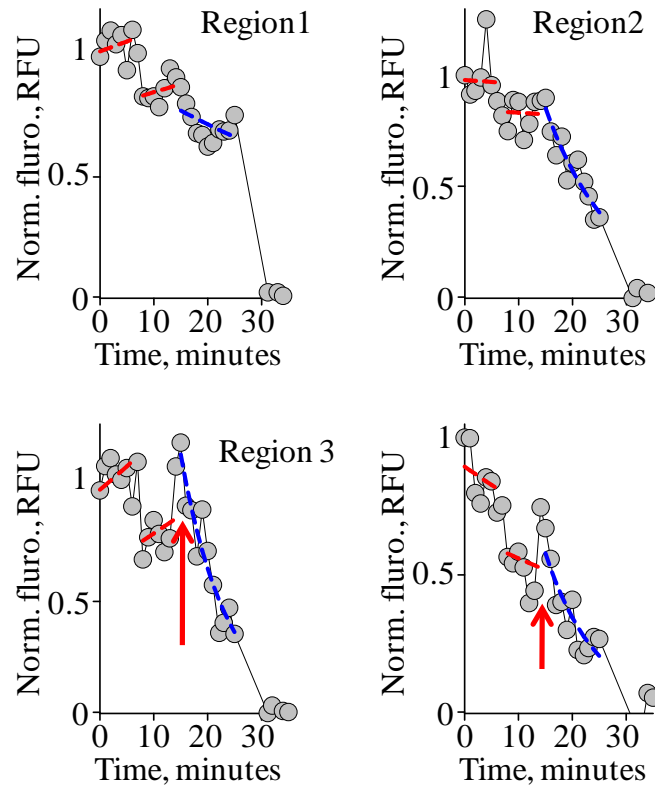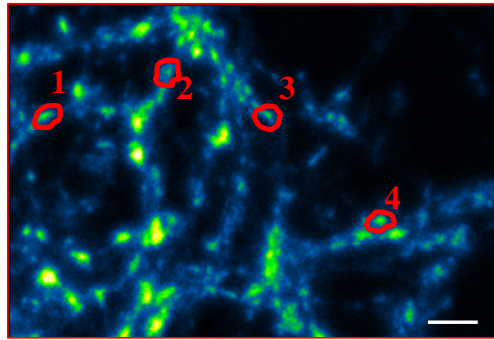
***Figure 6.5: Example fluorescence traces from a typical experiment for ROIs that
were not selected for future analysis. (a)*** *Typical region from the example experiment
as in figure 6.4a.* ***(b)*** *Traces from four ROIs which did not pass the selection criteria as
χ^2 was above the threshold. Values of χ^2 for these regions are listed in table 6.2. Scale
bar:* ***(a)*** *10 μm*

Table 6.2: χ2 of four example disregarded regions showing substantial movement.

Region	Stage 1, χ^2 x 10^{-3}	Stage 2, χ^2 x 10^{-3}	Stage 3, χ^2 x 10^{-3}
1	3.54	1.80	3.58
2	16.10	3.94	3.64
3	10.93	15.66	8.61
4	8.80	14.82	2.62

The *RP*, which gave the total size of the recycling pool was estimated by two methods. First, *RP* was measured by taking the fluorescence signal at t = 0 (i.e. the fluorescence at the start of imaging, having taken the background fluorescence into account). This we denoted as '*RP 1st frame*'. Secondly, the fluorescence signal immediately after loading was estimated, by extrapolating the fit for K_{sp} back to the time of loading, which we denoted as '*RP wash*'. By taking spontaneous destaining during the wash process into account using the second method, the estimate of *RP* was obviously on average larger.

6.4.5. Variability of synaptic recycling parameters within and between experiments
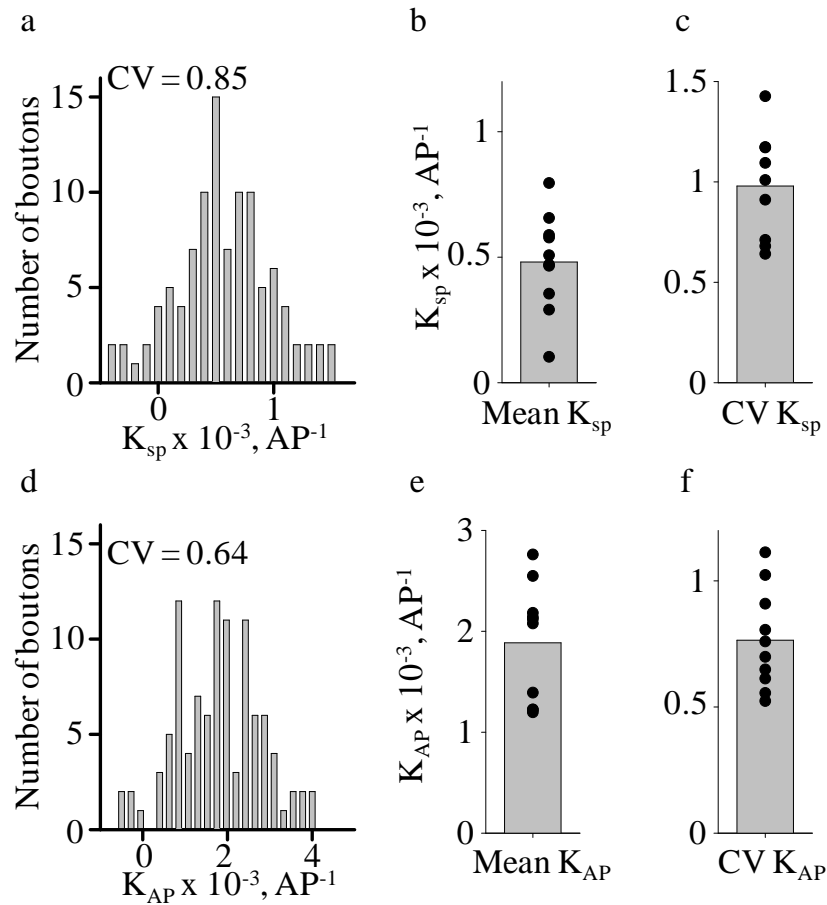
Figure 6.6: Distribution of K_{sp} and K_{AP} in a typical experiment and averaged over all experiments. (a), (d) Distribution of K_{sp} (a) and KAP (d) in the example experiment. (b), (e) mean values of K_{sp} (b) and K_{AP} (e) in individual experiments (scatter plot) and mean of the means (bar chart). (c), (f) mean values of CV for K_{sp}(c) and K_{AP} (f) in individual experiments (scatter plot) and mean of the means (bar chart). (a), (d) n=105 boutons. (b), (c), (e), (f) N = 714 boutons from N=10 independent experiments.

The distributions of K_{sp} and K_{AP} in the experiment depicted in figures 6.2 – 6.5 both showed substantial heterogeneity amongst individual boutons from the same coverslip (figure 6.6a, d. CV = 0.85 and 0.64 respectively). The mean values of K_{sp} and K_{AP} from all boutons in individual experiments also substantially varied among experiments

(figure 6.6b and e. Scatter plots) but gave an average observed value of 0.48 ± 0.06 x

10^{-3} AP^{-1} and 1.89 ± 0.18 x 10^{-3} AP^{-1} (figure 6.6b and e, bars). Between experiments,

the CVs also varied (figure 6.6c and f, scatter plot), and had a mean value of 0.98 ± 0.09

for the CV of K_{sp} and 0.76 ± 0.06 for the CV of K_{AP} (figure 6.6c and f, bars)
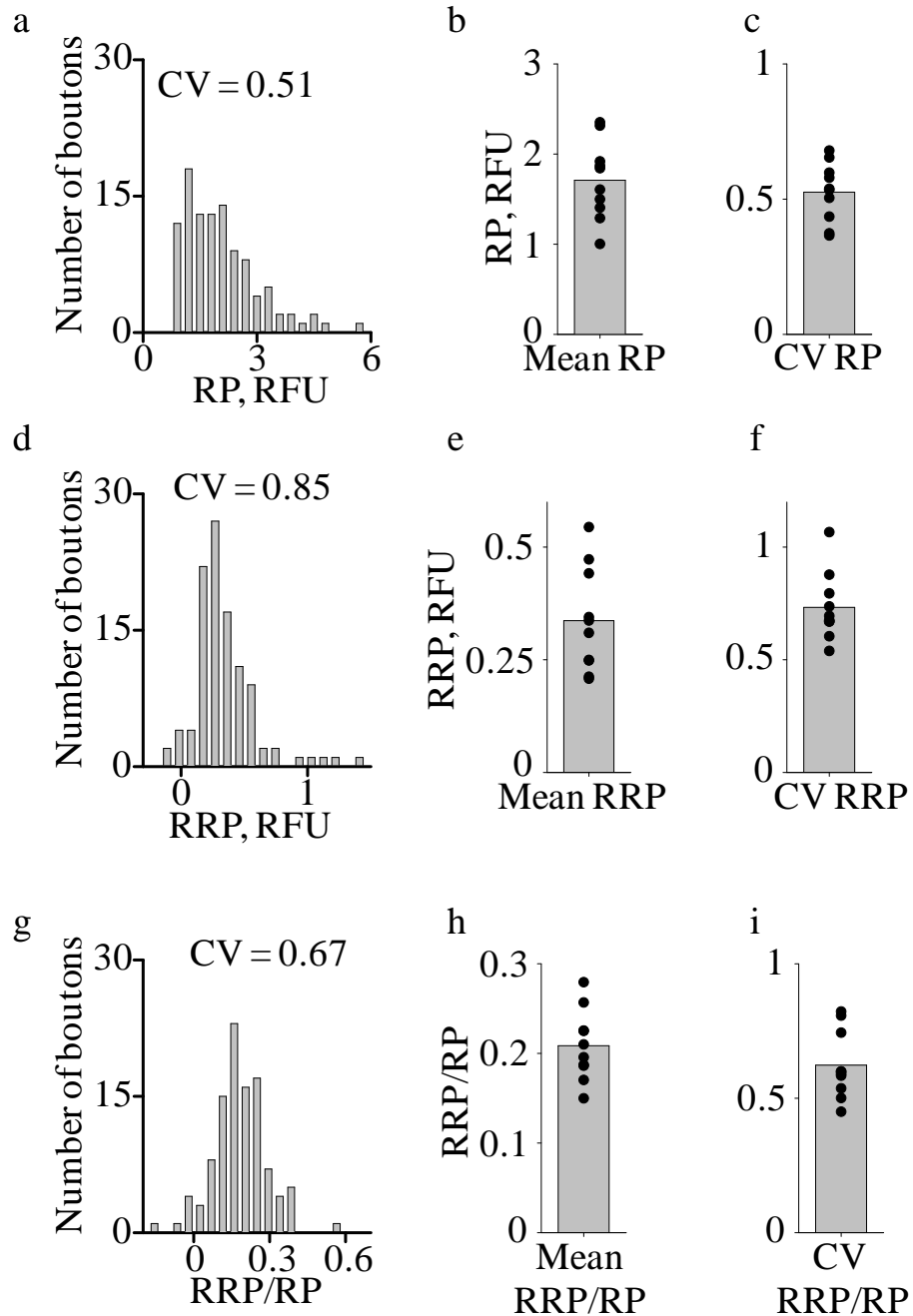
Figure 6.7: Distribution of RP, RRP, and RRP/RP in a typical experiment and

averaged over all experiments. (a), (d), (g) Distribution of RP (a), RRP (d), and

*RRP/RP(**g**) in the example experiment. (**b**), (**e**), (**h**) mean of RP (**b**), RRP (**e**) and*

*RRP/RP (**h**) for each experiment (scatter plot) and mean of the means (bar chart). (**c**),*

*(**f**), (**i**) mean CV for RP (**c**), RRP (**f**) and RRP/RP (**i**) for each experiment (scatter plot)*

*and mean of the means (bar chart). (**a**), (**d**), (**g**) n=105 boutons. (**b**), (**c**), (**e**), (**f**), (**h**), (**i**)*

N = 714 boutons from N=10 independent experiments.

Next we looked at the distributions of the *RP* (measured at the first frame), the *RRP* and

the ratio *RRP/RP* in the same example experiment (figure 6.7). The CV for *RP* was

lower compared to other vesicle pool size measurements (*RRP* and *RRP/RP*). This

difference in variation arose from the method for estimating the different values: to

estimate *RP*, only two mono-exponential fits were used (to fit stage 1 and 4), whereas to

estimate *RRP* and *RRP/RP*, three exponential fits were used. Similar to K_{AP} and K_{sp}, the

mean from each experiment and the mean of the means were calculated (figure 6.7b),

giving a mean value of *RP* as 1.71 ± 0.14 RFU.

The estimation of *RRP* showed large heterogeneity in the example experiment (figure

6.7d, CV = 0.85), and a mean of 0.34 ± 0.04 RFU between all experiments (figure 6.7e).

The *RRP*/*RP* varied to a lesser extent compared to *RRP* (figure 6.7g, CV = 0.67). The

RRP/RP was 0.21 ± 0.01 among all experiments, indicating that roughly 20% of

vesicles from the recycling pool are fusion-competent (figure 6.7h). In conclusion, all

observed synaptic vesicle recycling parameters showed variable degrees of

heterogeneity both between individual boutons from the same coverslip, and amongst

experiments.

6.4.6. Correlations between synaptic vesicle recycling parameters
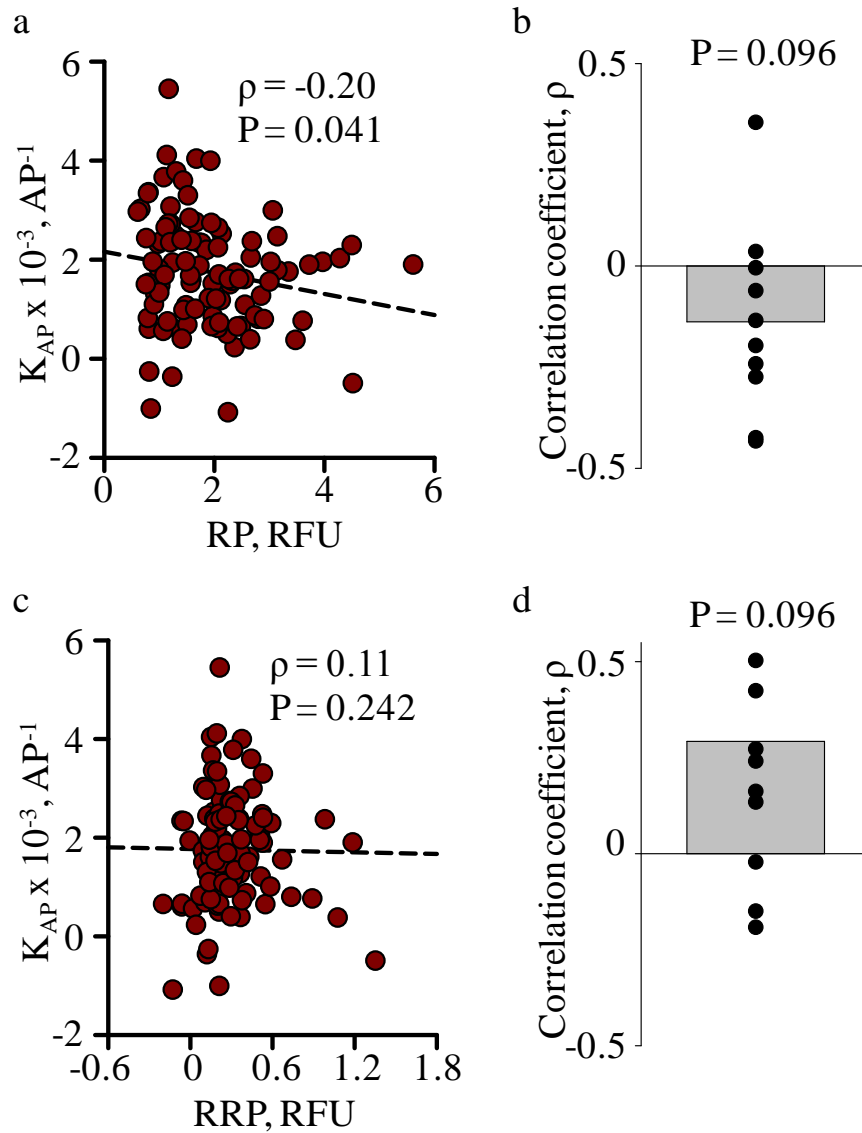
Figure 6.8: Lack of correlation between K_{AP} and RP, and K_{AP} and RRP. (a)

Relationship between RP and K_{AP} in the example experiment. ρ = -0.20, P = 0.041,

Spearman rank correlation. (b) Correlation coefficients for all experiments (scatter

graph), and mean ρ (P = 0.096, one sample T-test) (c) Relationship between RRP and

K_{AP} for the example experiment. ρ = 0.11, P = 0.242, Spearman rank correlation. (d)

Correlation coefficients for all experiments (scatter graph), and mean ρ (P = 0.096, one

*sample T-test) (**a**), (**c**) n=105 boutons. (**b**), (**d**) N = 714 boutons from N=10 independent*

experiments.

Next, we looked at whether there was any correlation between specific parameters.

First, we investigated the relationship between K_{AP} and RP, to test the assumption that

vesicles at the AZ fuse independently and hence follow a binomial model was valid

(figure 6.8a). The assumption that vesicles fuse independently from one another allowed

for the possibility of multivesicular release, especially at larger synapses or those with

high release probability. If this was the case, K_{AP} should not theoretically depend on the

size of RP. If however the fusion of an individual vesicle inhibited further fusion of

other vesicles at the same AZ, we would expected K_{AP} to have a negative correlation

with RP (Stevens et al. 1995).

In the example experiment, we observed that K_{AP} and RP had only weak negative

correlation, with a coefficient of $\rho = -0.20$ (figure 6.8a). However, when we calculated

the correlation coefficient for each experiment (figure 6.8b, scatter plot) and the mean

of all values of ρ ($\rho = -0.14 \pm 0.07$, figure 6.8b, bar plot), we found that ρ for all

experiments was not significantly different from zero (figure 6.8b). This indicated that

there was no significant correlation between K_{AP} and RP, suggesting the assumption that

vesicles fuse independently was valid and hence follow a binomial distribution. Indeed

we also did not find any significant correlation between K_{AP} and RRP within the

example experiment (figure 6.8c), and when averaged over all experiments (figure 6.8d)
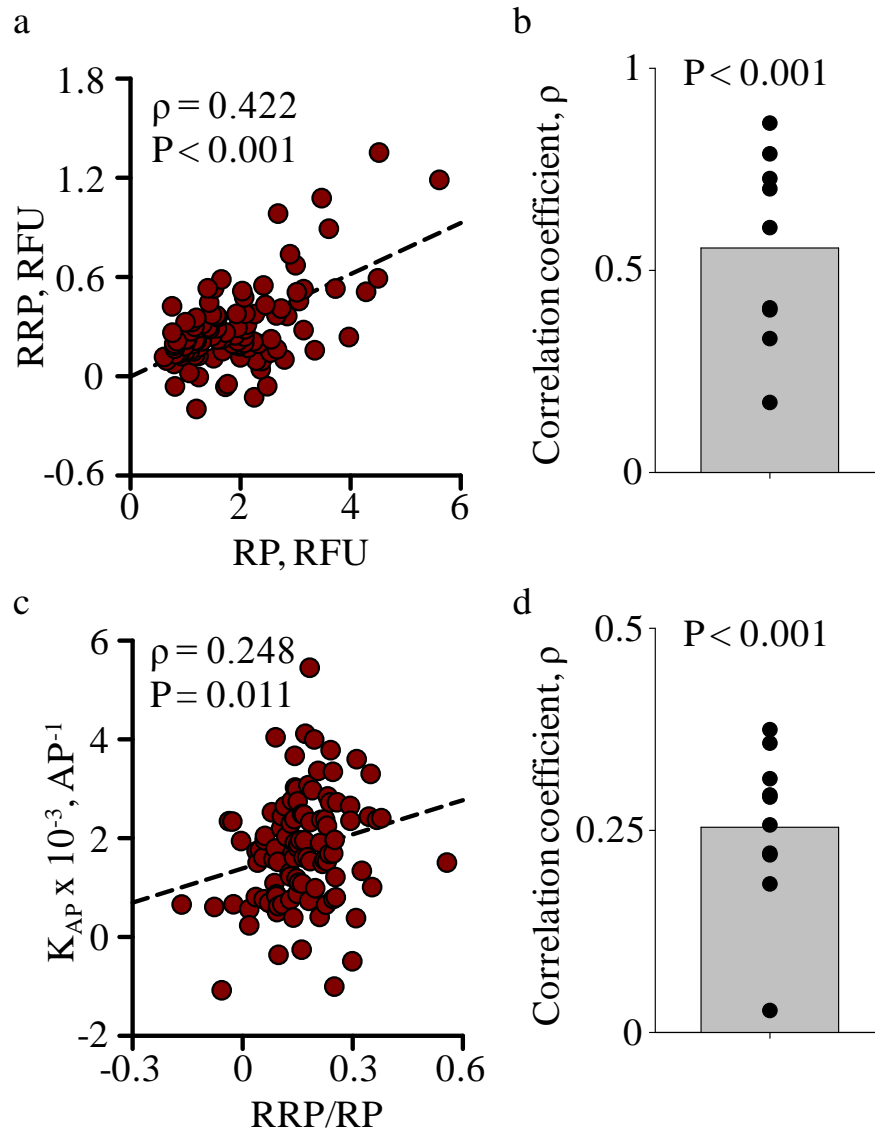
Figure 6.9: Relationship between RP and RRP, and K_{AP} and RRP/RP. *(a) Correlation*

between RP and RRP for the example experiment. ρ = 0.422, P < 0.001, Spearman rank

correlation. (b) Correlation coefficients for all experiments (scatter graph), and mean ρ

(P < 0.001, one sample T-test) (c) Correlation between RRP/RP and K_{AP} for the

example experiment. ρ = 0.248, P = 0.011, Spearman rank correlation. (d) Correlation

coefficients for all experiments (scatter graph), and mean ρ (P < 0.001, one sample T-

test) (a), (c) n=105 boutons. (b), (d) N = 714 boutons from N=10 independent

experiments.

As expected if the size of the RP and RRP both scaled with the size of the synapse (Murthy et al. 2001; Schikorski et al. 1997), we found a strong, positive correlation between *RP* and *RRP* in the example experiment (figure 6.9a). This correlation was evident in all experiments (figure 6.9b), with an average coefficient of $\rho = 0.51 \pm 0.06$.

Finally, we looked at the correlation between *RRP/RP* and K_{AP} (figure 6.9c and d). As expected from the equation $K_{AP} = RRP / RP \cdot p_v$ we found a significant positive correlation between these two parameters (figure 6.9c and d). However the observed correlation was relatively weak (mean correlation coefficient $\rho = 0.28 \pm 0.04$). This suggested that p_v should also vary among individual boutons. Therefore, we investigated the variability of p_v between synapses in more detail in the rest of this chapter to determine its contribution to the variability of P_{rel} (equation 6.2)

6.4.7. Estimating of true biological variability of K_{AP}, RRP/RP and p_v.

To test to what degree p_v varied, we first looked at the underlining sources of variation of K_{AP} and *RRP/RP*, to determine the contribution of experimental error and true biological variation to the observed variation. For each parameter the experimentally observed coefficient of variation CV_{Exp}, could be described as the sum of two independent variations:

$$CV_{Exp} = CV_{Biol} + CV_{Err} \hspace{3cm} \textbf{Equation 6.8}$$

where CV_{Biol} is the true biological variation in the parameter arising from differences among individual boutons, and CV_{Err} is the variation due to experimental error. Our aim was to estimate CV_{Err} and then CV_{Biol} as:

$$CV_{Biol} = CV_{Exp} - CV_{Err}$$

for both K_{AP} and RRP/RP.

In order to estimate CV_{Err} we performed Monte Carlo analysis of experimental noise. For each experiment we first generated a model fluorescence decay profile using the average values of K_{AP}, K_{sp}, and RRP/RP. Next, using the empirical noise distribution (e.g. experimentally determined χ^2 values) we simulated fluorescence decay profiles with noise and determined K_{AP}, K_{sp}, and RRP/RP in each profile using monoexponential fitting procedure as for the real experimental data.

On average, CV_{Exp} was higher for K_{AP} than for RRP/RP between most experiments (figure 6.10a, bar chart), although the degree to which CV_{Exp} for K_{AP} was larger varied between experiments (figure 6.10a, paired scatter points). Interestingly, the experimental error CV_{Err} for K_{AP} was lower than that for RRP/RP, although not significant (figure 6.10b). Finally, this allowed us to estimate CV_{Biol} for both K_{AP} and RRP/RP (figure 6.10c). If the assumption that p_v varied between boutons was true, the CV_{Biol} for K_{AP} should be higher than CV_{Biol} for RRP/RP. Indeed in nearly all experiments CV_{Biol} for K_{AP} was higher than that for RRP/RP (figure 6.10c, scatter plot). This result validates the idea that p_v varies amongst boutons, and hence increases the heterogeneity of P_{rel}.
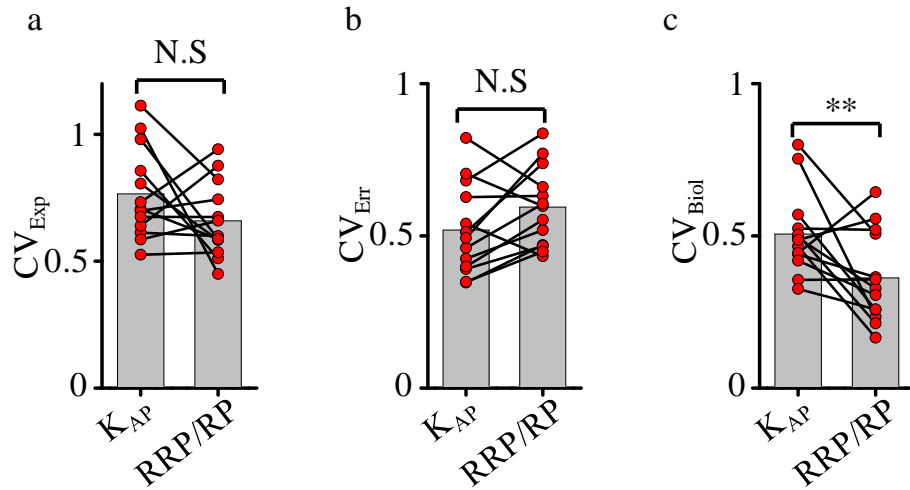
Figure 6.10: of the coefficient of variation (CV) for K_{AP} and RRP/RP. (a) *The measured CV_{Exp} of K_{AP} and RRP/RP for each experiment (scatter plot) and the means (bars)* ***(b)*** *Modelled estimate of CV_{Err} of K_{AP} and RRP/RP for each experiment (scatter plot) and the means (bars)* ***(c)*** *The variation arising from biological heterogeneity, CV_{Biol} of K_{AP} and RRP/RP for each experiment (scatter plot) and the means (bars). **P = 0.02, paired T-test*

6.5. Discussion

Current knowledge of neurotransmitter release mechanisms in the CNS strongly rely on studies of large or giant synapses, such as hippocampal mossy fibre connections or at the calyx of Held. These synapses are large enough to be patch-clamped to control the presynaptic membrane potential, allowing for direct measurements of synaptic properties. However, the majority of synapses in the CNS are too small (~ 1 μm scale) to allow such methods. Although recent studies have identified many of the molecules involved in activity dependent exo- and endocytosis at small central synapses a quantitative understanding of the variability of presynaptic recycling parameters has lagged behind.

In this chapter, we used a common technique of measuring presynaptic vesicle recycling (styryl dyes, in this case SRC1) applied to a new experimental paradigm, to simultaneously measure RP, RRP, K_{sp} and K_{AP} at the level of individual boutons from dissociated hippocampal cultures. Our main goals were to estimate the variability in the measured parameters, and to deduce whether the average release probability of vesicles in the RRP (p_v) varied amongst boutons. We measured the heterogeneity of the AP-evoked SRC1 destaining rate K_{AP}, which is proportional to the average number of vesicles released per AP, N_{AP}, and hence directly related to the synaptic release probability P_{rel}. We found that the biological heterogeneity of K_{AP}, and hence P_{rel}, could not solely be described by the variability of the RRP/RP, but was also dependent on the variability in p_v.

What was the source of the variation in p_v? Our colleague Yaroslav Ermolyuk performed similar SRC1 destaining experiments in hippocampal cultures, and combined

them with Ca^{2+} imaging experiments. He observed a strong correlation between p_v and the magnitude of AP-evoked presynaptic Ca^{2+} influx amongst synaptic boutons located on the same axon. This suggested that the average number of active VGCCs that trigger release of individual RRP vesicles varies among synapses.

6.6. Conclusions

Our results argue that heterogeneity of release probability P_{rel} in small CNS synapses is determined not only by the variability of the *RRP/RP* size, but also by inter-synaptic differences in the average exocytosis probability of individual release ready vesicles, p_v.

7. Effect of FHM1 mutations on vesicular release in small hippocampal synapses

7.1. Introduction

As discussed in the general introduction (section 1.6.9), there is controversy surrounding the effects of FHM1 mutations on P/Q-type Ca^{2+} channel function. In particular, it is not well understood whether FHM1 mutations lead to increase or decrease of neurotransmitter release at the level of individual synapses (Hans et al. 1999; Tottene et al. 2002; Tottene et al. 2005; Cao et al. 2005)

Following on from the results discussed in chapter 6, the average fusion probability of an individual vesicle docked at the AZ is heterogeneous amongst synaptic boutons. We also have data indicating that this variation is strongly correlated to the magnitude of AP-evoked presynaptic Ca^{2+} influx (Ermolyuk et al., in submission). If FHM1 mutations cause an increase in single-channel Ca^{2+} influx via VGCCs as has been proposed in a number of studies (Tottene et al. 2002; Tottene et al. 2005), this could lead to an increase of p_v in synapses harbouring FHM1 mutations compared to WT controls.

Using the SRC1 fluorescent imaging approach described in chapter 6, we wanted to measure synaptic vesicle recycling in cultures containing FHM1 mutations. We were interested to understand whether the spontaneous and evoked destaining rates (K_{sp} and K_{AP}) were increased at S218L and R192Q HOM and HET synapses, as a number of studies have suggested that neurotransmission is increased by these mutations at several synapses (van den Maagdenberg et al. 2004; van den Maagdenberg et al. 2010)

We also wanted to investigate whether the sizes of the *RP* and *RRP* were modified by the S218L and R192Q mutation. Several studies have pointed to activity-dependent

homeostatic changes in the size of vesicular pools (Murthy et al. 2001; Thiagarajan et al. 2005). The regulation of neurotransmission by FHM1 mutations therefore could possibly lead to a change in the size of the vesicular pools, *RP* and *RRP*.

With our imaging method, we had an opportunity to simultaneously estimate K_{sp}, K_{AP}, *RP*, *RRP* and the release rate R_{rel} in individual synaptic boutons in both mutated and WT cultures. Unlike other studies which recorded average values from a large number of synapses via electrophysiological methods, we could discern estimates for these factors at the level of individual synapses and so hope to answer whether FHM1 mutations lead to a gain- or loss-of-function.

In addition to studying synaptic recycling at FHM1 containing synapses, we also looked at the effects of KO of the CACNA1A gene with encodes P/Q-type Ca^{2+} channels (Kaja et al. 2007). The HET mouse KO can be used as a model of EA2 (Ophoff et al. 1996), as EA2 in humans is associated with loss-of-function of P/Q-type Ca^{2+} channels (Riant et al. 2008; Labrum et al. 2009). Finally, P/Q-type Ca^{2+} channels are the dominant subtype in neurotransmitter release regulation at hippocampal synapses (Cao et al. 2004), and hence we were interested to establish the effect of the HOM KO on vesicle recycling.

7.2. Specific Aims

- Compare synaptic vesicle recycling in WT, HET and HOM cultures harbouring the FHM1 mutations S218L and R192Q, using the SRC1 destaining protocol discussed in chapter 6. In particular, we want to understand whether the mutations lead to any differences in the values of K_{sp}, K_{AP}, RP, RRP/RP, and R_{rel}

- Examine the effect of different external Ca^{2+} concentrations on synaptic vesicle recycling in neurons expressing FHM1 mutations.

- Compare recycling parameters in cultures containing and lacking P/Q-type Ca^{2+} channels, as a model of episodic ataxia type 2.

7.3. Results

7.3.1. Main Findings

- At current stage we could not find significant differences in parameters describing neurotransmitter release in S218L and R192Q cultures when compared to the WT controls.

- We found that vesicular release significantly varies among cultures prepared from different litters of the same animal strain.

- Reducing extracellular Ca^{2+} concentration does not unmask any effect of the S218L mutation on vesicular exocytosis.

- Knock out of the CACNA1A gene, and hence removal of P/Q-type Ca^{2+} channels causes a small but significant decrease in the *RRP/RP*

7.3.2. The S218L mutation does not appear to affect vesicle recycling in hippocampal cultures
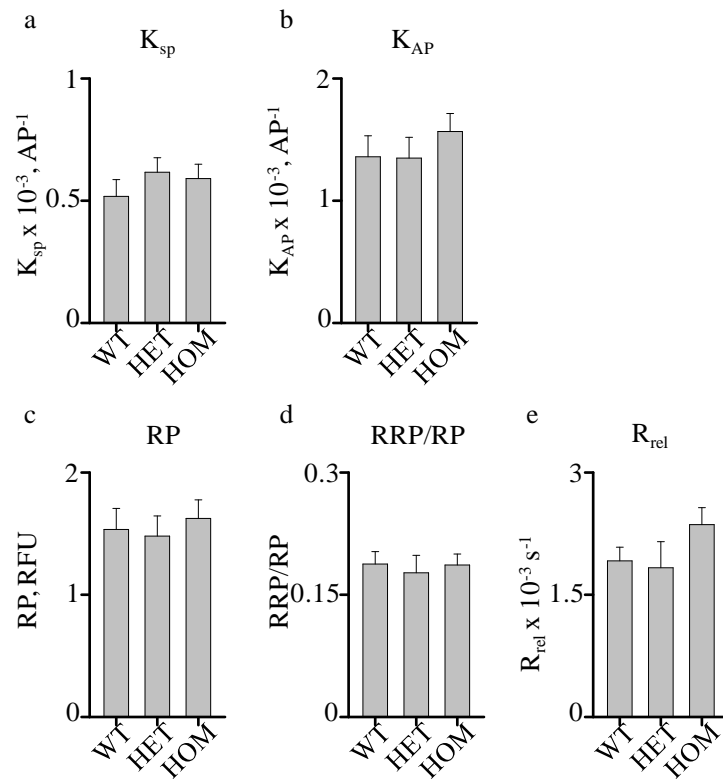
Figure 7.1: Unnormalised synaptic transmission parameters from synapses harbouring the S218L mutation. (a) K_{sp}, (b) K_{AP}, (c) RP, (d) RRP/RP, (e) R_{rel}. WT: n= 770 boutons from N = 12 independent experiments, from M = 3 litters. HET: n= 1113 boutons from N = 12 independent experiments, from M = 3 litters. HOM: n= 990 boutons from N = 13 independent experiments, from M = 3 litters. The table denotes P-values for one way analysis of variance (ANOVA)

	a) K_{sp}	b) K_{AP}	c) RP	d) RRP/RP	e) R_{rel}
P-value	0.523	0.565	0.816	0.888	0.089[†]

[†]*Kruskal-Wallis one way ANOVA*

We applied our experimental paradigm discussed in chapter 6 to cultures harbouring the S218L FHM1 mutation (figure 7.1). For control purposes, we carried out at least one

experiment each on WT, HET and HOM from the same litter on the same day. Initial

analysis of the data revealed that there was no significant difference in any of the

measured parameters, K_{sp}, K_{AP}, RP, RRP/RP, and R_{rel} (figure 7.1a-e). There was a small

increase in the values of K_{sp} (15%), K_{AP} (18%) and R_{rel} (23%) for HOM compared to

WT, although this was not significant (figure 7.1b and e).
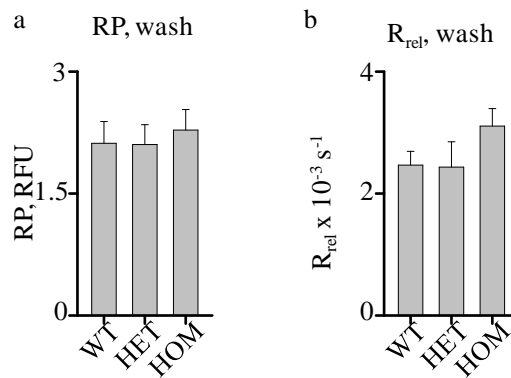
Figure 7.2: RP and R_{rel} measured from the start of dye wash-out. (a) RP wash, (b) R_{rel}

wash. WT: n= 770 boutons from N = 12 independent experiments, from M = 3 litters.

HET: n= 1113 boutons from N = 12 independent experiments, from M = 3 litters.

HOM: n= 990 boutons from N = 13 independent experiments, from M = 3 litters. The

table denotes P-values for one way analysis of variance (ANOVA)

	a) *RP*	b) R_{rel}
P-value	0.858	0.143

We also calculated the size of RP and R_{rel} from the start of the wash, to understand

whether this would uncover any differences between genotypes (see chapter 2, section

2.5.5). Previously reported studies at the NMJ have revealed that spontaneous

exocytosis is increased in S218L synapses (van den Maagdenberg et al. 2010). If this

was the case at hippocampal synapses, it could lead to an underestimation of the size of the *RP* and hence R_{rel} in S218L synapses when calculated at the start of imaging using our protocol. Using this method to calculate *RP* and R_{rel}, we still observed no significant difference between genotypes, although again there was an increase in R_{rel} among HOM cultures (figure 7.2a-b).

7.3.3. The neuronal culture is a large source of variation
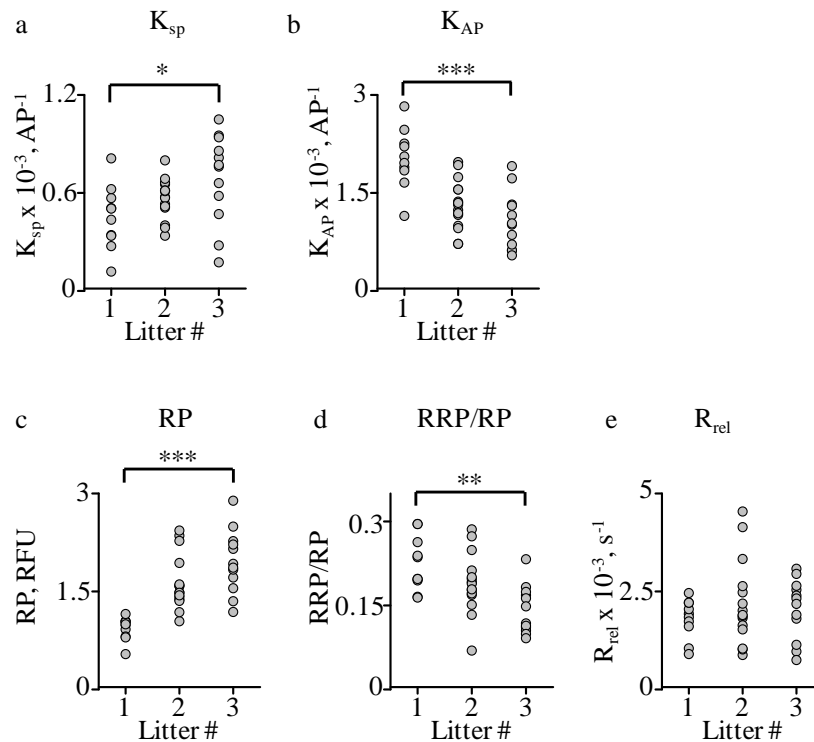
***Figure 7.3: S218L data grouped according to litter of culture. (a)** K_{sp}, **(b)** K_{AP}, **(c)** RP, **(d)** RRP/RP, **(e)** R_{rel}. WT: n= 770 boutons from N = 12 independent experiments, from M = 3 litters. HET: n= 1113 boutons from N = 12 independent experiments, from M = 3 litters. HOM: n= 990 boutons from N = 13 independent experiments, from M = 3 litters. The table denotes P-values for one way analysis of variance (ANOVA)*

	a) K_{sp}	b) K_{AP}	c) *RP*	d) *RRP/RP*	e) R_{rel}
P-value	*0.028[†]	***<0.001[†]	***<0.001[†]	**0.002[†]	0.525

[†]*Hom-Sidak method*

As we found no significant difference in synaptic vesicle release between S218L mutated and WT cultures, we analysed our data further (figure 7.3). We grouped together cultures from the same litter which were prepared on the same day (figure 7.3). A typical litter contained several mice of different genotypes, each of which was used to produce a unique set of coverslips (one coverslip counts for one experiment). In order to investigate whether possible variations in the culturing protocol produced any variation in the measured parameters we compared the groups of experiments performed on cultures from the same litter.

By applying the one-way ANOVA tests as before, we found that the culture produces a significant variability in the destaining rates K_{sp} and K_{AP} and in the vesicle pool sizes RP and RRP/RP (figures 7.3a-d, see table for P-values). The release rate (figure 7.3e) did not significantly vary with the litter, although as the product of K_{AP} and RP, release rate was still affected by the litter variation. To compensate this variability we calculated the mean of each parameter within each of the three litters. We then used this mean to normalise parameters within each litter. This normalisation was preferable to using the mean of the WT cultures in each litter, as this would not hold if there was uneven numbers of HOM, HET and WT experiments.

7.3.4. Normalisation data within each litter does not affect the initial findings
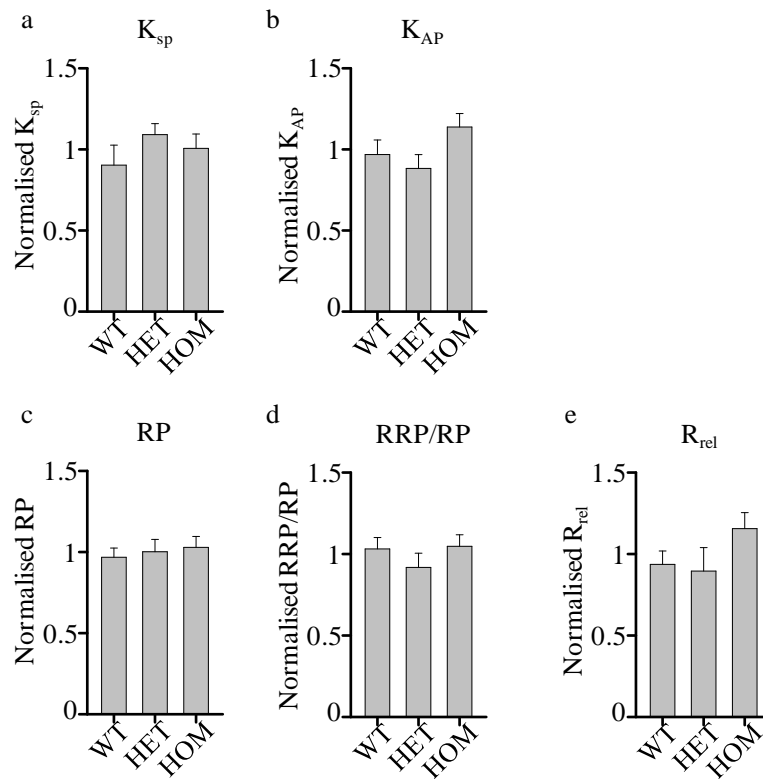
Figure 7.4: Effect of the S218L mutation on synaptic transmission properties

normalised to the mean of each litter. *(a)* K_{sp}, *(b)* K_{AP}, *(c)* RP, *(d)* RRP/RP, *(e)* R_{rel}.

WT: n= 770 boutons from N = 12 independent experiments, from M = 3 litters. HET:

n= 1113 boutons from N = 12 independent experiments, from M = 3 litters. HOM: n=

990 boutons from N = 13 independent experiments, from M = 3 litters. The table

denotes P-values for one way analysis of variance (ANOVA)

	a) K_{sp}	b) K_{AP}	c) RP	d) RRP/RP	e) R_{rel}
P-value	0.400	0.112	0.814	0.434	0.208

We grouped experiments by litters and calculated the mean of each parameter. This

value was used to normalise all the data from each litter (figure 7.4). Although the

increase in K_{sp}, K_{AP} and R_{rel} in HOM cultures was still present, we again did not find any significant difference between genotypes for any of the measured parameters.

7.3.5. Lowering external calcium does not unmask any effect of the S218L mutation
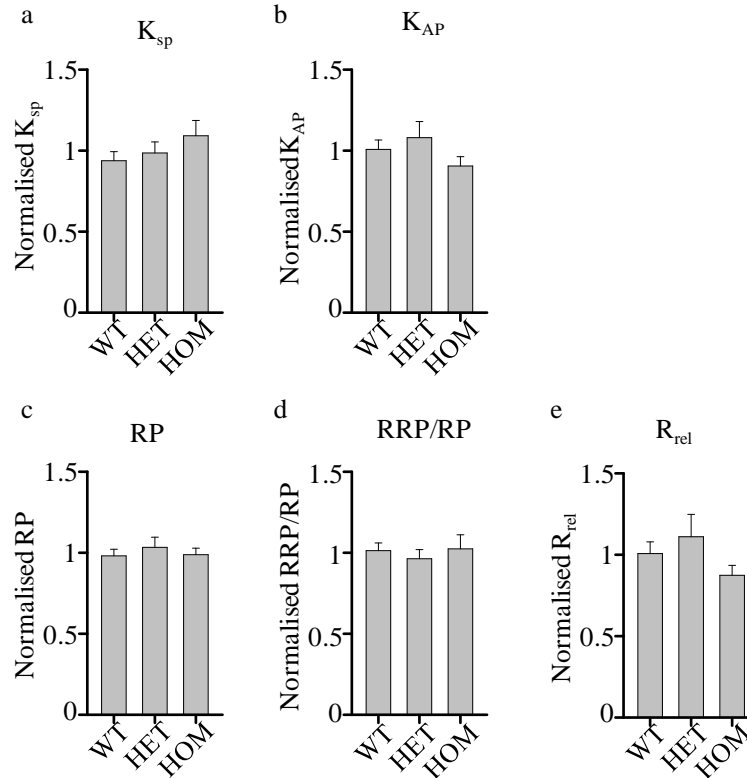
Figure 7.5: Effect of the S218L mutation on synaptic transmission properties in 1 mM external Ca²⁺. *(**a**) K_{sp}, (**b**) K_{AP}, (**c**) RP, (**d**) RRP/RP, (**e**) R_{rel}. WT: n = 1130 boutons from N = 17 independent experiments, from M = 5 litters. HET: n = 844 boutons from N = 15 independent experiments, from M = 5 litters. HOM: n = 1238 boutons from N = 13 independent experiments, from M = 5 litters. The table denotes P-values for one way analysis of variance (ANOVA)*

	a) K_{sp}	b) K_{AP}	c) RP	d) RRP/RP	e) R_{rel}
P-value	0.322	0.274	0.711	0.777	0.335[†]

[†]*Kruskal-Wallis one way ANOVA*

As we found no differences in synaptic transmission parameters arising from the S218L mutation, we investigated whether reduced external Ca^{2+} would unmask any effect. A previous report suggested that synaptic transmission in NMJ synapses harbouring the S218L mutation is enhanced 2.5 times compared to WT in 0.2 mM extracellular Ca^{2+} (van den Maagdenberg et al. 2010). We decided to perform our experiments in 1 mM to analyse any difference in mutant and WT cultures (figure 7.5). Again, we normalised data to the means for each litter. However, as in 2 mM external Ca^{2+}, we did not find any significant differences in any parameter between genotypes.

7.3.6. A less severe FHM1 mutation also has little effect on synaptic transmission
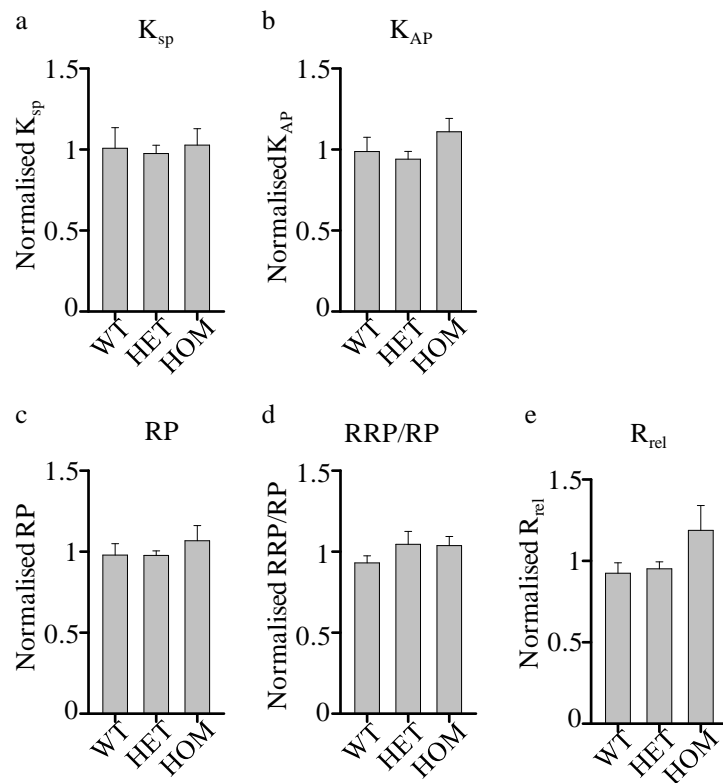
Figure 7.6: Effect of the R192Q mutation on synaptic neurotransmission. (a) K_{sp}, (b) K_{AP}, (c) RP, (d) RRP/RP, (e) R_{rel}. WT: n = 562 boutons from N = 9 independent

experiments, from M = 2 litters. HET: n = 727 boutons from N = 9 independent experiments, from M = 2 litters. HOM: n = 527 boutons from N = 6 independent experiments, M = 2 litters. The table denotes P-values for one way analysis of variance (ANOVA)

	a) K_{sp}	b) K_{AP}	c) RP	d) RRP/RP	e) R_{rel}
P-value	0.936	0.324	0.580	0.360	0.094[†]

[†]*Kruskal-Wallis one way ANOVA*

Alongside the S218L transgenic mouse strain, we had also obtained a second FHM1 mutated mouse strain from the laboratory of our collaborator Arn van den Maagdenberg. The R192Q mutation leads to a less severe phenotype in human patients compared to the S218L mutation, but we were interested to know whether similar trends in synaptic transmitter parameters were present. A previous report has suggested that spontaneous neurotransmission is increased by 81% in NMJ synapses harbouring the R192Q mutation (van den Maagdenberg et al. 2004). We performed our experimental protocol on cultures from R192Q mutant litters in 2 mM external Ca^{2+}, and analysed and normalised in the same way as for S218L (figure 7.6). The results showed similar increases in K_{AP} (12 %) and the R_{rel} (28%) as for S218L (figures 7.6b and e), although again they were not significant.

7.3.7. The CACNA1A KO decreases the evoked neurotransmitter release rate and the relative size of the RRP
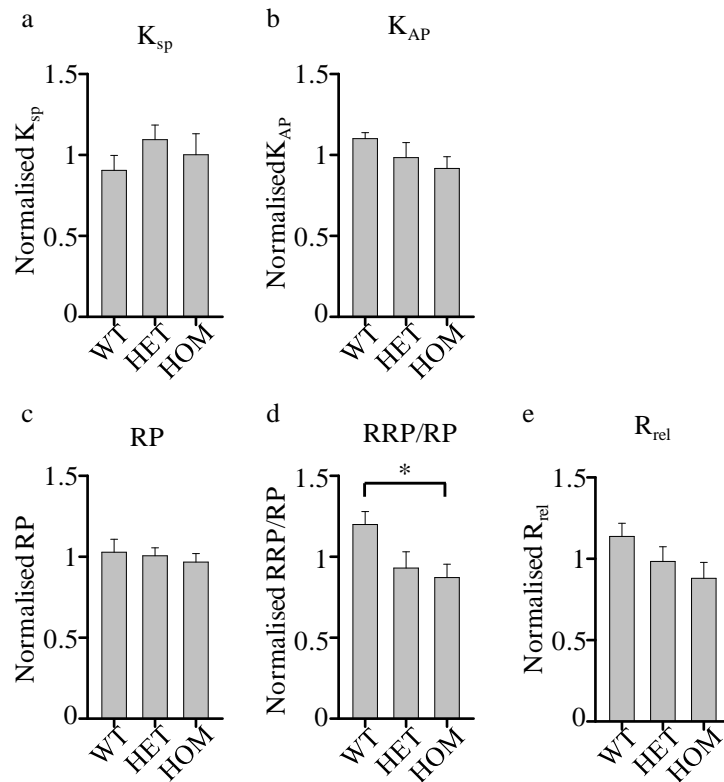
***Figure 7.7: Synaptic neurotransmission properties in hippocampal cultures from CACNA1A KO mice. (a)** K_{sp}, **(b)** K_{AP}, **(c)** RP, **(d)** RRP/RP, **(e)** R_{rel}. WT: n = 1062 boutons from N = 10 independent experiments, from M = 3 litters. HET: n = 924 boutons from N = 10 independent experiments, from M = 3 litters. HOM: n= 928 boutons from N = 10 independent experiments, from M = 3 litters. The table denotes P-values for one way analysis of variance (ANOVA)*

	a) K_{sp}	b) K_{AP}	c) RP	d) RRP/RP	e) R_{rel}
P-value	0.456	0.199	0.783	*0.031[†]	0.144

[†]*Hom-Sidak method*

Finally, we analysed data from cultures from CACNA1A KO mice. There was a small but non significant decrease in K_{AP} for KO synpases, but no similar effect in K_{sp} (figure 7.7a-b). Although we saw no difference in the size of the RP (figures 7.7c), we did observe a significant difference in the *RRP/RP* (figure 7.7d). There was also no significance in the R_{rel} (figure 7.7e).

7.4. Discussion

With this set of data, we aimed to contribute to the discussion of how FHM1 mutations in P/Q-type Ca^{2+} channels affect synaptic vesicle recycling. By simultaneously measuring several parameters characterising neurotransmitter release at the level of individual boutons, we aimed to discover whether FHM1 mutations led to a gain- or loss-of-function. However, our results were inconclusive.

In S218L synapses, there was a small increase in K_{sp} and K_{AP}, but this was not significant, and the increase in K_{AP} was abolished in 1 mM Ca^{2+}. This was in contrary to previous reports, where there was an increase in both spontaneous and evoked neurotransmission in S218L NMJ synapses when measured in low external Ca^{2+} (van den Maagdenberg et al. 2010). The non-significant trend in K_{AP} was also observed at R192Q synapses, which have again shown an increase in evoked neurotransmission in previous reports (van den Maagdenberg et al. 2004). The differences in our results to the published data could be due to the type of synapse under consideration (increased neurotransmission has been shown at the NMJ for instance), or to alternative experimental approaches: our results take into account results from individual synapses, whereas previous data has been pooled across many synapses.

We saw an increase in the release rate in both the S218L and R192Q data (although at 1 mM this trend was reversed). This could suggest that there is a gain-of-function effect at mutated synapses, which could be due to an increase in Ca^{2+} current at these synapses (Tottene et al. 2002; Tottene et al. 2005). However, due to the large variation in data, considerably more data will need to be collected to ascertain whether this and other trends are truly significant. Also, further multi-level data analysis should be performed to reduce variability from the litter and culture.

Interestingly, we did not observe a firm trend in the data from S218L and R192Q HET synapses. For example the value of K_{AP} (figures 7.4b and 7.6b) in the HET genotype was comparable to the WT, whereas K_{sp} in HET S218L (figure 7.4a) was increased to a similar extent as the HOM. However, as the data is not statistically significant, conclusions about the level of expression of the mutated P/Q-type channel in HET synapses cannot be drawn.

Knock-out of the P/Q-type Ca^{2+} channel leads to decrease in K_{AP} in HOM cultures, with a corresponding decrease in the release rate, although this was not significant. The relative size of the *RRP/RP* is significantly lower in HOM KO cultures (P = 0.031 one way ANOVA). However, as with FHM1, more data will need to be collected before these results can be used as a model of EA2, as there was no significant difference between WT and HET KO.

7.5. Conclusions

The current set of data needs to be expanded and analysed more effectively in order to draw out clear conclusions.

8. VGCCs and miniature release.

This chapter contains the data presented in the paper "Stochastic opening of presynaptic calcium channels contributes to spontaneous neurotransmitter release" which is in preparation for publication. This paper was the result of a collaborative project, and I am deeply indebted to my colleagues for allowing me to include their data in this chapter to aid continuity of the story. Where their data has been used, full acknowledgement has been noted.

8.1. Introduction

AP-independent miniature neurotransmission had been shown to occur at the majority of synapses. There is strong evidence to suggest spontaneous neurotransmission is not just a 'leak' of neurotransmitter, but that it has important physiological functions, such as regulation of dendritic protein expression (Sutton et al. 2004), maintenance of dendritic spines (McKinney et al. 1999), and modulation of neuronal firing properties (Carter et al. 2002) as discussed in the introduction (section 1.5). It has been proposed that spontaneously released vesicles are drawn from a different pool than those released in response to APs (Fredj et al. 2009), (Sara et al. 2005), and that they activate distinct sets of postsynaptic receptors (Atasoy et al. 2008) [although see (Hua et al., 2010a), (Wilhelm et al., 2010a)].

Recently, there has been an increased interest in elucidating the molecular mechanisms behind miniature release, and there are several discrepancies and controversies remaining to be resolved. In particular, the Ca^{2+} regulation of spontaneous release has been incompletely studied. Although a proportion of minis are truly Ca^{2+}-independent, the majority are Ca^{2+}-dependent under physiological conditions, and mini frequency has been shown to be reduced at lower extracellular Ca^{2+} levels (Groffen et al. 2010; Xu et

al. 2009). Doc2b and synaptotagmin-1 (syt1) have been proposed as the Ca^{2+} sensors for Ca^{2+}-sensitive miniature release (Groffen et al. 2010; Xu et al. 2009) although a recent report argues that Doc2 proteins support spontaneous neurotransmission by a Ca^{2+}-independent mechanism (Pang et al. 2011).

It is widely accepted that synchronous AP-evoked release is triggered by fast local Ca^{2+} transients via opening of VGCCs (Schneggenburger et al. 2005). This local increase of Ca^{2+} concentration (the equivalent of tens of micromoles per litre), located in the vicinity of readily releasable synaptic vesicles is sufficient to bind to the low affinity syt1 sensor, and trigger release. If syt1 is also the Ca^{2+} target for spontaneous release, this implies that syt1-mediated minis may also rely on a high local Ca^{2+} signal, but what is the source of this signal? Fast Ca^{2+} discharge from presynaptic stores has previously been reported (Emptage et al. 2001; Llano et al. 2000), and might provide transient Ca^{2+} signals, but it is unclear whether these transients are sufficient to be sensed by syt1 at docked vesicles.

An alternative hypothesis to explain the syt1-dependence of miniature release is that stochastic opening of presynaptic VGCCs at resting membrane potentials generates transient Ca^{2+} domains analogous to those that occur in response to APs, albeit likely much smaller. It has been shown previously that VGCCs can open spontaneously, or 'flicker', at resting membrane potentials (Awatramani et al. 2005; Yu et al. 2010). Furthermore, it was suggested that the opening of a single VGCC produced sufficient Ca^{2+} influx to trigger AP-dependent exocytosis (Bennett et al. 2000; Stanley 1993; Weber et al. 2010). Combined with evidence to suggest that the major Ca^{2+} sensor, syt1, triggers both evoked and spontaneous release (Xu et al. 2009) , this mechanism for

miniature release could provide a direct link between spontaneous and evoked neurotransmission, and this chapter is aimed at filling in that link.

Here we used electrophysiological, optical, pharmacological and genetic methods to test the roles of presynaptic VGCCs in spontaneous neurotransmission at small hippocampal synapses. We show that a substantial fraction of minis in unstimulated neurons is mediated by P/Q- and N-type VGCCs. Moreover these VGCC-dependent minis have the same sensitivity to the slow Ca^{2+} chelator EGTA as evoked release, consistent with the formation of Ca^{2+}-nanodomains around release sensors. We further show that an increased P/Q-type Ca^{2+} channel opening probability at resting membrane potentials (caused by the FHM1 mutation S218L) enhances spontaneous release and its sensitivity to extracellular Ca^{2+} when recorded via whole-cell patch clamp methods. Stochastic channel opening can thus directly trigger exocytosis in the absence of APs.

8.2. Specific aims

The specific aims of this chapter are:

- Compare the effects of different VGCC blockers on presynaptic Ca^{2+} influx.
- Evaluate whether miniature neurotransmission is dependent on VGCC opening.
- Test whether miniature release is increased in neurons expressing mutated S218L P/Q-type channels

8.3. Results

8.3.1. *Major findings*

- P/Q- and N-type VGCCs mediate roughly a quarter of mEPSCs in small hippocampal synapses.

- This fraction of VGCC-dependent minis show a similar sensitivity to the slow Ca^{2+} chelator EGTA as evoked release, consistent with the formation of Ca^{2+} nanodomains around release sensors.

- Miniature release in neurons containing the P/Q-type VGCC mutation S218L is increased, and has a stronger sensitivity to both ω-aga and extracellular Ca^{2+}.

- Stochastic opening of presynaptic VGCCs can directly trigger exocytosis in the absence of APs.

8.3.2. *The non-specific VGCC blocker cadmium increases resting calcium, whereas the specific toxins ω-agatoxin-IVA and ω-conotoxin MVIIA have no effect*

To examine the role of presynaptic VGCCs in spontaneous neurotransmitter release in cultured hippocampal neurons, it was important to find a VGCC blocker with no indirect or non-specific effects. Previous data on the contribution of VGCCs to spontaneous neurotransmission is controversial. Inhibition of N-type VGCCs with the neurotoxic peptide ω-conotoxin MVIIA resulted in a decrease in miniature inhibitory post synaptic current (mIPSC) frequency in the brainstem (Missler et al. 2003). However, the non-specific inorganic VGCC blocker Cadmium (Cd^{2+}) had no effect in hippocampal or neocortical preparations (Scanziani et al. 1995), (Vyleta et al. 2011) and in hypothalamic neurons, VGCC blockers actually increased the spontaneous release frequency (Druzin et al. 2002), (Hirasawa et al. 2003).
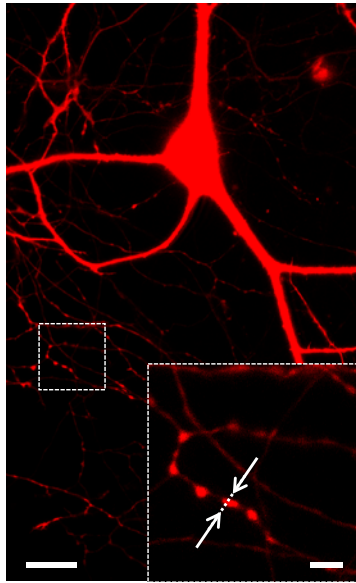
Figure 8.1:Presynaptic Ca2+ imaging to determine effects of VGCC blockers. Alexa 568 fluorescence image of a typical cultured hippocampal neuron, whole-cell loaded with 200 μM Alexa 568 and 200 μM Fluo-4. Inset: Typical axonal projection from the boxed region, showing several putative boutons. Arrows indicate position of the line-scan used to measure Ca2+ dynamics, illustrated in figure 8.2. Scale bars: (main) 20 μm, (inset) 4 μm. Data acquired by Y. Ermolyuk

Our colleague Yaroslav Ermolyuk (who has expertise in imaging presynaptic Ca^{2+} dynamics) kindly tested the specific effect of 100 µM Cd^{2+}, 0.25 µM ω-agatoxin-IVA (ω-aga) and 5 µM ω-conotoxin MVIIA (ω-ctx) on presynaptic Ca^{2+} dynamics, using the Ca^{2+} indicator Fluo-4. Cultured cells were whole-cell loaded with both the morphological tracer Alexa Fluor 568 (200 μM, to identify presynaptic boutons) and the high-affinity fluorescent Ca^{2+} indicator Fluo-4 (200 μM). Axons were identified and AP-evoked Fluo-4 transients were recorded before and after VGCC blocker application from individual boutons, using line scanning at 500 Hz (Figure 8.1; 8.2 a, b). Presynaptic Ca^{2+} dynamics were compared under different conditions using the ratio of

the Fluo-4 Ca^{2+}-sensitive fluorescence (green, G) to the Alexa Fluor 568 Ca^{2+}-independent fluorescence (red, R) (Oertner et al. 2002)
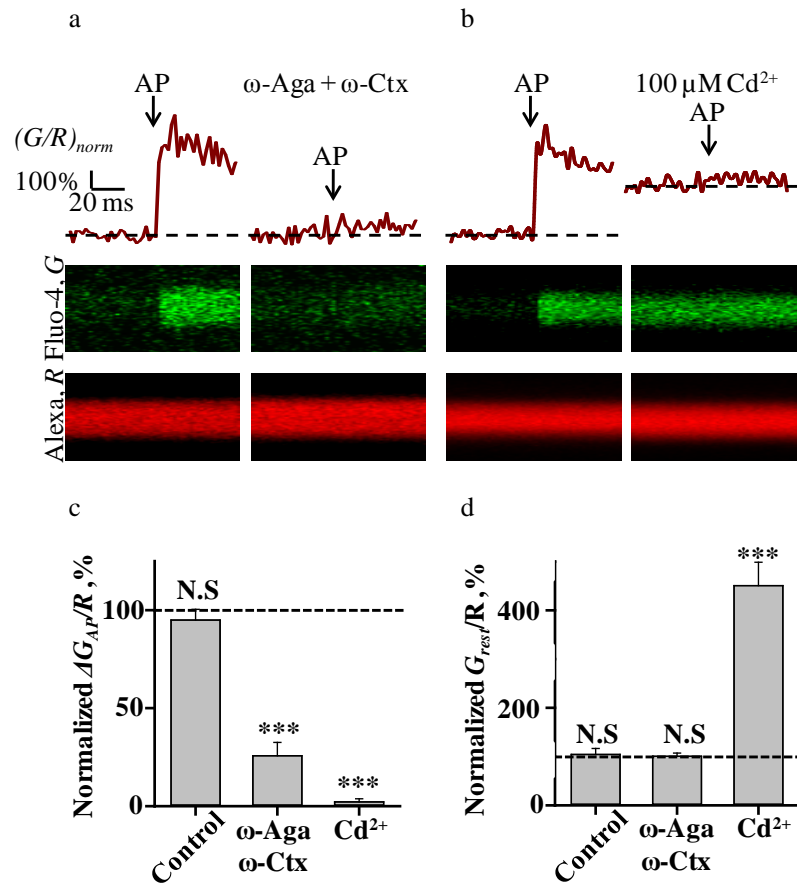
Figure 8.2: Differential effects of Cd^{2+} and specific VGCC blockers on presynaptic Ca^{2+} dynamics. (a) Fluorescence responses to a single AP obtained from line scan experiments averaged over 5 sweeps, before (left) and after (right) application of ω-aga and ω-ctx. Top panel, normalised fluorescence traces, bottom panel, raw Fluo-4 (green) and Alexa 568 (red) fluorescence profiles. (b) As for A, but before and after application of Cd^{2+}. (c) Summary graph of effect of toxins and Cd^{2+} on AP-evoked Ca^{2+} transients. (d) Summary graph of change in resting Ca^{2+} after toxin and Cd^{2+} application. Data are means ± s.e.m. N = 9 (control), N = 18 (ω-aga and ω-ctx), N =

13 (Cd^{2+}) boutons from 4 independent experiments for each condition. *** P < 0.001,

N.S P > 0.7, T-test. **Data acquired by Y. Ermolyuk**

Application of ω-aga and ω-ctx greatly decreased the AP-evoked Ca^{2+} fluorescence transient, $\Delta G_{AP}/R$ (by 74.3 ± 6.4 %, s.e.m, figure 8.2 a, c), confirming previous reports that the majority of AP-evoked Ca^{2+} influx is via N- and P/Q-type VGCC s (Li et al. 2007; Mintz et al. 1995; Rusakov et al. 2004).

Cd^{2+} produced a near total block of Ca^{2+} influx (98.7 ± 1.6 %, figure 8.2b, c). However, Cd^{2+} increased resting Ca^{2+} fluorescence (G_{rest}/R) robustly and significantly (451 ± 48 % of the initial amount, figure 8.2d) which was in stark contrast to the resting Ca^{2+} in the presence of ω-aga and ω-ctx, (101 ± 7 %, figure 8,2 d), which did not change significantly compared to control levels. The massive increase in the presence of Cd^{2+} could be explained by increased intracellular levels of Ca^{2+} (Xu et al. 2011) or by binding of Cd^{2+} to the Ca^{2+} indicator (Oyama 2002; Regehr et al. 1995). Cd^{2+} is also known to have adverse effects on other ionic channels (for instance, TRPM7 channels (Thévenod 2010; Elinder et al. 2003) and chloride channels (Maduke et al. 2000)) and it has also been reported to disrupt Ca^{2+} homeostasis (Xu et al. 2011). Independent of the mechanism, the apparent increase in intracellular Ca^{2+} would be likely to distort data on the impact of Ca^{2+} on neurotransmission, moreover the presence of Cd^{2+} might have adverse effects on neurotransmission itself (Angleson et al. 2001). For these reasons we decided to avoid the potential confounding effects of Cd^{2+} and instead used the specific neurotoxic blockers ω-aga and ω-ctx for the rest of the study.

8.3.3. Acute blockade of P/Q- and N-type channels inhibits the majority of AP-evoked neurotransmitter release.

We recorded from synaptically coupled pairs of neurons to confirm that excitatory postsynaptic currents (EPSCs) depend on P/Q-type and N-type VGCCs. Consistent with previous reports (Cao et al. 2004; Mintz et al. 1995; Wu et al. 1994), ω-aga and ω-ctx strongly inhibited the amplitude of EPCSs (Figure 8.3ω-aga by 79.5 ± 4.9 %, and ω-aga and ω-ctx applied together by 87.9 ± 3.5 %).
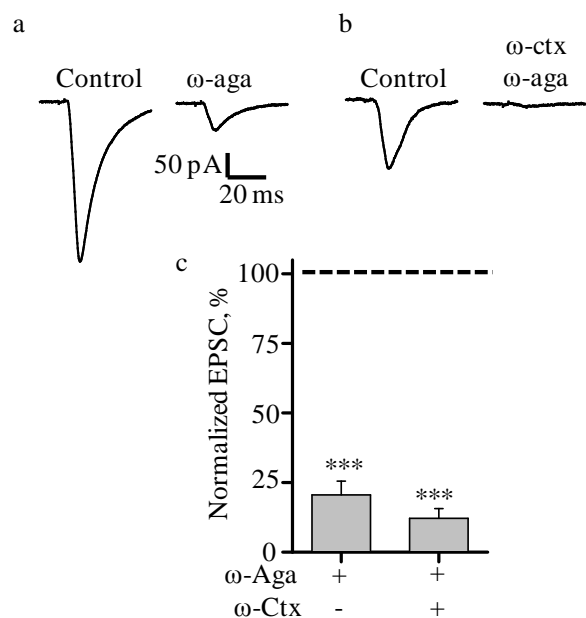
Figure 8.3: Blockade of VGCCs inhibits the majority of AP-evoked release. (a, b)Typical traces showing the EPSC response to an escape current in a synaptically connected cell, before and after ω-aga application (a) and before and after ω-aga and ω-ctx application (b). Scale bar 20 ms, 50 pA. (c) Application of ω-aga decreased EPSC amplitude by 79.5 ± 4.9% and ω-aga + ω-ctx by 87.9 ± 3.5%. ω-aga, N=7 cells, ω-aga + ω-ctx, N=8 cells. *** P < 0.001, T-test.

8.3.4. A proportion of miniature release is inhibited by blockade of VGCCs.

Next, we assessed the effects of VGCC blockers on miniature release. mEPSCs were continuously recorded in the presence of TTX before and after application of either ω-aga alone, or both ω-aga and ω-ctx. Traces from two typical experiments illustrating the block of mEPSCs after ω-aga application (figure 8.4 a) and after ω-aga and ω-ctx application (figure 8.5 a) are shown (baseline mEPSC frequency and amplitude varied widely between individual cells). We analysed mEPSCs and binned them into one minute intervals to ascertain the time-course of blockade by toxins (figures 8.4b and 8.5b). The mEPSC frequency decreased rapidly, stabilising within 5 - 10 minutes after addition of the toxins. Therefore we measured the effect of VGCC blockade on minis frequency between 10 - 20 min after application of the toxins. Blockade of VGCC did not alter the access resistance of the patch (figures 8.4c and 8.5c), which was monitored by applying a test pulse (5 mV, 200 ms) every two minutes (figures 8.4c and 8.5c, inset). Additionally, we did not observe any noticeable change in the mEPSC amplitude before and after toxin application (figures 8.4d and 8.5d).

Importantly, the application of specific VGCC blockers significantly decreased the mEPSC frequency (figure 8.6). ω-aga decreased mEPSC frequency by $19.7 \pm 4.9\%$. When both toxins were added, the frequency decreased by $26.9 \pm 3.7\%$. Thus, our data indicate that in WT cultures, approximately 25% of the miniature release at hippocampal synapses depends on the opening of P/Q- and N-type VGCCs.
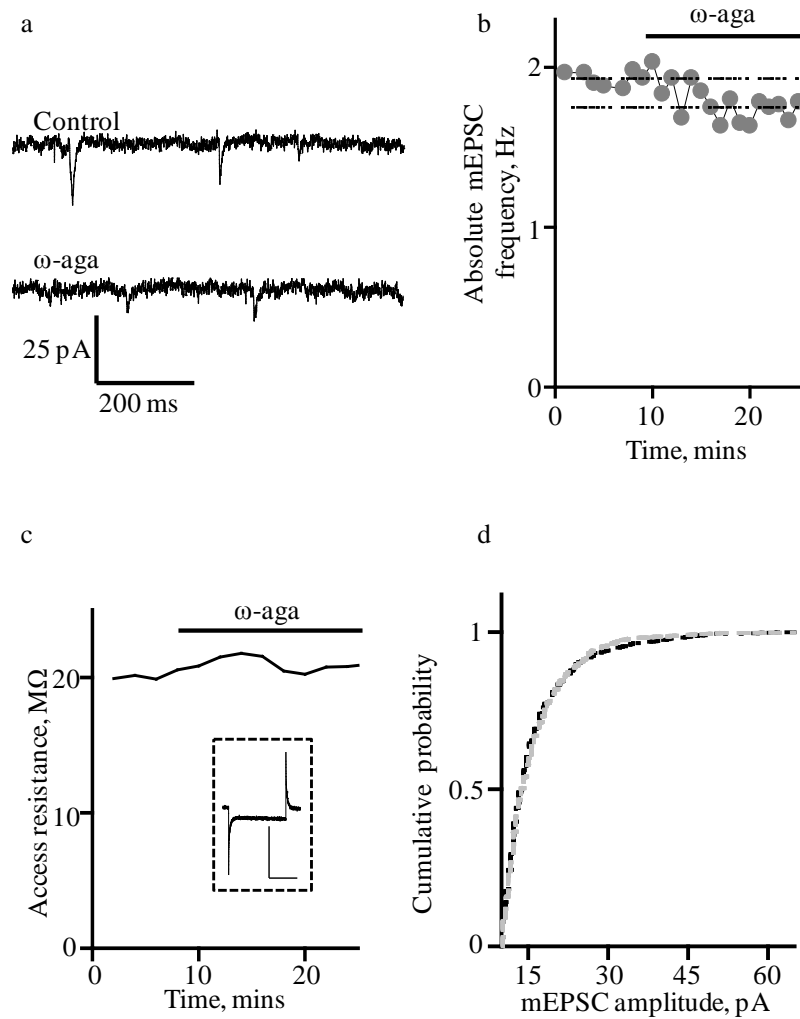
Figure 8.4: Application of ω-aga decreases mini frequency but not amplitude in a representative experiment. (a) *mEPSC traces illustrating the effect of ω-aga on*

frequency. ***(b)*** *Time course of application of ω-aga.* ***(c)*** *Access resistance was stable*

during this experiment, measured by eliciting a test pulse (inset) at two minute intervals.

(d) *Cumulative amplitude before (black) and after (grey) ω-aga application shows no*

significant difference, P = 0.57, Kolmogorov-Smirnov Test.
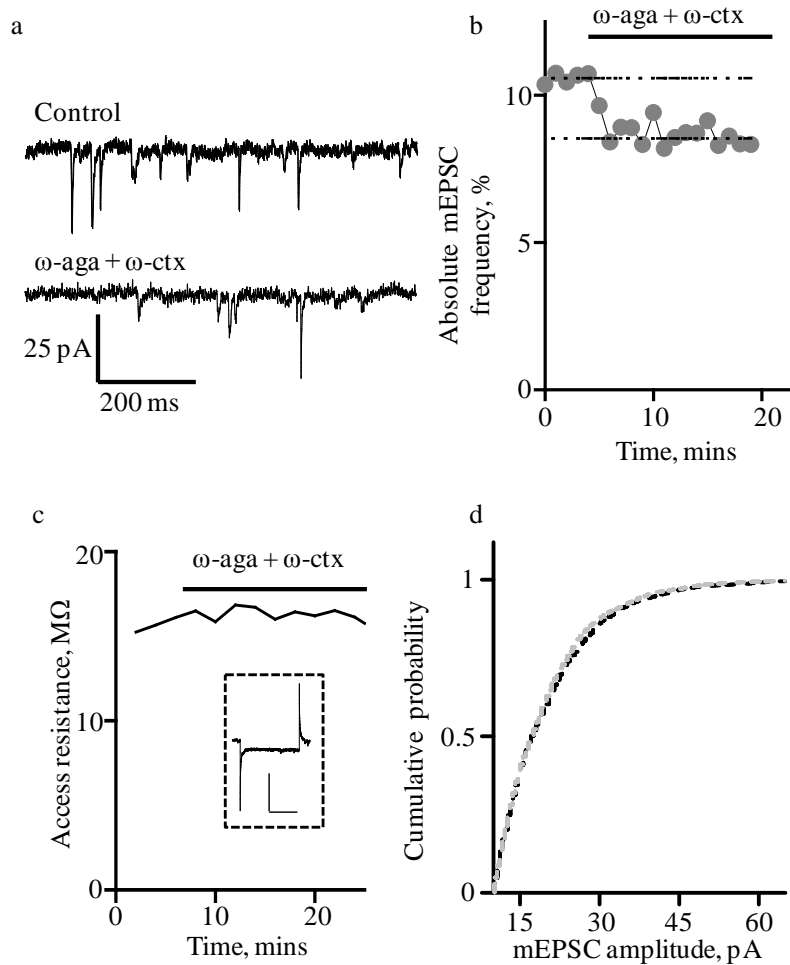
***Figure 8.5: Application of ω-aga + ω-ctx decreases mini frequency but not amplitude
in a representative experiment. (a)*** *mEPSC traces illustrating the effect of ω-aga + ω-
ctx on frequency.* ***(b)****Time course of application of ω-aga and ω-cono toxins.* ***(c)*** *Access
resistance during a typical experiment, measured by eliciting a test pulse (inset) at two
minute intervals.* ***(d)*** *Cumulative amplitude before (black) and after (grey) ω-aga + ω-
ctx application. P = 0.28, Kolmogorov-Smirnov Test.*
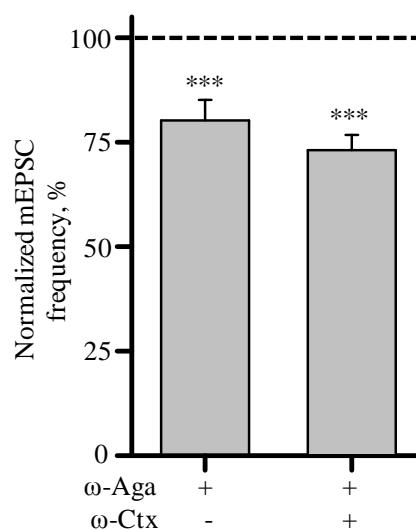
Figure 8.6: Application of VGCC blockers significantly decreases mEPSC frequency.

Application of ω-aga decreased mEPSC frequency by 19.7 ± 4.9% and ω-aga + ω-ctx by 26.9 ± 3.7%. ω-aga, N=14 cells, ω-aga + ω-ctx, N=19 cells. *** P < 0.001, T-test.

8.3.5. AP-evoked release and VGCC-dependent minis are affected to a similar extent by intracellular Ca^{2+} chelation.

Influx via presynaptic VGCCs contributed to roughly 25% of spontaneous neurotransmitter release, but the mechanism behind this release is not known. In the previous Ca^{2+} monitoring experiments (figures 8.1 and 8.2), we showed that blocking VGCCs with specific toxins did not have an effect on resting Ca^{2+} levels. However, the method we used to measure resting Ca^{2+} before and after toxin application was limited by the variation in fluorescence measurements (figure 8.2, G_{rest}/R, coefficient of variation CV ~30 %). By taking the Ca^{2+} dissociation constant of Fluo-4 into account (~ 350 nM), the 30 % variation of G_{rest}/R limits the sensitivity of resting Ca^{2+} concentration to 20 – 40 nM (Maravall et al. 2000). Therefore, it was possible that toxin

application decreased resting Ca^{2+} levels in this range. Furthermore, it has been shown that VGCCs can control resting Ca^{2+}, and that variation in the membrane potential between -80 mV and -60 mV can cause a VGCC-mediated change in resting Ca^{2+} in the range of tens of nM (Awatramani et al. 2005; Yu et al. 2010). These VGCC-mediated changes in resting Ca^{2+} evoked by small depolarisations are nearly completely blocked by the slow Ca^{2+} chelator EGTA (Awatramani et al. 2005; Yu et al. 2010; Christie et al. 2011). Therefore, we tested whether VGCC-dependent minis could be abolished by EGTA. The two possibilities are: If VGCC-dependent minis are abolished by EGTA, this would suggest that any role VGCCs play is through altered resting Ca^{2+} levels. If these minis are not abolished by EGTA, the role of VGCCs is not likely to be due to altered resting Ca^{2+} levels, but rather through direct EGTA-resistant Ca^{2+} nanodomains triggered by individual VGCC openings.

To study the effects of EGTA on minis, we made use of a membrane-permeable AM ester derivative of the slow Ca^{2+} buffer EGTA, EGTA-AM. EGTA-AM is passively loaded into cells to generate intracellular EGTA. Initially, we measured the time course of mEPSC blockade by bath-applied 20 µM EGTA-AM. mEPSCs were recorded as described previously, and EGTA-AM added after 10 minutes. After blockade of minis by EGTA-AM , $62.2 \pm 4.7\%$ of minis were remaining (figure 8.7a) and this proportion remained stable thereafter(figure 8.7a). It would have been ideal to measure baseline mEPSC frequency, followed by blockade with EGTA-AM then subsequent inhibition by toxins all in an individual cell. However, this would require the whole-cell patch to last more than fourty-five minutes, and consequently was not technically possible due to degradation of the patch over time. Therefore, we pre-incubated cells in 20 µM EGTA-AM for 20 minutes before patching and applying toxins. We observed that applying ω-

aga and ω-ctx together decreased mini frequency by 29.0 ± 7.8% after incubation in

EGTA-AM (figure 8.7b). VGCC-dependent miniature release is thus only partially

affected by EGTA.
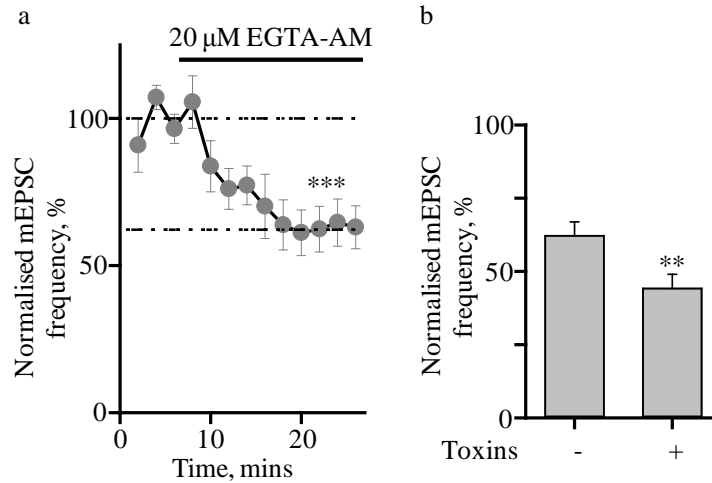
Figure 8.7: Inhibition of miniature release by ω-aga and ω-ctx is not occluded by

chelating intracellular Ca^{2+} with EGTA-AM. (a) Average time course of EGTA-AM

blockade of minis. EGTA-AM inhibited 37.8 ± 4.7% of mEPSCs. N = 9 cells, *** P <

0.001, T-test. *(b)* ω-aga + ω-ctx inhibited a further 29.0 ± 7.8% of minis in EGTA-AM

pre-treated cultures. N = 7 cells, ** P < 0.01, T-test

Failure to occlude the effect of ω-aga and ω-ctx by EGTA-AM implies that VGCC-

dependent minis are not triggered by slow fluctuations in global intraterminal [Ca^{2+}]$_{rest}$.

We therefore tested an alternative hypothesis, namely that VGCC-mediated minis might

be directly triggered by the formation of spontaneous single channel Ca^{2+}-nanodomains

around release sensors, akin to those that underlie AP-evoked exocytosis. Indeed the

slow Ca^{2+} buffer EGTA only has a modest effect on AP-evoked neurotransmission

(Bucurenciu et al. 2008; Rozov et al. 2001). If VGCC-dependent miniature release

was directly triggered by the formation of local Ca^{2+} nanodomains it should show the same sensitivity to intracellular EGTA as AP-evoked release.

What is the sensitivity to EGTA of VGCC-dependent miniature release? We used an algebraic calculation to compare the effects of VGCC blockers in control conditions (figure 8.6) and in the presence of EGTA-AM (figure 8.7 b), to estimate the proportion of VGCC-mediated minis which were blocked by EGTA-AM.

We denoted:

$R_{Control}^{Total}$ Average mini frequency under control conditions

$R_{Control}^{VGCC}$ Average mini frequency mediated by VGCCs in control conditions

R_{EGTA}^{Total} Average mini frequency after EGTA-AM application

R_{EGTA}^{VGCC} Average mini frequency mediated by VGCCs after EGTA-AM

application

The specific effect of EGTA-AM loading on the VGCC-dependent component of spontaneous release is:

$$\frac{R_{EGTA}^{VGCC}}{R_{Control}^{VGCC}}$$

The data we have presented to this point can be denoted as:

Data 1: The specific effect of VGCCs on mini frequency after blockade by EGTA-AM.

$$\frac{R_{EGTA}^{VGCC}}{R_{EGTA}^{Total}} = 29.0 \pm 7.8 \ \% \ (\text{SEM}), \text{ data from figure 8.7b (right hand bar), N=7 cells}$$

Data 2: The specific effect of VGCCs on mini frequency under control conditions.

$$\frac{R_{Control}^{VGCC}}{R_{Control}^{Total}} = 26.9 \pm 3.6 \ \% \ (\text{SEM}), \text{ data from figure 8.6 (right hand bar), N=13 cells}$$

Data 3: The specific effect of EGTA-AM on mini frequency under control conditions.

$$\frac{R_{EGTA}^{Total}}{R_{Control}^{Total}} = 62.2 \pm 4.8 \ \% \ (\text{SEM}), \text{ data from figure 8.7a, N=7 cells}$$

These three data sets can be combined to calculate the specific effect of EGTA-AM loading on the VGCC-dependent component of spontaneous release, by:

$$\frac{R_{EGTA}^{VGCC}}{R_{Control}^{VGCC}} = \frac{\left(R_{EGTA}^{VGCC} \Big/ R_{EGTA}^{Total} \right)}{\left(R_{Control}^{VGCC} \Big/ R_{Control}^{Total} \right)} \cdot \left(\frac{R_{EGTA}^{Total}}{R_{Control}^{Total}} \right)$$

or more simply,

$$\frac{R_{EGTA}^{VGCC}}{R_{Control}^{VGCC}} = \frac{Data1}{Data2} \cdot Data3$$

If we were to calculate this equality from the mean experimental values, we would bias our estimate. Therefore we estimated the specific effect of EGTA-AM loading on the

VGCC-dependent component of spontaneous release by bootstrap analysis. We

independently re-sampled each set of the experimental data and simulated the estimate

(N = 1000 simulations). The standard deviation was also estimated with this method.

$$\frac{R_{EGTA}^{VGCC}}{R_{Control}^{VGCC}} \approx 67.7 \pm 20 \text{ %}.$$
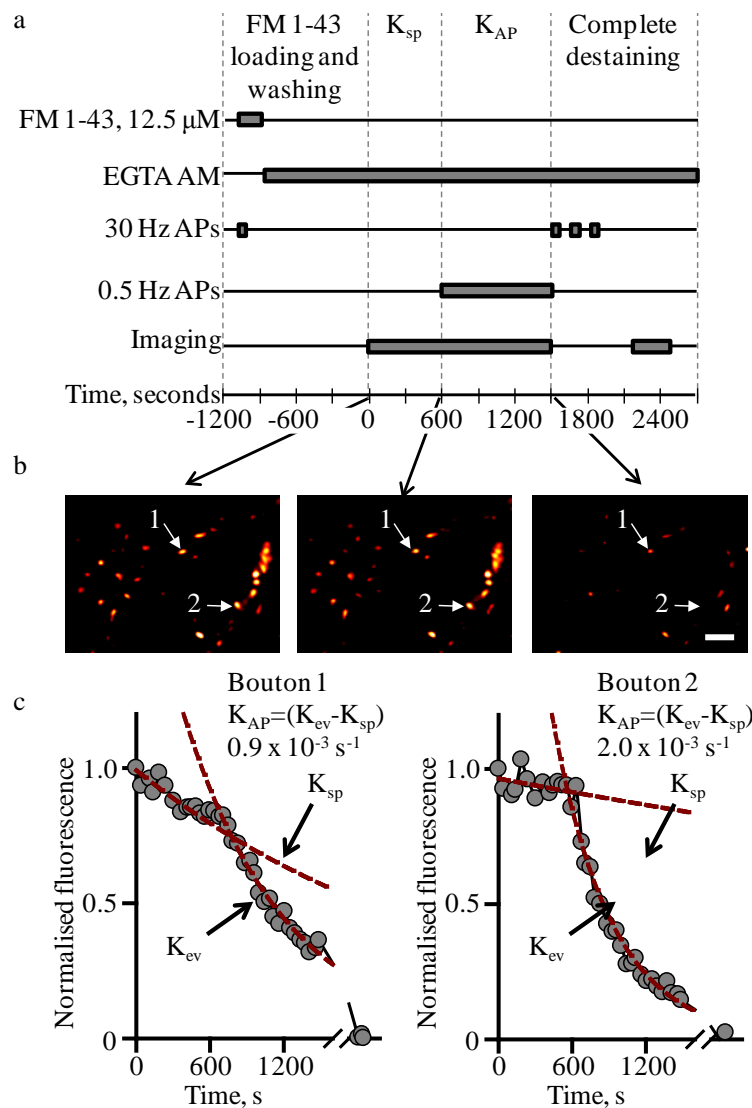
Figure 8.8: Experimental paradigm and example traces of FM 1-43 destaining in the

presence and absence of EGTA-AM. (a) Experimental paradigm (b)Typical

fluorescence loss in several synaptic boutons over the time course of a control

experiment. Arrows point to individual boutons inspected in c. (c) Fluorescence

destaining profiles for two example boutons. Exponential fits of the spontaneous

destaining rate K_{sp} and the evoked destaining rate K_{ev} are shown by red dashed lines.

The effective specific AP-evoked FM 1-43 destaining rate in each bouton was

*calculated by $K_{AP} = K_{ev} – K_{sp}$. Scale bar: (**b**) 5 µm.*

How does this value compare with the EGTA sensitivity of AP-evoked neurotransmitter

release under the same experimental conditions? We investigated this question using

optical recording methods, as in paired recordings dialysis of the presynaptic axon could

possibly disrupt the EGTA equilibrium (figure 8.8).

We first labeled recycling vesicles with the fluorescent styryl dye FM 1-43 using high

frequency stimulation, and then measured the rate of FM 1-43 fluorescence de-staining

(which is proportional to vesicular release rates in individual synapses (Branco et al.

2008; Gaffield et al. 2006)), either in the presence or in the absence of EGTA-AM

(Figure 8.8a, b). As described in chapter 6, to determine the AP-evoked FM 1-43 de-

staining rate (K_{AP}), we subtracted the spontaneous de-staining rate measured at rest (K_{sp})

from the de-staining rate measured during low frequency (0.5 Hz) AP stimulation (K_{ev}):

$K_{AP} = K_{ev} – K_{sp}$ (Figure 8.8c). When we averaged over a large number of boutons, K_{AP}

was roughly 10-fold larger than K_{sp}, but both K_{sp} and K_{AP} were significantly reduced in

the presence of EGTA-AM compared to the DMSO control (figure 8.9a and b).
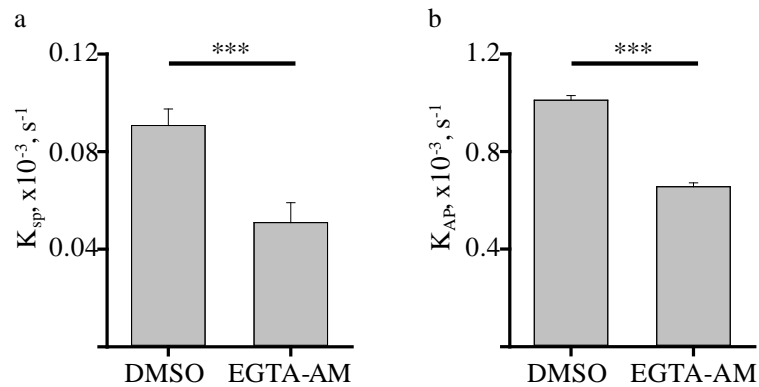
Figure 8.9: EGTA-AM significantly decreases both K_{sp} and K_{AP}. Effect of EGTA-AM incubation on (a) K_{sp} and (b) K_{AP} FM 1-43 destaining rates. Data are means ± s.e.m of all analysed boutons. Control (0.5% DMSO), N = 905 boutons from n = 5 independent experiments; EGTA-AM, N=899 boutons from n = 5 independent experiments. *** P < 0.001, Mann-Whitney rank test.

It should be noted that although K_{sp} is related to the mEPSC frequency recorded in the presence of TTX, the absolute value of K_{sp} can also be affected by spontaneous AP activity, by incomplete FM 1-43 loading of spontaneously recycling synaptic vesicles during high frequency stimulation [e.g. (Sara et al. 2005)], and by non-specific loss of FM 1-43 fluorescence. In contrast, the specific AP-evoked FM 1-43 de-staining rate K_{AP} was corrected to these factors and therefore the decrease of K_{AP} in EGTA-AM loaded neurons (~33%, Figure 8.9b) should report the specific reduction of AP-evoked vesicular release by EGTA-AM. Strikingly, this decrease in AP-evoked exocytosis by EGTA-AM was almost identical to the EGTA-AM inhibition of VGCC-dependent mEPSCs (~ 32%, figure 8.10).
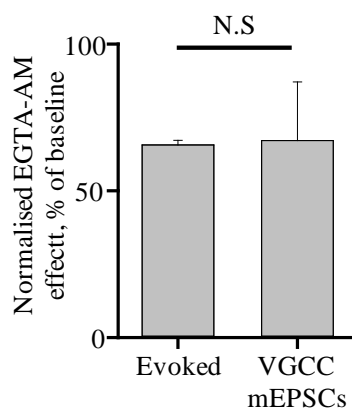
Figure 8.10: AP-evoked release and VGCC-dependent minis have a similar sensitivity to Ca^{2+} chelation by EGTA. Comparison of the EGTA-AM blockade of the AP-evoked release (data from figure 8.9 b) and the VGCC-mediated miniature release (data from figure 8.6 and 8.7). N.S, $P > 0.25$, Mann-Whitney rank test.

8.3.6. The S218L mutation in the P/Q-type VGCC increases the rate of spontaneous channel opening and leads to an increase in the frequency of VGCC-mediated mEPSCs.

The close agreement between the effects of EGTA on evoked exocytosis and on VGCC-dependent minis suggests that both forms of exocytosis depended on similar local intraterminal Ca^{2+} concentration changes. This is consistent with VGCC-dependent minis being directly triggered by the spontaneous opening of presynaptic VGCCs at resting membrane potentials. A consequence of this model is that increasing the opening probability of VGCCs at the resting membrane potential should be sufficient to increase the mEPSC frequency and its sensitivity to extracellular Ca^{2+}. To test this prediction we took advantage of the FHM1 mutation S218L KI mice described in chapter 7 (Pietrobon 2007). Importantly, at the level of individual channels, the S218L mutation increases P/Q-type channel open probability by shifting its activation voltage to more negative

values, and therefore enhances spontaneous channel opening and Ca^{2+} entry at near resting membrane potentials (Tottene et al. 2005; van den Maagdenberg et al. 2010). Thus, if stochastic opening of presynaptic VGCCs is directly linked to spontaneous release, the S218L mutation should increase the frequency of mEPSCs, enhance the sensitivity of spontaneous release to blockade of P/Q-type VGCCs, and potentiate the dependence of mEPSC frequency on extracellular Ca^{2+} concentration.

We used cultures made from the S218L KI mice. By measuring VGCC-dependent minis in these mice, we were able to determine whether the increased opening probability led to an increase in mini frequency and sensitivity to ω-aga and extracellular Ca^{2+} concentration. An increase in mini frequency in S218L neurons would be consistent with a role for spontaneous VGCC openings in supporting VGCC-dependent minis.

Our colleagues Rainer Surges and Ivan Pavlov carried out electrophysiological mEPSC recording experiments which confirmed the prediction that on average mEPSC frequency was significantly higher in S218L KI cultures than in the WT littermates (figure 8.12a and b). Due to the huge variability mEPSC frequency it was difficult to plot the absolute means, but the cumulative probability was significantly different (figure 8.12b).

a WT

25 pA
200 ms

S218L

b

c ω-Aga

d 0.5 mM Ca^{2+}
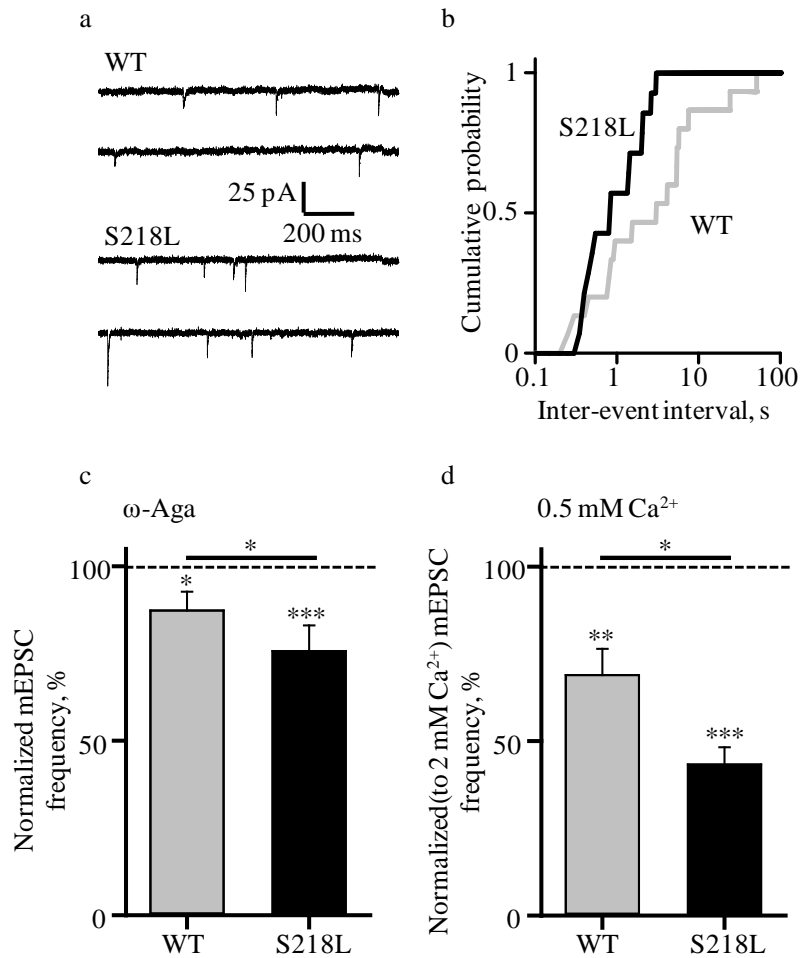
Figure 8.11: The S218L mutation in P/Q-type Ca^{2+} channels enhances miniature

release. (a) Example mEPSC traces recorded in WT and S218L KI cultures. The

average mEPSC amplitude were similar in both genotypes (WT: 11.2 ± 0.8 pA, S218L

KI: 11.6 ± 0.8 pA) (b) Cumulative probability of the average mEPSC inter-event

intervals shows increase in frequency of minis in S218L KI preparations. WT: N = 15,

S218L: N = 14 cells. P < 0.02 Kolmogorov-Smirnoff test. (c) Normalised mEPSC

frequency decrease in the presence of ω-aga shows increased sensitivity of S218L KI

neurons to P/Q-type VGCC blockade. WT: N = 9 and S218L KI: N = 10 cells. (d)

S218L KI neurons have increase sensitivity to changes in extracellular Ca^{2+}

concentration. WT: N = 9 and S218L KI: N = 8 cells. * P < 0.05, ** P < 0.01, *** P < 0.001, T-test. **Data acquired by R. Surges and I. Pavlov**

During acute P/Q-type VGCC blockade with ω-Aga, we observed a significantly larger effect in S218L KI experiments than in WT counterparts. mEPSC frequency was reduced by 28.6 ± 4.5 % and 13.7 ± 5.1 %, respectively (figure 8.12c). The sensitivity of the cultures to extracellular Ca^{2+} changes was also increased in S218L KI cultures. When we reduced extracellular Ca^{2+} from 2 mM to 0.5 mM the mEPSC frequency decreased by 56.7 ± 4.6 % in S218L KI but by only 31.1 ± 7.5 % in WT cultures (figure 8.12d). These results supported the hypothesis that increased stochastic opening of mutated P/Q-type channels increased the frequency of VGCC-sensitive mEPSCs.

8.4. Discussion

In this chapter, we have detailed a body of work which suggests that roughly 25% of miniature release at small hippocampal synapses is directly triggered by opening of presynaptic VGCCs. Furthermore, we have shown that the slow Ca^{2+} buffer EGTA cannot occlude the effect of ω-aga and ω-ctx, pointing away from the hypothesis that VGCCs trigger minis via slow changes in intraterminal Ca^{2+} concentration. We observed a remarkably similar EGTA sensitivity for AP-evoked release and VGCC-dependent minis. This result indicates that VGCC-dependent mini release, like AP-evoked release, is triggered by VGCC opening and formation of Ca^{2+} nanodomains which in turn are sensed by the low affinity Ca^{2+} sensor Syt1. Further support for this hypothesis came from the finding that miniature release is enhanced in a P/Q-type VGCC mutation, that leads to an increase in open probability at resting membrane potential.

The combination of these results suggests that stochastic opening of VGCCs at resting membrane potential can trigger the same signalling cascade that is used during AP-evoked release, and furthermore these stochastic openings are sufficient for miniature release. As the probability of multiple VGCCs opening simultaneously in the same location is remote, this further suggests that the stochastic opening of a single VGCC may be sufficient to trigger release (Bennett et al. 2000; Stanley 1993; Weber et al. 2010; Bucurenciu et al. 2010).

Recent studies have suggested that AP-evoked and AP-independent neurotransmission are mediated by non-overlapping sources of Ca^{2+} (Glitsch 2008; Pang et al. 2006), different Ca^{2+} sensors (Groffen et al. 2010) or by separate pools of vesicles (Sara et al. 2005; Fredj et al. 2009; Cheung et al. 2010). Whilst synchronous AP-evoked release is mediated by the low affinity Ca^{2+} sensors syt1, synaptotagmin-2 and synaptotagmin-9 (Xu et al. 2007), it has previously been proposed that miniature release is controlled by Ca^{2+} sensors with higher Ca^{2+} affinity (Glitsch 2008; Groffen et al. 2010; Pang et al. 2011). In addition, rather than depending on transient local Ca^{2+} nanodomains, miniature release has been suggested to depend on slower global changes in presynaptic $[Ca^{2+}]$, such as those that occur by release from intracellular stores or by store-operated presynaptic Ca^{2+} entry (Emptage et al. 2001; Llano et al. 2000; Glitsch 2008; Simkus and Stricker 2002a; Simkus and Stricker 2002b; Wasser et al. 2009). However, blurring the distinction between evoked and miniature exocytosis, two recent reports argue that, under physiological conditions, miniature release is triggered by the AP-evoked neurotransmitter release sensor Syt1 (Xu et al. 2009; Pang et al. 2011). Consistent with this, the present study shows that a substantial proportion of AP-independent exocytosis

can be directly triggered by Ca^{2+} entry via presynaptic VGCCs that open stochastically at resting membrane potentials. It remains to be determined whether additional Ca^{2+} dependent components of spontaneous neurotransmission mediated by Ca^{2+} release from the intracellular stores act similarly via syt1 or via other Ca^{2+} release sensors. Other recent studies suggesting that miniature and AP-evoked recycling arises from the same pool of synaptic vesicles also agree with our results (Groemer and Rizzoli 2010b; Hua et al., 2010b).

Several studies have shown that blocking VGCCs does not change the rate of spontaneous release (Scanziani et al. 1995; Vyleta et al. 2011), which appears to contradict our results. However, these studies used the non-specific VGCC blocker Cd^{2+}, which we have shown has an adverse affect on resting Ca^{2+} concentrations (figure 8.2), Ca^{2+} homeostasis (Xu et al. 2011), and hence spontaneous release. We used the specific VGCC blockers ω-aga and ω-ctx, which had no such effects on these parameters, and consequently our data cannot be compared to data obtained using Cd^{2+}.

8.5. Conclusions

In this chapter, we have proposed a novel mechanism of spontaneous neurotransmitter release. Our results indicate that a proportion of miniature release is dependent on stochastic opening of presynaptic VGCCs at resting membrane potentials. Furthermore, these VGCC-mediated minis share an almost identical sensitivity to the slow Ca^{2+} buffer EGTA as AP-evoked neurotransmission, suggesting that this form of miniature release is triggered by the same signalling cascade. Finally, a naturally occurring mutation in the P/Q-type VGCC pore leads to an increase in the open probability of the channel at resting membrane potentials. Miniature release in these synapses was increased, as was their sensitivity to ω-aga and extracellular concentrations,

strengthening our hypothesis that stochastic opening of presynaptic VGCCs contribute to spontaneous neurotransmitter release.

9. Final conclusions

This piece of work sheds new light on Ca^{2+} regulation of synaptic vesicular release in cultured hippocampal neurons. Using a combination of optical and electrophysiological methods, we showed:

1. A large heterogeneity in the SRC1 evoked (K_{AP}) and spontaneous (K_{sp}) destaining rates amongst individual synaptic boutons, leading to the conclusion that both evoked and spontaneous transmitter release varies widely between synapses. The size of the *RP* and *RRP* is also very heterogeneous between individual boutons.

2. By analysing the true biological variability of both K_{AP} and the *RRP/RP*, we determined that the average fusion probability of an individual vesicle docked at the *RRP* (p_v) was also highly heterogeneous amongst boutons. The observation that p_v was highly variable underlies the molecular mechanism behind the variability of the probability of neurotransmitter release at a given synapse, P_{rel} (Koester et al. 2005; Branco et al. 2008).

3. Two human familial hemiplegic migraine mutations in the P/Q-type VGCC, S218L and R192Q do not appear to have a significant effect on the mean values of K_{AP}, K_{sp}, *RP*, *RRP/RP* or P_{rel} when compared with WT using SRC1 destaining methods, although K_{AP}, K_{sp} are increased.

4. P/Q- and N-type VGCCs mediate a quarter of mEPSCs in small hippocampal synapses. These VGCC-dependent minis demonstrate a similar sensitivity to the slow Ca^{2+} chelator EGTA as evoked release.

In order to fully clarify whether S218L and R192Q do indeed modify synaptic transmission, more experiments and further analysis will need to be performed.

References

Adams, Michael E (2004). Agatoxins: ion channel specific toxins from the American funnel web spider, Agelenopsis aperta. Toxicon 43, 637-644.

Adler, J. E., and Black, I. B. (1986). Sympathetic neuronal density and cell membrane contact regulate phenotypic expression in culture. Ann. N.Y. Acad. Sci. 486, 87-95.

Aggarwal, S. K., and MacKinnon, R (1996). Contribution of the S4 segment to gating charge in the Shaker K+ channel. Neuron 16, 1169-77.

Ahern, C. a, and Horn, R. (2004). Stirring up controversy with a voltage sensor paddle. Trends Neurosci. 27, 303-307.

Ahnert-Hilger, G., Holtje, M., Pahner, I., Winter, S., and Brunk, I. (2003). Regulation of vesicular neurotransmitter transporters. Review Physiology Biochemistry Pharmacology 150, 140-160.

Alford, Simon, Frenguellit, B. G., Schofield, J. G., and Collingridge, G. L. (1993). Characterization of Ca2+ signals induced in hippocampal CA1 neurones by the synaptic activation of NMDA receptors. J. Physiol. 469, 693-716.

Alés, E., Tabares, L., Poyato, J. M., Valero, V., Lindau, M., and Alvarez de Toledo, G. (1999). High calcium concentrations shift the mode of exocytosis to the kiss-and-run mechanism. Nature cell biology 1, 40-4.

Amos, W. (2003). How the confocal laser scanning microscope entered biological research. Biol. Cell 95, 335-342.

Anderson, P. a, and Greenberg, R. M. (2001). Phylogeny of ion channels: clues to structure and function. Comparative biochemistry and physiology. Part B, Biochemistry & molecular biology 129, 17-28.

Andrews, P. W. (1984). Retinoic acid induces neuronal differentiation of a cloned human embryonal carcinoma cell line in vitro. Dev. Biol. 103, 285-93.

Angleson, J. K. et al. (2001). Intraterminal Ca 2 + and Spontaneous Transmitter Release at the Frog Neuromuscular Junction Intraterminal Ca 2⁺ and Spontaneous Transmitter Release at the Frog Neuromuscular Junction. Journal of Neurophysiology, 287-294.

Aravanis, A. (2003). Imaging single synaptic vesicles undergoing repeated fusion events: kissing, running, and kissing again. Neuropharmacology 45, 797-813.

Aravanis, A. M. (2003). Single synaptic vesicles fusing transiently and successively without loss of identity. Nature 423, 643-647.

Arikkath, Jyothi, and Campbell, Kevin P (2003). Auxiliary subunits: essential components of the voltage-gated calcium channel complex. Current Opinion in Neurobiology 13, 298-307.

Arnot, M. I., Stotz, S. C., Jarvis, S E, and Zamponi, G W (2000). Differential modulation of N-type 1B and P/Q-type 1A calcium channels by different G protein subunit isoforms. The Journal of physiology 527 Pt 2, 203-12.

Atasoy, D., Ertunc, M., Moulder, K. L., Blackwell, J., Chung, ChiHye, Su, J., and Kavalali, Ege T (2008). Spontaneous and evoked glutamate release activates two populations of NMDA receptors with limited overlap. The Journal of neuroscience : the official journal of the Society for Neuroscience 28, 10151-66.

Atlas, D. (2001). Functional and physical coupling of voltage-sensitive calcium channels with exocytotic proteins: ramifications for the secretion mechanism. Journal of Neurochemistry 77, 972-985.

Atluri, P. P., and Regehr, W G (1998). Delayed release of neurotransmitter from cerebellar granule cells. The Journal of neuroscience: the official journal of the Society for Neuroscience 18, 8214-27.

Awatramani, G. B., Price, G. D., and Trussell, L. O. (2005). Modulation of transmitter release by presynaptic resting potential and background calcium levels. Neuron 48, 109-21.

Bain, G., Kitchens, D., Yao, M., Huettner, J. E., and Gottlieb, D. I. (1995). Embryonic stem cells express neuronal properties in vitro. Dev. Biol. 168, 342-357.

Bajjalieh, S. M., and Scheller, Richard H (1995). The biochemistry of neurotransmitter secretion. The Journal of biological chemistry 270, 1971-1974.

Balaji, J., and Ryan, T. A. (2007). Single-vesicle imaging reveals that synaptic vesicle exocytosis and endocytosis are coupled by a single stochastic mode. Proc. Natl. Acad. Sci. USA 104, 20576-20581.

Baldwin, M. L., Cammarota, M., Sim, A. T. R., and Rostas, J. A. P. (2006). Src family tyrosine kinases differentially modulate exocytosis from rat brain nerve terminals. Neurochem. Int. 49, 80-86.

Banker, G. A. (1980). Trophic interactions between astroglial cells and hippocampal neurons in culture. Science 209, 809-810.

Banker, G. A., and Goslin, K. (1988). Developments in neuronal cell culture. Nature 366, 185-186.

Barclay, J. et al. (2001). Ducky mouse phenotype of epilepsy and ataxia is associated with mutations in the Cacna2d2 gene and decreased calcium channel current in cerebellar Purkinje cells. The Journal of neuroscience: the official journal of the Society for Neuroscience 21, 6095-104.

Barrett, C. F., Cao, Y.-Q., and Tsien, Richard W (2005). Gating deficiency in a familial hemiplegic migraine type 1 mutant P/Q-type calcium channel. The Journal of biological chemistry 280, 24064-71.

Barrett, E. F., and Stevens, C F (1972). The kinetics of transmitter release at the frog neuromuscular junction. The Journal of physiology 227, 691-708.

Bean, B. P. (1989). Multiple types of calcium channels in heart muscle and neurons. Modulation by drugs and neurotransmitters. Annals of the New York Academy of Sciences 560, 334-45.

Bekkers, J M, Vidovic, M., and Ymer, S. (1996). Differential effects of histamine on the N-Methyl-D-Aspartate channel in hippocampal slices and cultures. Neuroscience 72, 669-677.

Bekkers, J M, and Stevens, C F (1991). Excitatory and inhibitory autaptic currents in isolated hippocampal neurons maintained in cell culture. Proc. Natl. Acad. Sci. USA 88, 7834-7838.

Benarroch, E. E. (2011). Na+, K+-ATPase: functions in the nervous system and involvement in neurologic disease. Neurology 76, 287-93.

Bennett, M K, Calakos, N., and Scheller, R H (1992). Syntaxin: a synaptic protein implicated in docking of synaptic vesicles at presynaptic active zones. Science (New York, N.Y.) 257, 255-9.

Bennett, M. R., Farnell, L., and Gibson, W. G. (2000). The probability of quantal secretion near a single calcium channel of an active zone. Biophysical journal 78, 2201-21.

Benson, D. L., Watkins, F. H., Steward, O., and Banker, G (1994). Characterization of GABAergic neurons in hippocampal cell cultures. J. Neurocytol. 23, 279-95.

Bergsman, J. B., and Tsien, R W (2000). Syntaxin modulation of calcium channels in cortical synaptosomes as revealed by botulinum toxin C1. The Journal of neuroscience : the official journal of the Society for Neuroscience 20, 4368-78.

Berninghausen, O., Rahman, M. A., Silva, J.-P., Davletov, B., Hopkins, C., and Ushkaryov, Y. A. (2007). Neurexin I beta and neuroligin are localized on opposite membranes in mature central synapses. J. Neurochem. 103, 1855-1863.

Bernstein, J. (1902). Untersuchungen zur Thermodynamik der bioelektrischen Ströme Erster Theil. Pflügers Archiv European Journal of Physiology 92.

Betz, W J, Mao, F, and Bewick, G. S. (1992). Activity-dependent fluorescent staining and destaining of living vertebrate motor nerve terminals. J. Neurosci. 12, 363-375.

Betz, W J, Mao, F, and Smith, C. B. (1996). Imaging exocytosis and endocytosis. Current opinion in neurobiology 6, 365-71.

Blaustein, R. O., and Miller, Christopher (2004). Shake, Rattle, or Roll? Nature 427, 499-500.

Bolay, H., Reuter, U., Dunn, A. K., Huang, Z., Boas, D. a, and Moskowitz, M. a (2002). Intrinsic brain activity triggers trigeminal meningeal afferents in a migraine model. Nature medicine 8, 136-42.

Bollmann, J. H., Sakmann, Bert, and Borst, J Gerard G (2000). Calcium Sensitivity of Glutamate Release in a Calyx-Type Terminal. Science 289, 953-957.

Bottenstein, J. E. (1979). Growth of a rat neuroblastoma cell line in serum-free supplemented medium. Proc. Natl. Acad. Sci. USA 76, 514-517.

Bourinet, E., Soong, T W, Sutton, K., Slaymaker, S., Mathews, E., Monteil, a, Zamponi, G W, Nargeot, J., and Snutch, T P (1999). Splicing of alpha 1A subunit gene generates phenotypic variants of P- and Q-type calcium channels. Nature neuroscience 2, 407-15.

Bouron, A. (2001). Modulation of spontaneous quantal release of neurotransmitters in the hippocampus. Prog. Neurobiol. 63, 613-35.

Boyer, C., Schikorski, T, and Stevens, C F (1998). Comparison of hippocampal dendritic spines in culture and in brain. J. Neurosci. 18, 5294-300.

Brain, K. L., and Bennett, M. R. (1995). Calcium in the nerve terminals of chick ciliary ganglia during facilitation, augmentation and potentiation. J. Physiol. 489, 637-648.

Branco, T., Staras, Kevin, Darcy, Kevin J, and Goda, Yukiko (2008). Local dendritic activity sets release probability at hippocampal synapses. Neuron 59, 475-85.

Brewer, G. J., Torricelli, J. R., Evege, E. K., and Price, P. J. (1993). Optimized survival of hippocampal neurons in B27-supplemented Neurobasal, a new serum-free medium combination. J. Neurosci. Res. 35, 567-76.

Brewer, G. J., and Cotman, C. W. (1989). Survival and growth of hippocampal neurons in defined medium at low density: advantages of a sandwich culture technique or low oxygen. Brain Res. 494, 65-74.

Brice, N. L., Berrow, N. S., Campbell, V., Page, K M, Brickley, K., Tedder, I., and Dolphin, a C. (1997). Importance of the different beta subunits in the membrane expression of the alpha1A and alpha2 calcium channel subunits: studies using a depolarization-sensitive alpha1A antibody. The European journal of neuroscience 9, 749-59.

Brose, Nils, Petrenko, A. G., Südhof, Thomas C, and Jahn, Reinhard (1992). Synaptotagmin : A Calcium Sensor on the Synaptic Vesicle Surface. Science 256, 1021-1025.

Buchhalter, J. R., and Dichter, M. A. (1991). Electrophysiological comparison of pyramidal and stellate nonpyramidal neurons in dissociated cell culture of rat hippocampus. Brain Res. Bull. 26, 333-8.

Bucurenciu, I., Bischofberger, J., and Jonas, Peter (2010). A small number of open Ca2+ channels trigger transmitter release at a central GABAergic synapse. Nature neuroscience 13, 19-21.

Bucurenciu, I., Kulik, A., Schwaller, B., Frotscher, M., and Jonas, Peter (2008). Nanodomain coupling between Ca2+ channels and Ca2+ sensors promotes fast and efficient transmitter release at a cortical GABAergic synapse. Neuron 57, 536-45.

Buraei, Z., and Yang, J. (2010). The beta subunit of voltage-gated Ca2+ channels. Physiol. Rev. 90, 1461-1506.

Börjesson, S. I., and Elinder, Fredrik (2008). Structure, function, and modification of the voltage sensor in voltage-gated ion channels.

Campos, F. V., Chanda, B., Roux, B., and Bezanilla, Francisco (2007). Two atomic constraints unambiguously position the S4 segment relative to S1 and S2 segments in the closed state of Shaker K channel. Proceedings of the National Academy of Sciences of the United States of America 104, 7904-9.

Cantí, C et al. (2005). The metal-ion-dependent adhesion site in the Von Willebrand factor-A domain of alpha2delta subunits is key to trafficking voltage-gated Ca2+ channels. Proceedings of the National Academy of Sciences of the United States of America 102, 11230-5.

Cantí, C, and Dolphin, a C. (2003). CaVβ subunit-mediated up-regulation of CaV2.2 currents triggered by D2 dopamine receptor activation. Neuropharmacology 45, 814-827.

Cao, Y.-Q., Piedras-Rentería, Erika S, Smith, G. B., Chen, G., Harata, Nobutoshi C, and Tsien, Richard W (2004). Presynaptic Ca2+ channels compete for channel type-preferring slots in altered neurotransmission arising from Ca2+ channelopathy. Neuron 43, 387-400.

Cao, Y.-Q., and Tsien, Richard W (2010). Different relationship of N- and P/Q-type Ca2+ channels to channel-interacting slots in controlling neurotransmission at cultured hippocampal synapses. The Journal of neuroscience : the official journal of the Society for Neuroscience 30, 4536-46.

Cao, Y.-Q., and Tsien, Richard W (2005). Effects of familial hemiplegic migraine type 1 mutations on neuronal P/Q-type Ca2+ channel activity and inhibitory synaptic transmission. Proc. Natl. Acad. Sci. USA 102, 2590-2595.

Carbone, E., and Lux, H. D. (1984). A low voltage activated fully inactivating Ca channel in vertebrate sensory neurons. Nature 310, 501-502.

Carter, A. G., and Regehr, Wade G (2002). Quantal events shape cerebellar interneuron firing. Nature neuroscience 5, 1309-18.

Casadio, A., Martin, K. C., Giustetto, M., Zhu, H., Chen, M., Bartsch, D., Bailey, C. H., and Kandel, E. R. (1999). A transient, neuron-wide form of CREB-mediated long-term facilitation can be stabilized at specific synapses by local protein synthesis. Cell 99, 221-37.

Castellano, A, Wei, X., Birnbaumer, L, and Perez-Reyes, E (1993a). Cloning and expression of a neuronal calcium channel beta subunit. The Journal of biological chemistry 268, 12359-66.

Castellano, A, Wei, X., Birnbaumer, L, and Perez-Reyes, E (1993b). Cloning and expression of a third calcium channel beta subunit. The Journal of biological chemistry 268, 3450-5.

Catterall, W A (1999). Interactions of presynaptic Ca2+ channels and snare proteins in neurotransmitter release. Annals of the New York Academy of Sciences 868, 144-59.

Catterall, W A (1986). Molecular properties of voltage-sensitive sodium and calcium channels. Annual review of biochemistry 55, 953-985.

Catterall, W A (2000). Structure and regulation of voltage-gated Ca2+ channels. Annual review of cell and developmental biology 16, 521-55.

Catterall, W A (1995). Structure and function of voltage-gated ion channels. Annual review of biochemistry 64, 493-531.

Catterall, William A (2011). Voltage-Gated Calcium Channels. Cold Spring Harbor perspectives in biology.

Catterall, William A, Perez-reyes, E., Snutch, Terrance P, and Striessnig, Joerg (2005). International Union of Pharmacology . XLVIII . Nomenclature and Structure-Function Relationships of Voltage-Gated Calcium Channels. Pharmacological Reviews 57, 411-425.

Catterall, William A, and Few, A. P. (2008). Calcium channel regulation and presynaptic plasticity. Neuron 59, 882-901.

Ceccarelli, B., Hurlbut, W. P., and Mauro, A. (1973). Turnover of transmitter and synaptic vesicles at the frog neuromuscular junction. J. Cell Biol. 57, 499-524.

Ceccarelli, B., and Hurlbut, W. P. (1980). Ca2+-dependent recycling of synaptic vesicles at the frog neuromuscular junction. The Journal of cell biology 87, 297-303.

Cha, A., Snyder, G. E., Selvin, P. R., and Bezanilla, Francisco (1999). Atomic scale movement of the voltage-sensing region in a potassium channel measured via spectroscopy. Nature 402, 809-813.

Chanda, B., Asamoah, O. K., Blunck, R., Roux, B., and Bezanilla, Francisco (2005). Gating charge displacement in voltage-gated ion channels involves limited transmembrane movement. Nature 436, 852-6.

Chang, B. S., and Lowenstein, D. H. (2003). Epilepsy. N. Engl. J. Med. 349, 1257-1266.

Chang, S Y, Yong, T. F., Yu, C. Y., Liang, M C, Pletnikova, O., Troncoso, J., Burgunder, J.-M., and Soong, T W (2007). Age and gender-dependent alternative splicing of P/Q-type calcium channel EF-hand. Neuroscience 145, 1026-36.

Chapman, E. R., Hanson, Phyllis I, An, S., and Jahn, Reinhard (1995). Ca2+ Regulates the Interaction between Synaptotagmin and Syntaxin 1. Journal of Biological Chemistry 270, 23667-23671.

Chaudhuri, D., Alseikhan, Badr a, Chang, Siao Yun, Soong, Tuck Wah, and Yue, David T (2005). Developmental activation of calmodulin-dependent facilitation of cerebellar P-type Ca2+ current. The Journal of neuroscience : the official journal of the Society for Neuroscience 25, 8282-94.

Chaudhuri, D., Chang, S.-Y., DeMaria, Carla D, Alvania, Rebecca S, Soong, Tuck Wah, and Yue, David T (2004). Alternative splicing as a molecular switch for Ca2+/calmodulin-dependent facilitation of P/Q-type Ca2+ channels. The Journal of neuroscience : the official journal of the Society for Neuroscience 24, 6334-42.

Chen, W.-S., Yueh, C.-Y., Huang, Y.-A., and Hwang, E. (2011). An inverted method for culturing dissociated mouse hippocampal neurons. Neurosci. Res. 70, 118-23.

Chesler, M. (1990). The regulation and modulation of pH in the nervous system. Prog. Neurobiol. 34, 401-27.

Cheung, G., Jupp, O. J., and Cousin, Michael a (2010). Activity-dependent bulk endocytosis and clathrin-dependent endocytosis replenish specific synaptic vesicle pools in central nerve terminals. The Journal of neuroscience: the official journal of the Society for Neuroscience 30, 8151-61.

Chioza, B., Wilkie, H., Nashef, L., Blower, J., McCormick, D, Sham, P., Asherson, P., and Makoff, A. J. (2001). Association between the α 1a calcium channel gene CACNA1A and idiopathic generalized epilepsy. Neurology 56, 1245-1246.

Christie, J. M., Chiu, D. N., and Jahr, C. E. (2011). Ca(2+)-dependent enhancement of release by subthreshold somatic depolarization. Nature neuroscience 14, 62-8.

Christie, S. B., and Blas, A. L. De (2003). GABAergic and glutamatergic axons innervate the axon initial segment and organize GABA(A) receptor clusters of cultured hippocampal pyramidal cells. J. Comp. Neurol. 456, 361-74.

Chu, P. J., Robertson, H. M., and Best, P. M. (2001). Calcium channel gamma subunits provide insights into the evolution of this gene family. Gene 280, 37-48.

Chung, Chihye, and Kavalali, Ege T (2006). Seeking a function for spontaneous neurotransmission. Nature neuroscience 9, 989-90.

Clayton, E. L., and Cousin, M. A. (2008). Differential labelling of bulk endocytosis in nerve terminals by FM dyes. Neurochem. Int. 53, 51-55.

Cochilla, A. J., Angleson, J. K., and Betz, W J (1999). Monitoring secretory membrane with FM1-43 fluorescence. Annu. Rev. Neurosci. 22, 1-10.

Coetzee, W. A. et al. (1999). Molecular diversity of K+ channels. Annals of the New York Academy of Sciences 868, 233-85.

Cole, K. S. (1949). Dynamic electrical characteristics of the squid axon membrane. Archives de Sciences Physiologiques 3, 253-258.

Cole, K. S., and Curtis, H. J. (1939). Electric Impedance of the Squid Giant Axon During Activity. The Journal of general physiology 22, 649-70.

Currie, K. P., and Fox, A P (1997). Comparison of N- and P/Q-type voltage-gated calcium channel current inhibition. J. Neurosci. 17, 4570-9.

Dale, H. H., Feldberg, W., and Vogt, M. (1936). Release of acetylcholine at voluntary motor nerve endings. The Journal of physiology 86, 353-80.

Darcy, K.J., Staras, K, Collinson, L. M., and Goda, Y (2006). Constitutive sharing of recycling synaptic vesicles between presynaptic boutons. Nat. Neurosci. 9, 1-7.

Davies, A. et al. (2006). The calcium channel alpha2delta-2 subunit partitions with CaV2.1 into lipid rafts in cerebellum: implications for localization and function. The Journal of neuroscience : the official journal of the Society for Neuroscience 26, 8748-57.

DeMaria, C D, Soong, T W, Alseikhan, B a, Alvania, R S, and Yue, D T (2001). Calmodulin bifurcates the local Ca2+ signal that modulates P/Q-type Ca2+ channels. Nature 411, 484-9.

Denier, C et al. (1999). High prevalence of CACNA1A truncations and broader clinical spectrum in episodic ataxia type 2. Neurology 52, 1816-21.

Denier, C., Ducros, A., Durr, A., Eymard, B., Chassande, B., and Tournier-Lasserve, E. (2001). Mutation Causing Episodic Ataxia Type 2. Archives of Neurology 58, 292-295.

Dichgans, M., et al. (2005). Mutation in the neuronal voltage-gated sodium channel SCN1A in familial hemiplegic migraine. Lancet 366, 371-7.

Dietrich, D., Kirschstein, T., Kukley, M., Pereverzev, Alexej, Brelie, C. von der, Schneider, T., and Beck, H. (2003). Functional specialization of presynaptic Cav2.3 Ca2+ channels. Neuron 39, 483-96.

Diriong, S., Lory, P., Williams, M E, Ellis, S B, Harpold, M M, and Taviaux, S. (1995). Chromosomal localiastion of the human genes for alpha1A, alpha1B and alpha1E Voltage dependent Ca2+ channel subunits. Genomics 30, 605-609.

Dodson, P. D., and Forsythe, Ian D (2004). Presynaptic K+ channels: electrifying regulators of synaptic terminal excitability. Trends in neurosciences 27, 210-7.

Dolphin, A. C. (2006). A short history of voltage-gated calcium channels. British Journal of Pharmacology, 56-62.

Dolphin, A. C. (2009). Calcium channel diversity: multiple roles of calcium channel subunits. Current opinion in neurobiology 19, 237-44.

Dolphin, A. C. (2003). Subunits of Voltage-Gated Calcium Channels. Journal of Bioenergetics and Biomembranes 35, 599-620.

Doyle, D. A. (1998). The Structure of the Potassium Channel: Molecular Basis of K+ Conduction and Selectivity. Science 280, 69-77.

Dreier, J. P., Jurkat-Rott, K, Petzold, G. C., Tomkins, O., Klingebiel, R., Kopp, U. a, Lehmann-Horn, F, Friedman, a, and Dichgans, M (2005). Opening of the blood-brain barrier preceding cortical edema in a severe attack of FHM type II. Neurology 64, 2145-7.

Druzin, M., Haage, D., Malinina, E., and Johansson, S. (2002). Dual and opposing roles of presynaptic Ca2+ influx for spontaneous GABA release from rat medial preoptic nerve terminals. The Journal of Physiology 542, 131-146.

Ducros, A. et al. (2001). THE CLINICAL SPECTRUM OF FAMILIAL HEMIPLEGIC MIGRAINE ASSOCIATED WITH MUTATIONS IN A NEURONAL CALCIUM CHANNEL. The Neuroscientist : a review journal bringing neurobiology, neurology and psychiatry 345, 17-24.

Dulubova, I, Sugita, S., Hill, S., Hosaka, M., Fernandez, I., Südhof, T C, and Rizo, J (1999). A conformational switch in syntaxin during exocytosis: role of munc18. The EMBO journal 18, 4372-82.

Duran, C., Thompson, C. H., Xiao, Q., and Hartzell, H. C. (2010). Chloride channels: often enigmatic, rarely predictable. Annual review of physiology 72, 95-121.

Durell, S. R., Shrivastava, I. H., and Guy, H Robert (2004). Models of the structure and voltage-gating mechanism of the shaker K+ channel. Biophysical journal 87, 2116-30.

Durr, A. (2010). Autosomal dominant cerebellar ataxias: polyglutamine expansions and beyond. Lancet neurology 9, 885-94.

Dutzler, R., Campbell, E. B., and MacKinnon, Roderick (2003). Gating the selectivity filter in ClC chloride channels. Science (New York, N.Y.) 300, 108-12.

Eckert, R., and Chad, J. E. (1984). Inactivation of Ca channels. Progress in biophysics and molecular biology 44, 215-67.

Elinder, F., and Rhem, P. (2003). Metal ion effects on ion channel gating. Quarterly Reviews of Biophysics 36, 373-427.

Ellis, S. B., et al. (1988). Sequence and Expression of mRNAs Encoding the alpha1 and alpha2 Subunits of a DHP-Sensitive Calcium Channel. Science 241, 1661-1664.

Emptage, N. J. (1999). Calcium on the up: supralinear calcium signaling in central neurons. Neuron 24, 495-7.

Emptage, N. J., Reid, C. A, and Fine, A (2001). Calcium stores in hippocampal synaptic boutons mediate short-term plasticity, store-operated Ca2+ entry, and spontaneous transmitter release. Neuron 29, 197-208.

Ertel, E. A. et al. (2000). Nomenclature of voltage-gated calcium channels. Neuron 25, 533-535.

Erulkar, S. D., and Rahamimoff, R. (1978). The role of calcium ions in tetanic and post-tetanic increase of miniature end-plate potential frequency. Journal of Physiology 278, 501-511.

Evans, R. M., and Zamponi, G.W. (2006). Presynaptic Ca2+ channels--integration centers for neuronal signaling pathways. Trends in neurosciences 29, 617-24.

Far, O. E. L. et al. (1993). Synaptotagmin associates with presynaptic calcium channels and is a Lambert-Eaton myasthenic syndrome antigen. Ann. N.Y. Acad. Sci. 707, 382-385.

Fasshauer, D, Eliason, W. K., Brünger, a T., and Jahn, R (1998). Identification of a minimal core of the synaptic SNARE complex sufficient for reversible assembly and disassembly. Biochemistry 37, 10354-62.

Fath, T., Ke, Y. D., Gunning, P., Götz, J., and Ittner, L. M. (2009). Primary support cultures of hippocampal and substantia nigra neurons. Nat. Protoc. 4, 78-85.

Fatt, P., and Katz, B. (1952). The electrical properties of crustacean muscle fibres. Journal of Physiology 120, 171-204.

Fedulova, S. a, Kostyuk, P. G., and Veselovsky, N. S. (1985). Two types of calcium channels in the somatic membrane of new-born rat dorsal root ganglion neurones. The Journal of physiology 359, 431-46.

Felix, R., Gurnett, C. A., Waard, M. D., Campbell, K. P, and Roche, I. J. (1997). Dissection of Functional Domains of the Voltage-Dependent Ca2+ Channel alpha2delta Subunit. Nature 17, 6884-6891.

Fernández-Chacón, R. et al. (2001). Synaptotagmin I functions as a calcium regulator of release probability. Nature 410, 41-9.

Fesce, R., Grohovaz, F., Valtorta, F., and Meldolesi, Jacopo (1994). Neurotransmitter release: fusion or "kiss-and-run"? Trends in Cell Biology, 1-4.

Finlin, B. S., Shao, H., Kadono-okuda, K., Guo, N., and Andres, D. A. (2000). Rem2, a new member of the Rem/Rad/Gem/Kir family of Ras-related GTPases. Biochemistry Journal 347, 223-231.

Fletcher, C F et al. (2001). Dystonia and cerebellar atrophy in Cacna1a null mice lacking P/Q calcium channel activity. FASEB 15, 1288-90.

Forsythe, I D (1994). Direct patch recording from identified presynaptic terminals mediating glutamatergic EPSCs in the rat CNS, in vitro. J. Physiol. 479, 381-387.

Fredj, N. B., and Burrone, J. (2009). A resting pool of vesicles is responsible for spontaneous vesicle fusion at the synapse. Nature neuroscience 12, 751-8.

Freise, D. et al. (2000). Absence of the gamma subunit of the skeletal muscle dihydropyridine receptor increases L-type Ca2+ currents and alters channel inactivation properties. The Journal of biological chemistry 275, 14476-81.

Friedman, H. V., Bresler, T., Garner, C. C., and Ziv, N. E. (2000). Assembly of new individual excitatory synapses: time course and temporal order of synaptic molecule recruitment. Neuron 27, 57-69.

Fusco, M. De, Marconi, R., Silvestri, L., Atorino, L., Rampoldi, L., Morgante, L., Ballabio, A., Aridon, P., and Casari, G. (2003). Haploinsufficiency of ATP1A2 encoding the Na+/K+ pump alpha2 subunit associated with familial hemiplegic migraine type 2. Nature genetics 33, 192-6.

Gaffield, M. A., and Betz, William J (2006). Imaging synaptic vesicle exocytosis and endocytosis with FM dyes. Nat. Protoc. 1, 2916-2921.

Gancher, S. T., and Nutt, J. G. (1986). Autosomal dominant episodic ataxia: a heterogeneous syndrome. Mov Disord 1, 239-253.

Gandhi, C. S., Loots, E., and Isacoff, E Y (2000). Reconstructing voltage sensor-pore interaction from a fluorescence scan of a voltage-gated K+ channel. Neuron 27, 585-95.

Gandhi, S. P., and Stevens, C F (2003). Three modes of synaptic vesicular recycling revealed by single-vesicle imaging. Nature 423, 607-613.

Gao, B. et al. (2000). Functional Properties of a New Voltage-dependent Calcium Channel Auxiliary Subunit Gene (CACNA2D2) . 275, 12237-12242.

Gasser, U. E., and Hatten, M. E. (1990). Neuron-glia interactions of rat hippocampal cells in vitro: glial-guided neuronal migration and neuronal regulation of glial differentiation. J. Neurosci. 10, 1276-1285.

Geiger, J. R., and Jonas, P (2000). Dynamic control of presynaptic Ca(2+) inflow by fast-inactivating K(+) channels in hippocampal mossy fiber boutons. Neuron 28, 927-939.

Geppert, M., Goda, Y, Hammer, R E, Li, C, Rosahl, T. W., Stevens, C F, and Südhof, T C (1994). Synaptotagmin I: a major Ca2+ sensor for transmitter release at a central synapse. Cell 79, 717-27.

Gerlai, R. (1996). Gene-targeting studies of mammalian behavior: is it the mutation or the background genotype? Trends Neurosci. 19, 177-181.

Gersdorff, H von, Vardi, E., Matthews, G, and Sterling, P. (1996). Evidence that vesicles on the synaptic ribbon of retinal bipolar neurons can be rapidly released. Neuron 16, 1221-7.

Gersdorff, Henrique von, and Matthews, Gary (1994). Dynamics of synaptic vesicle fusion and membrane retrieval in synaptic terminals. Nature 367, 735-739.

Giessel, A. J., and Sabatini, Bernardo L (2011). Boosting of Synaptic Potentials and Spine Ca Transients by the Peptide Toxin SNX-482 Requires Alpha-1E-Encoded Voltage-Gated Ca Channels. PloS one 6, e20939.

Glauner, K. S., Mannuzzu, L. M., Gandhi, C. S., and Isacoff, E Y (1999). Spectroscopic mapping of voltage sensor movement in the Shaker potassium channel. Nature 402, 813-7.

Glitsch, M. D. (2008). Spontaneous neurotransmitter release and Ca2+--how spontaneous is spontaneous neurotransmitter release? Cell calcium 43, 9-15.

Goadsby, P. J., Charbit, A. R., Andreou, A. P., Akerman, S., and Holland, P. R. (2009). Neurobiology of migraine. Neuroscience 161, 327-41.

Goda, Y., and Stevens, C F (1994). Two components of transmitter release at a central synapse. Proceedings of the National Academy of Sciences of the United States of America 91, 12942-6.

Goda, Y., and Südhof, T. C. (1997). Calcium regulation of neurotransmitter release: reliably unreliable? Current opinion in cell biology 9, 513-518.

González, J. C., Albiñana, E., Baldelli, P., García, a G., and Hernández-Guijo, J. M. (2011). Presynaptic muscarinic receptor subtypes involved in the enhancement of spontaneous GABAergic postsynaptic currents in hippocampal neurons. The European journal of neuroscience 33, 69-81.

Gordon-Weeks, P. (1987). Isolation of synaptosomes, growth cones and their subcellular components. In Neurochemistry. A Practical Approach A. Turner and H. Bachelard, eds. (IRL Press, Oxford, UK), pp. 1–26.

Gossler, A., Joyner, A. L., Rossant, J., and Skarnes, W. C. (1989). Mouse embryonic stem cells and reporter constructs to detect developmentally regulated genes. Science 244, 463-5.

Granseth, B., Odermatt, B., Royle, S. J., and Lagnado, L (2006). Clathrin-mediated endocytosis is the dominant mechanism of vesicle retrieval at hippocampal synapses. Neuron 51, 773-786.

Graus, F., Lang, B, Pozo-Rosich, P., Saiz, A., Casamitjana, R., and Vincent, A (2002). P / Q type calcium-channel antibodies in paraneoplastic cerebellar degeneration with lung cancer P / Q type calcium- channel antibodies in paraneoplastic cerebellar degeneration with. Neurology 59, 764-766.

Groffen, A. J. A., Friedrich, R., Brian, E. C., Ashery, U., and Verhage, Matthijs (2006). DOC2A and DOC2B are sensors for neuronal activity with unique calcium-dependent and kinetic properties. Journal of neurochemistry 97, 818-33.

Groffen, A. J. et al. (2010). Doc2b is a high-affinity Ca2+ sensor for spontaneous neurotransmitter release. Science (New York, N.Y.) 327, 1614-8.

Grosse, G., Tapp, R., Wartenberg, M., Sauer, H., Fox, P. a, Grosse, J., Gratzl, M., and Bergmann, M. (1998). Prenatal hippocampal granule cells in primary cell culture form mossy fiber boutons at pyramidal cell dendrites. J. Neurosci. Res. 51, 602-11.

Guida, S. et al. (2001). Complete loss of P/Q calcium channel activity caused by a CACNA1A missense mutation carried by patients with episodic ataxia type 2. American journal of human genetics 68, 759-64.

Gurnett, C., Dewaard, M., and Campbell, K. (1996). Dual Function of the Voltage-Dependent Ca Channel alpha2delta Subunit in Current Stimulation and Subunit Interaction. Neuron 16, 431-440.

Guy, H R, and Seetharamulu, P. (1986). Molecular model of the action potential sodium channel. Proceedings of the National Academy of Sciences of the United States of America 83, 508-12.

Görtz, P., Fleischer, W., Rosenbaum, C., Otto, F., and Siebler, M. (2004). Neuronal network properties of human teratocarcinoma cell line-derived neurons. Brain Res. 1018, 18-25.

Haan, J, Terwindt, G M, Maagdenberg, a M. J. M. van den, Stam, a H., and Ferrari, M D (2008). A review of the genetic relation between migraine and epilepsy. Cephalalgia 28, 105-13.

Hagiwara, S., Ozawa, S., and Sand, O. (1975). Voltage clamp analysis of two inward current mechanisms in the egg cell membrane of a starfish. J. Gen. Physiol. 65, 617-644.

Hagiwara, S., and Byerly, L. (1981). Calcium channel. Annual review of neuroscience 4, 69-125.

Hagler, D. J., and Goda, Y., (2001). Properties of Synchronous and Asynchronous Release During Pulse Train Depression in Cultured Hippocampal Neurons Properties of Synchronous and Asynchronous Release During Pulse Train Depression in Cultured Hippocampal Neurons. Journal of Neurophysiology 85, 2324-2334.

Halling, D. B., Aracena-Parks, P., and Hamilton, S. L. (2005). Regulation of voltage-gated Ca2+ channels by calmodulin. Science's STKE : signal transduction knowledge environment 2005, re15.

Hama, H., Hara, C., Yamaguchi, K., and Miyawaki, A. (2004). PKC signaling mediates global enhancement of excitatory synaptogenesis in neurons triggered by local contact with astrocytes. Neuron 41, 405-15.

Han, Y., Kaeser, P. S., Südhof, T. C., and Schneggenburger, R.(2011). RIM determines Ca^2+ channel density and vesicle docking at the presynaptic active zone. Neuron 69, 304-316.

Hans, M. et al. (1999). Functional consequences of mutations in the human alpha1A calcium channel subunit linked to familial hemiplegic migraine. J. Neurosci. 19, 1610-1619.

Hanson, P I, Roth, R., Morisaki, H., Jahn, R, and Heuser, J. E. (1997). Structure and conformational changes in NSF and its membrane receptor complexes visualized by quick-freeze/deep-etch electron microscopy. Cell 90, 523-35.

Harata, N C (2006). Kiss-and-run and full-collapse fusion as modes of exo-endocytosis in neurosecretion. J. Neurochem. 97, 1546-1570.

Harata, N., Pyle, J. L., Aravanis, a M., Mozhayeva, M., Kavalali, E T, and Tsien, R W (2001). Limited numbers of recycling vesicles in small CNS nerve terminals: implications for neural signaling and vesicular cycling. Trends in neurosciences 24, 637-43.

Harata, N., Ryan, T. A., Smith, S J, Buchanan, J., and Tsien, R W (2001). Visualizing recycling synaptic vesicles in hippocampal neurons by FM 1-43 photoconversion. Proc. Natl. Acad. Sci. U.S.A. 98, 12748-12753.

Harrison, R. G. (1910). The outgrowth of the nerve fiber as a mode of protoplasmic movement. J. Exp. Zool. 142, 5-73.

Hartley, R. S., Margulis, M., Fishman, Paul S, Lee, Virginia M, and Tang, C.-min (1999). Between human NTera2 (NT2N , hNT) neurons grown on astrocytes. J. Comp. Neurol. 10, 1-10.

Hayashi, T., McMahon, H., Yamasaki, S., Binz, T., Hata, Y., Südhof, T C, and Niemann, H. (1994). Synaptic vesicle membrane fusion complex: action of clostridial neurotoxins on assembly. The EMBO journal 13, 5051-61.

Hess, P (1990). Calcium channels in vertebrate cells. Annual review of neuroscience 13, 337-56.

Hess, P., and Tsien, R. W. (1984). Mechanism of ion permeation through calcium channels. Nature 309, 453-456.

Heuser, J. E., and Reese, T. S. (1973). Evidence for recycling of synaptic vesicle membrane during transmitter release at the frog neuromuscular junction. J. Cell Biol. 57, 315-344.

Higgins, D., Waxman, a, and Banker, G (1988). The distribution of microtubule-associated protein 2 changes when dendritic growth is induced in rat sympathetic neurons in vitro. Neuroscience 24, 583-92.

Hille, B. (2001). Ion cannels of excitatble membranes 3rd ed. (Sinauer Associates).

Hillman, D., Chen, S, Aung, T. T., Cherksey, B., Sugimori, M., and Llinás, R. R. (1991). Localization of P-type calcium channels in the central nervous system. Proceedings of the National Academy of Sciences of the United States of America 88, 7076-80.

Hirasawa, M., and Pittman, Q. J. (2003). Nifedipine facilitates neurotransmitter release independently of calcium channels. Proceedings of the National Academy of Sciences of the United States of America 100, 6139-44.

Hodgkin, A. L. (1964). The Ionic Basis of Nervous Conduction. Science (New York, N.Y.) 145, 1148-54.

Hodgkin, A. L., and Huxley, A. F. (1952). A quantitative description of membrane current and its application to conduction and excitation in nerve. Journal of Physiology 117, 500-544.

Hodgkin, A. L., and Huxley, A. F. (1939). Action Potentials Recorded from Inside a Nerve Fibre. Nature 144, 710-711.

Hodgkin, A. L., and Huxley, A. F. (1945). Resting and action potentials in single nerve fibres. Journal of phyiology 104, 176-195.

Hodgkin, A. L., and Katz, B. (1949). The effect of sodium ions on the electrical activity of the giant axon of the squid. Journal of Physiology 108, 37-77.

Hofmann, F, Biel, M, and Flockerzi, V (1994). Molecular basis for Ca2+ channel diversity. Annual review of neuroscience 17, 399-418.

Hopf, F. W., Waters, J., Mehta, S., and Smith, S. J. (2002). Stability and plasticity of developing synapses in hippocampal neuronal cultures. J. Neurosci. 22, 775-781.

Hosey, M. M., Chien, A. J., and Puri, T. S. (1996). Structure and regulation of L-type calcium channels a current assessment of the properties and roles of channel subunits. Trends in cardiovascular medicine 6, 265-73.

Hua, Y., Sinha, R., Martineau, M., Kahms, M., and Klingauf, Jürgen (2010a). A common origin of synaptic vesicles undergoing evoked and spontaneous fusion. Nature neuroscience 13, 1451-3.

Hua, Y., Sinha, R., Martineau, M., Kahms, M., and Klingauf, Jürgen (2010b). A common origin of synaptic vesicles undergoing evoked and spontaneous fusion. Nature neuroscience 13, 1451-3.

Huber, K. M., Kayser, M. S., and Bear Mark F (2000). Role for Rapid Dendritic Protein Synthesis in Hippocampal mGluR-Dependent Long-Term Depression. Science 288, 1254-1256.

Huxley, A. F. (2002). Hodgkin and the action potential 1935-1952. J. Physiol. 538, 2-3.

Häusser, M. (2000). The Hodgkin-Huxley theory of the action potential. Nature Neuroscience 3, 1165.

Ikeda, Stephen R (1996). Voltage dependent modulation of N type calcium channels by G proteinbeta-gamma subunits. Nature 380, 225-258.

Imbrici, P., Jaffe, S. L., Eunson, Louise H, Davies, N. P., Herd, C., Robertson, R., Kullmann, Dimitri M, and Hanna, Michael G (2004). Dysfunction of the brain calcium channel CaV2.1 in absence epilepsy and episodic ataxia. Brain 127, 2682-92.

Inchauspe, C. G., Urbano, F. J., Guilmi, M. N. Di, Forsythe, I. D., Ferrari, M. D., van den Maagdenberg, A M J M, and Uchitel, O. D. (2010). Gain of function in FHM 1 Cav2.1 KI mice is related to the shape of the AP. Journal of Neurophysiology.

Inoue, A., Obata, K., and Akagawa, K. (1992). Cloning and sequence analysis of cDNA for a neuronal cell membrane antigen, HPC-1. Journal Biol Chem 267, 10613-9.

Isomoto, S., Kondo, C., and Kurachi, Y. (1997). Inwardly rectifying potassium channels: their molecular heterogeneity and function. Japanese Journal of Physiology 47, 11-39.

Jackson, A. C., and Nicoll, R. A. (2011). The expanding social network of ionotropic glutamate receptors: TARPs and other transmembrane auxiliary subunits. Neuron 70, 178-99.

Jarvis, S. E., and Zamponi, G. W. (2001). Interactions between presynaptic Ca2+ channels, cytoplasmic messengers and proteins of the synaptic vesicle release complex. Trends in pharmacological sciences 22, 519-25.

Jarvis, S. E, Barr, W., Feng, Z.-P., Hamid, J., and Zamponi, Gerald W (2002). Molecular Determinants of Syntaxin 1 Modulation of N-type Calcium Channels. J Biol Chem 277, 44399-44407.

Jarvis, S. E., and Zamponi, G. W. (2005). Masters or slaves? Vesicle release machinery and the regulation of presynaptic calcium channels. Cell calcium 37, 483-8.

Jay, S. D., Sharp, A. H., Kahl, S. D., Vedvick, T. S., Harpold, M M, and Campbell, K P (1991). Structural characterization of the dihydropyridine-sensitive calcium channel alpha 2-subunit and the associated delta peptides. The Journal of biological chemistry 266, 3287-93.

Jen, J. C., Graves, T D, Hess, E. J., Hanna, M G, Griggs, R. C., and Baloh, R. W. (2007). Primary episodic ataxias: diagnosis, pathogenesis and treatment. Brain 130, 2484-93.

Jen, J., Kim, G. W., and Baloh, R. W. (2004). Clinical spectrum of episodic ataxia type 2. Neurology 62, 17-22.

Jiang, Y., Ruta, V., Chen, J., Lee, Alice, and Mackinnon, R. (2003). The principle of gating charge movement in a voltage-dependent K+ channel. Nature 423, 42-48.

Jockusch, W. J., Praefcke, G. J. K., McMahon, H. T., and Lagnado, L. (2005). Clathrin-dependent and clathrin-independent retrieval of synaptic vesicles in retinal bipolar cells. Neuron 46, 869-78.

Jodice, C. et al. (1997). Episodic ataxia type 2 (EA2) and spinocerebellar ataxia type 6 (SCA6) due to CAG repeat expansion in the CACNA1A gene on chromosome 19p. Human molecular genetics 6, 1973-8.

Jones, K. H., and Senft, J. A. (1985). An improved method to determine cell viability by simultaneous staining with fluorescein diacetate-propidium iodide. J. Histochem. Cytochem. 33, 77-79.

Jones, M. V., and Westbrook, G. L. (1995). Desensitized states prolong GABAA channel responses to brief agonist pulses. Neuron 15, 181-91.

Jongh, K. S. De, Warner, C., and Catterall, W. A. (1990). Subunits of purified calcium channels. The Journal of biological chemistry 265, 14738-14741.

Joselevitch, C., and Zenisek, D. (2009). Imaging exocytosis in retinal bipolar cells with TIRF microscopy. J. Vis. Exp., 1-6.

Jouvenceau, A., Eunson, L. H., Spauschus, A., Ramesh, V., Zuberi, S. M., Kullmann, D. M., and Hanna, M. G. (2001). Human epilepsy associated with dysfunction of the brain P/Q-type calcium channel. Lancet 358, 801-7.

Jun, K. et al. (1999). Ablation of P/Q-type Ca(2+) channel currents, altered synaptic transmission, and progressive ataxia in mice lacking the alpha(1A)-subunit. Proceedings of the National Academy of Sciences of the United States of America 96, 15245-50.

Jurkat-Rott, K. et al. (2004). Variability of familial hemiplegic migraine with novel A1A2 Na / K -ATPase variants. Neurology 62, 1857-1861.

Kaech, S., and Banker, G. (2006). Culturing hippocampal neurons. Nat. Protoc. 1, 2406-15.

Kaeser, P. S., Deng, L., Wang, Yun, Dulubova, Irina, Liu, Xinran, Rizo, Josep, and Südhof, Thomas C (2011). RIM proteins tether Ca2+ channels to presynaptic active zones via a direct PDZ-domain interaction. Cell 144, 282-295.

Kaja, S., Ven, R. C. G. van de, Broos, L. A. M., Frants, Rune R, Ferrari, Michel, and Maagdenberg, Arn Plomp, J. J. van den (2007). Characterization of acetylcholine release and the compensatory contribution of non-Cav2.1 channels at motor nerve terminals of leaner Cav2.1-mutant mice. Neuroscience 144, 1278–1287.

Kammermeier, P. J., Ruiz-Velasco, V., and Ikeda, S R (2000). A voltage-independent calcium current inhibitory pathway activated by muscarinic agonists in rat sympathetic neurons requires both Galpha q/11 and Gbeta gamma. J Neurosci 20, 5623-9.

Kang, H., and Schuman, E M (1996). A requirement for local protein synthesis in neurotrophin-induced hippocampal synaptic plasticity. Science 273, 1402-6.

Kanumilli, S., Tringham, E. W., Payne, C. E., Dupere, J. R. B., Venkateswarlu, K., and Usowicz, M. M. (2006). Alternative splicing generates a smaller assortment of CaV2.1 transcripts in cerebellar Purkinje cells than in the cerebellum. Physiological genomics 24, 86-96.

Katoh, A., Jindal, J. A., and Raymond, J. L. (2007). Motor deficits in homozygous and heterozygous p/q-type calcium channel mutants. J Neurophysiol 97, 1280-7.

Katz, B. (1971). Quantal mechanism of neural transmitter release. Science 173, 123-6.

Katz, B., and Miledi, R. (1970). Further study of the role of calcium in synaptic transmission. J Physiol 207, 789-801.

Katz, B., and Miledi, R. (1969a). Spontaneous and evoked activity of motor nerve endings in calcium ringer. Journal of Physiology 203, 689-706.

Katz, B., and Miledi, R. (1969b). Tetrodotoxin-resistant electric activity in presynaptic terminals. Journal of Physiology 203, 459-487.

Kay, A. R. et al. (1999). Imaging synaptic activity in intact brain and slices with FM1-43 in C. elegans, lamprey, and rat. Neuron 24, 809-817.

Keen, J. H., Willingham, M. C., and Pastan, I. H. (1979). Clathrin-coated vesicles : isolation, dissociation and factor-dependent reassociation of clathrin baskets. Cell 16, 303-312.

Kempen, G. T. H. van, vanderLeest, H. T., Berg, R. J. van den, Eilers, P., and Westerink, R. H. S. (2011). Three distinct modes of exocytosis revealed by amperometry in neuroendocrine cells. Biophysical journal 100, 968-77.

Keynes, R. D., and Elinder, F (1998). On the slowly rising phase of the sodium gating current in the squid giant axon. Proceedings. Biological sciences / The Royal Society 265, 255-62.

Khosravani, H., and Zamponi, Gerald W (2006). Voltage-Gated Calcium Channels and Idiopathic Generalized Epilepsies. Physiological Reviews 86, 941-966.

King, A. E., Chung, R. S., Vickers, J. C., and Dickson, T. C. (2006). Localization of glutamate receptors in developing cortical neurons in culture excitotoxicity. J. Comp. Neurol. 294, 277-294.

Kleppner, S. R., Robinson, K. a, Trojanowski, J. Q., and Lee, V M (1995). Transplanted human neurons derived from a teratocarcinoma cell line (NTera-2) mature, integrate, and survive for over 1 year in the nude mouse brain. J. Comp. Neurol. 357, 618-32.

Klingauf, J, Kavalali, E T, and Tsien, R W (1998a). Kinetics and regulation of fast endocytosis at hippocampal synapses. Nature 394, 581-585.

Kloepper, T. H., Kienle, C. N., and Fasshauer, Dirk (2007). An Elaborate Classification of SNARE Proteins Sheds Light on the Conservation of the Eukaryotic Endomembrane System. Molecular Biology of the Cell 18, 3463-3471.

Klugbauer, N., Marais, E., and Hofmann, Franz (2003). Calcium Channel $\alpha 2$ Subunits: Differential Expression, Function, and Drug Binding. Journal of Bioenergetics and Biomembranes 35, 639-647.

Klyachko, V. a, and Jackson, M. B. (2002). Capacitance steps and fusion pores of small and large-dense-core vesicles in nerve terminals. Nature 418, 89-92.

Koester, H. J., and Johnston, D. (2005). Target cell-dependent normalization of transmitter release at neocortical synapses. Science 308, 863-866.

Koh, T.-W., and Bellen, H. J. (2003). Synaptotagmin I, a Ca2+ sensor for neurotransmitter release. Trends in Neurosciences 26, 413-422.

Koizumi, S., Bootman, M. D., Bobanović, L. K., Schell, M. J., Berridge, M. J., and Lipp, P. (1999). Characterization of elementary Ca2+ release signals in NGF-differentiated PC12 cells and hippocampal neurons. Neuron 22, 125-37.

Kraus, R. L., Sinnegger, M. J., Glossmann, H., Hering, S., and Striessnig, J (1998). Familial hemiplegic migraine mutations change alpha1A Ca2+ channel kinetics. J. Biol. Chem. 273, 5586-90.

Kraus, R. L., Sinnegger, M. J., Koschak, a, Glossmann, H., Stenirri, S., Carrera, P., and Striessnig, J (2000). Three new familial hemiplegic migraine mutants affect P/Q-type Ca(2+) channel kinetics. The Journal of biological chemistry 275, 9239-43.

Krovetz, H. S., Helton, T. D., Crews, A. L., and Horne, W. A. (2000). C-Terminal alternative splicing changes the gating properties of a human spinal cord calcium channel alpha 1A subunit. J Neurosci 20, 7564-70.

Kullmann, D. M. (2010). Neurological channelopathies. Annual review of neuroscience 33, 151-72.

Kullmann, D. M. (2002). The neuronal channelopathies. Brain 125, 1177-95.

Kuromi, H., and Kidokoro, Y. (1998). Two distinct pools of synaptic vesicles in single presynaptic boutons in a temperature-sensitive Drosophila mutant, shibire. Neuron 20, 917-25.

Kuromi, H., and Kidokoro, Y. (2004). Two synaptic vesicle pools, vesicle recruitment and replenishment of pools at the Drosophila neuromuscular junction. Journal of neurocytology 32, 551-65.

Labrum, R. W. et al. (2009). Large scale calcium channel gene rearrangements in episodic ataxia and hemiplegic migraine: implications for diagnostic testing. J. Med. Genet. 46, 786-791.

de Lanerolle, N. C., and Lee, T.-S. (2005). New facets of the neuropathology and molecular profile of human temporal lobe epilepsy. Epilepsy Behav. 7, 190-203.

Lange, R. P. J. de, Roos, A. D. G., and Borst, J. G. G. (2003). Two modes of vesicle recycling in the rat calyx of Held. J Neurosci 23, 10164-73.

Lasek, R. J., Gainer, H., and Barker, J. L. (1977). Cell-to-cell transfer of glial proteins to the squid giant axon. J.Cell Biol. 74, 501-523.

Lauritzen, M. (1994). Pathophysiology of the migraine aura. The spreading depression theory. Brain 117 (Pt 1, 199-210.

Laviv, T., Riven, I., Dolev, I., Vertkin, I., Balana, B., Slesinger, P. A., and Slutsky, I. (2010). Basal GABA regulates GABAbR conformation and release probability at single hippocampal synapses. Neuron 67, 253-267.

Leao, A. (1944). Spreading depression of activity in the cerebral cortex. Depression, 391-396.

Lecar, H., Larsson, H. P., and Grabe, M. (2003). Electrostatic model of S4 motion in voltage-gated ion channels. Biophysical journal 85, 2854-64.

Lee, A, Wong, S. T., Gallagher, D., Li, B., Storm, D. R., Scheuer, T, and Catterall, W. A. (1999). Ca2+/calmodulin binds to and modulates P/Q-type calcium channels. Nature 399, 155-9.

Letts, V. a et al. (1998). The mouse stargazer gene encodes a neuronal Ca2+-channel gamma subunit. Nature genetics 19, 340-7.

León, D., Sánchez-Nogueiro, J., Marín-García, P., and Miras-Portugal, M. a T. (2008). Glutamate release and synapsin-I phosphorylation induced by P2X7 receptors activation in cerebellar granule neurons. Neurochem. Int. 52, 1148-1159.

Li, Cai, Ullrich, B., Zhang, J. Z., Anderson, R. G. W., Brose, Nils, and Südhof, T. C. (1995). Ca2+ dependent and independent activities of neural and non-neural synaptotagmins. Nature 375, 594-599.

Li, L., Bischofberger, J., and Jonas, P. (2007). Differential gating and recruitment of P/Q-, N-, and R-type Ca2+ channels in hippocampal mossy fiber boutons. J Neurosci 27, 13420-9.

Li, Z., Burrone, J., Tyler, W. J., Hartman, K. N., Albeanu, D. F., and Murthy, Venkatesh N (2005). Synaptic vesicle recycling studied in transgenic mice expressing synaptopHluorin. Proceedings of the National Academy of Sciences of the United States of America 102, 6131-6.

Liang, H., DeMaria, Carla D, Erickson, M. G., Mori, M. X., Alseikhan, Badr a, and Yue, David T (2003). Unified mechanisms of Ca2+ regulation across the Ca2+ channel family. Neuron 39, 951-60.

Lipscombe, Diane (2005). Neuronal proteins custom designed by alternative splicing. Current opinion in neurobiology 15, 358-63.

Liu, H., Felix, R, Gurnett, C. a, Waard, M De, Witcher, D. R., and Campbell, K P (1996). Expression and subunit interaction of voltage-dependent Ca2+ channels in PC12 cells. J Neurosci 16, 7557-65.

Liu, L., Zwingman, T. A., and Fletcher, C. F. (2003). In vivo analysis of voltage-dependent calcium channels. Journal of bioenergetics and biomembranes 35, 671-85.

Llano, I., González, J., Caputo, C., Lai, F. A., Blayney, L. M., Tan, Y. P., and Marty, A. (2000). Presynaptic calcium stores underlie large-amplitude miniature IPSCs and spontaneous calcium transients. Nature neuroscience 3, 1256-65.

Llinas, R, Sugimori, M., Hillman, D. E., and Cherksey, B. (1992). Distribution and functional significance of the P-type, voltage-dependent Ca2+ channels in the mammalian central nervous system. Trends in neurosciences 15, 351-355.

Llinas, R., and Yarom, Y. (1981). Properties and distribution of ionic conductances generating electroresponsiveness of mammalian inferior olivary neurons in vitro. Journal of Physiology 315, 569-584.

Llinás, R., Sugimori, M., Lin, J. W., and Cherksey, B. (1989). Blocking and isolation of a calcium channel from neurons in mammals and cephalopods utilizing a toxin fraction (FTX) from funnel-web spider poison. Proceedings of the National Academy of Sciences of the United States of America 86, 1689-93.

Long, S. B., Tao, X., Campbell, E. B., and MacKinnon, R. (2007). Atomic structure of a voltage-dependent K+ channel in a lipid membrane-like environment. Nature 450, 376-82.

Lévêque, C., Far, O. el, Martin-Moutot, N., Sato, K., Kato, R., Takahashi, M., and Seagar, M. J. (1994). Purification of the N-type calcium channel associated with syntaxin and synaptotagmin. A complex implicated in synaptic vesicle exocytosis. J. Biol. Chem. 269, 6306-6312.

López-Muñoz, F., and Alamo, C. (2009). Historical evolution of the neurotransmission concept. Journal of neural transmission 116, 515-33.

Maagdenberg, Arn M J M van den et al. (2004). A CACNA1A knockin migraine mouse model with increased susceptibility to cortical spreading depression. Neuron 41, 701–710.

Maagdenberg, Arn M J M van den et al. (2010). High cortical spreading depression susceptibility and migraine-associated symptoms in Cav2.1 S218L mice. Ann. Neurol. 67, 85–98.

van den Maagdenberg, A. et al. (2010). High Cortical Spreading Depression Susceptibility and Migraine- Associated Symptoms in CaV2.1 S218L Mice. Ann. Neurol. 67, 85–98.

Madden, D. R. (2002). The structure and function of glutamate receptor ion channels. Nature reviews. Neuroscience 3, 91-101.

Maduke, M., Miller, C, and Mindell, J. A. (2000). A decade of CLC chloride channels: structure, mechanism, and many unsettled questions. Annual review of biophysics and biomolecular structure 29, 411-38.

Malgaroli, A, Ting, A. E., Wendland, B., Bergamaschi, A., Villa, A., Tsien, R W, and Scheller, R H (1995). Presynaptic component of long-term potentiation visualized at individual hippocampal synapses. Science (New York, N.Y.) 268, 1624-8.

Malgaroli, A., and Tsien, R. W. (1992). Glutamate-induced long-term potentiation of the frequency of miniature synaptic currents in cultured hippocampal neurons. Nature 357, 134-139.

Mantione, J., Kleppner, S., Miyazono, M., Wertkin, A., Lee, V., and Trojanowski, J. (1995). Human neurons that constitutively secrete Aβ do not induce Alzheimer's disease pathology following transplantation and long-term survival in the rodent brain. Brain Res. 671, 333-337.

Maravall, M., Mainen, Z. F., Sabatini, B L, and Svoboda, K (2000). Estimating intracellular calcium concentrations and buffering without wavelength ratioing. Biophysical journal 78, 2655-67.

Mark, L. P., Prost, R. W., Ulmer, J. L., Smith, M. M., Daniels, D. L., Strottmann, J. M., Brown, W. D., and Hacein-Bey, L. (2001). Pictorial review of glutamate excitotoxicity: fundamental concepts for neuroimaging. Am. J. Neuroradiol. 22, 1813-24.

Matsuyama, Z., Wakamori, M., Mori, Y, Kawakami, H., Nakamura, S., and Imoto, K. (1999). Direct alteration of the P/Q-type Ca2+ channel property by polyglutamine expansion in spinocerebellar ataxia 6. J Neurosci 19, RC14.

Matthews, C. C., Zielke, H. R., Wollack, J. B., and Fishman, P S (2000). Enzymatic degradation protects neurons from glutamate excitotoxicity. J. Neurochem. 75, 1045-52.

Matthiessen, H. P., Schmalenbach, C., and Müller, H. W. (1988). Interactions of astroglia-derived factors with hippocampal neurons. Ann. N.Y. Acad. Sci. 540, 416-9.

Mauch, D. H., Nägler, K., Schumacher, S., Göritz, C., Müller, E. C., Otto, A., and Pfrieger, F. W. (2001). CNS synaptogenesis promoted by glia-derived cholesterol. Science 294, 1354-7.

Maximov, A., Shin, O.-H., Liu, Xinran, and Südhof, T. C. (2007). Synaptotagmin-12, a synaptic vesicle phosphoprotein that modulates spontaneous neurotransmitter release. The Journal of cell biology 176, 113-24.

Maximov, A., Tang, J., Yang, X., Pang, Z. P., and Südhof, T. C. (2009). Complexin controls the force transfer from SNARE complexes to membranes in fusion. Science (New York, N.Y.) 323, 516-21.

Mazzanti, M., and Haydon, P. G. (2003). Astrocytes selectively enhance N-type calcium current in hippocampal neurons. Glia 41, 128-36.

McBain, C. J., and Mayer, M. L. (1994). N-methyl-D-aspartic acid receptor structure and function. Physiol. Rev. 74, 723-60.

McCleskey, E. W., Fox, A. P., Feldman, D. H., Cruz, L. J., Olivera, B. M., Tsien, R W, and Yoshikami, D. (1987). Omega-conotoxin: direct and persistent blockade of specific types of calcium channels in neurons but not muscle. Proceedings of the National Academy of Sciences of the United States of America 84, 4327-31.

McKinney, R. A., Capogna, M., Dürr, R., Gähwiler, B. H., and Thompson, S. M. (1999). Miniature synaptic events maintain dendritic spines via AMPA receptor activation. Nature neuroscience 2, 44-9.

Meinrenken, C. J., Borst, J Gerard G, and Sakmann, Bert (2002). Calcium secretion coupling at calyx of held governed by nonuniform channel-vesicle topography. J Neurosci 22, 1648-67.

Melliti, K., Grabner, M., and Seabrook, G. R. (2002). The familial hemiplegic migraine mutation R192q reduces G-protein-mediated inhibition of p/q-type (Cav2.1) calcium channels expressed in human embryonic kidney cells. The Journal of Physiology 546, 337-347.

Miesenbock, G., Angelis, D. A. De, and Rothman, James E (1998). Visualizing secretion and synaptic transmission with pH-sensitive green fluorescent proteins. Nature 394, 192-195.

Mikala, G., Bahinski, A., Yatani, A., Tang, S., and Schwartz, A. (1993). Differential contribution by conserved glutamate residues to an ion-selectivity site in the L-type Ca2+ channel pore. FEBS letters 335, 265-9.

Milani, D., Malgaroli, A., Guidolin, D., Fasolato, C., Skaper, S., Meldolesi, J, and Pozzan, T. (1990). Ca2+ channels and intracellular Ca2+ stores in neuronal and neuroendocrine cells. Cell calcium 11, 191-199.

Miller, C (2000). Ion channels: doing hard chemistry with hard ions. Current opinion in chemical biology 4, 148-51.

Min, M. Y., Rusakov, D. A., and Kullmann, D. M. (1998). Activation of AMPA, kainate, and metabotropic receptors at hippocampal mossy fiber synapses: role of glutamate diffusion. Neuron 21, 561-70.

Mintz, I. M., Adams, M E, and Bean, B. P. (1992). P-type calcium channels in rat central and peripheral neurons. Neuron 9, 85-95.

Mintz, I. M., Sabatini, B L, and Regehr, W G (1995). Calcium control of transmitter release at a cerebellar synapse. Neuron 15, 675-88.

Misiuta, I. E., Saporta, S., Sanberg, P. R., Zigova, T., and Willing, A. E. (2006). Influence of retinoic acid and lithium on proliferation and dopaminergic potential of human NT2 cells. J. Neurosci. Res. 679, 668-679.

Missler, M., Zhang, W., Rohlmann, A., Kattenstroth, G., Hammer, Robert E, Gottmann, K., and Südhof, Thomas C (2003). Alpha-neurexins couple Ca2+ channels to synaptic vesicle exocytosis. Nature 423, 939-48.

Miyawaki, H., and Hirano, T. (2011). Different correlations among physiological and morphological properties at single glutamatergic synapses in the rat hippocampus and the cerebellum. Synapse 65, 412-23.

Mochida, S., Sheng, Z. H., Baker, C., Kobayashi, H., and Catterall, W A (1996). Inhibition of neurotransmission by peptides containing the synaptic protein interaction site of N-type Ca2+ channels. Neuron 17, 781-8.

Morales, M., Colicos, M. A., and Goda, Y (2000). Actin-dependent regulation of neurotransmitter release at central synapses. Neuron 27, 539-50.

Moss, F. J. et al. (2002). The novel product of a five-exon stargazin-related gene abolishes Ca(V)2.2 calcium channel expression. The EMBO journal 21, 1514-23.

Munir, M., Lu, L., and Mcgonigle, P. (1995). Excitotoxic cell death and delayed rescue in human neurons derived from NT2 cells. J. Neurosci. 15, 7847-60.

Murthy, V N, and Stevens, C F (1999). Reversal of synaptic vesicle docking at central synapses. Nature neuroscience 2, 503-7.

Murthy, Venkatesh N, Schikorski, Thomas, Stevens, Charles F, and Zhu, Y. (2001). Inactivity produces increases in neurotransmitter release and synapse size. Neuron 32, 673-682.

Murthy, Venkatesh N, Sejnowski, T. J., and Stevens, Charles F (1997). Heterogeneous release properties of visualized individual hippocampal synapses. Neuron 18, 599-612.

Myoga, M. H., and Regehr, Wade G (2011). Calcium microdomains near R-type calcium channels control the induction of presynaptic long-term potentiation at parallel fiber to purkinje cell synapses. J. Neurosci. 31, 5235-43.

Müllner, C., Broos, L. a M., Maagdenberg, Arn M J M van den, and Striessnig, Jörg (2004). Familial hemiplegic migraine type 1 mutations K1336E, W1684R, and V1696I alter Cav2.1 Ca2+ channel gating: evidence for beta-subunit isoform-specific effects. The Journal of biological chemistry 279, 51844-50.

Neelands, T. R., King, A. P. J., Macdonald, R. L., Sochivko, D., Pereverzev, Alexey, Smyth, N., Gissel, C., and Schneider, T. (2011). Functional expression of L- , N- , P/Q- , and R-Type calcium channels in the human NT2-N cell line functional expression of L- , N- , P / Q- , and R-Type calcium channels in the human NT2-N cell line. J. Neurophysiol., 2933-2944.

Neher, E (1998). Vesicle pools and Ca2+ microdomains: new tools for understanding their roles in neurotransmitter release. Neuron 20, 389-99.

Neher, Erwin, and Marty, A. (1982). Discrete changes of cell membrane capacitance observed under conditions of enhanced secretion in bovine adrenal chromaffin cells. Proc. Natl. Acad. Sci. USA 79, 6712-6716.

Neher, Erwin, and Sakaba, T. (2008). Multiple roles of calcium ions in the regulation of neurotransmitter release. Neuron 59, 861-72.

Neusch, C., Weishaupt, J. H., and Bähr, M. (2003). Kir channels in the CNS: emerging new roles and implications for neurological diseases. Cell and tissue research 311, 131-8.

Neves, G., Gomis, a, and Lagnado, L (2001). Calcium influx selects the fast mode of endocytosis in the synaptic terminal of retinal bipolar cells. Proceedings of the National Academy of Sciences of the United States of America 98, 15282-7.

Neves, G., and Lagnado, L (1999). The kinetics of exocytosis and endocytosis in the synaptic terminal of goldfish retinal bipolar cells. J. Physiol. 515, 181-202.

Newcomb, R. et al. (1998). Selective peptide antagonist of the class E calcium channel from the venom of the tarantula Hysterocrates gigas. Biochemistry 37, 15353-62.

Nicholls, D. G., and Sihra, T. S. (1986). Synaptosomes possess an exocytotic pool of glutamate. Nature 321, 772-773.

Nowycky, M. C., Fox, Aaron P, and Tsien, Richard W (1985). Three types of neuronal calicum channel with different calcium agonist sensiticity. Nature 316, 440-443.

Oertner, T. G., Sabatini, Bernardo L, Nimchinsky, E. a, and Svoboda, Karel (2002). Facilitation at single synapses probed with optical quantal analysis. Nature neuroscience 5, 657-64.

Ophoff, R. A. et al. (1996). Familial hemiplegic migraine and episodic ataxia type-2 are caused by mutations in the Ca2+ channel gene CACNL1A4. Cell 87, 543-552.

Orita, S., Sasaki, T., Naito, A., Komuro, R., Ohtsuka, T., Maeda, M., Suzuki, H., Igarashi, H., and Takai, Y. (1995). Doc2: A novel brain protein having two repeated C2-like domains. Biomedical and biophysical research communications 206, 439-448.

Ostroff, L. E., Fiala, J. C., Allwardt, B., and Harris, Kristen M (2002). Polyribosomes redistribute from dendritic shafts into spines with enlarged synapses during LTP in developing rat hippocampal slices. Neuron 35, 535-45.

Overton, E. (1902). Beiträge zur allgemeinen Muskel- und Nervenphysiologie. Pflügers Archiv European Journal of Physiology 92.

Oyama, Y. (2002). Estimation of increased concentration of intracellular Cd2+ by fluo-3 in rat thymocytes exposed to CdCl2. Environmental Toxicology and Pharmacology 11, 111-118.

Oyler, G. A., Higgins, G. A., Hart, R. A., Battenberg, E., Billingsley, M., Bloom, F. E., and Wilson, M. C. (1989). The identification of a novel synaptosomal-associated protein, SNAP-25, differentially expressed by neuronal subpopulations. The Journal of cell biology 109, 3039-52.

O'Connor, D. T., Mahata, S. K., Mahata, M., Jiang, Q., Hook, V. Y., and Taupenot, L. (2007). Primary culture of bovine chromaffin cells. Nat. Protoc. 2, 1248-1253.

O'Connor, V. M., Shamotienko, O., Grishin, E., and Betz, H. (1993). On the structure of the "synaptosecretosome". Evidence for a neurexin/synaptotagmin/syntaxin/Ca2+ channel complex. FEBS letters 326, 255-260.

Palmer, M. J. (2010). Characterisation of bipolar cell synaptic transmission in goldfish retina using paired recordings. J. Physiol. 588, 1489-1498.

Pang, Z. P., Bacaj, T., Yang, X., Zhou, P., Xu, W., and Südhof, Thomas C (2011). Doc2 supports spontaneous synaptic transmission by a Ca(2+)-independent mechanism. Neuron 70, 244-51.

Pang, Z. P., Shin, O.-H., Meyer, A. C., Rosenmund, Christian, and Südhof, Thomas C (2006). A gain-of-function mutation in synaptotagmin-1 reveals a critical role of Ca2+-dependent soluble N-ethylmaleimide-sensitive factor attachment protein

receptor complex binding in synaptic exocytosis. The Journal of neuroscience : the official journal of the Society for Neuroscience 26, 12556-65.

Pang, Z. P., Sun, J., Rizo, Josep, Maximov, A., and Südhof, Thomas C (2006). Genetic analysis of synaptotagmin 2 in spontaneous and Ca2+-triggered neurotransmitter release. The EMBO journal 25, 2039-50.

Pathak, M. M., Yarov-Yarovoy, V., Agarwal, G., Roux, B., Barth, P., Kohout, S., Tombola, F., and Isacoff, Ehud Y (2007). Closing in on the resting state of the Shaker K(+) channel. Neuron 56, 124-40.

Payandeh, J., Scheuer, Todd, Zheng, N., and Catterall, William a (2011). The crystal structure of a voltage-gated sodium channel. Nature 475, 353-358.

Perin, M. S., Fried, V. A., Mignery, G. A., Jahn, Reinhard, and Südhof, Thomas C (1990). Phospholipid binding by a synaptic vesicle protein homologous to the regulatory region of protein kinase C. Nature 345, 260-263.

Pfeffer, S. R., and Kelly, R. B. (1985). The subpopulation of brain coated vesicles that carries synaptic vesicle proteins contains two unique polypeptides. Cell 40, 949-57.

Pfrieger, F. W., and Barres, B. A. (1997). Synaptic efficacy enhanced by glial cells in vitro. Science 277, 1684-7.

Piedras-Renteria, E. S., Watase, K., Harata, N., Zhuchenko, O., Zoghbi, H Y, Lee, C C, and Tsien, R W (2001). Increased expression of alpha 1A Ca2+ channel currents arising from expanded trinucleotide repeats in spinocerebellar ataxia type 6. The Journal of neuroscience : the official journal of the Society for Neuroscience 21, 9185-93.

Pietrobon, Daniela (2010). CaV2.1 channelopathies. Pflügers Archiv: European journal of physiology 460, 375-93.

Pietrobon, Daniela (2007). Familial hemiplegic migraine. Neurotherapeutics the journal of the American Society for Experimental NeuroTherapeutics 4, 274-84.

Pietrobon, Daniela (2005). Migraine: new molecular mechanisms. The Neuroscientist a review journal bringing neurobiology, neurology and psychiatry 11, 373-86.

Pietrobon, Daniela, and Striessnig, Jörg (2003). Neurobiology of migraine. Nature reviews. Neuroscience 4, 386-98.

Pinto, A. et al. (1998). Human autoantibodies specific for the alpha1A calcium channel subunit reduce both P-type and Q-type calcium currents in cerebellar neurons. Proceedings of the National Academy of Sciences of the United States of America 95, 8328-33.

Piontek, J., Regnier-Vigouroux, A., and Brandt, R. (2002). Contact with astroglial membranes induces axonal and dendritic growth of human CNS model neurons

and affects the distribution of the growth-associated proteins MAP1B and GAP43. J. Neurosci. Res. 67, 471- 483.

Pleasure, S. J., Page, C., and Lee, V M (1992). Pure, postmitotic, polarized human neurons derived from NTera 2 cells provide a system for expressing exogenous proteins in terminally differentiated neurons. J. Neurosci. 12, 1802-15.

Pleasure, S. J., and Lee, V M (1993). NTera 2 cells: a human cell line which displays characteristics expected of a human committed neuronal progenitor cell, J. Neurosci. Res. 35, 585-602.

Pocock, J., Cousin, M, Parkin, J., and Nicholls, D. (1995). Glutamate exocytosis from cerebellar granule cells: The mechanism of a transition to an L-type Ca2+ channel coupling. Neuroscience 67, 595-607.

Pohorille, A., Schweighofer, K., and Wilson, M. A. (2005). The origin and early evolution of membrane channels. Astrobiology 5.

Poirier, M. A., Hao, J. C., Malkus, P. N., Chan, C, Moore, M. F., King, D. S., and Bennett, M K (1998). Protease resistance of syntaxin.SNAP-25.VAMP complexes. Implications for assembly and structure. The Journal of biological chemistry 273, 11370-7.

Poirier, M. A., Xiao, W., Macosko, J. C., Chan, Charles, Shin, Y.-K., and Bennett, Mark K (1998). The synaptic SNARE complex is a parallel four-stranded helical bundle. Nature 5, 765-769.

Posson, D. J., Ge, P., Miller, Christopher, Bezanilla, Francisco, and Selvin, P. R. (2005). Small vertical movement of a K+ channel voltage sensor measured with luminescence energy transfer. Nature 436, 848-51.

Pozo, K., and Goda, Yukiko (2010). Unraveling mechanisms of homeostatic synaptic plasticity. Neuron 66, 337-51.

Pragnell, Marlon, Waard, Michel De, Mori, Yasuo, Tanabe, Tsutomu, Snutch, Terry P, and Campbell, Kevin P (1994). Calcium channel beta subunit binds to a conserved motif in the I-II cytoplasmic linker of the alpha subunit. Science 368, 67-70.

Pyka, M., Busse, C., Seidenbecher, C., Gundelfinger, E. D., and Faissner, A. (2011). Astrocytes are crucial for survival and maturation of embryonic hippocampal neurons in a neuron-glia cell-insert coculture assay. Synapse 65, 41-53.

Pyle, J. L., Kavalali, E T, Choi, S., and Tsien, R W (1999). Visualization of synaptic activity in hippocampal slices with FM1-43 enabled by fluorescence quenching. Neuron 24, 803-808.

Pyle, J. L., Kavalali, E T, Piedras-renteria, E. S., and Tsien, R W (2000a). Rapid reuse of readily releasable pool vesicles at hippocampal synapses. Neuron 28, 221-231.

Qin, N., Yagel, S., Momplaisir, M.-L., Codd, E. E., and D'Andrea, M. R. (2002). Molecular cloning and characterization of the human voltage-gated calcium channel alpha(2)delta-4 subunit. Molecular pharmacology 62, 485-96.

Rajakulendran, Sanjeev et al. (2010). Genetic and functional characterisation of the P/Q calcium channel in episodic ataxia with epilepsy. The Journal of physiology 588, 1905-13.

Ramaswami, M., Krishnan, K. S., and Kelly, R. B. (1994). Intermediates in synaptic vesicle recycling revealed by optical imaging of Drosophila neuromuscular junctions. Neuron 13, 363-375.

Randall, a, and Tsien, R W (1995). Pharmacological dissection of multiple types of Ca2+ channel currents in rat cerebellar granule neurons. The Journal of neuroscience : the official journal of the Society for Neuroscience 15, 2995-3012.

Regehr, W G, and Atluri, P. P. (1995). Calcium transients in cerebellar granule cell presynaptic terminals. Biophysical journal 68, 2156-70.

Regehr, Wade G, and Stevens, Charles F (2001). Physiology of synaptic transmission and short-term plasticity.

Reid, C. a, Bekkers, John M., and Clements, J. D. (2003). Presynaptic Ca2+ channels: a functional patchwork. Trends in Neurosciences 26, 683-687.

Reim, K., Mansour, M., Varoqueaux, F., McMahon, H T, Südhof, T C, Brose, N, and Rosenmund, C (2001). Complexins regulate a late step in Ca2+-dependent neurotransmitter release. Cell 104, 71-81.

Rendt, J., Erulkar, S., and Andrews, P. W. (1989). Presumptive neurons derived by differentiation of a human embryonal carcinoma cell line exhibit tetrodotoxin sensitive sodium currents and the capacity for regenerative responses. Exp. Cell Res. 180, 580-584.

Restituito, S., Thompson, R. M., Eliet, J., Raike, R. S., Riedl, M., Charnet, P., and Gomez, C. M. (2000). The polyglutamine expansion in spinocerebellar ataxia type 6 causes a beta subunit-specific enhanced activation of P/Q-type calcium channels in Xenopus oocytes. The Journal of neuroscience : the official journal of the Society for Neuroscience 20, 6394-403.

Rettig, J., and Neher, Erwin (2002). Emerging roles of presynaptic proteins in Ca++-triggered exocytosis. Science (New York, N.Y.) 298, 781-5.

Reuter, Harald (1979). Properties of two inward membrane currents in the heart. Annual review of physiology 41, 413-424.

Reuter, Harald (1967). The dependence of slow inward current in purkinje fibres on hte extracellular calcium concentration. Journal of Physiology 192, 479-492.

Riant, F. et al. (2005). ATP1A2 mutations in 11 families with familial hemiplegic migraine. Human mutation 26, 281.

Riant, F., Mourtada, R., Saugier-veber, P., and Tournier-lasserve, E. (2008). Large CACNA1A deletion in a family with episodic ataxia type 2. Arch. Neurol. 65, 817-820.

Richards, D. A., Bai, J., and Chapman, E. R. (2005a). Two modes of exocytosis at hippocampal synapses revealed by rate of FM 1-43 efflux from individual vesicles. J. Cell Biol. 168, 929-39.

Richards, D. A., Guatimosim, Cristina, Rizzoli, Silvio O, and Betz, William J (2003). Synaptic vesicle pools at the frog neuromuscular junction. Neuron 39, 529-541.

Richards, D. a, Guatimosim, C, and Betz, W J (2000). Two endocytic recycling routes selectively fill two vesicle pools in frog motor nerve terminals. Neuron 27, 551-9.

Richards, K. S., Swensen, A. M., Lipscombe, Diane, and Bommert, K. (2007). Novel CaV2.1 clone replicates many properties of Purkinje cell CaV2.1 current. The European journal of neuroscience 26, 2950-61.

Richards, Mark W, Butcher, A. J., and Dolphin, A. C. (2004). Ca2+ channel beta-subunits: structural insights AID our understanding. Trends in pharmacological sciences 25, 626-32.

Rizo, Josep, and Südhof, Thomas C (2002). Snares and Munc18 in synaptic vesicle fusion. Nature reviews. Neuroscience 3, 641-53.

Rizo, Josep, and Rosenmund, Christian (2008). Synaptic vesicle fusion. Nat. Struct. Mol. Biol. 15, 665-674.

Rizzoli, S O, and Betz, W J (2005). Synaptic vesicle pools. Nat. Rev. Neurosci. 6, 57-69.

Robertis, E. D. P. De, and Bennett, H. S. (1954). A SUBMICROSCOPIC AND NERVE COMPONENT SATELLITE OF SCHWANN. Experimental Cell Research 6, 543-545.

Rollenhagen, A., and Lübke, J. H. R. (2010). The mossy fiber bouton: the "common" or the "unique" synapse? Front Synaptic Neurosci. 2, 1-9.

Rosenberg, R. L., Tomiko, S. a, and Agnew, W S (1984). Single-channel properties of the reconstituted voltage-regulated Na channel isolated from the electroplax of Electrophorus electricus. Proceedings of the National Academy of Sciences of the United States of America 81, 5594-8.

Rosenmund, C, and Stevens, C F (1996). Definition of the readily releasable pool of vesicles at hippocampal synapses. Neuron 16, 1197-207.

Ross, W. N., Nakamura, T., Watanabe, S., Larkum, M., and Lasser-Ross, N. (2005). Synaptically activated Ca2+ release from internal stores in CNS neurons. Cell Mol. Neurobiol. 25, 283-295.

Rouze, N. C., and Schwartz, E. A. (1998). Continuous and transient vesicle cycling at a ribbon synapse. J. Neurosci. 18, 8614-8624.

Rozov, a, Burnashev, N., Sakmann, B, and Neher, E (2001). Transmitter release modulation by intracellular Ca2+ buffers in facilitating and depressing nerve terminals of pyramidal cells in layer 2/3 of the rat neocortex indicates a target cell-specific difference in presynaptic calcium dynamics. The Journal of physiology 531, 807-26.

Rusakov, D. a, Wuerz, A., and Kullmann, Dimitri M (2004). Heterogeneity and specificity of presynaptic Ca2+ current modulation by mGluRs at individual hippocampal synapses. Cerebral cortex (New York, N.Y.: 1991) 14, 748-58.

Ruta, V., Chen, J., and MacKinnon, Roderick (2005). Calibrated measurement of gating-charge arginine displacement in the KvAP voltage-dependent K+ channel. Cell 123, 463-75.

Ruth, P., Rohrkasten, A., Biel, Martin, Bosse, E., Regulla, S., Meyer, H. E., Flockerzi, Veit, and Hofmann, Franz (1989). Subunit of the DHP- Primary Structure of the beta subunit of the DHP-senstitve calcium channel from skeletal muscle. Science 245, 1115-1118.

Ryan, T. A., Reuter, H, Wendland, B., Schweizer, F. E., Tsien, R W, and Smith, S J (1993). The kinetics of synaptic vesicle recycling measured at single presynaptic boutons. Neuron 11, 713^724.

Sabatini, Bernardo L, and Regehr, Wade G (1996). Timing of neurotransmission at fast synapses in the mammalian brain. Nature 384, 170-172.

Sander, J. W. (2003). The epidemiology of epilepsy revisited. Current opinion in neurology 16, 165-70.

Sankaranarayanan, S., Angelis, D., D., R., E, J., and Ryan, T. A. (2000). The use of pHluorins for optical measurements of presynaptic activity. Biophys J 79, 2199-2208.

Sankaranarayanan, S., and Ryan, T. A. (2001). Calcium accelerates endocytosis of vSNAREs at hippocampal synapses. Nat. Neurosci. 4, 129-136.

Sankaranarayanan, S., and Ryan, T. a (2000). Real-time measurements of vesicle-SNARE recycling in synapses of the central nervous system. Nature cell biology 2, 197-204.

Saporta, S., Willing, A. E., Colina, L. O., Zigova, T., Milliken, M., Daadi, M. M., and Sanberg, P. R. (2000). In vitro and in vivo characterization of hNT neuron neurotransmitter phenotypes. Brain Res. Bull. 53, 263-8.

Sara, Y, Virmani, T., Deák, F., Liu, X, and Kavalali, E.T. (2005). An isolated pool of vesicles recycles at rest and drives spontaneous neurotransmission. Neuron 45, 563–573.

Sara, Yildirim, Mozhayeva, M. G., Liu, Xinran, and Kavalali, Ege T (2002). Fast vesicle recycling supports neurotransmission during sustained stimulation at hippocampal synapses. J. Neurosci. 22, 1608-1617.

Sather, W A, Tanabe, T, Zhang, J. F., Mori, Y, Adams, M E, and Tsien, R W (1993). Distinctive biophysical and pharmacological properties of class A (BI) calcium channel alpha 1 subunits. Neuron 11, 291-303.

Scanziani, M., Gahwiler, B. H., and Thompson, S. M. (1995). Presynaptic inhibition of excitatory synaptic transmission by muscarinic and metabotropic glutamate receptor activation in the hippocampus: are Ca2+ channels involved? Neuropharmacology 34, 1549-57.

Schenck, S., Wojcik, S. M., Brose, Nils, and Takamori, S. (2009). A chloride conductance in VGLUT1 underlies maximal glutamate loading into synaptic vesicles. Nature neuroscience 12, 156-62.

Schikorski, T, and Stevens, C F (1997). Quantitative ultrastructural analysis of hippocampal excitatory synapses. J. Neurosci. 17, 5858-5867.

Schikorski, T, and Stevens, C.F. (2001). Morphological correlates of functionally defined synaptic vesicle populations. Nat. Neurosci. 4, 391–395.

Schmalenbach, C., and Müller, H. W. (1993). Astroglia-neuron interactions that promote long-term neuronal survival. J. Chem. Neuroanat. 6, 229-37.

Schneggenburger, R, and Neher, E (2000). Intracellular calcium dependence of transmitter release rates at a fast central synapse. Nature 406, 889-93.

Schneggenburger, Ralf, and Forsythe, Ian D (2006). The calyx of Held. Cell Tissue Res. 326, 311-337.

Schneggenburger, Ralf, Sakaba, T., and Neher, Erwin (2002). Vesicle pools and short-term synaptic depression: lessons from a large synapse. Trends Neurosci. 25, 206-612.

Schneggenburger, Ralf, and Neher, Erwin (2005). Presynaptic calcium and control of vesicle fusion. Current opinion in neurobiology 15, 266-74.

Schorge, Stephanie, Leemput, J. van de, Singleton, A., Houlden, H., and Hardy, J. (2010). Human ataxias: a genetic dissection of inositol triphosphate receptor (ITPR1)-dependent signaling. Trends in neurosciences 33, 211-9.

Schorge, Stephanie, and Rajakulendran, Sanjeev (2011). The P/Q channel in human disease: Untangling the genetics and physiology. Membrane transport and signalling.

Segal, M., and Manor, D. (1992). Confocal microscopic imaging of [Ca2+]i in cultured rat hippocampal neurons following exposure to N-methyl-D-aspartate. J. Physiol. 448, 655-76.

Seoh, S. a, Sigg, D., Papazian, D M, and Bezanilla, F (1996). Voltage-sensing residues in the S2 and S4 segments of the Shaker K+ channel. Neuron 16, 1159-67.

Serra, S. A., Cuenca-león, E., Llobet, A., Rubio-moscardo, F., Plata, C., and Carreño, O. (2009). A mutation in the first intracellular loop of CACNA1A prevents P / Q channel modulation by SNARE proteins and lowers exocytosis. PNAS, 1-6.

Shafrir, Y., Durell, S. R., and Guy, H Robert (2008). Models of voltage-dependent conformational changes in NaChBac channels. Biophysical journal 95, 3663-76.

Sheng, Z.-H. (1997). Interaction of the synprint site of N-type Ca2+ channels with the C2B domain of synaptotagmin I. Proceedings of the National Academy of Sciences 94, 5405-5410.

Sheng, Zu-Hang, Rettig, J., Cook, T., and Catterall, William A (1996). Calicum-dependent interaction of N-type calicum channels with the synaptic core complex. Nature 379, 451-454.

Sherff, C. M., and Carew, T. J. (1999). Coincident Induction of Long-Term Facilitation in Aplysia: Cooperativity Between Cell Bodies and Remote Synapses. Science 285, 1911-1914.

Silverman, W. R., Roux, B., and Papazian, Diane M (2003). Structural basis of two-stage voltage-dependent activation in K+ channels. Proceedings of the National Academy of Sciences of the United States of America 100, 2935-40.

Simkus, C. R. L., and Stricker, C. (2002a). Properties of mEPSCs recorded in layer II neurones of rat barrel cortex. The Journal of Physiology 545, 509-520.

Simkus, C. R. L., and Stricker, C. (2002b). The contribution of intracellular calcium stores to mEPSCs recorded in layer II neurones of rat barrel cortex. The Journal of Physiology 545, 521-535.

Smith, C. B., and Betz, William J (1996). Simultaneous independent measurements of endocytosis and exocytosis. Nature 380, 531-534.

Soldatov, N. M. (2003). Ca2+ channel moving tail: link between Ca2+-induced inactivation and Ca2+ signal transduction. Trends in Pharmacological Sciences 24, 167-171.

Sollner, T., Whiteheart, S. W., Brunner, M., Erdjument-Bromage, H., Geromanos, S., Tempst, P., and Rothman, James E (1993). SNAP receptors implicated in vesicle targeting and fusion. Nature 362, 318-324.

Soong, Tuck Wah, DeMaria, Carla D, Alvania, Rebecca S, Zweifel, L. S., Liang, Mui Cheng, Mittman, S., Agnew, William S, and Yue, David T (2002). Systematic

identification of splice variants in human P/Q-type channel alpha1(2.1) subunits: implications for current density and Ca2+-dependent inactivation. The Journal of neuroscience : the official journal of the Society for Neuroscience 22, 10142-52.

Spadaro, Maria et al. (2004). A G301R Na+/K+ -ATPase mutation causes familial hemiplegic migraine type 2 with cerebellar signs. Neurogenetics 5, 177-85.

Spafford, J. D., and Zamponi, Gerald W (2003). Functional interactions between presynaptic calcium channels and the neurotransmitter release machinery. Current Opinion in Neurobiology 13, 308-314.

Spillane, J., Beeson, D. J., and Kullmann, Dimitri M (2010). Myasthenia and related disorders of the neuromuscular junction. Journal of neurology, neurosurgery, and psychiatry 81, 850-7.

Stanley, E F (1997). The calcium channel and the organization of the presynaptic transmitter release face. Trends in neurosciences 20, 404-9.

Stanley, E F, and Goping, G. (1991). Characterization of a calcium current in a vertebrate cholinergic presynaptic nerve terminal. J. Neurosci. 11, 985-993.

Stanley, Elise F. (2003). Syntaxin I modulation of presynaptic calcium channel inactivation revealed by botulinum toxin C1. European Journal of Neuroscience 17, 1303-1305.

Stanley, Elk F (1993). Single Calcium Channels and Acetylcholine at a Presynaptic Nerve Terminal. Cell 11, 1007-1011.

Staras, Kevin, Branco, T., Burden, J. J., Pozo, K., Darcy, K., Marra, V., Ratnayaka, A., and Goda, Yukiko (2010). A vesicle superpool spans multiple presynaptic terminals in hippocampal neurons. Neuron 66, 37-44.

Stea, A., Soong, T W, and Snutch, T P (1995). Determinants of PKC-dependent modulation of a family of neuronal calcium channels. Neuron 15, 929-40.

Stea, A., Tomlinson, W. J., Soong, T W, Bourinet, E., Dubel, S. J., Vincent, S. R., and Snutch, T P (1994). Localization and functional properties of a rat brain alpha 1A calcium channel reflect similarities to neuronal Q- and P-type channels. Proceedings of the National Academy of Sciences of the United States of America 91, 10576-80.

Stevens, C F, and Wang, Y (1995). Facilitation and depression at single central synapses. Neuron 14, 795-802.

Stevens, Charles F, and Williams, J. H. (2007). Discharge of the readily releasable pool with action potentials at hippocampal synapses. J. Neurophysiol. 98, 3221-3229.

Stratagene Cloning Systems (1998). NT2 Precursor Cells - Maintenance and Differentiation to hNT Neurons. World Wide Web Internet And Web Information Systems, 1-23.

Strock, J., and Diversé-pierluissi, M. A. (2004). Ca 2+ Channels As Integrators of G Protein-Mediated Signaling in Neurons. Molecular Pharmacology 66, 1071-1076.

Strong, M., Chandy, K. G., and Gutman, G. a (1993). Molecular evolution of voltage-sensitive ion channel genes: on the origins of electrical excitability. Molecular biology and evolution 10, 221-42.

Südhof, T. C. (2004). The synaptic vesicle cycle. Annual review of neuroscience 27, 509-47.

Südhof, T. C. (1995). The synaptic vesicle cycle: a cascade of protein protein interactions. Nature 375, 645-653.

Südhof, T. C., Baumert, M., Perin, M. S., and Jahn, Reinhard (1989). A synaptic vesicle membrane protein is conserved from mammals to drosophila. Neuron 2, 1475-1481.

Sun, J., Pang, Z. P., Qin, D., Fahim, A. T., Adachi, R., and Südhof, Thomas C (2007). A dual-Ca2+-sensor model for neurotransmitter release in a central synapse. Nature 450, 676-82.

Sutton, M. A., Wall, N. R., Aakalu, G. N., and Schuman, Erin M (2004). Regulation of dendritic protein synthesis by miniature synaptic events. Science (New York, N.Y.) 304, 1979-83.

Sutton, M. a, Ito, H. T., Cressy, P., Kempf, C., Woo, J. C., and Schuman, Erin M (2006). Miniature neurotransmission stabilizes synaptic function via tonic suppression of local dendritic protein synthesis. Cell 125, 785-99.

Sutton, R. B., Fasshauer, Dirk, Jahn, Reinhard, and Brunger, A. T. (1998). Crystal structure of a SNARE complex involved in synaptic ° resolution exocytosis at 2 . 4 A. Nature 395, 347-353.

Sätzler, K., Söhl, L. F., Bollmann, Johann H, Borst, J Gerard G, Frotscher, M., Sakmann, Bert, and Lübke, J. H. R. (2002). Three-dimensional reconstruction of a calyx of Held and its postsynaptic principal neuron in the medial nucleus of the trapezoid body. J. Neurosci. 22, 10567-10579.

Südhof, Thomas C, and Rothman, James E (2009). Membrane fusion: grappling with SNARE and SM proteins. Science 323, 474-477.

Takahashi, M, Seagar, M J, Jones, J. F., Reber, B. F., and Catterall, W a (1987). Subunit structure of dihydropyridine-sensitive calcium channels from skeletal muscle. Proceedings of the National Academy of Sciences of the United States of America 84, 5478-82.

Takei, K., Mundigl, O., Daniell, L., and Camilli, P. De (1996). The synaptic vesicle cycle: a single vesicle budding step involving clathrin and dynamin. J. Cell Biol. 133, 1237-1250.

Takeuchi, A., and Takeuchi, N. (1960). On the permeability of end-plate membrane during the action of transmitter. Journal of Physiology 154, 52-67.

Teng, H., Cole, J. C., Roberts, R. L., and Wilkinson, R. S. (1999). Endocytic active zones: hot spots for endocytosis in vertebrate neuromuscular terminals. J. Neurosci. 19, 4855-4866.

Thiagarajan, T. C., Lindskog, M., and Tsien, Richard W (2005). Adaptation to synaptic inactivity in hippocampal neurons. Neuron 47, 725-37.

Thomsen, L. L., Eriksen, M. K., Roemer, S. F., Andersen, I., Olesen, J., and Russell, M. B. (2002). A population-based study of familial hemiplegic migraine suggests revised diagnostic criteria. Brain: a journal of neurology 125, 1379 -91.

Thévenod, F. (2010). Catch me if you can! Novel aspects of cadmium transport in mammalian cells. Biometals : an international journal on the role of metal ions in biology, biochemistry, and medicine 23, 857-75.

Tokuoka, H., and Goda, Yukiko (2006). Myosin light chain kinase is not a regulator of synaptic vesicle trafficking during repetitive exocytosis in cultured hippocampal neurons. J. Neurosci. 26, 11606-14.

Tombaugh, G C, and Somjen, G. G. (1996). Effects of extracellular pH on voltage-gated Na+, K+ and Ca2+ currents in isolated rat CA1 neurons. J. Physiol. 493, 719-32.

Tombaugh, Geoffrey C (1998). Intracellular pH buffering shapes activity-dependent Ca2+ dynamics in dendrites of CA1 interneurons. J. Neurophysiol. 80, 1702-1712.

Tombola, F., Pathak, M. M., Gorostiza, P., and Isacoff, Ehud Y (2007). The twisted ion-permeation pathway of a resting voltage-sensing domain. Nature 445, 546-9.

Tombola, F., Pathak, M. M., and Isacoff, Ehud Y (2006). How does voltage open an ion channel? Annu. Rev. Cell Dev. Biol. 22, 23-52.

Tomita, S., Chen, Lu, Kawasaki, Y., Petralia, R. S., Wenthold, R. J., Nicoll, R. A., and Bredt, D. S. (2003). Functional studies and distribution define a family of transmembrane AMPA receptor regulatory proteins. J. Cell Biol. 161, 805-16.

Toru, S. et al. (2000). Spinocerebellar ataxia type 6 mutation alters P-type calcium channel function. J. Biol. Chem. 275, 10893-8.

Tottene, Angelita, Conti, R., Fabbro, A., Vecchia, D., Shapovalova, Maryna, Santello, M., Maagdenberg, Arn M J M van den, Ferrari, Michel D, and Pietrobon, Daniela (2009). Enhanced excitatory transmission at cortical synapses as the basis for facilitated spreading depression in Ca(v)2.1 knockin migraine mice. Neuron 61, 762-73.

Tottene, Angelita, Fellin, Tommaso, Pagnutti, Stefano, Luvisetto, Siro, Striessnig, Joerg, Fletcher, C., and Pietrobon, Daniela (2002). Familial hemiplegic migraine mutations increase Ca(2+) influx through single human CaV2.1 channels and

decrease maximal CaV2.1 current density in neurons. Proc. Natl. Acad. Sci. USA 99, 13284-13289.

Tottene, Angelita, Pivotto, F., Fellin, Tommaso, Cesetti, T., Maagdenberg, A. M. J. M. V. D., and Pietrobon, Daniela (2005). Specific kinetic alterations of human Cav2.1 calcium channels produced by mutation S218L causing familial hemiplegic migraine and delayed cerebral edema and coma after minor head trauma. J. Biol. Chem. 280, 17678 -17686.

Trimble, W. S., Cowan, D. M., and Scheller, R H (1988). VAMP-1 : A synaptic vesicle-associated integral membrane protein. Proceedings of the National Academy of Sciences of the United States of America 85, 4538-42.

Tsai, C.-C. et al. (2009). Dynasore inhibits rapid endocytosis in bovine chromaffin cells. Am. J. Physiol. Cell Physiol. 297, 397-406.

Tsien, R W, Lipscombe, D, Madison, D. V., Bley, K. R., and Fox, a P. (1988). Multiple types of neuronal calcium channels and their selective modulation. Trends in neurosciences 11, 431-8.

Tsunemi, T., Saegusa, Hironao, Ishikawa, Kinya, Nagayama, Shin, Murakoshi, Takayuki, Mizusawa, Hidehiro, and Tanabe, Tsutomu (2002). Novel Cav2.1 splice variants isolated from Purkinje cells do not generate P-type Ca2+ current. The Journal of biological chemistry 277, 7214-21.

Tsvetkov, E., Shin, R.-M., and Street, M. (2004). Glutamate uptake determines pathway specificity of long-term potentiation. Neuorn 41, 139-151.

Turner, T. J., and Dunlap, K. (1995). Pharmacological characterization of presynaptic calcium channels using subsecond biochemical measurements of synaptosomal neurosecretion. Neuropharmacology 34, 1469-1478.

Vanden Berghe, P., and Klingauf, Jürgen (2006). Synaptic vesicles in rat hippocampal boutons recycle to different pools in a use-dependent fashion. The Journal of physiology 572, 707-20.

Vanmolkot, K. R. J., Kors, E. E., et al. (2003). Novel mutations in the Na+, K+-ATPase pump gene ATP1A2 associated with familial hemiplegic migraine and benign familial infantile convulsions. Annals of neurology 54, 360-6.

Vanmolkot, K. R. J., Maagdenberg, Arn M J M van den, Haan, Joost, and Ferrari, Michel D (2003). New discoveries about the second gene for familial hemiplegic migraine, ATP1A2. The Lancet 2, 721.

Varley, Z. K., Pizzarelli, R., Antonelli, R., Stancheva, S. H., Kneussel, M., Cherubini, E., and Zacchi, P. (2011). Gephyrin regulates GABAergic and glutamatergic synaptic transmission in hippocampal cell cultures. J. Biol. Chem. 286, 20942-51.

Verderio, C. et al. (2004). SNAP-25 modulation of calcium dynamics underlies differences in GABAergic and glutamatergic responsiveness to depolarization. Neuron 41, 599-610.

Verhage, M, Vries, K. J. de, Røshol, H., Burbach, J. P., Gispen, W. H., and Südhof, T C (1997). DOC2 proteins in rat brain: complementary distribution and proposed function as vesicular adapter proteins in early stages of secretion. Neuron 18, 453-61.

Viard, P., Butcher, A. J., Halet, G., Davies, A., Nürnberg, B., Heblich, Fay, and Dolphin, A. C. (2004). PI3K promotes voltage-dependent calcium channel trafficking to the plasma membrane. Nature neuroscience 7, 939-46.

Vicario-Abejón, C, Collin, C., McKay, R. D., and Segal, M. (1998). Neurotrophins induce formation of functional excitatory and inhibitory synapses between cultured hippocampal neurons. J. Neurosci. 18, 7256-71.

Vicario-Abejón, C, Collin, C., Tsoulfas, P., and McKay, R. D. (2000). Hippocampal stem cells differentiate into excitatory and inhibitory neurons. Eur. J. Neurosci. 12, 677-88.

Vicario-Abejón, Carlos (2004). Long-term culture of hippocampal neurons. Curr. Protoc. Neurosci. 3, 1-13.

Viesselmann, C., Ballweg, J., Lumbard, D., and Dent, E. W. (2011). Nucleofection and primary culture of embryonic mouse hippocampal and cortical neurons. J. Vis. Exp., 2-5.

Vincent, Angela (2010). Autoimmune channelopathies: well-established and emerging immunotherapy-responsive diseases of the peripheral and central nervous systems. Journal of clinical immunology 30, 97-102.

Volsen, S. G. et al. (1995). The expression of neuronal voltage-dependent calcium channels in human cerebellum. Brain research. Molecular brain research 34, 271-82.

Vyleta, N. P., and Smith, Stephen M (2011). Spontaneous glutamate release is independent of calcium influx and tonically activated by the calcium-sensing receptor. The Journal of neuroscience : the official journal of the Society for Neuroscience 31, 4593-606.

Waard, Michel De, Hering, J., Weiss, N., and Feltz, A. (2005). How do G proteins directly control neuronal Ca2+ channel function? Trends in pharmacological sciences 26, 427-36.

Walker, D., and Waard, M De (1998). Subunit interaction sites in voltage-dependent Ca2+ channels: role in channel function. Trends in neurosciences 21, 148-54.

Wang, C., and Zucker, R. S. (1998). Regulation of synaptic vesicle recycling by calcium and serotonin. Neuron 21, 155-167.

Wasser, C. R., and Kavalali, E T (2009). Leaky synapses: regulation of spontaneous neurotransmission in central synapses. Neuroscience 158, 177-88.

Waters, J., and Smith, S.J. (2002). Vesicle pool partitioning influences presynaptic diversity and weighting in rat hippocampal synapses. J. Physiol. 541, 811-823.

Weber, A. M., Wong, F. K., Tufford, A. R., Schlichter, L. C., Matveev, V., and Stanley, Elise F (2010). N-type Ca2+ channels carry the largest current: implications for nanodomains and transmitter release. Nature neuroscience 13, 1348-50.

Weber, T., Zemelman, B. V., McNew, J. a, Westermann, B., Gmachl, M., Parlati, F., Söllner, T. H., and Rothman, J E (1998). SNAREpins: minimal machinery for membrane fusion. Cell 92, 759-72.

Weiss, N., Sandoval, A., Felix, Ricardo, Maagdenberg, A. Van den, and Waard, Michel De (2008). The S218L familial hemiplegic migraine mutation promotes deinhibition of Ca(v)2.1 calcium channels during direct G-protein regulation. Pflügers Archiv : European journal of physiology 457, 315-26.

Wheeler, D. B., Randall, a, and Tsien, R W (1996). Changes in action potential duration alter reliance of excitatory synaptic transmission on multiple types of Ca2+ channels in rat hippocampus. The Journal of neuroscience : the official journal of the Society for Neuroscience 16, 2226-37.

Wheeler, D. B., Randall, a, and Tsien, R W (1994). Roles of N-type and Q-type Ca2+ channels in supporting hippocampal synaptic transmission. Science (New York, N.Y.) 264, 107-11.

White, J. G., Amos, W. B., and Fordham, M. (1987). An evaluation of confocal versus conventional imaging of biological structures by fluorescence light microscopy. J. Cell Biol. 105, 41-8.

Wilhelm, B. G., Groemer, T. W., and Rizzoli, Silvio O (2010a). The same synaptic vesicles drive active and spontaneous release. Nature neuroscience 13, 1454-6.

Wilhelm, B. G., Groemer, T. W., and Rizzoli, Silvio O (2010b). The same synaptic vesicles drive active and spontaneous release. Nat. Neurosci. 13, 1454-1456.

Winterer, J., Stanton, P., and Müller, W. (2006). Direct monitoring of vesicular release and uptake in brain slices by multiphoton excitation of the styryl FM 1-43. BioTechniques 40, 343-350.

Winterfield, J. R., and Swartz, K. J. (2000). A hot spot for the interaction of gating modifier toxins with voltage-dependent ion channels. J. Gen. Physiol. 116, 637-644.

Witcher, D. R., Waard, M De, Sakamoto, J., Franzini-Armstrong, C., Pragnell, M, Kahl, S. D., and Campbell, K P (1993). Subunit identification and reconstitution of the N-type Ca2+ channel complex purified from brain. Science (New York, N.Y.) 261, 486-9.

Wu, L.-G., and Saggau, P. (1994). Pharmacological Identification of Two Types of Presynaptic Calcium Channels at CA3-CA1 Synapses of the Hippocampus. J Neurosci 14, 5613-5622.

Wu, W., Xu, J, Wu, X. S., and Wu, L. G. (2005). Activity-dependent acceleration of endocytosis at a central synapse. J Neurosci 25, 11676-11683.

Wu, Y., Yeh, F. L., Mao, Fei, and Chapman, E. R. (2009). Biophysical characterization of styryl dye-membrane interactions. Biophys. J. 97, 101-109.

Xie, X.-S., Crider, B. P., and Stone, D. K. (1989). Isolation and Reconstitution of the chloride transporter of clathrin-coated vesicles. The Journal of biological chemistry 264, 18870-18873.

Xu, B. et al. (2011). Calcium signaling is involved in cadmium-induced neuronal apoptosis via induction of reactive oxygen species and activation of MAPK/mTOR network. PloS one 6, e19052.

Xu, Jun, Mashimo, T., and Südhof, Thomas C (2007). Synaptotagmin-1, -2, and -9: Ca(2+) sensors for fast release that specify distinct presynaptic properties in subsets of neurons. Neuron 54, 567-81.

Xu, Jun, Pang, Z. P., Shin, O.-H., and Südhof, Thomas C (2009). Synaptotagmin-1 functions as a Ca2+ sensor for spontaneous release. Nature neuroscience 12, 759-66.

Xu-Friedman, M. a, Harris, K M, and Regehr, W G (2001). Three-dimensional comparison of ultrastructural characteristics at depressing and facilitating synapses onto cerebellar Purkinje cells. The Journal of neuroscience: the official journal of the Society for Neuroscience 21, 6666-72.

Yang, H., Cong, Rui, Na, L., Ju, G., and You, S.-W. (2010). Long-term primary culture of highly-pure rat embryonic hippocampal neurons of low-density. Neurochem. Res. 35, 1333-42.

Yang, J., Ellinor, P. T., Sather, William A., Zhang, J.-F., and Tsien, Richard W. (1993). Molecular determinants of Ca2+ selectivity and ion permeation in L-type Ca2+ channels. Nature 366, 158-161.

Yarov-Yarovoy, V., Baker, D., and Catterall, William a (2006). Voltage sensor conformations in the open and closed states in ROSETTA structural models of K(+) channels. Proceedings of the National Academy of Sciences of the United States of America 103, 7292-7.

Yataganas, X., Strife, A., Perez, A., and Clarkson, B. D. (1974). Microfluorimetric evaluation of cell kill kinetics with 1-beta-D-arabinofuranosylcytosine. Cancer Res. 34, 2795-806.

Yoshida, A., Oho, C., Omori, A., Kuwahara, R., Ito, T., and Takahashi, Masami (1992). HPC-1 Is Associated with Synaptotagmin and omega-Conotoxin Receptor. The Journal of biological chemistry 267, 24925-24928.

Yu, F. H., and Catterall, William a (2003). Overview of the voltage-gated sodium channel family. Genome biology 4, 207.

Yu, Y., Maureira, C., Liu, Xiuxin, and McCormick, David (2010). P/Q and N channels control baseline and spike-triggered calcium levels in neocortical axons and synaptic boutons. The Journal of neuroscience : the official journal of the Society for Neuroscience 30, 11858-69.

Zamponi, G W (2001). Determinants of G protein inhibition of presynaptic calcium channels. Cell biochemistry and biophysics 34, 79-94.

Zamponi, Gerald W, and Snutcht, T. P. (1998). Modulation of voltage-dependent calcium channels by G proteins. Curr. Opin. Neurobiol. 8, 351-356.

Zeller, M., and Strauss, W. L. (1995). Retinoic acid induces cholinergic differentiation of NTera 2 human embryonal carcinoma cells. Int. J. Devl. Neurosci. 13, 437-45.

Zenisek, D., Steyer, J. a, Feldman, M. E., and Almers, W. (2002). A membrane marker leaves synaptic vesicles in milliseconds after exocytosis in retinal bipolar cells. Neuron 35, 1085-97.

Zhang, X. H., and Poo, M.-ming (2002). Localized synaptic potentiation by BDNF requires local protein synthesis in the developing axon. Neuron 36, 675-88.

Zhong, H., Yokoyama, C. T., Scheuer, T, and Catterall, W a (1999). Reciprocal regulation of P/Q-type Ca2+ channels by SNAP-25, syntaxin and synaptotagmin. Nature neuroscience 2, 939-41.

Zhuchenko, O. et al. (1997). Autosomal dominant cerebellar ataxia (SCA6) associated with small polyglutamine expansions in the alpha1A voltage dependent calcium channel. Nature 15, 62-69.

Zimmerberg, J., Curran, M., Cohen, F. S., and Brodwick, M. (1987). Simultaneous electrical and optical measurements show that membrane fusion precedes secretory granule swelling during exocytosis of beige mouse mast cells. Proceedings of the National Academy of Sciences of the United States of America 84, 1585-9.